This electronic thesis or dissertation has been downloaded from the King's Research Portal at https://kclpure.kcl.ac.uk/portal/

Brain Metabolomics

A new comprehensive metabolic profiling approach to Alzheimer's disease pathology using LC-MS and GC-MS

Ebshiana, Amera Abugiala A

Awarding institution:
King's College London

The copyright of this thesis rests with the author and no quotation from it or information derived from it may be published without proper acknowledgement.

END USER LICENCE AGREEMENT

Unless another licence is stated on the immediately following page this work is licensed

under a Creative Commons Attribution-NonCommercial-NoDerivatives 4.0 International

licence. https://creativecommons.org/licenses/by-nc-nd/4.0/

You are free to copy, distribute and transmit the work

Under the following conditions:

- Attribution: You must attribute the work in the manner specified by the author (but not in any way that suggests that they endorse you or your use of the work).
- Non Commercial: You may not use this work for commercial purposes.
- No Derivative Works - You may not alter, transform, or build upon this work.

Any of these conditions can be waived if you receive permission from the author. Your fair dealings and other rights are in no way affected by the above.

Take down policy

If you believe that this document breaches copyright please contact librarypure@kcl.ac.uk providing details, and we will remove access to the work immediately and investigate your claim.

Download date: 05. May. 2023

Brain Metabolomics: A new comprehensive metabolic profiling approach to Alzheimer's disease pathology using LC-MS and GC-MS

AMERA EBSHIANA

A THESIS SUBMITTED IN PARTIAL FULFILMENT OF THE REQUIREMENTS FOR THE DEGREE OF DOCTOR OF PHILOSOPHY

SUPERVISORS:

DR. CRISTINA LEGIDO-QUIGLEY

DR. RICHARD PARSONS

INSTITUTE OF PHARMACEUTICAL SCIENCE

FACULTY OF LIFE SCIENCES & MEDICINE

KING'S COLLEGE LONDON

ACKNOWLEDGEMENTS

I thank God (ALLAH) the most merciful and the most gracious for giving me the strength, knowledge and patience to be able to complete this study.

I would like to express my sincere gratitude to Dr Cristina Legido-Quigley,for giving me the opportunity to undertake this project under her supervision and for her expert insight and valuable advice that have guided me through this PhD. I also wish to thank sincerely Dr. Stuart Snowdfor sharing ideas and discussion.

My thanks go to all PhD colleagues in my research group for the friendship throughout my studies and to technicians at the institute of pharmaceutical science - king' college London. I would like to acknowledge the Libyan Cultural attaché of Libyan embassy for funding my study and for giving me this great opportunity

My special thanks go to my parents, Abugiala and Najat, my sisters and brothers for their constant encouragement and endless love. I would like also to thank my loved husband Mahmoud for his continuous motivation and caring, and wish him good luck in his PhD.

Last but not least, I would like to tell my daughters, Rancy, Sarah and Sadan, my joy and happiness that I love you and sorry for not being around at all times.

ABSTRACT

Alzheimer's disease (AD) is the most common form of dementia characterized by memory loss and other cognitive abilities that worsen overtime to interfere with daily life. AD's incidence and financial burden is rapidly increasing worldwide. Considering brain disease pathology starts 20 years before symptoms become noticeable, detecting molecules capable of precise diagnosis of disease before development of symptoms is a priority. This thesis investigates the possibility of using metabolomics to detect AD associated metabolites and to measure the abundance of a range of small molecule metabolites in human brain to examine how these metabolites are associated with severity of AD pathology and expression of symptoms. A project plan was designed to investigate brain metabolic profiling of AD samples. Initially rat brain samples were used to develop a method capable of the coverage of a wide range of metabolites using Liquid chromatography quadrupole time of flight mass spectrometry (LC- Q-TOF-MS) combining two separation techniques reversed phase (RP) and Hydrophilic liquid chromatography (HILIC). After this, gas chromatography mass spectrometry (GC-MS) analysis was employed with the aim of developing untargeted analysis and expanding the metabolome, thus identifying new and novel AD predictor metabolites to help elucidate and understand brain metabolism. Later, a brain invial dual extraction (IVDE) method was tested and applied to plasma of control and AD groups using a multimodal strategy that combines both LC-MS and GC-MS data. Finally, human brain samples from control, asymptomatic and AD patients were analysed using the developed untargeted LC&GC-MS brain IVDE method. Results revealed unsaturated fatty acids and sphingolipid metabolism to be significantly dysregulated in the brains of patients with varying degrees of Alzheimer pathology.

TABLE OF CONTENT

LIST OF FIGURES

LIST OF TABLES

LIST OF ABBREVIATIONS

AA	Arachidonic acid
AD	Alzheimer's Disease
Aβ	Amyloid beta peptide
ACAT1	acyl-cholesterol-acyltransferase-1
ASM	Asymptomatic
ADL	Activities of daily living
ADAS-Cog	Alzheimer's Disease Assessment Scale-Cognitive Subscale
ADNI	Alzheimer's Disease Neuroimaging Initiative
ANOVA	One-way Analysis of Variance
APCI	Atmospheric pressure chemical ionization
APP	Amyloid Precursor Protein
APPI	Atmospheric pressure photo ionization
APOE	Apolipoprotein E
AQ	Aqueous
BACE	β-secretase
℃	Centigrade Celsius
CB	Cerebellum
CDR	Clinical dementia rating
CE-MS	Capillary electrophoresis-mass spectrometry
Cer	Ceramide
CERAD	Consortium to establish a registry for alzheimer's disease
CNS	Central nervous system
COX	Cyclooxygenases
CSF	Cerebrospinal fluid
Da	Daltons

DG	Diacylglycerol
DHA	Docosahexaenoic acid
DI-MS	Direct Infusion Mass Spectrometry
DNA	Deoxyribonucleic acid
DOPA	dihydroxy-phenylalanine
DTI	Diffusion tensor imaging
EOAD	Early onset alzheimer's disease
ESI	Electrospray ionization
EPA	Eicosapentanoic acid
FAA	Free amino acids
FDG	Fluro-2-deoxy-D-glucose
FL	Full loop
GABA	Gamma-aminobutyrate
GC-MS	Gas chromatography-mass spectrometry
GSK3B	Glycogen synthase kinase 3 beta
HCA	Hierarchical clustering analysis
H_2O	Water
H_2O_2	Hydrogen Peroxide
HILIC	Hydrophilic Liquid Interaction Chromatography
HMDB	Human Metabolome Database
ITG	Inferior temporal gyrus
IS	Internal standard
IVDE	In-vial dual extraction
LCECA	Liquid chromatography – electrochemical detection
LC-MS	Liquid chromatography-mass spectrometry
LOX	Lipoxygenases
LPC	Lyso Phosphatidylcholine
LOAD	Late onset alzheimer's disease
LOD	Limit of detection
MAPK	Mitogen-activated protein kinase

MCI	Mild cognitive impairment
MDMS-SL	Multi-dimensional mass spectrometry-based shotgun lipidomics
MFG	Middle frontal gyrus
MTBE	Methyl-tert-Butyl Ether
Mg	Milligram
µg	Microgram
MRI	Magnetic resonance imaging
MRS	Magnetic resonance spectroscopy
MCI	Mild cognitive impairment
MMSE	Mini mental state examination
MRS	Magnetic resonance spectroscopy
MVA	Multivariate analysis
MS	Mass spectrometry
MSTFA	N-methyl-N-(trimethylsilyl)-trifluoroacetamide
mRNA	Messenger ribonucleic acid
m/z	Mass to charge ratio
NAQ	Non-aqueous
NIA-AA	National institute of aging- Alzheimer's association
NFT	Neurofibrillary tangles
NINCDS-ADRDA	National Institute of Neurological and Communicative Disorders and Stroke-Alzheimer's Disease and Related Disorders
NMR	Nuclear Magnetic Resonance spectroscopy
NPC	Normal Phase Chromatography
OPLS-DA	Orthogonal Projections to latent structures discriminant analysis
PA	Palmitic acid
PCA	Principal component analysis
PET	Positron emission tomography
PC	Phosphatidylcholine
PE	Phosphatidylethanolamine

PI	Phosphatidylinositol
PiB	Pittsburgh compound B
PLNO	Partial Loop with Needle Overfill
PMI	Post Mortem Interval
P-tau	Phosphorylated-tau
PLS-DA	Partial least squares discriminant analysis
PLA2	Phospholipase A2
PP2A	Protein phosphatase 2 A
PS	Phosphatidylserine
PUFA	Polyunsaturated fatty acids
PlsEtn	ethanolamine plasmalogens
Q TOF-MS	Quadrupole time-of-flight mass spectrometry
QC	Quality control
RSD	Relative standard deviation
RT	Retention time
ROC	Receiver Operating Characteristic
ROS	Reactive oxygen species
RP	Reversed Phase
SD	Standard deviation
SM	Sphingomyeline
SMase	Sphingomyelinase
S/N	Signal to noise
SPHL	Sphingolipid
TG	Triacylglyceride
T-tau	Total-tau
TMCS	trimethylchlorosilane
UVA	Univariate Analysis

PUBLICATIONS

2015

Metabolomic Method: UPLC-q-ToF Polar and Non-Polar Metabolites in the Healthy Rat Cerebellum Using an In-Vial Dual Extraction (Chapter 2).

Ebshiana AA, Snowden SG, Thambisetty M, Parsons R, Hye A, et al. (2015) Metabolomic Method: UPLC-q-ToF Polar and Non-Polar Metabolites in the Healthy Rat Cerebellum Using an In-Vial Dual Extraction. PLOS ONE10(4): e0122883. https://doi.org/10.1371/journal.pone.01228837

Author Contributions

Ebshiana AA: Performed the experiments, analysed the data, contributed reagents/materials/analysis tools, wrote the paper.

Snowden SG: Performed the experiments, analysed the data, contributed reagents/materials/analysis tools, wrote the paper.

Parsons R: Wrote the paper.

Hye A: Wrote the paper.

Thambisetty M: Wrote the paper.

CLQ: Conceived and designed the experiments, Wrote the paper.

2017

Association between fatty acid metabolism in the brain and Alzheimer disease neuropathology and cognitive performance: A nontargeted metabolomic study(Chapter 5).

Snowden SG, Ebshiana AA, Hye A, An Y, Pletnikova O, et al. (2017) Association between fatty acid metabolism in the brain and Alzheimer disease neuropathology and cognitive performance: A nontargeted metabolomic study. PLOS Medicine 14(3): e1002266. https://doi.org/10.1371/journal.pmed.1002266

Author Contributions

Ebshiana AA: conceptualization, data curation, investigation, methodology, paper writing, review and editing.

Snowden SG: conceptualization, data curation, formal analysis, investigation, methodology, visualization, writing paper original draft.

Hye A: conceptualization, funding acquisition, resources, paper writing, review and editing.

YA: conceptualization, data curation, formal analysis, visualization, paper writing, review and editing.

Pletnikova O: conceptualization, paper writing, review and editing.

O'Brien R: conceptualization, paper writing, review and editing.

Troncoso J: conceptualization, paper writing, review and editing.

CLQ: conceptualization, data curation, funding acquisition, methodology, project administration, resources, supervision, paper writing, review and editing.

Thambisetty M: conceptualization, funding acquisition, project administration, resources, supervision, paper writing, review and editing.

Multimodal Metabolomics Combining UPLC-qToF-MS and GC-MS Data in Plasma and Brain Tissue (Chapter 4).

Ebshiana, A.A.; Snowden, S.G.; Legido-Quigley, C. Multimodal Metabolomics Combining UPLC-qToF-MS and GC-MS Data in Plasma and Brain Tissue. Preprints 2017, 2017040080 (doi: 10.20944/preprints201704.0080.v1).

Author Contributions

Ebshiana AA: conceived and designed the experiments, performed the experiments, analysed the data, wrote the paper.

Snowden SG: conceived and designed the experiments, performed the experiments, analysed the data, wrote the paper.

CLQ: conceived and designed the experiments, contributed reagents/materials/analysis tools, wrote the paper.

CHAPTER 1: Introduction

1.1 General Introduction

In human body, the brain along with spinal cord make up the central nervous system (CNS). The brain is composed of cerebrum, cerebellum and brainstem. The cerebrum consists of two cerebral hemispheres, each hemisphere is composed of four lobes (regions), namely; frontal, temporal, parietal and occipital lobe, with each lobe having a certain function. The brain's anatomy can be seen in Figure 1.1. The brain and the central nervous system represent a major cause of global morbidity and mortality, with over 600 recognised neurological diseases [1, 2] including developmental disorders such as Down's syndrome and autism spectrum disorders[3, 4], seizure disorders such as epilepsy [5] and neurodegenerative dementias including Alzheimer's and Parkinson's disease [6, 7].

Recently, 'metabolomics' has been introduced as a tool aiming to meausre metabolic composition, allowing the measurement of abundance and distribution of metabolites in the Biosystems, such as, biofluids (plasma, serum and cerebrospinal fluid(CSF)), cells and tissue, using different analytical platforms. Unlike biofluids, brain metabolomics entails many challenges including limited accessibility, samples extraction (in terms of brain homogeneity), along with other parameters as consistency in selecting analytical platform for metabolite analysis and data treatment strategies. In addition, different brain areas have different metabolite composition, that is produced in the brain under pathological conditions, and also each region has its own specificity to disease pathology with some brain regions being more vulnerable to disease than other areas. Mechanisms underlying the differential regional vulnerability to disease remains to be elucidated, especially in Alzheimer's disease.

The work presented in this thesis will focus on studying Alzheimer's disease (AD) in brain. AD is a devastating disease not only to patients but to their families and society, it was rated as second leading cause of death in 2015 in the United Kingdom(UK), just after ischemic heart disease. A more detailed section on AD and application of metabolomics in the AD field will be presented in this chapter.

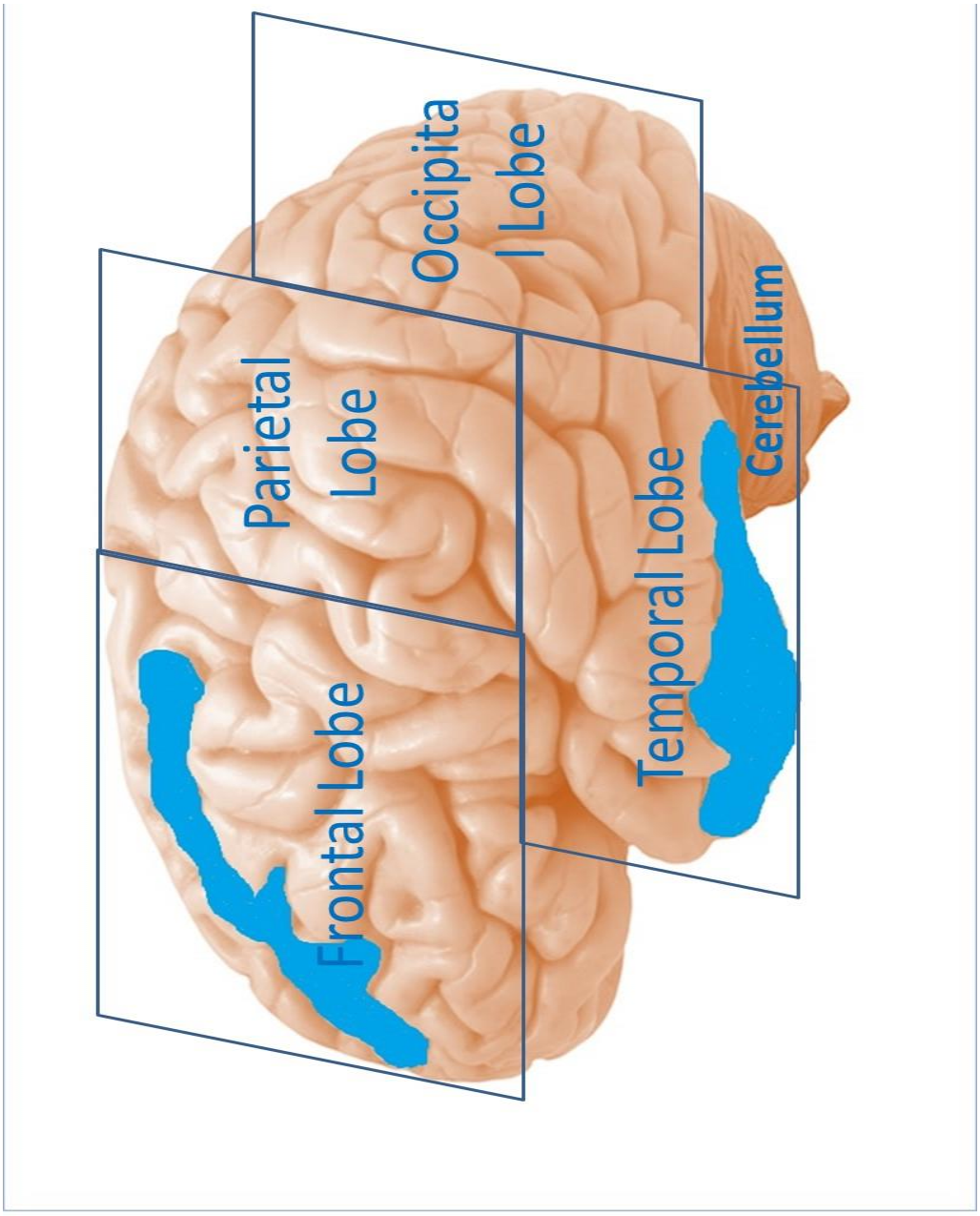

Figure 1.1 Human brain structure showing four main functional lobes of cerebral cortex. . Areas highlited in blue in the frontal and temporal lobes are Medial frontal gyrus (MFG) and Inferior temporal gyrus (ITG) respectively. These two regions along with cerebellum have been used in Chapter 5 & 6 of this thesis. Figure drawn using pain and power point.

1.2 Introduction to Alzheimer's Disease (AD)

1.2.1 AD Prevalence, incidence and types

Alzheimer's disease (AD) is a progressive neurodegenerative disorder. AD was first described by Alois Alzheimer's in 1970 when he described symptoms he observed in Auguste Deter, a 51 years old woman with disorientation and memory loss symptoms described as ″sometimes stronger, sometimes weaker″ [8]. Following her death four and half years later, Dr. Alois examined her brain and observed brain atrophy and abnormal deposition in and around the nerve cells, these were later identified as ″ Plaque″ and ″ Tangle fibre″. These observations lead to further studies in dementia and in particular AD.

AD is the most common form of dementia accounting for around 60% of cases. Indicative signs of AD are cognitive impairment, memory loss and disorientation resulting in a decline in the person's ability to plan, solve problems, or undertake daily activities [9], [10]. There is still no definitive method of diagnosing AD as the pathogenesis of the disease is still yet to be fully understood. Moreover, a slight decrease in AD incidence in high income countries was suggested, potentially due to better education, treatment and awareness of AD risk factors such as cardiovascular disease, excess alcohol, smoking and depression, to lead to less number of people with dementia [11]. However, it was estimated that in developed countries around 60 % of people with dementia have low income, with this expected to rise to about 70 % in 2040 [12].

Worldwide, there has been an increase in the prevalence of age related neurodegenerative diseases. In Europe, around eight million individuals have AD, and dementia-related healthcare is estimated at 113 billion Euros a year. [13]. In the United Kingdom (UK) dementia cases are expected to rise to about 76 million by 2030, while at present in the UK there are an estimated 500,000 people living with Alzheimer's [14].

There are two main forms of AD, Familial AD and Sporadic AD. Familial AD is known as early onset AD (EOAD). It accounts for 5% of all AD cases, occurring in people below age of 65yrs [15]. Three genes are currently associated with the onset of familial AD namely presenilin 1, presenilin 2 and amyloid precursor protein (APP). Presenilin 1 and presenilin 2 were reported to provoke plaque via the γ secretase enzyme complex [16]. Further to this, polymorphisms in the gene coding for APP cause dramatic increase in amyloid peptide isoform production [17]. Sporadic AD is the most common form of the disease, accounting for over 95% of cases, also known as late onset AD(LOAD). Incidence of LOAD occurs at the age of 65yrs or older. There are many risk factors for sporadic AD including age, apolipoprotein (APOE) , diet and nutrition. APOE is a risk gene, and the e4 allele APOE gene is considered the most significant risk factors of AD[18] and has been identified to be associated with late onset AD [19] (more details can be seen in section 1.4.2).

1.2.2 Alzheimer's Disease Pathology

The extracellular deposition of senile plaques composed of amyloid beta peptide(Aβ) in AD brain was documented by Dr. Alzheimer. Later he also described intracellular neurofibrillary tangles composed of phosphorylated protein tau. These pathological characteristics begin in the entorhinal cortex and Hippocampus and then proceed to other cortical areas, leading to neuronal damage and death [20]. In AD brain, these two features in association with brain atrophy were defined as the main AD pathology hallmarks (Figure 1.2).

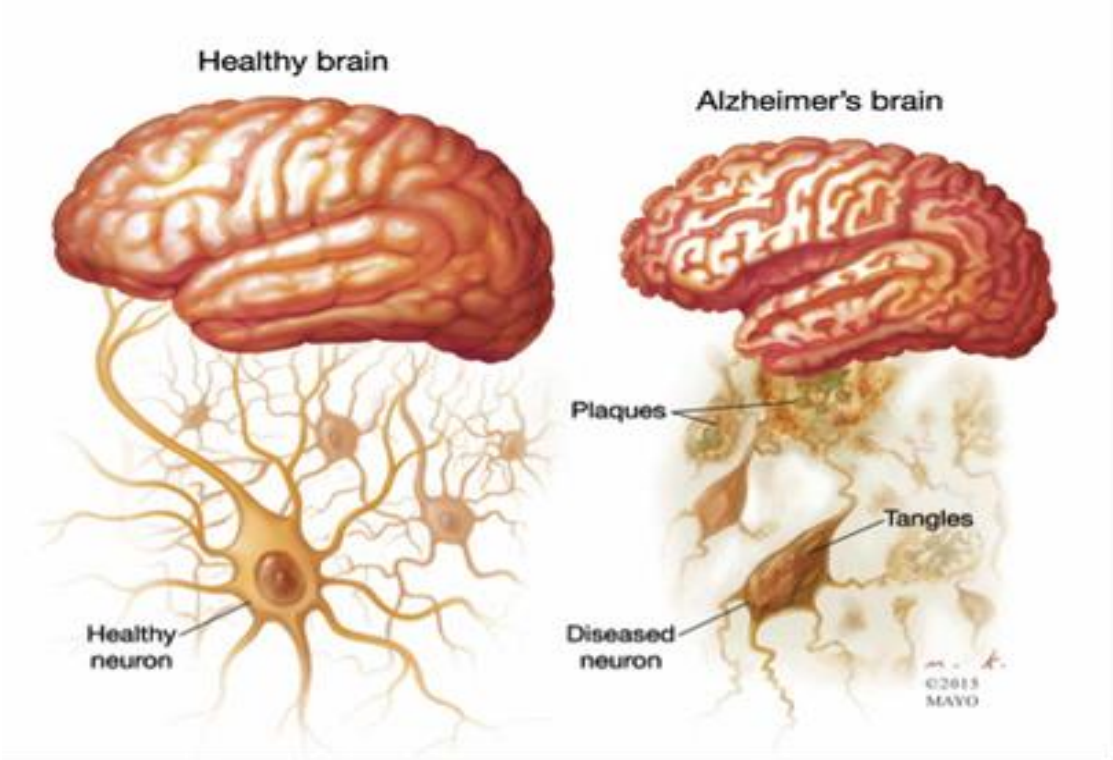

Figure 1.2 Pathological hallmarks of Alzheimer's disease: Healthy(left) versus AD(right) brain and neurons: both Amyloid plaques and tau tangles can be seen outside and inside neurons respectively in AD brain(right) accompanied with brain atrophy (reduction in brain volume). Image adapted from psychneuro.wordpress.com

1.2.2.1 Amyloid pathology

The first hallmark of AD is the extracellular deposition of Aβ peptide around the nerve cells. This is known as 'neurotic plaques'. Aβ has 38-42 amino acids which form when the amyloid precursor protein (APP) is cleaved first by β secretase 1(BACE 1), releasing the APP from the cell [21], the remaining fragments of APP are cleaved by γ- secretase [22, 23] causing the release of more Aβ, and the released Aβ will aggregate to form Aβ oligomers in the extracellular space. The insoluble form of these oligomers is known as 'Aβ Plaques' [24].

The two leading isoforms of Aβ (formed during the γ- secretase cleavage) are Aβ40 (residue with 40 amino acids) and Aβ42 (residue with 42 amino acids). In AD brain Aβ42 was identified to contribute more to Aβ aggregation and formation due to it is lower solubility [25]. The mechanism behind the role of $A\beta_{42}$ and its high production in AD

brain is still unclear. Some studies proposed that plaque formation is an immune system response to microbes in the brain [26, 27], others, suggested a possible role of metal ions as plaque initiaton [28, 29]. The hypothesis that $A\beta_{42}$ is causative of AD is the 'Amyloid cascade model'(Figure 1.3). Low levels of $A\beta_{42}$ are reported in AD Cerebrospinal Fluid (CSF) in comparison to controls [30, 31], these changes in CSF develop even prior to Aβ plaque formation in AD brain, and at present CSF levels are a surrogate marker of amyloid burden in the brain [32].

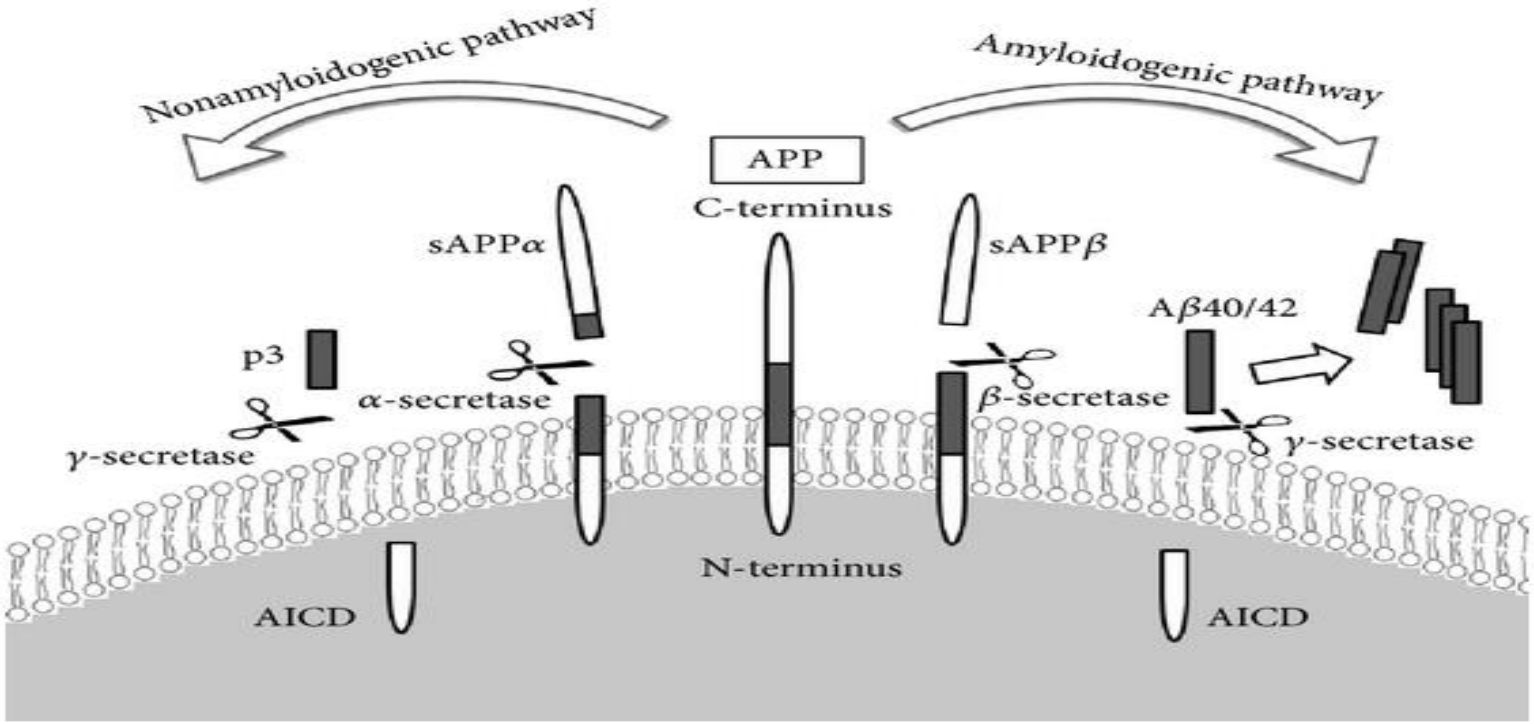

Figure 1.3 Amyloid precursor protein (APP) metabolism into amyloidogenic and non-amyloidogenic pathway. Amyloid precursor protein (APP) is a ubiquitously expressed integral membrane protein that can be processed in two distinct pathways. In the nonamyloidogenic pathway, APP is cleaved within the Aβ domain by the α-secretase enzyme. However, in the amyloidogenic pathway, APP is first cleaved by β-secretase (BACE1), instead of α-secretase, at the N-terminus of the Aβ domain, and this is followed by γ-secretase cleavage at the C-terminus. This sequence of events generates the Aβ amylogenic peptides, which can aggregate into oligomers and form extracellular neurotoxic plaques in the brain. Both pathways release identical APP intracellular C-terminal domain (AICD). This figure was obtained from [3].

1.2.2.2 Tau pathology

The second pathology hallmark in AD brain is known as neurofibrillary tangles (NFT). NFT are tau deposits inside neuronal cells formed as a result of abnormal hyper-phosphorylation or glycosylation of tau protein in AD brain. Tau protein is a microtubule-associated protein [33], which binds with microtubulin to help maintain cell structural stability. Dissociation of the tau protein from microtubulin causes the aggregation of unbounded tau protein leading to tangle formation inside neurons, followed by synaptic dysfunction, axonal loss and disruption of intracellular communication[34, 35]. The reason for this aggregation is known as the tau hypothesis [36, 37]. The process of tau phosphorylation and dephosphorylation is regulated by different phosphatase and kinase enzymes and deterioration in this process may contribute to the accumulation of NFT. Consequently, more and more AD research is focusing on studying tau (T-tau) and phosphorylated tau (P-tau) as a potential AD biomarkers.

1.2.2.3 Other pathological changes

In addition to Aβ plaque and NFT, oxidative stress, mitochondrial dysfunction, metal dyshaemostasis and lipid peroxidation were reported as pathological characteristics of AD brain. Oxidative stress involves the production of Reactive Oxygen Species(ROS). Many studies observed the overproduction of Hydrogen Peroxide (H_2O_2, an oxidative stress marker) in the presence of Aβ plaque, suggesting Aβ role in promoting oxidative stress [38-40]. A possible mechanism is Aβ plaques causing mitochondrial dysfunction via cytochrome c oxidase inhibition leading to endoplasmic reticulum (ER) stress and cellular dysfunction [41, 42] or by directly disrupting mitochondrial membrane permeability as Aβ deposits were found in mitochondria [43, 44].

Mitochondrial dysfunction is linked to deterioration in glucose metabolism [45]. In the brain, the energy required for cells to perform adequately is obtained from phosphorylation of Adenosine Triphosphate, which is generated in the mitochondria through glucose oxidation. Thus, damage in mitochondria causes glucose

hypometabolism (reduction in glucose metabolism). Brain glucose hypometabolism has been investigated and indeed observed in many studies [46-49].

Tau pathology has also been associated to oxidative stress. As mentioned previously tau phosphorylation is regulated by a balance between tau kinase and tau phosphatase activities. Treatment with ROS stimulates tau hyperphosphorylation, this involves the increase in activity of kinase (glycogen synthase kinase-3 (GSK3β)) [50] and a decrease in the activity of phosphatase (protein phosphatase 2A (PP2A)) [51]. To find therapeutic approaches, studies looked at inhibiting GSK3β, but this did not hinder hyperphosphorylation of tau or DNA damage in mitochondria, suggesting GSK3β translocation may produce other than tau hyperphosphorylation [52]. In addition to mitochondria, microglial cells were recently identified as ROS producers in tauopathies. However, the mechanism behind this is unclear and further studies are needed to investigate this novel area of research.

Furthermore, metal dyshaemostasis has been linked with oxidative stress. In AD brain metal dyshaemostasis has been reported to take place mainly due to the action of three metal ions namely; Zinc (Zn^{+2}), Cupric(Cu^{+2}) and Ferric (Fe^{+3}) [53-55]. High level of these three ions were found in Aβ deposits proposing a role in AD pathology. Zn^{+2} and Cu^{+2} can block Ca^{+2} influx into neurons inhibiting N-methyl-D-aspartate (NMDA) receptors. Zn^{+2} and Cu^{+2} can also bind to tyrosine and histidine in Aβ initiating peptide aggregation [28, 29, 56]. This interaction is believed to lead to production of ROS [28, 29, 57, 58]. Fe^{+3} in its reduced form (Fe^{+2}), is an oxidant agent leading to production of H_2O_2 and thus causing oxidative stress. This advocates a pivotal function for metal ions in AD pathology, possibly through initiating Aβ aggregation and producing ROS.

Recently, there has been a shift in focus towards the role of lipids, mainly phospholipids and sphingolipids, in AD brain pathogenesis. This interest has risen from the findings of “adipose inclusions” or “lipoid granules” in brain tissue from AD patients. This was observed by Alois Alzheimer when he first described the disease pathology. Findings suggest that Aβ production relies on cholesterol levels within β- and γ-secretase

membrane [59]. Deterioration in phospholipids metabolism has therefore also been proposed to contribute to AD pathogenesis, but its mechanism remains unclear.

Phospholipid are the main class of membrane lipids, playing a vital role in regulating cell functions [60]. Several studies have shown irregularity in phospholipid levels in AD brain, including low concentration of phosphatidylcholines (PC) [61-63], PI [64-66] phosphatidyethanolamine (PE) [62, 64], and ethanolamine plasmalogens (PlsEtn) [63, 66, 67] with these lipid level also observed to be dysregulated in blood [68-70]. Opposite trends were observed in the CSF with high phospholipid concentration observed in AD patients [71, 72].

Sphingolipids are another lipid class which play important roles in signal transmission and cell recognition [73], this class includes ceramides and sphingomyelines. High Ceramides abundance was found in AD brain and plasma [74-76]. In AD brain, sphingomyelinase (SMase), is an enzyme that induces the breakdown of sphingomyelines to ceramides and thus high Cer and low sphingomyelines level were seen [74, 75]. Inhibition of SMase demonstrated to reduce both ceramide and Aβ deposition [77]. Other publications reported opposite trends for sphingomyelines in brain [66, 78], which was also reflected in CSF of AD samples [79, 80].

The role of cholesterol has been widely studied and it is thought to contribute the most in AD brain pathogenesis, with high level of cholesterol measured in AD brain. Cholesterol plays a vital role to maintain the integrity and fluidity of cell membranes, and to facilitate cell signalling [81]. Cholesterol is converted to cholesteryl esters via acyl-cholesterol-acyltransferase-1 (ACAT 1), leading to increase Aβ production due to the cholesteryl ester accumulation intracellularly [82, 83]. Moreover, it was reported that cholesterol rich environments promote Aβ deposition and affect the γ and β secretase activity [84, 85] Further evidence is the reduced level of cholesteryl esters and thus Aβ release by inhibiting ACAT1 [86].

1.3 Criteria and methods for AD diagnosis (Diagnosis criteria)

A set of diagnostic criteria for AD was designed in 1984 by the National Institute of Neurological and Communicative Disorders and Stroke and the Alzheimer's Disease and Related Disorders Association (NINCDS-ADRDA) [87]. The guidelines indicated that diagnosis require assessment of patient's symptoms, medical history, mental status and also neuropsychological testing. AD is deemed a clinical diagnosis as identified by the 1984 criteria, with definite diagnosis only visible by post mortem examination of the brain and the presence of the AD hallmarks. However, it was later found that these pathological changes may occur in the brain 20-30 years before the clinical onset of dementia.

AD is still deemed a clinical diagnosis, though now it is established that AD has a symptomatic pre-clinical dementia phase, where pathological changes such as Aβ, T-tau and P-tau accompanied with brain atrophy are present but patients have no development of cognitive or behavioural problems. Thus, a new criteria incorporating this pre-clinical stage was necessary in order to help with early diagnosis and treatment intervention [88].

In 2011 a new criterion was established by NIA-AA (the National Institute of Aging in collaboration with Alzheimer's Association) [89], this revised criteria provided two main improvements. 1) extending AD into three phases, namely an asymptomatic, pre-clinical phase, a symptomatic pre-clinical dementia phase (also known as Mild Cognitive impairment (MCI)) and a dementia phase. 2) merging the biomarkers research in AD diagnosis to enhance our understanding for pathological changes as well as for early intervention strategies. The NIA-AA recommendations call for identifying biomarkers that can increase sensitivity and specificity in the diagnosis of underlying AD including imaging techniques (see section 1.4.1 for more details). AD biomarkers were defined as ″ parameters (physiological, biochemical, anatomic) that can be measured in vivo and that reflect specific features of disease-related pathophysiological processes″ [90].

Current diagnostic procedures rely on clinicians to observe a combination of clinical examination and neuropsychological assessment and involve evaluating patient's medical history, mental cognition and general physical health. The first step involves history taking to eliminate the presence of other causes leading to the dementia. This involves

checking existing conditions, such as diabetes, depression or heart disease that is not well managed, also reviewing medications and diet habits. Following history taking, cognitive impairment can be assessed by several cognitive tests. These tests assess many different mental abilities including memory, concentration, attention span, language, communication skills and orientation. Specialist carrying out these tests consider that test scores may be influenced by different factors including for example a person's level of education.

The Mini Mental State Exam (MMSE) is the most common mental state screening test that clinicians use. It comprises 30 questions (with a maximum score of 30) divided into 6 sections [91]. A typical MMSE form and interpretation scores can be observed in Figure 1.4.

MINI MENTAL STATE EXAMINATION (MMSE)

Name:

DOB:

Hospital Number:

One point for each answer **DATE:**			
ORIENTATION Year Season Month Date Time	...../ 5	...../ 5	...../ 5
Country Town District Hospital Ward/Floor	...../ 5	...../ 5	...../ 5
REGISTRATION Examiner names three objects (e.g. apple, table, penny) and asks the patient to repeat (1 point for each correct. THEN the patient learns the 3 names repeating until correct).	...../ 3	...../ 3	...../ 3
ATTENTION AND CALCULATION Subtract 7 from 100, then repeat from result. Continue five times: 100, 93, 86, 79, 65. (Alternative: spell "WORLD" backwards: DLROW).	...../ 5	...../ 5	...../ 5
RECALL Ask for the names of the three objects learned earlier.	...../ 3	...../ 3	...../ 3
LANGUAGE Name two objects (e.g. pen, watch).	...../ 2	...../ 2	...../ 2
Repeat "No ifs, ands, or buts".	...../ 1	...../ 1	...../ 1
Give a three-stage command. Score 1 for each stage. (e.g. "Place index finger of right hand on your nose and then on your left ear").	...../ 3	...../ 3	...../ 3
Ask the patient to read and obey a written command on a piece of paper. The written instruction is: "Close your eyes".	...../ 1	...../ 1	...../ 1
Ask the patient to write a sentence. Score 1 if it is sensible and has a subject and a verb.	...../ 1	...../ 1	...../ 1
COPYING: Ask the patient to copy a pair of intersecting pentagons 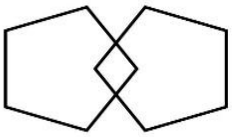	...../ 1	...../ 1	...../ 1
TOTAL:	...../ 30	...../ 30	...../ 30

MMSE scoring
24-30: no cognitive impairment
18-23: mild cognitive impairment
0-17: severe cognitive impairment

OME Oxford Medical Education

Figure 1.4 Mini-Mental State Examination (MMSE)form and score interpretation. Healthy controls with non-cognitive impairment are expected to score 30, the greater the impairment the lower the expected outcome score from the examination. MMSE obtained online from oxford medical education.

Additionally, there are many neuropsychological tests that can help to evaluate both cognitive and behavioural functions such as the Alzheimer's Disease Assessment Scale-Cognitive subscale (ADAS-Cog), which consists of two parts, one that measures cognitive functions and one that measures non-cognitive functions like mood and behaviour. This is to differentiate between normal and impaired cognitive functioning[92]. Other scales can also be employed such as the Global Deterioration Scale [93] and the Clinical Dementia Rating, applied to assess dementia severity in a score range from 0 to 3, and to also assess the effects of cognitive loss on everyday activities [94, 95]. Both tests combine mental cognition, functional symptoms and neuropsychiatric aspects in a single approach.

Other AD-stage descriptors rely on brain pathology. The staging of AD-related to neurofibrillary pathology described in 1991 and defined as 'braak staging' can differentiate initial, intermediate, and late phases of the disease process in both a symptomatic and symptomatic individual [96]. The Neuropsychological Battery for the Consortium to Establish a Registry for Alzheimer's Disease (CERAD) with criteria for Aβ plaque scoring system, which ranks the amount of Aβ plaques identified histochemically in several regions [97].

1.4 Biomarkers in AD

1.4.1 Brain neuroimaging

Imaging techniques have been used to measure brain region volumes. Atrophy was observed early in hippocampus and entorhinal cortex is suggested to be associated with memory impairment and an increased risk of AD [98, 99]. Imaging techniques, Magnetic Resonance Imaging (MRI), uses radio waves and magnets to create a detailed view of brain, it is also employed to help diagnose and monitor treatment for various conditions in the body including heart, abdomen, chest, and pelvis. In AD, MRI has focused on detecting reduced hippocampal volume, this reduction in hippocampal volume was reported at 10 % – 15 % and 20 % – 25 % in MCI and AD brain compared to healthy brain respectively [100]. MRI comparing healthy and AD brain can be seen in Figure 1.5. Further findings show reduction in brain hippocampus volume by 12% in mild AD [101] and 37% in moderate AD [102] compared to controls, also calculating AD diagnosis using the volume of hippocampus at 85% sensitivity and 82% specificity with higher values obtained after correction to age [102].

Besides, Diffusion Tensor Imaging (DTI) has become a leading method in identification of white matter integrity in several brain regions. White matter changes in parietal, temporal areas, and also in frontal regions have been detected in persons with AD and MCI compared to normal controls [103], suggesting that these changes occur early in the disease process and thus with a possibility of applying it to early diagnosis [103-105]. DTI could predict conversion from MCI to AD dementia but at present it was only recommended for research purposes.

Magnetic resonance spectroscopy (MRS), is a technique which employs the theory of Nuclear Magnetic Resonance along with MRI, permitting metabolite quantification in vivo by brain tissue scanning. The combination of data from hippocampal brain atrophy with MRS has improved diagnostic performance. For instance, this combination enables the quantification of N-Acetyl Aspartate (NAA) levels that are shown to be decreased in AD [106]. More details about MRS and its applicability for biomarker discovery can be viewed in the following literature [107].

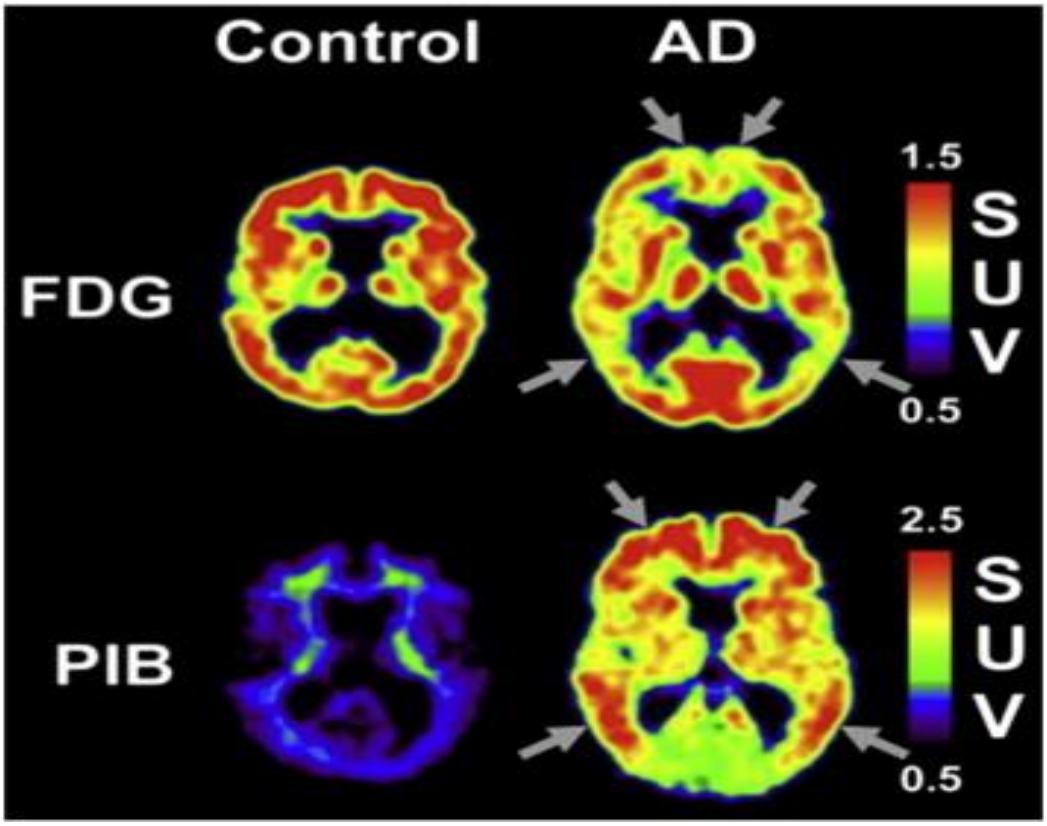

Figure 1.5 Example of FDG and PIB Positron Emission Tomography: The upper image is an example of fluoro-2-deoxy-D-glucose (FDG) PET imaging. The control demonstrates normal FDG uptake, whilst arrows on the AD image shows a typical pattern of FDG hypometabolism or Aβ deposition. The lower image depicts Pittsburgh Compound B (PiB) PET imaging of Aβ in brain of Control (left) and AD (right), with high Aβ retention observed in AD [108]

An alternative imaging based approach is Positron emission tomography (PET). This technique works by identifying a radiolabelled positron emitting nuclei called ”Tracers”. Once the tracer is injected in the body, it binds with molecules of interest, then PET is applied to obtain 3D of the tracer intensity. PET scanning enables the imaging of Aβ load in brain of live patients via Pittsburg compound B(PiB) that binds to Aβ. Furthermore, FDG (Fluro-2-deoxy-D-glucose) is a glucose analogue that has been utilized to monitor regional glucose metabolism and uptake, it can show glucose hypometabolism in AD brain particularly in temporo-parietal [109] and inferior-parietal lobes [110]. These changes have been reported as AD features and conversion predictors from MCI to AD. PET scan of PiB and FDF comparing healthy and AD brain can be seen in Figure 1.5.

1.4.2 Genetic (APOE4)

APOE is a class of protein involved in the metabolism of fats in the body. APOE comes in several forms, or alleles, namely ε 2, ε 3 and ε 4. As stated before, APOE ε4 is the biggest genetic risk factor in LOAD. Individuals having at least one APOE ε4 alleles are at increased risk of developing AD compared to those carrying ε3 allele (most common allele), while the ε2 allele decreases risk. For example, people who inherit two ε4 alleles are at seven fold risk of developing AD higher than those with the E3 allele [111].

A study by Mayeux *et al*. looked into AD diagnosis in 2188 individuals with AD and those individuals with other types of dementia. Findings revealed that APOE genotyping alone has sensitivity and specificity at 65% and 68% respectively, which is not sufficient to be used as a diagnostic test [112].

APOE is linked to the production and aggregation of Aβ and tau [113, 114]. However, the mechanism behind this is still unclear. APOE can promote Aβ degradation, APOE ε 4 apart is the allele found to be less efficient at catalysing the reaction compared to other lipoprotein alleles and thus the existence of this allele could be responsible for the Aβ accumulation and the dysfunction of cholinergic neurotransmission [115].

1.4.3 AD protein markers in CSF

For protein markers such as Aβ and tau to be used successfully in the clinical environment, they need to be detected in biofluids like CSF, plasma or urine. In the literature, Aβ analysis in urine and plasma were inconsistently reported [116, 117]]. However promising results have been acquired from CSF analysis of Aβ [30, 118-120] T-tau [118, 120, 121] and P-tau analysis [120, 121]. Despite the difficulty and discomfort in CSF samples collection procedure, CSF reflects brain pathology quite well as it is in direct contact with brain.

In AD CSF, a decrease in $A\beta_{42}$ and increase in both T-tau and P-tau levels are observed. The diagnostic power of these proteins ranges between 69% and 91%, combined data of the 2 proteins increased diagnostic sensitivity and specificity to range between 86% and

96% [122, 123]. Despite the promising accuracy of these proteins, for early AD the accuracies are lower and alone they can not be used to assist clinician with differential diagnosis like predicting conversion from MCI to AD, however they could be used for aiding later stage diagnostics [124].

1.5 Metabolomics

The discovery of biomarker in AD can be invisigated using large scale " Omic" technologies, which provide universal detection to characterise and quantify thousands of molecules in biological systems in a holistic manner. Omic technologies including: genomics (The study of the structure, function and expression of all the genes in an organism), transcriptomics (The study of the mRNA within a cell or organism), proteomics (The study of proteomes and their functions) and more recently metabolomics. Overview of the “omics” cascade can be found in Figure 1.6.

There has been a particular focus on identifying genes and proteins as potential candidates in the field of AD biomarkers. So far, no single biomarker has shown to meet the criteria for AD biomarker. However, the development in analytical techniques enables the detection of small molecule metabolites(<1500Da). This new approach that allow the measurement of many small molecules is known as "metabolomics" or "metabonomics".

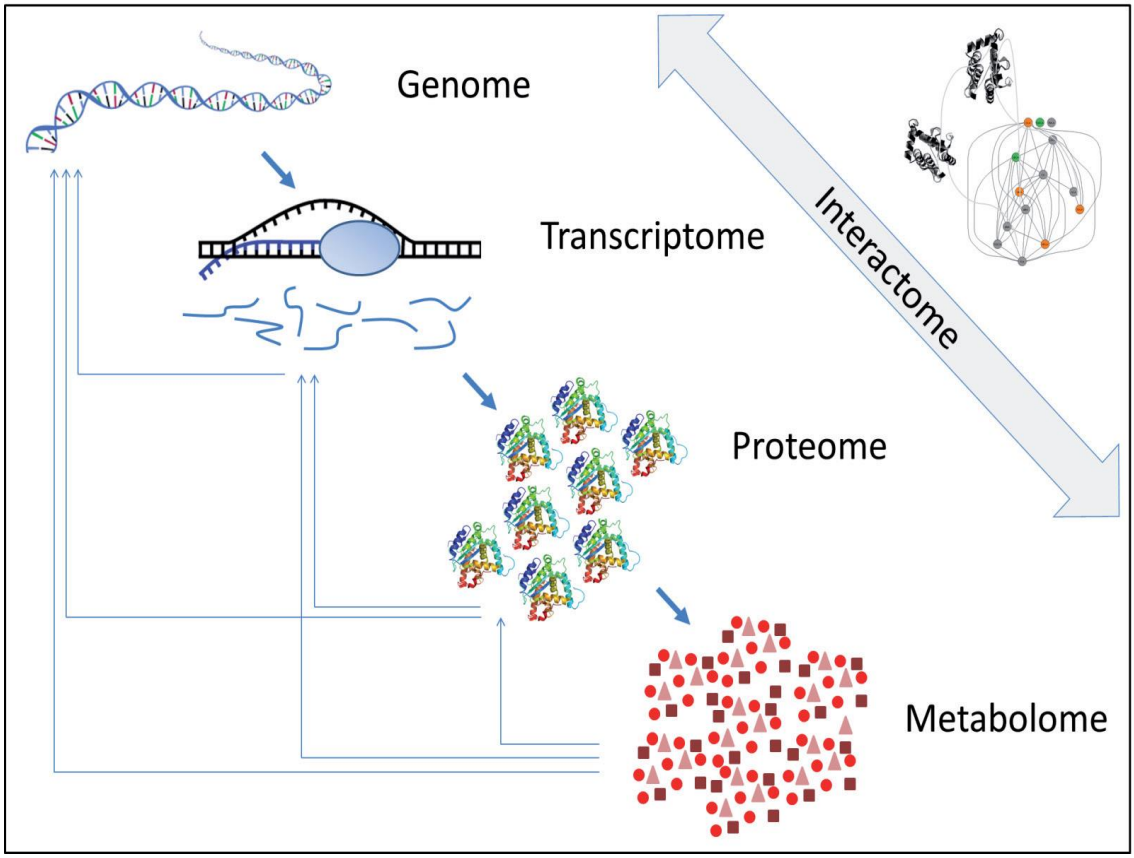

Figure 1.6 overview of omics approaches and systems biology. The upper right part shows the complex biological pathways and interactions that could happen across the entire network [125].

The terms " metabonomics" and"metabolomics" have been introduced by Nicholson Group at Imperial College London and Fiehn group at The Max-Planck Institute of Molecular Plant Physiology in 1999 and 2002, respectively [126, 127].

" Metabolomics refers to the study of the global, dynamic endogenous metabolic profiles in a living system (tissue, cell or organism) under a given set of conditions, such as diseases (e.g., cancer and diabetes), pathophysiological stimuli (e.g., xenobiotics) or genetic modifications" [128], while metabonomics has been described as the “quantitative measurement over time of the metabolic responses of an individual or population to drug treatment or other intervention” [129]. These two terms are used interchangeably with the same analytical and data analysis procedures [130].

Metabolomics has become a tool to drive biomarkers research in different areas of life sciences including drug development and diagnostic strategies [131-135]. It helps with our understanding of disease in different areas including: mechanisms of disease diagnostic biomarkers, mechanisms of drug action for drug discovery as well as monitoring disease to predict individual variation in drug response phenotypes [131, 132, 135].

1.5.1 Metabolomics Approaches

Approaches for metabolomic biomarker discovery in biological systems can be classified as targeted or untargeted metabolomics. The difference between the two approaches depends on whether the methodology used is designed to identify and quantify a specific number of metabolites of interest (Targeted) or to a larger set of metabolites restricted only by the sensitivity and applicability of the analytical platforms and data processing employed (untargeted). The nontargeted approach allows for the identification and semi-quantification of many metabolites in a biological system and without having prior knowledge of the nature and the identity of the measured metabolites. It aims to achieve qualitative and semi-quantitative information, which can be used to compare fingerprints of metabolites that change in response to external stimuli, i.e. exposure to a toxic compound. Consequently, untargeted metabolomics can provide a platform to uncover the involvement of the metabolic pathways that may not have been predicted. Hence untargeted metabolomics is often hypothesis-generating or hypothesis-refining rather than having a defined hypothesis [136, 137]. The untargeted approach is employed throughout this thesis.

The concept of untargeted approach is to extract and analyse a wide range of molecules. Metabolites comprise downstream products of the genomes, transcriptomes, proteomes and monitoring these metabolites can help to track the mechanism of disease pathology (Figure 1.6). Furthermore, metabolomics is low cost and time efficient and applicable to different biological samples like CSF, plasma, cells and tissue [138].

Due to the nature of biological systems, metabolites exist at a wide range of concentrations and exhibit various physicochemical properties. This can make extraction and analysis difficult. For example, the analysis of highly abundant molecules may require a dilution step for accurate analysis but those molecules at low concentration will be diluted to below their limit of detection. In addition, in untargeted metabolomics, problems can arise with coelution of features resulting in mass spectrometry (MS) effects known as “ion suppression”. To solve this, improved separation and detection techniques are required.

Another drawback can be the cost and the long time required in data treatment and statistical modelling when comparing to a targeted approach. Despite all these disadvantages, untargeted approaches are gaining more popularity especially with an increase in demand for biomarkers.

metabolomics is totally dependent in advancements in analytical platforms, particularly Mass Spectrometry (MS). Therefore, designing metabolomics using MS has some important parameters to consider especially in the study of brain tissue. In the case of this thesis, the extraction and analysis of brain tissue is challenging compared to many biofluids. Further, additional steps, as sample treatment prior to metabolic analysis is needed, this include tissue homogenizationis to guarantee optimal extraction and hence optimal separation and detection of metabolites. Besides, in biological samples the presence of proteins can influence accuracy, precision and instrument lifetime, hence deproteinisation as a pre-treatment step can be incorporated, mainly using organic solvents to precipitate proteins.

Figure 1.7, summarizes the key parameters in designing a metabolomics study. The first parameter is the study design also termed as experimental design. This term considers all aspects from sampling to data collection. Maintaining consistent study design is essential to guarantee the accuracy of the biological variation observed in the metabolome and ensure that variation is not introduced during the study, many times due to sample handling, sample preparation and storage [139, 140].

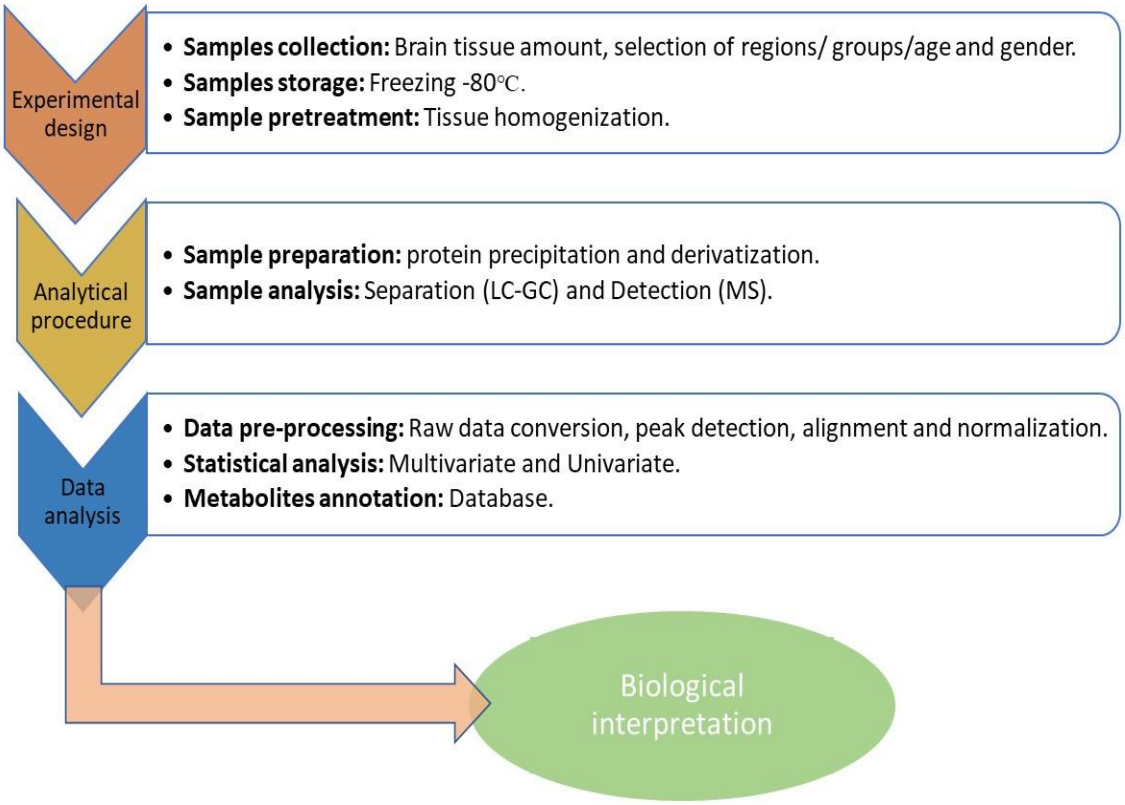

Figure 1.7 Overview of metabolomics analysis workflow.

The study design needs to be established by the research team before commencing sampling and analysis. This is especially important in large scale studies requiring samples for which factors such as age, gender, sample size and randomization need to be considered. All these factors help to achieve reliable study results and to avoid redesigning due to lack of stringent control [141, 142]. The next step involves selecting analytical platforms and usually a combination of analysis platforms are therefore necessary for accurate and wide range metabolite measurements.

The next section will discuss Mass spectrometry (MS) and Nuclear magnetic resonance spectroscopy (NMR) as the most commonly used analytical techniques in AD metabolomics research.

1.5.2 Analytical platforms in metabolomics

Current developments in analytical platforms have enabled the detection and measurement of metabolites in biological samples simultaneously. These techniques are NMR and MS. The platform of choice applied in this thesis is MS.

1.5.2.1 Nuclear Magnetic Resonance Spectroscopy

NMR spectroscopy is a powerful and commonly used analytical technique, it has the advantages of high reproducibility and resolution power providing details on chemical structure and require minimal sample pre-treatment prior to analysis. [143-145]. The working scope involves applying magnetic field around an atom, as a result each atom absorbs certain resonance frequency (electromagnetic radiation) thus providing more data about molecular structure and marker molecules elucidation.

The main limitations of this technique is the relative insensitivity which can be improved by introducing high magnetic field. This consequently would affect the working condition of surrounding computers and monitors equipments [146]. Furthermore, the high cost of instrument itself and maintenance, the difficulty in interpreting obtained spectrum would add extra expenses as specialist operator required.

Regardless of these limitations, NMR remains a highly powerful biomarker instrument for non-invasive thus non-destructive technique allowing reanalysis of the same sample again either by NMR or another analytical technique. As a result, NMR has been widely used in pharmaceutical and toxicology research [144, 147, 148]

1.5.2.2 Mass Spectrometry

MS-based metabolomics has contributed to major advances in biomedical knowledge. It has, therefore, become a crucial application in biomarker discovery especially in AD [149, 150]. MS is an essential and extensively used ionization technique for comprehensive profiling of lipids (known as Lipidomics) and other metabolites. MS

technology can be time consuming but displays high sensitivity and resolution [151] compared to NMR which has lower sensitivity. In this thesis MS was chosen as the preferred analytical technique.

MS is an effective technique owing to high sensitivity, specificity, and ability to identify either by matching with internal, external standard or database match. One drawback of MS is quantification. To achieve accurate quantification of metabolites isotope labelled standards need to be added at the time of analysis. This procedure is pricey and impractical for untargeted analysis. Therefore, in untargeted metabolomics the relative abundance of metabolites (expressed as peak area or peak intensity) is used to compare between samples. Another main disadvantage is ion suppression that takes place in the ionization stage of analysis resulting in decrease in ionization efficiency. This occurs when large number of molecules enter the source and compete for charge and ionization causing a molecule not to be ionized and detected. Ion suppression can be overcome by introducing separation techniques such as chromatography prior to MS detection as this will be discussed in the section below.

1.5.2.3 Chromatographic separation prior to MS analysis

Metabolomics has been developing alongside other analytical techniques such as separation science (often chromatography) coupled to a detector. These chromatographic techniques include Gas chromatography (GC), Liquid chromatography (LC), and Capillary electrophoresis (CE).

In GC, the mobile liquid phase is replaced with an inert gas (mainly helium) with long stainless steel or glass column stationary solid phases. Separation is based on analyte volatility and choosing the optimal temperature gradient. Also, a derivatization step (alkylation or silylation) is required to improve analyte volatility. This would add extra steps to sample treatment which in turn increase analytical variation and analysis time. Capillary GC has high resolution and separation efficiency and sensitivity enhancement due to the long distances travelled by the analyte. The column length which can reach 300

meters, allows separation of isomers like in case of unsaturated fatty acids. The electron impact ionization energy usually is set to 70 -80 eV so that the MS spectra could be compared with the a gas chromatography-mass spectrometry (GC-MS) library which is acquired at the same voltage [152, 153].

GC-MS is the analytical method that combine the advantages of GC and MS, it can effectively separate thermally stable and volatile molecules [154]. GC-MS can identify and quantify substance in a sample, providing mass spectrum of each substance and GC retention time (RT). It was used in environmental, food and pharmaceutical analysis [154-156]. GC-MS has many features including capability to separate compounds in complex mixture in short time with high reproducibility, selectivity and sensitivity. Table 1.1 summarize the advantages and disadvantages of different analytical techniques applied in metabolomics.

LC has solid stationary phase of derivatised silica particles in stainless steel column. It can analyse thermolabile and non-volatile samples (analytes) providing a fast selective and sensitive approach without need to derivatization. Analytes are separated into their individual components by distribution between a stationary solid phase and a mobile liquid phase. The affinity to both phases is determined based on the difference in physicochemical properties of the analyte. The liquid solvent passes at high pressure through the column helping molecules in the mixture to interact with both mobile and stationary phases. For example, lipids will interact with nonpolar stationary phases and move slowly through the column to achieve optimal separation and detection. The term LC covers various modes of separation. This depend on the type of analyte, stationary phase and mobile phase used which can alter mode of interaction and analyte separation. These modes are Normal Phase Chromatography (NPC), Reversed Phase Chromatography (RP), and Hydrophilic Liquid Interaction Chromatography (HILIC). This current work applied RP and HILIC both coupled to MS.

RP Chromatography: RP is the most commonly used form of LC mainly for non-polar compound separation. It accounts for 80% of HPLC separation with high reproducibility and applicability and ease of use [157, 158]. Separation is based on analyte partition

between a nonpolar stationary phase and a polar mobile phase. The stationary phase is composed of silica porous particles where hydrophobic ligands like octadecyl (C18) groups are irreversibly bonded. The mobile phase is usually composed of mixture of H_2O and organic solvent (eg: acetonitrile or methanol) and an aqueous buffer. Non-polar analytes are more strongly retained due to interaction with the hydrophobic groups in the stationary phases. The more lipophilic a mobile phase the more quickly lipids will elute from RP column. HPLC-MS combines the advantage of both HPLC and MS, allowing for the separation of metabolites of a wide range of molecular weight and polarity with high throughput and high sensitivity.

HILIC Chromatography: HILIC is a modern variant of NPC [159]. HILIC emerges as an important technique for the analysis of very polar compounds and is inverse to RP. The stationary phase is polar and is used with highly organic mobile phase containing a small proportion of H_2O or buffer.

The connection of LC with MS and the advancement in developing LC-MS has resulted in a collection of ionization modes. Atmospheric pressure (API) includes electrospray ionization (ESI), APCI (Atmospheric pressure chemical ionization) and APP (Atmospheric pressure photo ionization) [160, 161]. The development of API technology in particular ESI has enabled the LC-MS to gain popularity as one of most powerful analytical platforms and ionization techniques with broad applicability in the metabolomics field. These techniques are common in untargeted analysis because of their soft ionization capability that aid identification of unknown metabolites as well as the ability to ionize metabolites at broad polarity range.

In the last decade, the improvement of more efficient LC (known as Ultra performance LC (UPLC)) offers high pressure flow and enhance peak resolution and capacity. The ESI to which large voltage is applied to produce a spray of fine droplets is where the ionization occurs. This produces an electric field between capillary and cone (counter electrode). Based on the analytes of interest this voltage can be positive or negative ionization. Once ions are formed, they are focused into the mass analyser and separated into m/z. Mass

analysers separate ions by their m/z, then the electronic current produced is recorded in the detector and this result in obtaining mass spectrum.

.

Different types of mass analysers have been developed that can be coupled with LC. In the current study, QTOF including tandem and hybrid instrument have been employed and will be briefly discussed below.

Several mass spectrometers combine different types of analysers, referred to as hybrid instruments. Mass spectrometers can be performed in tandem mode (two MS/MS) Tandem MS is feasible with a TOF instrument, typically combining quadrupole and collision cell between the source and TOF analyser. This hybrid QTOF mass analyser has become popular providing ability to select ions for MS/MS fragmentation with high resolution and accurate mass measurements. The QTOF has been used for small molecules analysis in this thesis.

CE-MS is high efficient analytical platform that is used in metabolomics research. CE is inexpensive separation technique that is suitable for separating highly polar and ionic metabolites based on charge and size. The use of CE-MS in metabolomics is uncommon owing to poor robustness and detection sensitivity [162, 163]. Other techniques such as comprehensive two-dimensional chromatography (GC×GC–MS) [164], (LC x LC-MS) methods [165, 166], supercritical fluid chromatography (SFC-MS) [167] and Direct infusion (DI-MS) [168] have also been used. See Table 1.1 for more details.

Table 1.1 Summary of advantages and disadvantages of analytical techniques used in metabolomics research. Table reproduced from [125]

Analytical Platform	**Strengths**	**Weaknesses**
Nuclear Magnetic Resonance spectroscopy (NMR)	Offers detail on chemical structure of unknown compounds, high reproducibility and quantification, Provide structural elucidation for metablites identification. require minimal sample preparation prior to analysis like derivatization or separation.	High costs of instrument, operation need skilled operator, relatively insensitive
Magnetic Resonance Spectroscopy (MRS)	Non-invasive in vivo technique, high reproducibility and gives information on metabolites chemical Structure hence helping in identification,	relatively insensitive expensive, specialist operator required
Gas Chromatography-Mass Spectrometry (GC-MS)	Highly reproducible, handy to run, high sensitive and selectivity, structural data confirmation by matching with database.	Need samples derivatisation step, less structural information than LC-MS, long Separation time.
Direct Infusion Mass Spectrometry (DI-MS)	High throughput, high sensitivity, confirmation possible with comparison to standards, structural details can be obtained from fragmentation.	Need sample pre-treatment, interference and ion-suppression issues, less structural information than NMR and MRS

Liquid Chromatography Mass Spectrometry (LC-MS)	Easy to run, high sensitivity and selectivity, excellent tool for non-targeted analysis, fragmentation provides some structural data	Need sample pre-treatment to enable metabolites extraction, less structural details compared to MRS and NMR, require long analysis time
Liquid Chromatography electrochemical detection (LCECA)	High-throughput, high selectivity, less expensive compared to LC–MS, easy to operate.	Molecules require oxidation or reduction to enable detection, large volume of waste solvent produced, provide low structural data.
Capillary Electrophorsis (CE-MS).	High selectivity, separation and high throughput, low volume of waste solvent produced	poor sensitivity, also robustness, and reproducibility problems experienced that were improved in current instruments, need trained operator owing to difficulties in optimization

1.5.3 Data analysis methods in metabolomics

Following untargeted MS based metabolomics a data matrix is obtained. This matrix is very large and finding data treatment strategies to extract this data and to obtain metabolites that are responsible for biological alteration in a cohort is crucial.

Prior to data processing, data need to undergo a set of pre-processing steps including data conversion, alignment, scaling and normalization. Software for data pre-treatment in untargeted approaches is available such as XCMS and Mzmine for LC-MS, TagFinder and metab for GC-MS and JDAMP for CE-MS. This is then followed by data statistical analysis where the data matrix will undergo further analysis to select the significant features (markers). There are two kinds of data statistical analysis, widely used in metabolomics, these are Univariate analysis (UVA) and Multivariate analysis (MVA).

UVA, is used to determine if the variable selected significantly differs between the groups in the samples, this is divided into 1) parametric methods which assume that the data follows a normal distribution, well known are student's t-test to compare between two groups and one-way Analysis of Variance (ANOVA) to compare between more than two sets of samples. 2) non-parametric methods which assume that data does not exemplify normal distribution such as the Mann-Whitney test to compare between two groups of samples and the Kruskal-Wallis test to compare between more than two groups.

MVA is used to facilitate the process of extracting the metabolites of interest from a large data matrix in untargeted metabolomics. The first step involves applying Principal component analysis (PCA), an unsupervised method that is used in metabolomics to visualise the relationship among groups. This allow to simply evaluate and check trends by means of clustering of the data and check for outliers, given the sample identity is unknown. Constructing models such as PLS, PLS-DA and OPLS-DA can be used further as supervised multivariate analysis to provide superior information in what are the differences between groups and for biomarker discovery [169].

Validated predictive tool used to evaluate model quality are R^2 (explained variance) and Q^2 (predicted variance), return scores of R^2=0.5, Q^2=0.4 (SIMCA online - www. http://umetrics.com/manual/simca-online). Later, variable importance in the projection'(VIP) [170] and S-plot can be used to estimate the importance of each variable in the projection and it can also be used to enable the selection of statistically significant variables. An informative table describing the various forms of data analysis in metabolomic studies was gathered in a review by Madsen et al [171] and can be found in Table 1.2.

Finally, the selected potential markers, can be subjected to the in-house database search, such as HMDB (Human Metabolome Database) and Metlin (MS/MS metabolite database) to elucidate the structural information of metabolites and hence annotation.

Table 1.2 Data analysis methods frequently employed for disease diagnosis and biomarker identification in metabolomics.

Technique	Typical use	Description and comments
Univariate testing [172, 60]	Identification of potential biomarkers	Univariate analysis where the corresponding p-values are the standard scientific measure of significance. Multiple testing is prone to false positives unless corrected significance limit is used
Principal component analysis (PCA) [173, 54]	Data overview	Standard multivariate analysis method to provide an overview of a large dataset. Useful for identifying outliers, clusters and trends in the data. Is not a classification method
Partial least squares discriminant analysis (PLS-DA) [174, 55, 65]	Classification and biomarker identification	Classification variant of PLS. Works best with homogeneous classes. Biomarker identification possible, but not as straight forward as with OPLS-DA
Orthogonal projection to latent structures discriminant analysis (OPLS-DA) [175, 66]	Classification and biomarker identification	Classification variant of OPLS method. Ability to separate between-class from within-class variability. Straight forward interpretation and identification of potential biomarkers
Support vector machines (SVM) [176, 69]	Classification (non-linear)	High flexibility in modeling non-linearities. Careful model selection reduces possibility of overfitting. Potential biomarker identification more complex compared to linear methods,, except when linear variant is used (LS-SVM)

1.6 Metabolomics applications in AD research

1.6.1 AD metabolomics in CSF

The analysis of CSF is very useful in AD metabolomics, this is because CSF is in direct contact with brain and its composition is believed to reflect the brain metabolic production. Hence it is more likely to observe the changes in AD pathology in CSF compared to other biofluids [177]. However, collection procedure requires high skills (trained clinician) and can be painful [178].

In metabolomics, few studies have used HPLC coupled with electrochemical array detection (ECA). Kaddurah Daouk,et al has employed LC-ECA to analyse 114 CSF samples (38 CN, 36 MCI and 40 AD patients) from three groups. Patients presenting AD and MCI showed AD individual to have elevated levels methionine, 5-hydroxyindoleacetic acid , vanillylmandelic acid, xanthosine and glutathione compared to CN, suggesting these metabolites to be associated with AD pathology[179]. Moreover, a correlation with the concentration of $A\beta_{1-42}$, P-tau and T-tau proteins in CSF was investigated. Results demonstrated an association of xanthine, vanillylmandelic acid abundance with T-tau protein in CSF, indicating that purine pathway may be involved in T-tau aggregation and pathology generation. Furthermore, the same study observed increase in 5- hydroxyindoleacetic acid in both MCI and AD compared to CN groups, suggesting disturbances in these metabolites are related to $A\beta_{42}$ and thus amyloidgenic pathway [179].

In another study, the same group combined the metabolic information acquired from using both HPLC-ECA and GC-TOF MS platforms [180]. CSF Samples from 40 AD and 38 CN patients were studied. Following GC-TOF MS analysis and statistical evaluation, two metabolites with unknown identity were observed at high level, showing association with the disease. However, failure to annotate these metabolites prevented biological interpretation [180]. Metabolites involved in oxidative stress and neurotransmitter pathways have been investigated in post mortem ventricular CSF samples (15 CN with autopsy-confirmed diagnoses vs 15 AD) using LC-ECA. Findings showed a decrease in

norepinephrine and its related metabolites and suggest further investigation of these metabolites in preclinical patient samples [181].

Complementary chromatographic separation techniques coupled to UHPLC-MS have been used in CSF analysis to improve metabolome coverage. Using RP and HILIC/UHPLC-MS, a study of 45 CSF samples (15CN ,15MCI and 15AD) revealed changes in metabolic pathway by nearly 30% in MCI and 60% in AD compared to CN samples. The same results were reflected in plasma samples from the same patients showing clear correlation between biofluids [182]. Another study used the same platform and identified 17 significantly different metabolites in 4 groups (CN, MCI with progression to AD, MCI without progression to AD and AD), thet were able to predict AD development with values above 95% for sensitivity and specificity [184].

In MCI patients who progressed to AD, increased levels of dopamine-quinone or methylsalsolinol (neurotoxic metabolites) and a decreased level of taurine (a neuroprotective metabolite) were reported [183]. Furthermore, the model showed changes in histidine level that were previously reported and metabolic fingerprints were investigated using CE-MS of 85 CSF samples form patients with four different cognitive status (age matched control, MCI patients at time of sample collection and AD patients. Some patients with MCI had converted to AD while others remained stable based on two years period of clinical follow up. After analysis and data processing, 71 metabolites with high importance were selected. Following multivariate analysis, ten polar metabolites were selected as potential biomarkers of AD conversion [184].

Other work compared AD and healthy subjects to look at disease phenotype [185]. CSF samples (51 CN, 53 mild AD, and 26 moderate AD) were analysed by GC-MS followed by LCMS/MS, over 340 metabolites were determined. Discriminant analysis showed cysteine and uridine as the best metabolite to predict AD with sensitivity and specificity values of 75% [185]. NMR based metabolomics was also used to analyse CSF samples and to differentiate between CN and AD [182, 186, 187].

1.6.2 AD metabolomics in plasma and serum

Peripheral blood samples have the advantages of being easy to obtain and non-invasive. Samples can be collected repeatedly on intervals to monitor changes but are further away from the brain, and in contact with other tissues and organs which affects the interpretation of the data (14). In addition, blood can show the altered brain metabolite levels in AD in part to the increased porosity of the blood brain barrier causing molecules to leak into the blood from the brain and vice versa.

CSF, plasma and urine samples were analysed and differences in free amino acids(FAA) and dipeptides concentration in AD compared to CN groups were determined in the three biofluids by LC-ESI-MS^2. Highlighting the importance of FAA and dipeptides metabolism in the pathogenesis of AD [188].

Some studies have attempted to investigate to what extent metabolic changes seen in CSF reflected in other biofluids. A work by Trushina *et al* utilised CSF and plasma samples (15 CN, 15 MCI and 15 AD) correlation between both biofluids, with results showing increase in metabolic pathways affected in MCI and AD samples as disease progressed [182]. Interestingly, the same pathways were also altered in the plasma of same patients revealing clear correlation between biofluids [182].

Metabolic fingerprints of plasma samples were carried out by Li *et al* with the purpose of detecting potential metabolic biomarkers. Plasma samples (20 CN vs 20 AD) were analysed by UHPLC-MS, they demonstrated 9 metabolites (including lysophosphatidylcholines, typtophan and sphingosines) changed between CN and AD samples suggesting them as potential biomarkers [189]. Another study also utilized UHPLC-MS (for the analysis of lipids) in addition to GCxGC-MS (for the analysis of fatty acids, amino acids, sterols and sugars) to increase metabolic space in order to screen biomarkers metabolites that lead to AD progression [190].

As mentioned previously, a close link between lipid metabolism and AD has been established leading to special interest in profiling lipids and investigating lipid-related

metabolites in blood as potential markers using metabolomics. This interest has risen from the findings of "adipose inclusions" or "lipoid granules in brain tissue" as observed by Alois Alzheimer when he first described the disease [191, 125]. To study lipids as a potential early marker, Tukiainen *et al* used NMR to analyse serum samples (26 CN VS 19 MCI). Information from 3 groups of metabolites (lipoprotein, polar metabolites and lipids) were compared. Moreover, the same study reported association between AD risk factors in MCI patients and low level of omega 3 fatty acids, sphingomyelines and PCs [192]. LC-MS analysis of plasma samples reported lysophospholipid (18:1) as early marker that decrease with AD progression from CN to MCI to AD patients [166].

Over 800 lipids were detected in plasma by applying novel untargeted multidimensional on MS based shotgun lipidomics approach (MDMS-SL). AD patients showed significant depletion in sphingomyelines and elevation in Ceramides, suggesting this may be either due to high ceramide production in the brain or increase in sphingomyelines hydrolysis [193].

High cholesterol in plasma samples from patients carrying the APOE e4, was proposed as high risk of early onset at age of less than 65 years old [194]. This matched the results in other study presenting cholesterol and demosterol as markers for AD [195]. Both metabolites were analysed by LC-MS and quantified. Results showed a significant decrease in demosterol and cholesterol in AD samples, with these results proved by analysing 109 plasma samples as validation step [195]. More lipids have been reported to be associated with AD, these include cholesteryl esters [196], PlsEtn [197, 198].

In addition to RP-MS, DI-MS was used in human studies to perform lipid profiling in serum samples, with metabolites detected implicating PUFA, amino acids, and eicosanoid pathway [199, 200]. DI-MS was also utilized by other groups for blood metabolites profiling and changed concentration of phospholipids [201], diglycerides [202] and sphingolipids [193] were reported.

Another research investigated serum samples and reported depletion in oleamide and monoglycerides levels accompanied with increased level of acylcarnitine suggesting the findings to be a good ground to further understand disease progression [203].

1.6.3 Other biofluids

Urine and saliva have also been examined in the search for AD biomarkers as they are very easy to collect [188, 204]. In a study urine samples were analysed and found that altered levels of 5- L-glutamylglycine and L-glutamamine were detected in AD compared to CN [207].

Altered metabolites in AD pathology were identified and related to various biochemical processes including dopamine, L-Dopa and arginine metabolism[188]. A study found increased levels of 7- ketocholesterol and sphingosine-1-phosphate as potential predictive metabolites in AD conversion. These metabolites were also reported by other groups to distinguish CN and MCI from AD patient in saliva samples [205, 206].

Urine is another biofluid from which potential metabolites have been quantified with results consistent with CSF and blood metabolite study in AD. Urine has the advantage of being non-invasive and hence ideal for preclinical diagnosis in conjunction with CSF and blood biomarkers, however it can also have many drug metabolites.

Cui et al, analysed the blood serum and urine of 46 AD compared to 36 healthy CN subjects using (UPLC-QTOF-MS). Significantly three serum and two urine metabolites were selected as potential biomarkers namely LysoPC (18:0), LysoPC (18:2), palmitic amide, L-glutamine and 5L-glutamylglycine [Area under the curve (AUC $\geq$ 0.7)]. Palmitic amide increase was associated with the prevention of the breakdown of neuroprotective cannabinoid while in AD; urinal 5L-glutamylglycine was linked to the reduced GABA associated with memory impairment, increased L-glutamine level was linked to reduction in brain protection [207].

In another study, Peng et al used $^{12}C/^{13}C$ labelled LC-MS in the analysis of urine from 12 transgenic mice in comparison to 12 CN mice for the detection of potential biomarkers at different mice ages. Significant metabolites biomarkers identified included methionine, taurine, desaminotyrosine, N1-acetylspermidine, and 5-hydroxyindoleacetic acid. In the plasma, elevated levels of methionine and its product of metabolism homocysteine have been associated with increased Aβ aggregation in AD, while decreased taurine levels influenced synaptic transmission in the AD brain due to its function as a neurotransmitter. The role of the elevated desaminotyrosine was unknown but decreased 5-hydroxyindoleacetic acid a metabolite of serotonin was linked to AD via neurotransmitter alteration and reduced N1-acetylspermidine levels was related to disruption in cell membrane [208].

1.7 Metabolomics studies in AD brain tissue

Compared to biofluids, brain has different areas and regions making the study of this organ very complex. Careful considerations of study design in term of area have to be used, together with sample collection interval to post mortem and metabolite extraction.

Metabolomics studies have analysed different brain regions. The scarcity and difficulty in obtaining human brain samples is another challenge that hinders the extensive study of this organ. Early changes in AD brain are believed to occur first in the hippocampus and cortex then to the medial temporal lobe which is involved in the deficits in memory. In this sense, the analysis of different regions of brain would provide greater specificity and assurance particularly to study the neurophysiological pathway of the disease.

1.7.1 AD human brain tissue studies

In a study carried out by Graham et al using ^{1}H NMR to analyse the polar metabolites of post mortem human brain tissue (15 CN vs 15 AD), there were significantly increased levels of alanine (15.4%) and taurine (18.9%) in the neocortex region of AD brain, with the ratio of these metabolites (i.e alanine/carnitine) suggested to be powerful discriminating as biomarker of AD [ROC and (AUC)=0.76; $p<0.01$] [209]. Furthermore,

the same group have performed metabolic fingerprints of human brain neocortex (15 AD vs 15 CN) using UHPLC-MS in the positive and negative ionization modes. Following multivariate and statistical analysis, a total of 66 candidate molecules were reported to be statistically different [210].

A number of studies have looked at brain lipid metabolites in brain, owing to the brain rich fat nature and previously mentioned fat inclusions in AD brain. A study by Farooqui et al. found an increase in PlsEtn abundance with age, however this noticeably deceases following age of 40 [211]. Selective and marked reduction has also been found in the PlsEtn abundance were observed at lower level in AD individuals (70%) compared to those with normal brain particularly in the grey matter of brain as disease progress [67]. The same findings were reported by Wood et al. when they analysed frontal cortex grey matter and reported the decrease in PtdEtn abundance in AD individuals with no change observed in MCI individuals [212].

Another study, included human brain regions from 22 Subjects with no dementia (n=5), very mild dementia (n=3), mild dementia (n=4), moderate dementia (n=6) and severe dementia (n=4). After analysis by DI-MS a significant reduction in sulfatide levels were observed. Sulfatides deficiency by 93% and 58 % in the gray and white matter respectively were seen at the earliest clinical stage of AD [213]. This result were also observed on a study of the mouse model [214].

1.7.2 AD animal models and brain tissue studies

The use of animal models particularly in AD research tackle the challenges associated with obtaining human brain samples and thus animal model studies used in metabolomics to study AD pathogenesis are in increase. Many transgenic mouse models (Tg), were used in AD investigations. The most widely used models known to develop amyloid plaque pathology through the expression of APP are Tg2576 and TgCRND8. Other models known as biogenic transgenic mice that express mutant presenilin protein (APP/PS1 or APP/PS2) in addition to APP mutant are also popular [215-217].

Most recently, Pan *et al.* have performed longitudinal profile of brain and plasma metabolome at 8, 10, and 12 months using APPswe/PS1deltaE9 double transgenic and wild-type (WT) mice. A panel of metabolites were selected following multivariate analysis and metabolic pathway analysis finding perturbed polyamine metabolism in both plasma and brain samples [218]. Two years earlier, González-Domínguez et al. reported changes in purine metabolism, amino acid, phospholipids, dopamine and energy metabolism occurred in the different brain regions. Potential biomarkers identified were linked with phospholipid and sphingomyelin components of fatty acids with the decreased polyunsaturated fatty acids (PUFA) levels particularly docosa-hexanoic acid (DHA). The decreased levels of PUFA implied that oxidative stress was involved in AD, while accumulation of short chain fatty acid phospholipids was implicated in AD membrane disruption [219].

A study conducted by Lalande *et al*, using ^{1}H NMR to discover metabolites in the tissue extracts of five different brain regions namely rhinal cortex, frontal cortex, midbrain, hippocampus, and cerebellum of the 39 AβPPsweTg2576 mice model compared controls at 1, 3, 6, 11 months. Metabolite perturbations were observed with significantly decreased levels of myo-inostol, glutamate, creatine, N-acetylaspartate (NAA) and phosphocholine in the hippocampus and rhinal cortex at 1 month and 3-months old mice. Low levels of metabolites were linked to reduced neuronal function, neurotransmission at the synapses, like glutamate, N-acetylaspartate and NAA and creatine reductions were implicated in low cellular energy. At 11 months there were metabolite perturbations in all areas of the brain with the exception of the frontal cortex [220]. Further brain regions have been investigated in AD animal model studies using NMR and MS [2, 219, 221]. Table 1.3 summarize AD brain tissue metabolomics studies in animal models and human.

Table 1.3 animal and human brain tissue metabolomics studies in AD research

Animal model	Analysed region	Analytical platform	Altered metabolites	Ref
APPTg2576 mice (n=9) and WT(n=10)	Frontal cortex	NMR	Myo-inositol, Taurine, Choline, GSH, Glutamate, Glutamine, Succinate, Aspartate, Lactate, Alanine, gamma-aminobutyric acid, N-acetylaspartate.	[222]
APP (V717F) Tg , APP Tg, Apoe (-/-) , APP Tg, Apoe (+/+) mice	Cerebellum, cortex	MS	Sulfatide	[214]
APP-PS1(n=10) WT(n=10)	Parietal, temporal, occipital and frontal cortices, Hippocampus thalamus	HR-MAS	N-acetyl aspartate, acetate, myo-inositol and scyllo-inositol.	[223]
TgCRND8 mice(n=10) and their controls(n=12).	Cortex, frontal cortex, cerebellum, hippocampus, pons, midbrain, olfactory bulb and striatum	NMR	Gamma-amino butyric acid, glutamine glutamate, N-acetyl-aspartate, taurine, choline, creatine phosphocholine, phosphocreatine, succinate, free fatty acids, iso-leucine, leucine, lactate, valine, aspartate, glycine.	[224]
TgCRND8 mice (n = 6) and controls (n = 6)	Cerebellum	FT-ICR/MS	Total of 29 metabolites significantly altered i including: Phenylalanine, amino acids, amino acid conjugates, Tyrosine Tryptophan, Histidine, Methionine, sulfoxide L-Argininosuccinate, Phenylacetylglutamine, O-Oxalylhomoserine and N-Methyl-L-glutamate.	[225]

TASTPM n= (7-8) Tg, WT(n=5-9)	Whole brain	MRS ^{1}H MRS	Myo-inositol, Succinate, glycerophosphocholine and choline.	[226]
Tg AAP/PS1 mice (n = 30 and WTC57BL/6 controls (n = 30)	Hippocampus, cerebellum, cortex, striatum and olfactory bulb	UHPLC-ESI-QTOF/ MS and GC-EI-ITQ/ MS	N-acetyl-aspartate, valine, 2, adenine, adenosine, cholesterol, glutamate, dopamine, glucose-6-phosphate, taurine, glycerol, Phosphoribosyl-AMP, hypoxanthine guanosine, histidine, aspartate, inosine, myo-inositol, maleate, serine, creatinine, pyroglutamate, Pyrophosphate, lactate, urea, xanthine.	[219]
senescence-accelerated mouse prone 8 (SAMP8) (n=18)	Hippocampus	GC-MS	Cholesterol, oleic acid, and phosphoglyceride, alanine,serine, glycine, aspartic acid, glutamate, and gamma-aminobutyric acid, malic acid, butanedioic acid, fumaric acid, and citric acid, N-acetyl-aspartic acid and decreased pyroglutamic acid, urea, and lactic acid.	[227]
APPswe Tg2576 mice (n = 39) and WT (n = 44) at 1, 3, 6 and 11 months of age	Rhinal cortex, frontal cortex, midbrain, hippocampus, cerebellum	1H NMR	glutamate (Glu) and N-acetylaspartate (NAA), myo-inositol, creatine, phosphocholine, and gamma aminobutyric acid, creatine, and taurine.	[220]
APP(Tg2576) (n=3), PS1-M146L(n=3), WT (n=6)	Hippocampus	RP/GC-MS	Alteration in carbohydrates, amino acid s, nucleotide, energy and neurotransmitter metabolic pathway.	[221]
TgTASTPM mice (n = 16) and WT (n = 5)	Whole brain	GC-EI-MS	Threonine, L-serine, D-fructose, L-valine, L-, zymosterol.	[228]

APP/PS1 (n=6) and WT(N=6) mice	Whole brain	NMR	N-acetyl aspartic acid, gamma aminobutyric acid, creatine, ascorbate.	[229]
TgCRND8 mice	Hippocampal tissue	LC-LTQ-Orbitrap	Disturbance in eicosanoids in arachidonic acid metabolism, fatty acid beta-oxidation disorders as well as glucose metabolism.	[230]
Transgenic AAP/PS1 mice (n = 30) and WT C57BL/6 controls (n = 30)	Hippocampus, cortex, cerebellum, olfactory bulb	LC-QYOF/MS	Acylcarnitines, amino acids, steroids choline, dopamine, acetate glycerol-3-phosphate, phospholipids lyso-phospholipids, acetyl-spermidine, nucleotides, Pyruvate, tyrosine and urea.	[231]
APP/PS1deltaE9 mice (n = 8) and WT C57BL/6 J (n = 9) at 6, 8, 10, 12, and 18 months age	Whole brain	UHPLC-QqQ-MS	Biogenic amines (phenylalanine, tryptophan and Tyrosine), lysophosphotidylcholines, phosphotidylcholines, sphingolipids. Acylcarnitines(a (C10:1 and C12:1), (Putrescine,creatinine, hydroxyproline and proline), spermidine and spirmine.	[232]
TgAPP/PS1 mice and WT composed of controls (n = 10), AD (n = 10), G-Rg1 (n = 10) and G-Rg2 (n = 10)	Whole brain	LC/MS	hypoxanthine, dihydro-sphingosine, hexadeca-sphinganine, phyto-sphingosine, LPC C 16:0, LPC C 18:0 , LPC C 13:0, LPC C 15:0, LPC C 18:1, and LPC C 18:3 in AD mice.	[233]
Human Samples	**Brain regions used**	**Analytical platform**	**Altered metabolites**	**Ref**
AD (n = 21) and age matched controls (n = 19)	Whole brain, region not specified	UHPL-ESI-MSE	Cystine arginine, pentose 5-phosphate Aspartic acid, glutamic acid, Glutamine, uric acid, guanosine, Serine, hypoxanthine, Pantothenic acid, pyruvate, succinate, tryptophan, valeine, inosine , xanthine, Prolin, hydroxyproline Xanthosine.	[234]

AD (n=17), CN (n=5)	Hippocampus, entorhinal cortex, inferior parietal, superior temporal and middle frontal gyrus.	DI-MS	Ceramide, Sulfatide	[213]
AD (n = 15), healthy age matched controls (n = 15)	Brodmann and neocortex region	NMR	Hypoxanthine, acetate, carnitine, ethanolamine choline, creatine, alanin, aspartate, Inosine, lactate, taurine leucine, myo-inositol, tyrosin, N-acetyl aspartic acid, nicotinate, succinate, valine and serine.	[209]
AD (n=13), CN (n=4)	Hippocampal region and the cerebellum	MRS	N-acetyl aspartate, gamma-aminobutyric acid.	[214]
AD (n = 15) and elderly controls (n = 15)	Brodmann and neocortex region	LC-ESI-QTOF-MS	66metabolites in + and – ESI mode identified as significantly altered ions.	[210]
AD (n=9), CN (n=9)	Cingulate, middle-temporal gyrus, sensory, motor, entorhinal cortex, hippocampus and cerebellum	GC-MS	Alteration in glucose clearance/utilization, the urea cycle, and amino-acid metabolism.	[235]
Samples composed of AD I–II (n = 7), AD III–IV (n = 27), AD V–VI (n = 40) of Braak and Braak stages and controls (n = 38)	Frontal and entorhinal cortex	LC-ESI QTOF MS/MS	Glycine, xanthosine, inosine, and deoxy-guanosine di-phosphate guanine.	[236]
AD (n=34), MCI (n=19) and CN (n=28)	Frontal cortex white and grey matter	DI-MS	Mono and diacylglycerols (DG), the very-long-chain fatty acid 26:0, Ethanolamine plasmalogens, phosphatidylethanolamines.	[212]

AD (n=16). CN (n=8)	Temporal, parietal, cerebellar cortex and Caudate nucleus	HPLC	Glycerophosphocholine and glycerophosphoethanolamine.	[237]
Patients with gradual pre-mortem memory loss (n = 9) and controls (n = 9)	Frontal lobe	UPLC-ESI-MS/MS	l-phenylalanine and l-lactic acid were identified as biomarker candidates in AD brain.	[238]
AD (n=10), CN (n=10)	Frontal, occipital and parietal lobe	RP-MS	spermine and spermidine.	[239]
80 years old AD (n = 12) and controls (n = 12), and 60 years controls (n = 11).	Superior frontal gyrus, cerebellum and hippocampus	LC-ESI MS and HPLC-UV	Gamma aminobutyric acid, glutamine, glutamate L-arginine, agmatine, putrescine L-citrulline, L-ornithine, spermine, spermidine.	[240]
AD (N=6), CN (n=8)	Frontal gyrus	DI-MS	Sulfatide	[241]
AD (n = 8), ALS (n = 11)	Frontal cortex	1H NMR	Glutamine, acetate, lactate, alanine, glutamate, creatine	[242]
AD (=7), CN (n=9)	Frontal and parietal region	31P NMR	Phosphomonoesters, phosphocholine, phosphodiesters phosphoethanolamine, and the glycerophosphorylcholine and glycerophosphorylethanolamine.	[243]

1.8 Aims of the thesis

Considering the outcomes of this literature review, a project plan was designed to investigate metabolic composition of AD brain samples. Initially, rat brain samples were used to develop extraction methods capable of comprehensive coverage of wide range of metabolites using UPLC-MS Q-TOF combining two separation techniques (RP and HILIC) (chapter 2). As the project progressed, more coverage of metabolites with different physical properties was studied using multi-analytical platforms, here GC-MS analysis was employed with the aim of developing another untargeted analysis method and to expand the metabolome (chapter 3). Until this stage, the focus was on brain tissue. In addition, the applicability of the developed LC& GC-MS method was tested using plasma of control and AD groups (chapter 4).

The overall aim of the thesis was to identify a panel of candidate metabolites which would enable understand disease mechanisms and/or monitor disease progression in humans. Hence in the last chapters (chapter 5 & 6) human brain samples from control, asymptomatic and AD were analysed using the developed untargeted LC&GC-MS brain In vial dual extraction (IVDE) method.

CHAPTER 2: Comprehensive LC-MS analysis of rat cerebellum: An untargeted metabolomics approach

2.1 Introduction

Despite the importance of the brain and the pathological burden associated with it, we are still relatively ignorant of its mechanisms, as such it is hoped that developing a better understanding of cerebral metabolism will help to unlock the secrets of the brain. The biggest challenges of working with both human and animal brain tissue are twofold; firstly is the lack of available sample material, and secondly reproducible extraction of metabolites from the sample tissue. These obstacles make the development of analytical approaches that maximise the metabolites that can be reproducibly measured from small tissue samples an important challenge.

Due to the wide range of concentrations at which these metabolites are present and their diverse chemical structure, it is challenging to obtain comprehensive analysis of all metabolite classes using a single metabolomics method [244-247]. Therefore, many comprehensive metabolomic approaches that aim to maximise metabolite coverage utilise a combination of analytical platforms including, NMR and MS (coupled to separation chromatography such as GC, LC and CE [248, 249]. These multi-platform approaches will measure metabolites with a wide range of concentrations and physiochemical properties, however applying more platforms to increase metabolite coverage will significantly increase both the cost and time required for the analysis, and more importantly a greater amount of tissue will be required. As a result of this it is important to maximise the number of metabolites measured from a single sample.

LC coupled to MS is one of the most widely-used analytical techniques for metabolite fingerprinting and has been used to analyse a range of metabolite classes in a variety of biological matrices. Advantages and selection of this analytical technique was explained in detail in the introduction. Mainly related to the advance in MS technology that is time consuming with high sensitivity and resolution [151]. LC-Q TOF-MS has been therefore used to achieve an assorted number of scan modes to help detect specific polar and non-polar metabolites.

As discussed in the previous chapter, metabolomics uses modern techniques to analyse various biological samples by enhancing the separation and detection process. Moreover,

it is important to point out that different metabolites significantly differ in their physicochemical properties (solubility, polarity, and molecular weight). To date there have been a small number of metabolomic studies that have looked at the metabolite composition of brain tissue of post-mortem human brain[210, 250, 251] for the screening of neurodegenerative disorders while recently animal models have been widely used in AD [2, 252, 253], opening new research directions and leading the way toward the detection of specific biomarkers for the development of personalized diagnostic tools and treatments [254]. ^{1}H-NMR was used to measure the metabolite composition in the hippocampus, cortex, frontal cortex, midbrain and cerebellum of CRND8 mice identifying 23 metabolites from tissue samples ranging in mass from 10 - 50 mg [2]. Graham *et al*. lyophilized and milled ≈5 g of human post mortem brain tissue from which 50 mg was taken forward for extraction and subsequent analysis by UPLC-TOF-MS, from which 1264 ions were detected [255].

The whole process of extraction and analysis was prepared to be carried out in the same vial, thus reducing analytical variation and sample lose by reducing extraction steps. Each phase was analysed separately by LC-MS (RP for non-polar upper layer and HILIC for polar lower layer), using an optimal gradient, the method was designed to expand metabolic coverage from low sample aliquot and to enhance the reproducibility of the overall process. Furthermore, minimizing the risk of metabolite loss by external factors like drying. In this chapter, focus was placed on upper phase of the analysis of non-polar component in the brain IVDE method as well as polar metabolites present in the lower layer are of great interest, thus HILIC analysis was performed. The methodreveal the ability to extract wide variety of non-polar metabolites (i.e. Sphingolipids metabolism, phospholipids metabolism and glycerol esters) and polar metabolites (i.e. Carnitines, amino acids metabolism, neurotransmitter metabolism, tricarboxylic acid cycle and energy metabolism) with high reproducibility.

Aims of this chapter therefore was firstly to develop a modified version of the two phase in-vial dual extraction (IVDE) method described by Whiley *et al*. [256] to obtain both polar and non-polar metabolites from a single small sample of brain tissue. Secondly, to develop a robust hydrophilic liquid interaction chromatography (HILIC) method to

analyse polar metabolites of the aqueous phase, and a reversed phase (RP) method for the analysis of the non-polar metabolites of the non-aqueous phase of the IVDE.

2.2 Materials and Methods

2.2.1 Chemicals and Reagents

All solvents, water, methanol, acetonitrile, ammonium formate, formic acid and methyl tertiary butyl ether (MTBE), were LC-MS grade purchased from Sigma-Aldrich (Poole, UK). Four internal standards, heptadecanoic acid (≥ 98% purity), tripentadecanoin (≥ 98% purity) for the reversed phase, and L-serine$^{13}C_3{}^{15}N$ (95%) & L-valine$^{13}C_5{}^{15}N$ (95% purity) for HILIC, were purchased from Sigma-Aldrich. In-vial dual extractions were performed in amber glass HPLC vials with fixed 0.4 mL inserts (Chromacol, Welwyn Garden City, UK).

2.2.2. Samples

Experimental tissue material was obtained from the cerebellum of adult male Sprague dawley rats obtained from the Biomedical Services Unit, King's College London, which had been dissected from rats euthanized as per Schedule 1 of the Animal (Scientific Procedures) Act 1986. The cerebellum was isolated according to the Springer protocol for the dissection of rodent brain regions [257] , samples were weighed and subsequently stored at -80^{o}C. The cerebellum was sectioned on sterile glass slides (Thermo Scientific, Menzel-Glazer slides) using a sterile scalpel; both scalpel and slide were cooled in liquid nitrogen to reduce sample thawing during sectioning. Sectioned tissue samples were transferred to Eppendorf tubes containing a clean, pre-cooled, 5mm stainless steel ball bearing.

2.2.3 Experimental Design

In this study two primary experiments were performed to assess the precision and sensitivity of the IVDE, instrument methods and tissue homogenisation as well as to determine the effect of sample mass on metabolite recovery. The first experiment was

designed to assess the combined variability of the IVDE and instrument methods. This was done by homogenising a single piece (18 mg) of rat cerebellum, removing sample mass and tissue homogenisation as sources of variability. The homogenate was split into 7 aliquots of 50 µl which underwent parallel extractions prior to injection on both HILIC and RP methods (Figure 2.1A). The second experiment was designed to assess the effect of the mass of tissue extracted and tissue homogenisation on method sensitivity and precision. To do this 15 tissue samples ranging from 3 - 17 mg were homogenised and extracted in parallel prior to analysis (Figure 2.1B). Sensitivity was assessed in terms of the number of metabolite features that were routinely detected, whilst precision was assessed in terms of the variability (coefficient of variation) of the abundance of internal standard and metabolite peaks, as well as the degree of compositional similarity between samples as determined by principal component analysis (PCA). A graphical description of the analytical workflow used in this study is shown in Figure 2.1

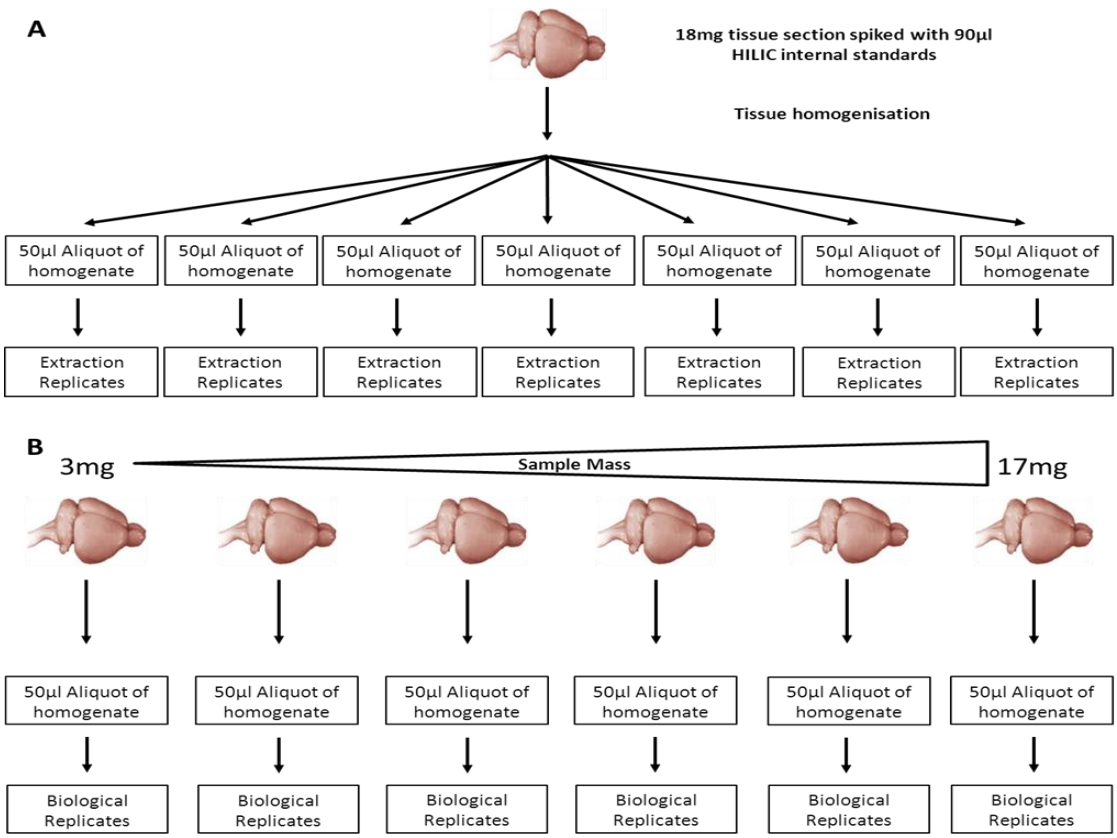

Figure 2.1 Graphical representation of the experimental designs used. A) Experiment 1, a single 18 mg brain section was homogenised then 7 parallel extractions were performed on 50 µl aliquots of homogenate. B) Experiment 2, brain sections ranging from 3 – 17 mg were homogenised and extracted.

2.2.4 Tissue homogenisation

Prior to homogenisation 20 µl of methanol and 5 µl of HILIC internal standard cocktail (2.5 mM L-serine$^{13}C_3{}^{15}N$ and L-valine$^{13}C_5{}^{15}N$ in methanol:water (4:1)) were added per mg of sample material. The tissue was then homogenised using a Tissueyzer (Qiagen-Germany) in 10 cycles of 30 seconds at 25 KHz, subsequently a 50 µl aliquot of homogenate was transferred to a Chromacol HPLC vial (400 µl fixed insert).

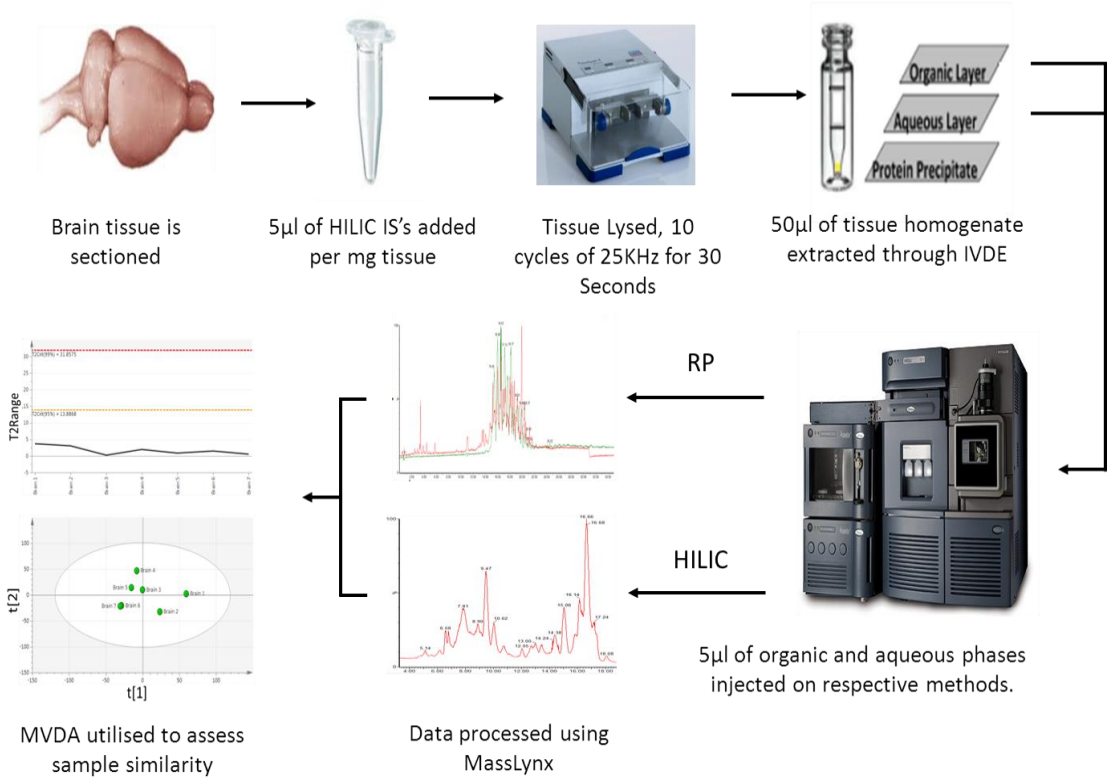

Figure 2.2 schematic representation of the applied analytical pipeline from tissue sectioning to IVDE and onto data processing and analysis.

2.2.5 In-vial dual extraction of brain tissue

Subsequently 10µl of water was added to the homogenate, vials were then vortex for 5 min, after which 250µl of MTBE containing tripentadecanoin (10 µg/ml) and heptadecanoic acid (10 µg/ml) was added, after which samples were again vortexed at

room temperature for 60 minutes. Following the addition of a further 40 µl of water containing 0.15 mM ammonium formate to enhance phase separation, samples were then centrifuged at 2500 × *g* for 30 minutes at 4° C. This resulted in a clear separation of MTBE (upper) and aqueous (lower) phases, with protein precipitate aggregated at the bottom of the vial.

2.2.6 LC-MS analysis of IVDE non-polar phase

LC-MS analysis was performed on a Waters Acquity ultra-performance liquid chromatogram (UPLC) system coupled to a Waters Premier quadrupole time-of-flight (Q-TOF) mass spectrometer (Waters, Milford, MA, USA). The needle height in the autosampler was set to 13 mm, with 5 µl of sample extract injected onto an Agilent Poroshell 120 EC-C8 column (150 mm × 2.1 mm, 2.7 µm). Separation was performed at 55 ^{o}C with a flow-rate of 0.5 ml/min using 10 mM ammonium formate in water (mobile phase A) and 10 mM ammonium formate in methanol (mobile phase B). For analysis in the positive mode, the gradient began at 80% mobile phase B, increasing linearly to 96% B after 15 minutes and was held isocratic for 13 minutes, after which initial conditions were restored in 2 minutes ahead of 7 minutes of column re-equilibration. For analysis in the negative ionisation mode the gradient began at 75% B, increasing linearly to 96% B at 23 minutes, then increasing further to 100% B by 35 minutes, after which initial conditions were restored to allow 7 minutes of column re-equilibration. In the positive mode, a capillary voltage of 3.2 kV and a cone voltage of 45 V was applied. The desolvation gas flow was 400 L/hour and the source temperature was 120 °C. In the negative mode, a capillary voltage of 2.6 kV and a cone voltage of 45 V were used. Desolvation gas flow and source temperature were fixed at 800 L/h and 350 ^{o}C, respectively. All analyses were acquired using the lock spray to ensure accuracy and reproducibility; A reference solution (leucine-enkephalin) was used as lock mass (*m/z* 556.2771 and 278.1141) at a concentration of 200 ng/mL to update accurate mass data values and a flow rate of 10 µL/min. Data were collected in the centroid mode over the mass range m/z 50–1000 with an acquisition time of 0.1 seconds/scan. Analysis settings for both positive and negative mode were used as stated by Whiley et al [256].

2.2.7 LC-MS analysis of IVDE polar phase

The auto sampler needle height was set at 2 mm, with analysis of 5 µl of aqueous phase extract being analysed on a Merck Sequant column (150 × 4.6 mm, 5 µm particle size) coupled to a Merck Sequant guard column (20 × 2.1 mm). A 40 minutes room temperature gradient (0.3 ml/min) was applied using 0.1% formic acid in water (mobile phase A) and 0.1% formic acid in acetonitrile (mobile phase B). The gradient began at 80% mobile phase B, followed by a linear reduction to 20% mobile phase B after 30 minutes, initial conditions were then restored to allow 10 minutes of column re-equilibration. Mass spectral data was acquired between 75-1000 Da in both positive and negative ionisation modes. The applied mass spectrometry conditions were the same as for the reversed non-polar phase method.

2.2.8 Data processing and metabolite identification

The generated data was processed using MarkerLynx (Masslynx 4.1-Waters Corporation) which provides automated peak detection based on peak alignment and normalization to total peak area. The reversed phase data were processed with a mass tolerance of 0.01 daltons (Da), a mass window of 0.05 Da, and a RT window of 12 seconds and a peak width of 10 seconds. The HILIC data was processed with a mass tolerance of 0.01 daltons (Da), a mass window of 0.05 Da, RT window 18 seconds, and peak width of 20 seconds. Processed data was evaluated using principal component analysis (PCA) performed using SIMCA 13.0.3 (Umetrics, Umeå, Sweden). The data in all the generated PCA models was logarithmically transformed (base 10) and scaled to unit variance (UV). The performance of the PCA models generated was assessed based on the cumulative correlation coefficients (R^2Y[cum]), and predictive performance based on seven-fold cross validation (Q^2[cum]). Hotelling's T^2 plots were used to assess the departure of samples from the origin in the model plane, which will show the distance of a sample to calculate average observation (i.e. an average metabolite composition). The DModX plots corresponds to the residual standard deviation of an observation in the x-variables, it was used to assess the distance of an observation to the fitted model.

Metabolite annotation was performed by searching the *m/z* of measured metabolite features in a range of publicly accessible metabolite databases including the human metabolome database (HMDB), METLIN and LipidMaps. Once potential explanatory metabolites had been identified an annotation was confirmed by matching the fragmentation pattern of the peak being annotated to the fragmentation pattern shown for given metabolites within the databases. This method of annotation does possess a small inherent bias towards common well-studied metabolites, as standards are readily available for these compounds thus allowing fragmentation spectra to be more easily generated than less common metabolites.

2.3 Results and Discussion

2.3.1 Assessing the precision and performance of IVDE and instrument methods (Experiment 1)

The first step in assessing the precision of the (IVDE) and both the RP and HILIC methods was to determine the recovery of the four internal standards (Figure 2.3). In the RP method heptadecanoic acid was measured in the negative mode and tripentadecanoin was measured in the positive. The recovery of both standards was consistent, with CVs of 2.5% and 4.4% for heptadecanoic acid and tripentadecanoin respectively (Figure 2.3A). In the HILIC method the internal standards were measured in both the positive and negative ionisation modes. In the positive data, the recovery of internal standards is highly consistent, with coefficient of variation (CV) of 2.4% and 3.7% (Figure 2.3B) for the serine and valine standards respectively. In the negative mode, recovery is more variable than the positive mode, with CVs of 9.1% and 5.7% (Figure 2.3C) for serine and valine respectively. The standard recoveries suggests that the IVDE and both HILIC and RP methods have good precision with all internal standard measurements having CVs less than 15% [258], with mass spectrometry in the negative mode adding more variability than the positive mode.

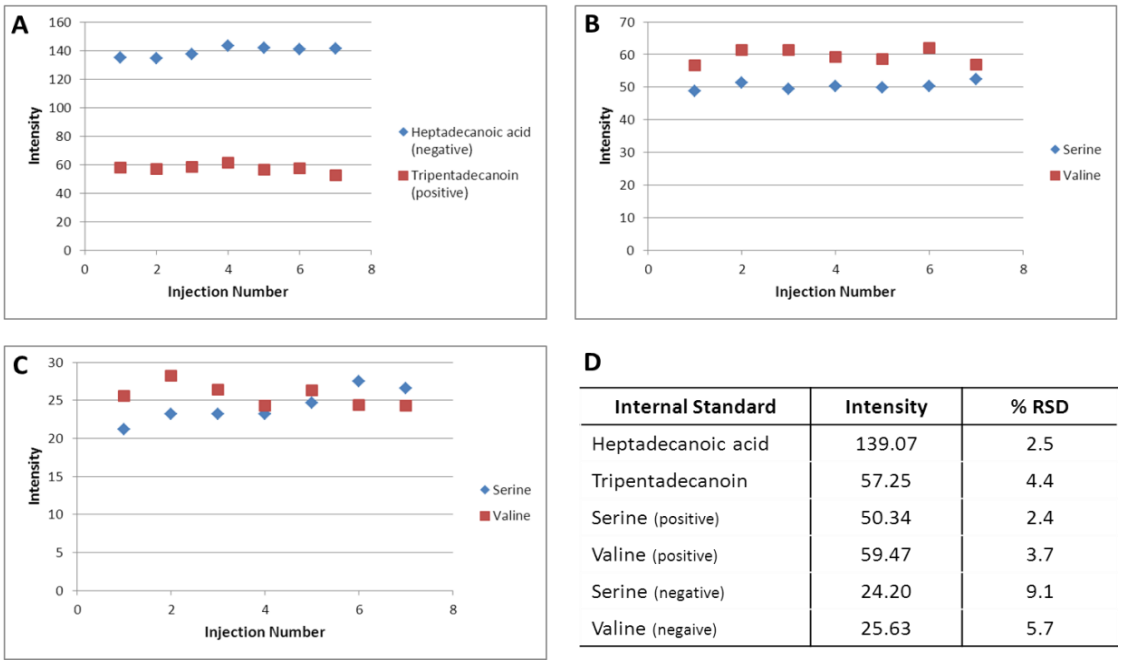

D

Internal Standard	Intensity	% RSD
Heptadecanoic acid	139.07	2.5
Tripentadecanoin	57.25	4.4
Serine (positive)	50.34	2.4
Valine (positive)	59.47	3.7
Serine (negative)	24.20	9.1
Valine (negaive)	25.63	5.7

Figure 2.3 Recoveries of HILIC and RP internal standards in experiment 1. A) Plot of intensity of RP internal standards heptadecanoic acid (negative) and t ripentadecanoin (positive), B) plot of intensity of HILIC internal standards in positive ionisation mode, C) plot of intensity of HILIC internal standards in negative ionisation mode, D) average intensity and coefficient of variance of all internal standards.

The next step in determining the method's performance was to identify the number of metabolite features measured following HILIC and RP separation and to assess the precision of these peaks. This was done by initially identifying the features present in all samples, then identifying those features measured in at least 85% of samples, with a minimum cut-off of peaks present in at least 70% of samples analysed (Table 2.1 and Table 2.2). In total, 5,841 metabolite features were measured in 100% of samples for both the HILIC (3713 metabolite features) and RP (2128 metabolite features) methods. When a 70% sample presence cut off was applied, 12,274 metabolite features were identified with 6,570 and 5,704 metabolite features measured in the HILIC and RP methods respectively. The measured metabolite features show good precision, with 3,468 of the 5,841 (59.4%) peaks observed in 100% of samples, and 6,362 of the 12,274 (51.8%) of the peaks measured in at least 70% of samples have CVs of <15%. In general, the features with CV's of ≥15% are lower in abundance, with peaks with CVs <15% with an average abundance 6.62, with peaks with CVs ≥15% having an average of 1.93 potentially accounting for the lower precision. It is also interesting to note that the metabolite features

that are measured in all samples have a higher average abundance (4.76) than those measured in 85% (2.04) and 70% (1.83). This is due to these groups possessing more peaks that are close to the limit of detection (LOD), with the peak falling below the LOD in some samples accounting for the missing values.

Table 2.1 Measured metabolite features in the HILIC method in experiment 1. Showing the number of metabolite peaks identified and their relative variability in 100%, 85% and 70% of 7 sample replicates. a percentage of samples [a] peak is detected in, [b] coefficient of variance of peak intensity between samples.

	HILIC Positive			HILIC Negative			HILIC Total		
%RSD	100%[a]	85%[a]	70%[a]	100%[a]	85%[a]	70%[a]	100%[a]	85%[a]	70%[a]
< 5[b]	141	155	170	103	113	127	244	268	297
5-10[b]	416	507	598	605	668	726	1021	1175	1324
10-15[b]	305	436	582	460	618	726	765	1054	1308
15-30[b]	417	635	889	803	1204	1539	1220	1839	2428
> 30[b]	149	286	406	314	540	807	463	826	1213
Total	1428	2019	2646	2285	3143	3925	3713	5162	6570

Table 2.2 Measured metabolite features in the RP method in experiment 1. Showing the number of metabolite peaks identified and their relative variability in 100%, 85% and 70% of 7 sample replicates. [a] percentage of samples a peak is detected in, [b] coefficient of variance of peak intensity between samples.

	RP Positive			RP Negative			RP Total		
%RSD	100%[a]	85%[a]	70%[a]	100%[a]	85%[a]	70%[a]	100%[a]	85%[a]	70%[a]
< 5[b]	124	261	278	202	253	455	326	514	733
5-10[b]	193	418	450	504	628	1112	697	1046	1562
10-15[b]	69	115	197	346	418	941	415	533	1138
15-30[b]	112	246	329	402	484	1009	514	730	1338
> 30[b]	50	134	226	126	340	707	176	474	933
Total	548	1174	1480	1580	2123	4224	2128	3297	5704

Table 2.3 Measured metabolite features in the HILIC method in experiment 2. Showing the number of metabolite peaks identified and their relative variability in 100%, 93%, 87%, 80% and 73% of 15 samples replicates. [a] percentage of samples a peak is detected in, [b] coefficient of variance of peak intensity between samples.

	HILIC Positive					HILIC Negative					HILIC Total				
%RSD	100%[a]	93%[a]	87%[a]	80%[a]	73%[a]	100%[a]	93%[a]	87%[a]	80%[a]	73%[a]	100%[a]	93%[a]	87%[a]	80%[a]	73%[a]
< 5[b]	38	49	56	68	81	33	39	44	55	61	71	88	100	123	142
5-10[b]	322	408	431	467	509	217	302	283	344	372	539	710	714	811	881
10-15[b]	426	566	601	644	685	222	353	386	495	566	648	919	987	1139	1251
15-30[b]	406	583	742	793	884	501	751	1115	1142	1348	907	1334	1857	1935	2232
> 30[b]	454	610	827	1078	1254	219	362	514	735	977	673	972	1341	1813	2231
Total	1646	2216	2657	3050	3413	1192	1807	2342	2771	3324	2838	4023	4999	5821	6737

Table 2.4 Measured metabolite features in the RP method in experiment 2. Showing the number of metabolite peaks identified and their relative variability in 100%, 93%, 87%, 80% and 73% of 15 sample replicates. [a] percentage of samples a peak is detected in, [b] coefficient of variance of peak intensity between samples.

	RP Positive					RP Negative					RP Total				
%RSD	100%[a]	93%[a]	87%[a]	80%[a]	73%[a]	100%[a]	93%[a]	87%[a]	80%[a]	73%[a]	100%[a]	93%[a]	87%[a]	80%[a]	73%[a]
< 5[b]	168	184	195	229	238	9	9	14	14	14	177	193	209	243	252
5-10[b]	203	213	220	231	235	7	11	30	38	38	210	224	250	269	273
10-15[b]	65	72	93	140	156	46	81	127	191	196	111	153	220	331	352
15-30[b]	103	119	147	166	182	267	271	754	1314	1363	370	390	901	1480	1545
> 30[b]	49	62	89	135	184	266	388	901	1524	1591	315	450	990	1659	1775
Total	588	650	744	901	995	595	760	1826	3081	3202	1183	1410	2570	3982	4197

Having considered the behaviour of individual metabolite peaks, the final step in assessing the method performance was to look at the similarity of the overall composition of the analysed samples. Principal component analysis (PCA) was performed on all 12,274 metabolite features that were identified in at least 70% of samples (Figure 2.4A). This PCA revealed little structure within the data, with the first component accounting for only 25.3% of the total variability with a predictive performance of Q^2 = -0.10, with the first two components accounting for just 43.9% of variability with a predictive performance of Q^2 = -0.21. The distance of a sample's metabolite composition to a calculated average composition was assessed using the Hotelling's T^2 range plot (Figure 2.4B). This plot shows that all of the samples were compositionally similar both to each other and the calculated average, with all samples having a T^2 of < 5 with the 95% confidence interval set at 13.88. The distance of samples to the model was assessed using the DModX plot (Figure 2.4C), which showed that the samples had a low residual of difference to the fitted model, with all of the observations falling below the Dcritical (0.05) threshold. This combined with the Hotelling's T^2 showed that all of the samples were compositionally similar and that there were no outliers to the model.

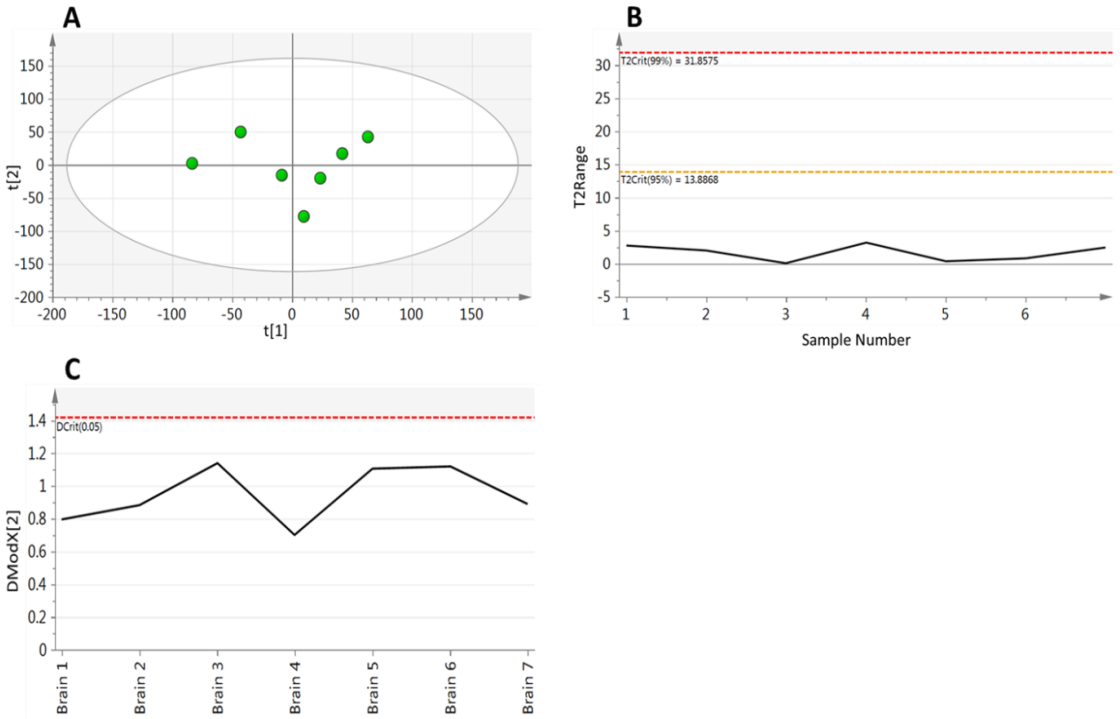

Figure 2.4 Principal component analysis (components = 2, R2 X – 0.439, Q2 –0.210) of metabolite features identified in at least 70% of samples in experiment 1. A) Scores plot and B) Hotelling's T2 and C) DModX plot.

2.3.2 Assessing the effect of tissue homogenisation and sample mass on method performance and precision (experiment 2).

As with assessing the performance of the IVDE and instrument methods, the first step in assessing the effect of tissue homogenisation and sample mass is to look at the recovery of the internal standards. As in experiment 1 both HILIC internal standards were observed in positive and negative ionisation modes (Figure 2.5B and 2.5C). In the positive mode, the CVs of the internal standard recoveries were 13.5% and 14.7% for serine and valine respectively. In the negative mode CVs of the internal standard recoveries were 14.9% and 14.4% for serine and valine respectively. In the RP data heptadecanoic acid was measured in the negative mode with a CV of 13.4%, and tripentadecanoin was measured in the positive mode with a CV of 3.8%. The recovery of the HILIC internal standards was more variable in these samples than in experiment 1, suggesting that the tissue homogenisation step was contributing significantly to analytical variability. This is further supported by no increase in the variability of tripentadecanoin which was spiked into the sample after tissue

homogenisation. The recovery of the HILIC internal standards in the quality control samples, which are pooled after tissue homogenisation, were more consistent than in the analytical samples, and comparable with experiment 1 with CVs of 3.8% and 4.8% in positive and 5.3% and 7.1% in negative for serine and valine respectively, further supporting the hypothesis that tissue homogenisation is contributing significantly to the observed variability. Having shown this, it was important to assess the relationship between the mass of tissue extracted and the recovery of the internal standards (Figure 2.5). Spearman's correlation was used to assess the relationship between standard recovery and sample mass, this analysis revealed no significant correlations showing that internal standard recovery is independent of the sample mass extracted.

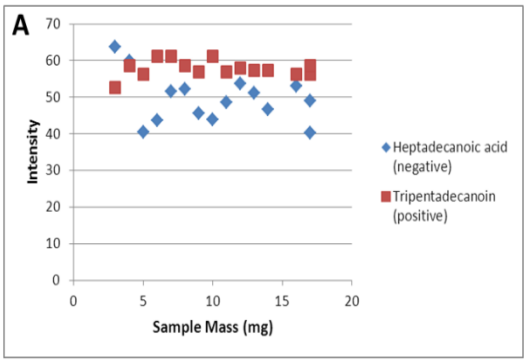

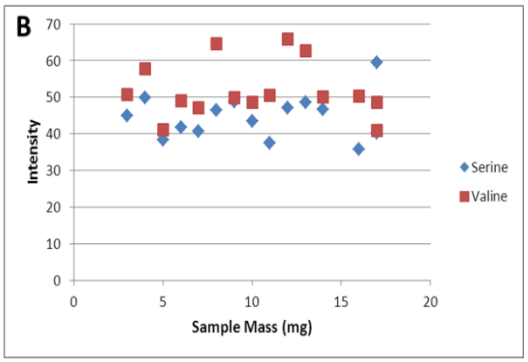

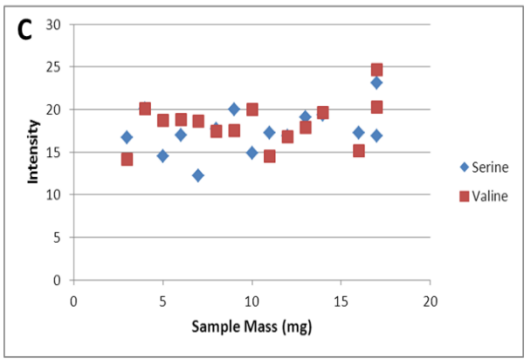

D

Internal Standard	Intensity	% RSD
Heptadecanoic acid	49.56	13.4
Tripentadecanoin	57.79	3.8
Serine (positive)	44.65	13.5
Valine (positive)	51.86	14.7
Serine (negative)	17.52	14.9
Valine (negative)	18.28	14.4

Figure 2.5 Recoveries of HILIC and RP internal standards in experiment 2. A) Plot of intensity of RP internal standards heptadecanoic acid (negative) and tripentadecanoin (positive), B) plot of intensity of HILIC internal standards in positive ionisation mode, C) plot of intensity of HILIC internal standards in negative ionisation mode, D) average intensity and coefficient of variance of all internal standards.

The next step in assessing the method performance was to determine the number of metabolite features measured and the precision of these peaks. As in experiment 1 this was

initially done by identifying peaks that were measured in all samples, working down to a cut-off peaks present in at least 73% of samples (Table 2.3 and 2.4). In total 4,021 peaks were measured in 100% of samples, with 2,838 and 1,183 measured in HILIC and RP methods respectively, 10,934 peaks measured in 73% of samples with 6,737 and 4,197 measured in HILIC and RP data respectively. The precision of the measured peaks was lower than was observed in experiment 1 with 1,726 of 4,021 (43.7%) of the peaks observed in 100% of samples and 3,151 of 10,934 (28.8%) of peaks observed in 70% of samples having CVs of <15%. The finding of higher sample-to-sample variability of the measured metabolite features lends further support to the hypothesis of tissue homogenisation as a source of variability within the method.

Having considered metabolite features individually it was important to consider the composition of samples as a whole. As in experiment 1 PCA was applied to all metabolite features that were measured in at least 73% of samples (Figure 2.6). The analysis revealed little structure within the data, with the first component accounting for only 22.3% of total variability with a poor predictive performance of $Q^2 = 0.07$, with the second component only explaining a further 13.1% of variability ($Q^2 = 0.05$) (Figure 2.6A). The Hotelling's T^2 plot (Figure 2.6B) shows that all samples fall within the 95% confidence interval ($T^2 = 8.19$), with all bar one sample having a $T^2 < 4$, demonstrating that the samples were compositionally similar both to each other and to the calculated average. The DModX plot (Figure 2.6C) showed that all samples had a low residual of difference to the fitted model with all of the observations falling below the Dcritical (0.05) threshold. This combined with the Hotelling's T^2 plot showed that all samples were compositionally similar and that there were no outliers to the model.

Whilst all samples were compositionally similar it was important to determine the effect of the extracted tissue mass on metabolite composition. Looking at the PCA scores plot (Figure 2.6A) it can be seen that there was no bias in the distribution of samples based on the tissue mass, with low and high mass samples clustering together within the plot showing that they possessed high levels of compositional similarity. As well as looking at the effect of sample mass on the compositional similarity it was important to assess its effect on the abundance of individual metabolites. Figure 2.7 shows the abundance of 9

annotated metabolites from both HILIC and RP methods plotted against the tissue mass, these plots show no relationship between metabolite abundance and sample mass, with the strongest correlation being for glutamate (r = -0.24). This data shows that using between 3-17 mg of sample material had no effect on the overall sample composition or the abundance of individual metabolites, showing this method can provide broad metabolite coverage when sample material is limited.

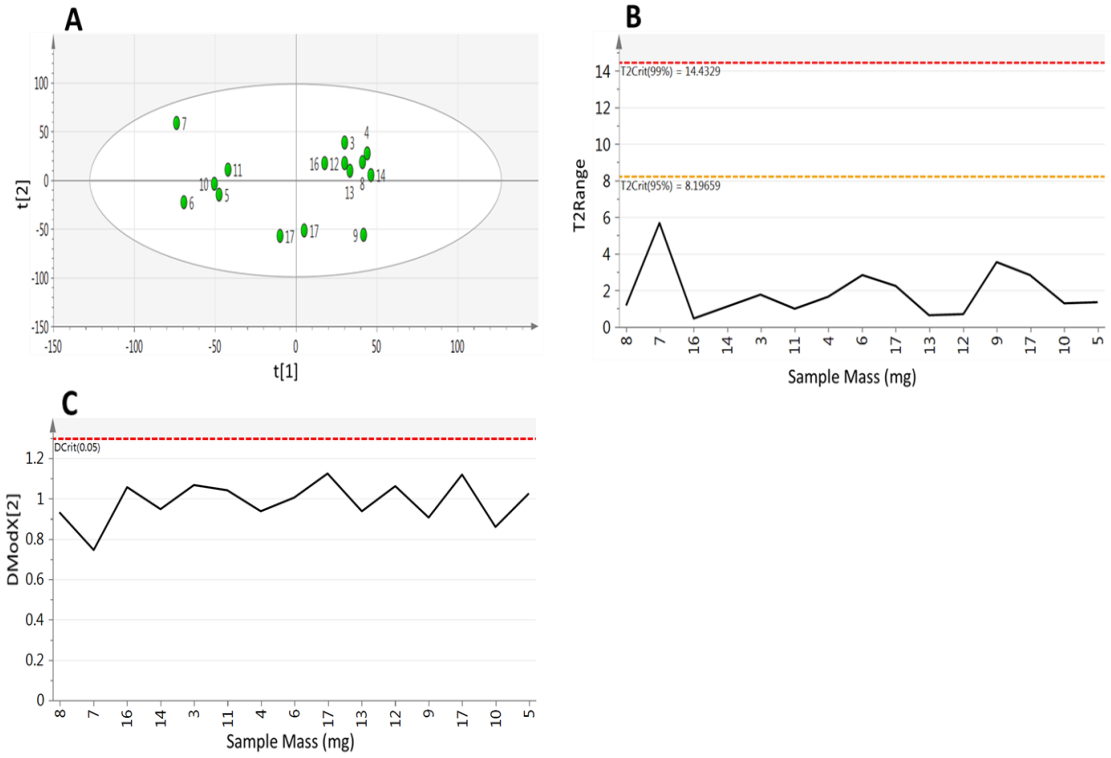

Figure 2.6 Principal component analysis of 15 brain samples ranging from 3 – 17 mg (components = 2, R^2X 0.354, Q^2 0.049) of metabolite features identified in at least 73% of samples in experiment 2. A) Scores plot where point labels represent sample mass B) Hotelling's T^2 and C) DModX plot of analytical samples.

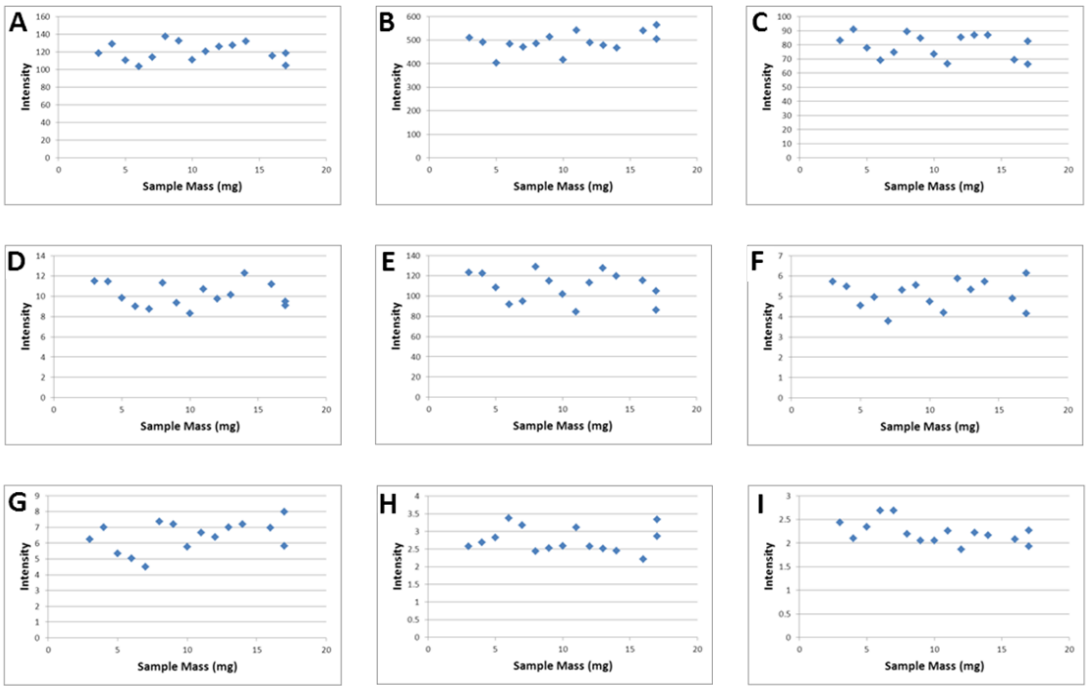

Figure 2.7 Plots of sample mass in mg against intensity for 9 annotated metabolites. A) taurine B) hypoxanthine C) glutamate D) pantothenate E) aspartate F) glcosylceramide (36:1) G) phosphatidylethanolamine (38:4) H) ceramide (38:1) I) triglyceride (48:3).

2.3.3 IVDE method optimization

Extraction solvents

For the extraction of metabolites from human brain, there are various methods. Traditional method includes Folch "a gold standard" method which involves lipids extraction using chloroform as the extraction solvent. The traditional Folch method procedure results in formation of protein precipitate in the middle between the chloroform lower layer and methanol upper layer [259]. This makes the sample collection a hard process. In contrast, in IVDE, MTBE results in protein pellet formation at the bottom of the vial with two solvents layers located above protein precipitate, allowing for low risk of column blockage by protein and direct and simple injection of solvent layers in to the LC-MS, which in turn minimises analytical variability due to sample collection and transfer (This is managed by adjusting needle height automatically).

The traditional Folch method using chloroform with a glass-glass homogenization method has been compared to bead mechanical homogenization with MTBE, with the later providing significantly improved efficiency and reduced time for sample preparation [260].However, no change in term of lipid species composition were observed when comparing the two extraction methods. Extensive testing of MTBE extraction performed by Matyash et al [261], shows that the use of MTBE provides similar or better recoveries of species of most lipid classes when compared with the Folch or Bligh and Dyer methods [259, 262].

MTBE was used as extraction solvent for the upper lipidome phase as in the original plasma IVDE method. Furthermore, the described brain IVD Extraction method has the advantages of performing extraction and analysis within the same vial. A study examined seven extraction methods along with series of chromatographic and detection methods, this resulted in the design of "all in one" extraction and increasing metabolic coverage. This emphasized the importance of expanding metabolic range through sample pre-treatment optimization [263]. Another study has investigated combining the polar and non-polar fractions "Dual Extraction" concluded the that the best protocol for non-polar and polar metabolite profiling is by aqueous extraction using water: methanol preceding extraction using organic solvent of dichloromethane: methanol [264]. Chen et al 2013 also developed a MTBE extraction protocol using limited amounts of tissue, resulting polar and non-polar fractions were pooled, evaporated and reconstituted in the appropriate solvent for UHPLC/MS analysis. However, this required separate extraction, drying down, and multiple transfer steps that will increase the risk of variability and probably sample contamination [265]. In this regard, unsaturated lipids species for example can be easily oxidized, thus steps of drying down and transfer must be carried out carefully to avoid metabolite modification and sample loss.

Development of LC-MS parameters

Although the injection of pure organic solvent (MTBE) is not recommended, no effect was noticed in terms of separation and reproducibility of early eluting peaks. Apart from the simplicity of the extraction and injection procedure offered by IVDE method, most

importantly, it eliminates the drying and re-suspension step that would reduce the instrumental variability and oxidation effect on lipids species. High throughput analysis is being widely preferred. The gradient length for the positive mode RP analysis has a run time of 51 min with the negative having a shorter run time of 35 min due to fewer species ionising in the negative mode such as DG species that do not ionise well in this mode and thus less separation time was needed.

2.3.4 Putative metabolites annotation

Having demonstrated the sensitivity and reproducibility of the metabolite features measured by the analytical method, the final step is to demonstrate its biological relevance by linking the data directly to metabolism by annotating metabolites from a variety of chemical classes and across a range of concentrations. To do these 200 metabolites, 100 from both the HILIC and RP methods were annotated (Appendix A Tables 2.1 and 2.2). The annotated metabolites come from a wide range of metabolite classes including amino acids, purines, phospholipids and glycerides, across 3.5 orders of magnitude ranging in abundance from 0.1 to 576.9. There is limited overlap between the two analytical methods with no identified metabolites in common, this limited overlap demonstrates the necessity of using complementary separation techniques like HILIC and RP chromatography to obtain a comprehensive view of all chemical space. These annotations enable the method to be easily compared as basal metabolite abundance in the rat's healthy cerebellum and provide valuable information allowing the method to be accurately replicated by other laboratories.

The features were preliminary identified using open access databases such as human metabolome database (HMDB) (www.hmdb.ca/) and the equivalent METLIN (METaboliteLINK) database (http://metlin.scripps.edu/). Using the HMDB allowed an indication of the molecular classes.

A set of rules were enforced in the identification database searching process to be as consistent as possible. These rules are listed and explained below as following:

- 0.05 Dalton (Da) error

The use of 0.05 Da as mass error for database search. This falls within the accuracy of the Waters Xevo® MS and confirmed by our external calibration.

- Polarity

The features in each instance realistically ionise in the polarity being observed. For example, Triacylglycerides generally only observed in positive ionization mass spectrometry (unless they have formed adduct in the ionization source).

- Human Biology

HMDB search retrieve feature search and indicates the human biology of whether this feature has been extracted from human tissue and reported in the literature.

- Retention Time

RT and chemical properties of the feature like partition coefficient were considered. For example, molecules with similar polarity often elute in the same region of the chromatogram and metabolites with small or even negative log(p) elute early in the RP chromatogram. This was taken in consideration when completing database search.

- MS^2 fragmentation

All data was collected by Waters Xevo QTOF which used MS^e technique, two collision energies applied that grant data collection at two levels. The first level obtained data using 5 V of collision energy, the second level obtained data at higher collision energy of 50 V. This can assist in structural elucidation and to simultaneously collect accurate mass, parent ion and fragmentation data.

From identification results listed in Appendix A, Table 2.1 & 2.2, annotation suggests different classes of lipids and polar molecules upon performing HILIC and RP analysis respectively.

.

2.4 Conclusions

The method described in this chapter combined both RP and HILIC is shown to be capable of measuring over 4,000 metabolite features from as little as 3 mg of tissue with a high degree of reproducibility. This performance is an improvement on previously described methods in both the number of metabolite features measured and the sample mass from which they were extracted. A single extraction method producing both a polar and non-polar phase will reduce the required sample mass as well as reduce analytical variability by reducing the number of steps involved in sample preparation. The polar phase was analysed in positive and negative modes following separation on a HILIC in which 2,838 metabolite features were consistently measured, representing metabolites including amino acids, sugars and purine bases. The non-polar phase was also analysed in positive and negative modes following separation on reverse phase from which 1,183 metabolite features were consistently measured, representing metabolites such as phosphatidylcholines, sphingolipids and triacylglycerides. It is hoped that the low required sample mass and improved sensitivity of this method will provide a valuable tool with which to analyse the previously poorly explored area of cerebral metabolism, hopefully providing new insights into the functioning of the brain as well as the mechanisms of pathology of neurological disorders.

In the next chapter, the aim was to expand the metabolome range using GC-MS analysis. This is to test the applicability of using the remaining extract volume from the LC-MS brain IVDE method (presented in this chapter). Brain tissue is very precious and i wanted to explore the ability to develop a GC-MS method directly from the same vial to extract new classes of metabolites and increase the metabolic coverage.

Chapter 3: GC-MS Metabolomics of rat brain tissue: An untargeted approach

3.1 Introduction

Multi-parallel techniques are required in metabolic fingerprinting in order to gain a broad metabolic profile, especially in tissue, which contains both non-polar and polar metabolites [244, 266]. Among all these techniques, NMR and MS are the main detection techniques used in metabolomics research [249, 267, 268].

MS is often coupled to chromatographic technology and this called combined techniques which combine the advantage of separation power of chromatographic technology (i.e. LC, GC and CE) and the high sensitivity and selectivity of MS spectrometry, allow a much finer degree of compound identification than each unit used separately [249, 269]. However, the downside to increasing metabolite coverage will be a significant increase in the amount of tissue required.

The first combined instrument was the GC-MS in 1950s and has been described as the gold standard in metabolomics allowing quantification and identification of thousands of compounds in biological samples. It is a quick and accurate technique that offer screening of hundreds of metabolites from different chemical groups after sample extraction and derivatization making it an efficient technique for diagnosis and screenig [270-272] even though it has its own limitations [273, 274] .

GC-MS is still one of the most popular global analysis methods due to the fact that GC offers a stable, sensitive and high-resolution separation system and electron impact (EI) and a mass spectrometer providing each component a mass spectrum. EI is a hard ionisation method which can offer a lot of information about the identity of a compound through fragmentation and there are a number of databases available assisting with compounds identification. In the case of LC-MS, metabolite identification is more time consuming as the ESI interface does not cause fragmentation of molecular ions as EI does and there are few available ESI mass spectral libraries. The major disadvantage of GC-MS is that compounds must be volatile and thermo-stable. Non-volatile, polar compounds could be converted into volatile compounds through derivatization prior to analysis, this possibly causes variability and concentration losses during sample preparation [275-278].

The aim of this chapter therefore was to develop GC-MS method to maximise brain metabolite coverage analysis for comprehensive metabolomic approaches. This involve using remaining extract of brain IVDE LC-MS analysis (discussed in Chapter 2). Extraction solvent was directly analysed using GC-MS following derivatisation. Firstly, the analysis conditions were optimized and tested. Secondly, large number of metabolites including sugars, sterols, organic acids, fatty acids and other cyclic metabolites were efficiently detected by this GC-MS method. The unique identity of metabolites identified demonstrates the need to combine complementary separation techniques (e.g. HILIC-LCMS, RP-LCMS and GC-MS) in the study of chemical composition of tissue to obtain a global view of metabolome.

3.2Materials and Methods

3.2.1 Chemicals and Reagents

LC-MS grade water, LC-MS grade acetonitrile, were purchased from VWR international (UK), LC-MS grade methanol, N, O-Bis(trimethylsilyl)trifluoro-acetamide (BSTFA) with 1% trimethylchlorosilane (TMCS), N-Methyl-N-(trimethylsilyl)trifluoroacetamide (MSTFA), and LC-MS grade toluene were purchased from Sigma-Aldrich (UK).

3.2.2 Brain Materials

Brain tissue samples used for the experimental design were obtained from rat cerebellums which were harvested as per Schedule 1 of the Animal (scientific procedures) Act of 1986-King's College London.

3.2.3 Extraction procedure

The extraction procedure involved brain preparation according to brain IVDE method (described in Chapter 2), the remaining of both non-aqueous (NAQ) and aqueous (AQ) phase extract after the LC-MS analysis was split for the purpose of derivatization prior to GC-MS analysis. Since very few studies have used GC-MS for the analysis of brain tissue, more optimization and validation to develop untargeted GCMS method was required.

3.2.3.1 GC-MS derivatisation Procedure of NAQ and AQ phase

The derivatisation procedure involved adding 80 µL of upper NAQ phase **or** 40 µL of lower AQ phase into separate vials. This amount was dried down under a stream of nitrogen gas at 37^{o}C. Samples were then re-suspended in 1:1 solution of acetonitrile and the derivatising agents N, O-Bis (Trimethylsilyl) trifluoroacetamide (BSTFA) and 1% Trimethylchlorosilane, and were incubated at 37^{o}C for 1 hour using Thermo-scientific Reacti-therm III heating module. Following incubation, samples were again dried down under nitrogen using Thermo-scientific Reacti-VAP III evaporation unit and were subsequently re-suspended in 25µl of toluene for analysis. Full details of the experimental design and optimization process performed to obtain the above-mentioned GC-MS derivatisation procedure for NAQ and AQ phase can be found below in Section 3.2.4.

3.2.4 Experimental Design of GC-MS brain IVDE method

In this study we performed four experiments for GC-MS method optimization. Experiment One, was designed to assess the impact of sample volume on method performance. This was done by preparing 5 individual IVDE, then different sample volume ranging from 20 µL to 80 µL for the NAQ (Upper phase) and 10 µL to 40 µL for the AQ (Lower phase) were taken, this underwent parallel derivatization (02:01 sample: reagent) and injected into the GC-MS (Figure 3.1).

Experiment two, was designed to assess the effect of derivatising agent volume on method performance. This was done by preparing 5 individual IVDE. Different sample volume to derivatising agent volume (04:01,02:01 and 01:01) were investigated.

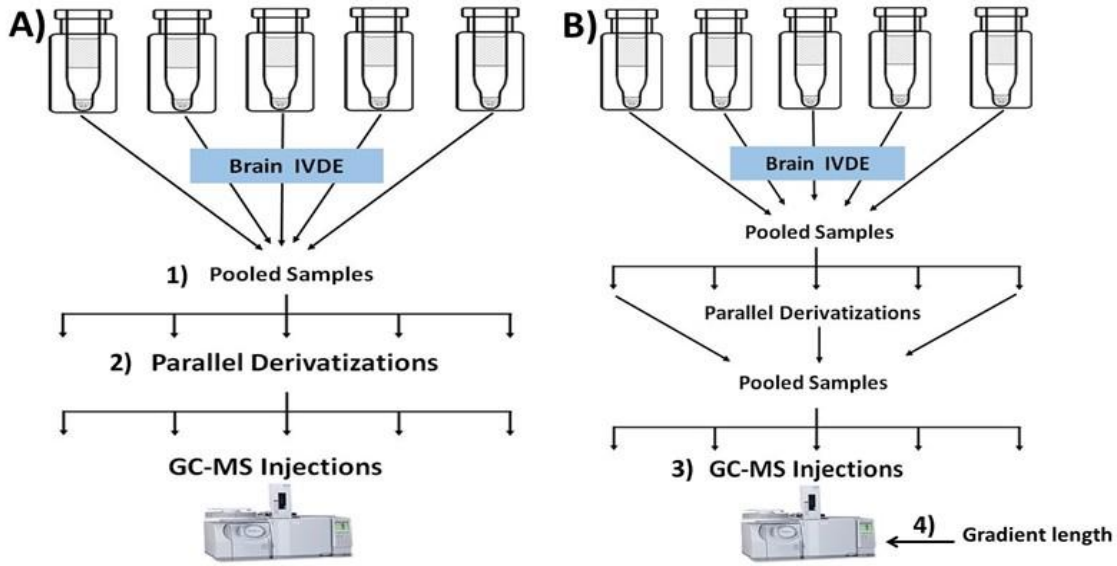

Figure 3.1: **Graphical representation of the experimental designs used.** A) Experiment 1, involved preparing 5 independent IVDE extracts followed by 5 parallel derivatization using different sample volumes. B) Experiment 2, involved preparing 5 independent IVDE extracts followed by 5 parallel derivatization prior using different sample volumes to derivatising agent ratio. B) Experiment 3, involved preparing 5 independent IVDE extracts followed by 5 parallel derivatization using different sample injection volumes into the GC-MS. B) Experiment 4, involved preparing 5 independent IVDE extracts followed by 5 parallel derivatizations prior using different gradient lengths.

Experiment Three, aimed to determine the effect of increasing the volume of sample injected (0.5 µL, 1 µL, 2 µL and **4 µL**) on the number and intensity of metabolite peaks (Figure 3.2). While experiment Four, aimed to determine the effect of gradient length on the observed metabolite peaks number and abundance. To do this, 5 parallel derivatisation of both Aqueous (short= 22mins, medium**= 33mins** and long= 50mins) and Non-Aqueous (short= 32mins, **medium= 49mins** and long= 64mins) gradients was performed (Figure 3.2).

Further experiment, involved applying the optimal parameters selected from experiment 1,2,3 and 4. This experiment purpose is to identify the number of metabolite features measured following GC-MS analysis and to assess the precision of these peaks. This involved preparing seven independent IVDE's and derivatisation of both AQ and NAQ phases. Additionally, the normalization method was tested. This involved applying signal

to noise threshold (S/N) followed by Total Ion Count (TIC) normalization. To do this, extraction blanks were prepared by performing IVDE extraction without adding plasma or tissue homogenate and this was used to perform noise filtering based on signal to noise ratio>5 to remove features (mass/RT) that could interfere and give false signal of metabolites.

3.2.5 GC-MS Analysis Set-up

GC-MS analysis was carried out on a Shim adzu QP-2010 with an AOC-20S auto sampler and AOC-20i auto injector (Shimadzu, Kyoto, Japan). The aqueous (AQ) phase was analysed in split less mode with 4µl of sample injected on a BP5MS capillary column (length 30m, thickness 0.25mm, diameter 0.25mm). The carrier gas (helium) pressure was 79.5Kpa, with a total flow of 125ml/min, a column flow of 1.18ml/min, a linear velocity of 40cm/sec and a purge flow of 6ml/min. The gradient temperature started at 80^{o}C and was held for 5 minutes followed by a linear increase of 10^{o}C per minute to 200^{o}C, where the rate of increase was slowed to 2^{o}C per minute to a final temperature of 225^{o}C and was held for 4 minutes. Analysis of 1µl non-aqueous phase (NAQ) was performed in the split less mode on the same column. The carrier gas (helium) pressure was set to 86.2Kpa with a total flow of 122.8ml/min a column flow of 1.16ml/min, a linear velocity of 40cm/sec and a purge flow of 6ml/min. The gradient temperature started at 100^{o}C and was held for 5 minutes followed by a linear increase of 15^{o}C per minute to 250^{o}C, where the rate of increase was slowed to 2^{o}C per minute to a final temperature of 310^{o}C where it was held for 4 minutes. Mass spectral analysis of both phases was performed using electron ionisation between 50 and 600 *m/z* with an ion source temperature of 200^{o}C, an interface temperature of 280^{o}C with a scan speed of 833 and an event time of 0.2 seconds.

3.2.6 Data Processing and Analysis

GCMS Real Time Analysis (Shimadzu, Kyoto, Japan) was used to acquire GC-MS data. This later imported to GCMS Postrun Analysis file converting utility where GC-MS raw data were converted to mzXML format. Next, the converted data files were imported into XCMS software package in R for data pre-treatment which was followed by normalization

to total peak area (S/N=3 and S/N=5) in Excel. Both raw and normalized data were used to test the reproducibility of the optimized GC-MS protocol. The workflow proposed here is shown in Figure 3.3. Metabolite identification was achieved by using NIST and IEM libraries in GCMS Postrun Analysis software (Shimadzu, Kyoto, Japan).

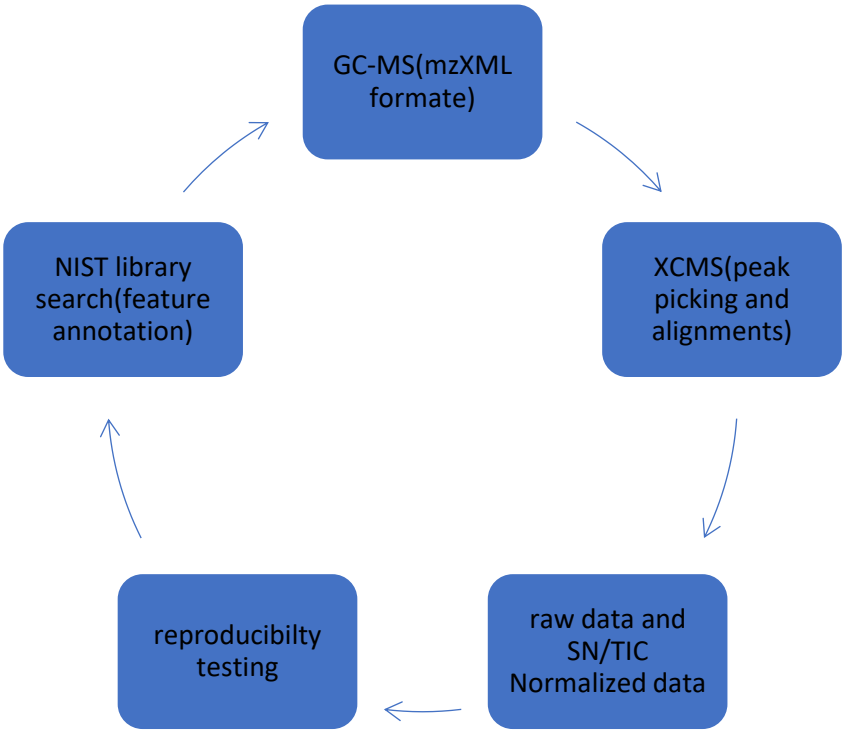

Figure 3.2 Proposed workflow of GC-MS Data processing.

3.3 Results and Discussions

3.3.1 GC-MS materials selection

- AQ phase sample volume optimization

Sustainable use of sample further itself and therefore LC-MS over fill loop optimization of the IVDE lower AQ phase was tested. The AQUITY UPLC® system was set to different injection loop volumes. These mainly fall into two modes: Full Loop mode (FL) and Partial

Loop with Needle Overfill (PLNO). Both injection modes were compared using LC-MS. This was only applied for the AQ phase due to the small volume of the lower AQ phase (50µL) returned after LC-MS analysis. To recover more sample volume, PLNO was applied and I.S recovery (% RSD) and signal intensity were observed and compared with FL (which was used for the LC-MS brain IVDE method in Chapter 2). It was observed that using PLNO mode caused 11% drop in signal intensity which would cause loss of the low concentration metabolites with low reproducibility also for IS compared to that observed with FL. This showed that FL provided better recovery than PLNO. Therefore, FL was selected and the method optimization for the AQ phase was carried out using the 50µL volume.

- Derivatization procedure selection

The method used for derivatisation was based on previously published sterol targeted GC-MS method [260] and this method was adapted and modified. This method needs a long extraction time, often for several hours and requires large quantities of samples and organic solvents, some of which are toxic. Moreover, this method can also expose samples to excessive heat or oxygen which might cause the oxidation of active ingredients and the reaction between different components. Modification of this method to a simple derivatisation step was applied to both the NAQ and AQ phases (for details see section 3.2.3.1). We were able to detect many compounds including but not limited to sugars, sterols and fatty acids with high reproducibility.

GC-MS in full scan mode is used for untargeted metabolic profiling and the detection of new metabolites [279]. As mentioned previously, GC-MS has limitations in the analysis of polar compounds due to their low volatility therefore compounds for analysis must first be derivatised to increase volatility and stability. Prior to analysis by GC-MS, derivatisaing agents like a silylating reagents are used to derivatise amine, and thiol groups. There are two main classes of silylating reagents: those producing trimethylsilyl (TMS) derivatives including N,O-bis-(trimethylsilyl) trifluoroacetamide (BSTFA) and N-methyl-N-(trimethylsilyl)-trifluoroacetamide (MSTFA), and those producing tert butyldimethylsilyl (TBDMS) derivative which produced by reaction with N-methyl-N-(tert-

butyldimethylsilyl) trifluoroacetamide (MTBSTFA) [280]. Often higher reproducibility and resolution can be achieved by GC-MS when compared to LC-MS with the latter advantage over the classical GCMS procedures is the reduced complexity in sample preparation by elimination of derivatisation steps before the chromatographic separation.

Several parameters were investigated at this stage including the selection of the derivatising reagent, reconstitution solvent, incubation temperature and time. The selection of these parameters are important aspects to achieve the optimal metabolites analysis using GC-MS.

To start with, two silylation reagents MSTFA and BSTFA were compared. This accomplished by samples dried by nitrogen then, 40µL of derivatizing reagent was added to the NAQ and AQ residue, then peaks were integrated with no significant difference were observed. Owing to BSTFA low cost, it was decided to be used in this study.

Toluene and acetonitrile were tested as reconstitution solvents for polar as well as catalyst in the derivatization reaction. Figure 3.4 shows the GC-MS analysis results. It can be clearly seen that under the same GC-MS condition, toluene provides a better peak shape and more information than acetonitrile. In chromatogram A (Acetonitrile), peaks are fronting and not separated while in chromatogram B (Toluene), peaks are sharp and well separated. Thus, toluene was chosen as the dissolving solvent. Additionally, different reaction time (includes 30-60 and 120 mins) and temperature (37°C -57°C and 75°C) were employed and 37°C for 60min was selected to be the optimal reaction conditions. Hexane is usually favoured as an extraction solvent for GC-MS analysis of non-polar metabolites, For the non-polar (MTBE) phase, toluene and hexane were tested as reconstitution solvent to extract the non-polar and semi polar metabolites. Following derivatization and drying down, both toluene and hexane were tested as reconstituting solvents and no difference was observed.

A B

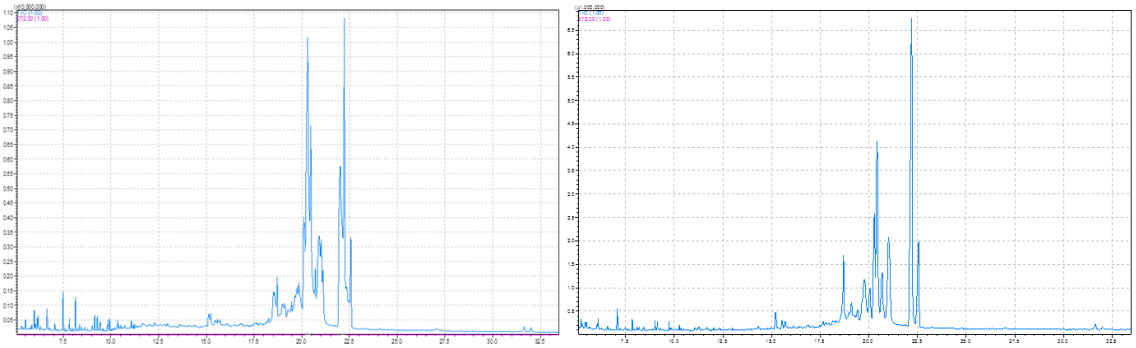

Figure 3.3 Total ion current chromatograms of rat brain A) Acetonitrile as the redissolving solvent. B) Toluene as the redissolving solvent.

3.3.2 GC-MS Method Optimization and parameter selection

- Sample Volume (Experiment One):

The first step in validating the method was to determine if increasing the volume of sample material derivatised would increase the number and intensity of the observed peaks. 80uL for the NAQ and 40uL for the AQ was used as the maximum sample volume that can be recovered from the IVDE after it being injected in to the LC-MS. It can be noticed that the effect of increasing sample volume was proportional to the number of peaks and abundance of metabolites peaks. Additionally, applying normalization using S/N cut off of 3 and 5 has improved the number of peaks (Figure 3.5). The abundance of five identified metabolites were also reported (Figure 3.6). Metabolites relative abundance was dramatically increased with increasing sample volume.

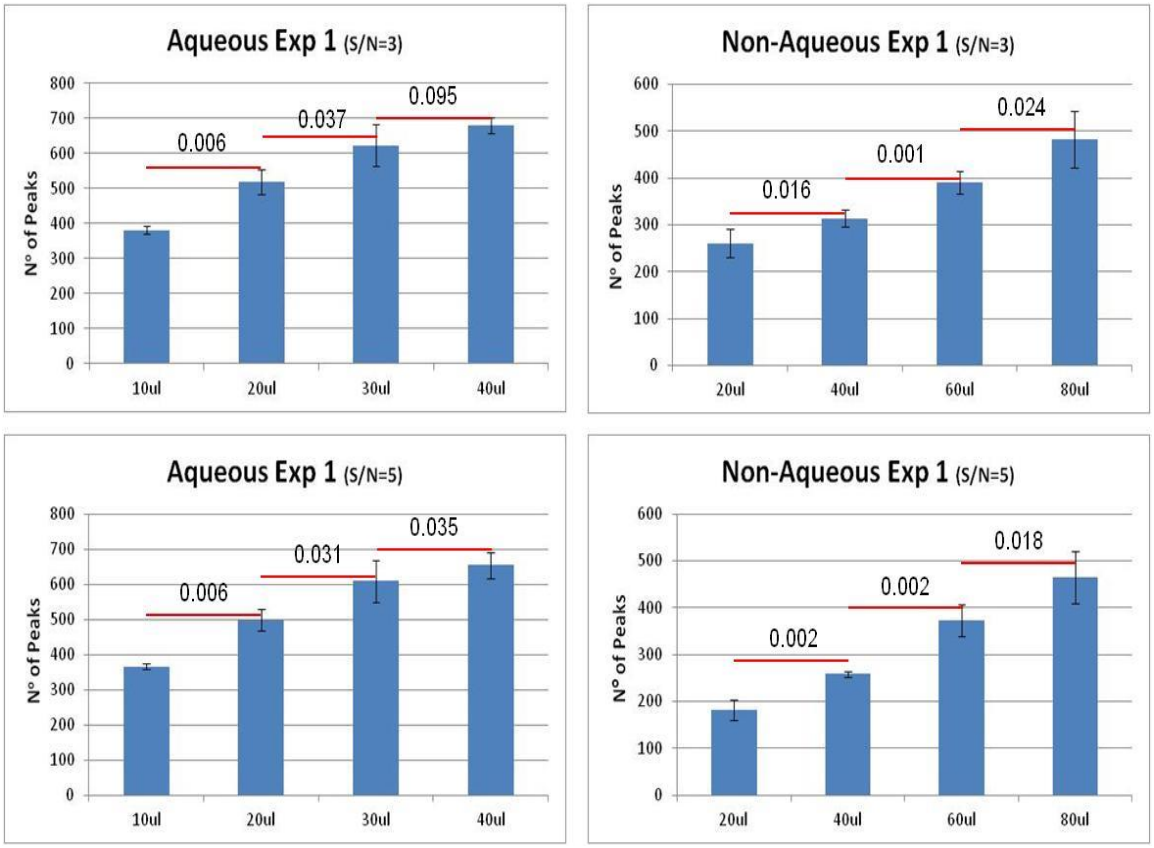

Figure 3.4 Number of peaks obtained at different sample volumes for AQ and NAQ phase with signal to noise normalization threshold of 3 and 5. Error bars signify standard deviation.

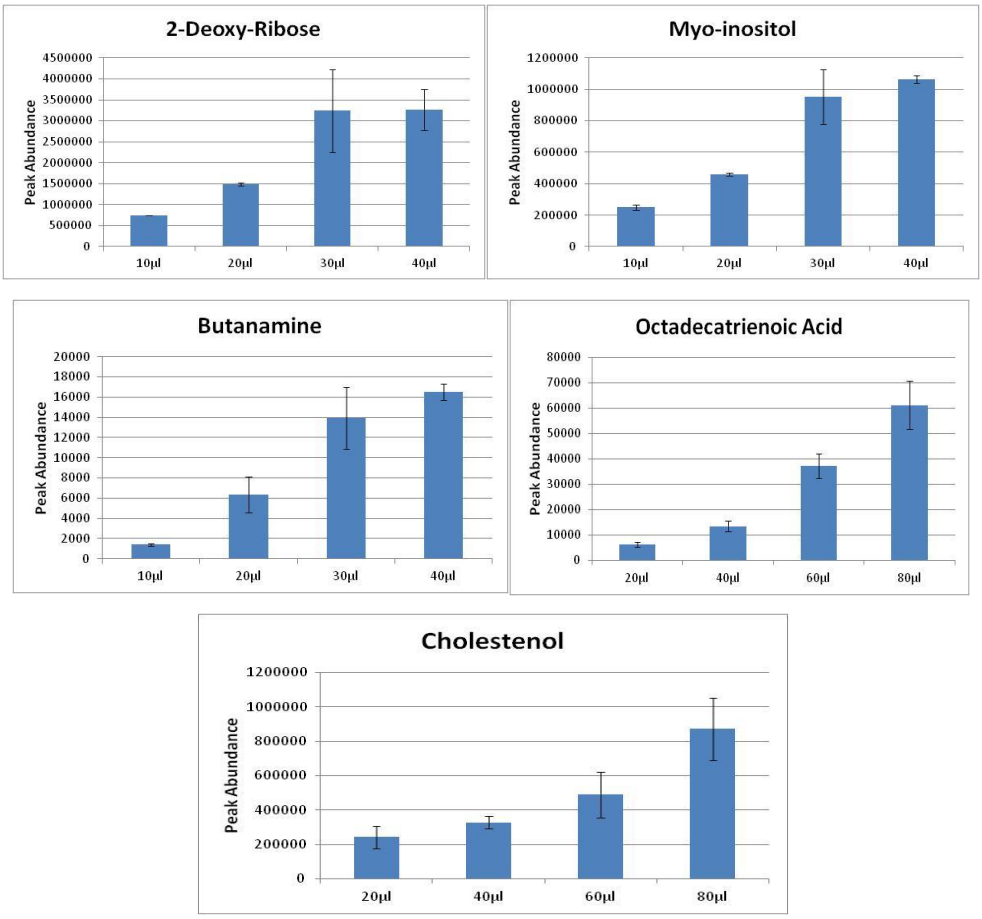

Figure 3.5 Peak intensity of 5 annotated metabolites using different sample volumes. Error bars signify standard deviation.

- **Derivatising reagent (Experiment Two):**

A slight increase can be seen in the number of peaks detected at 02:01 ratio compared with 04:01 ratio, with no difference or less peaks detected in 01:01 compared to 02:01 ratio (Figure 3.7). Furthermore, up on observation of individual metabolite abundance (Figure 3.8), the 04:01 ratio showed inconsistent trends, hence better peak intensity was reported at 01:01 ratio for most metabolites.

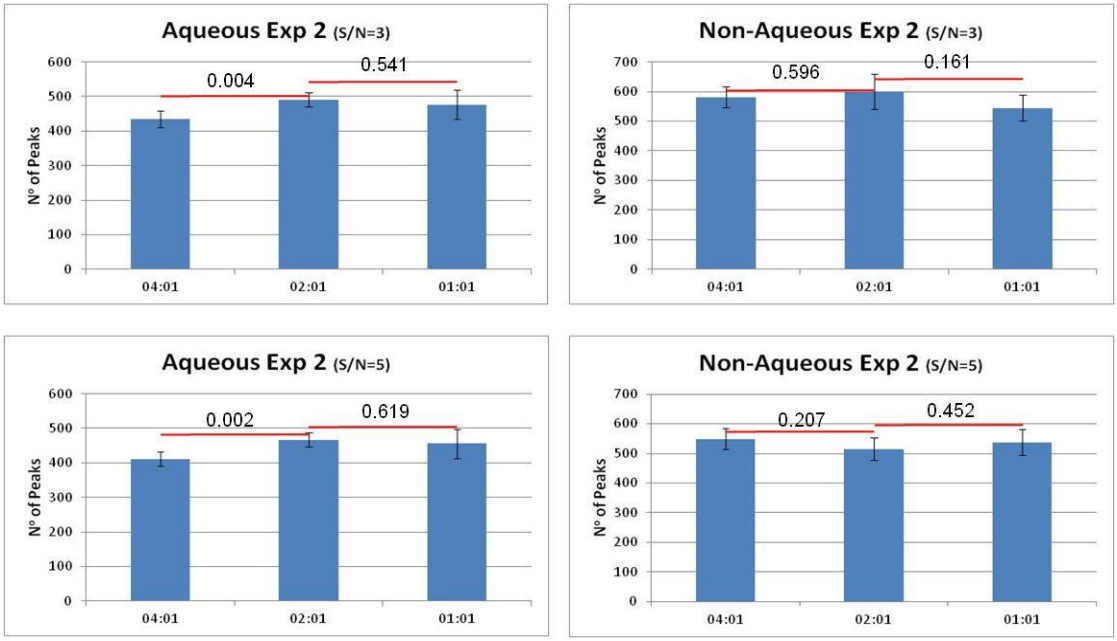

Figure 3.6 Number of peaks at different sample to derivatising agent ratio following signal to noise normalization. Error bars signify standard deviation.

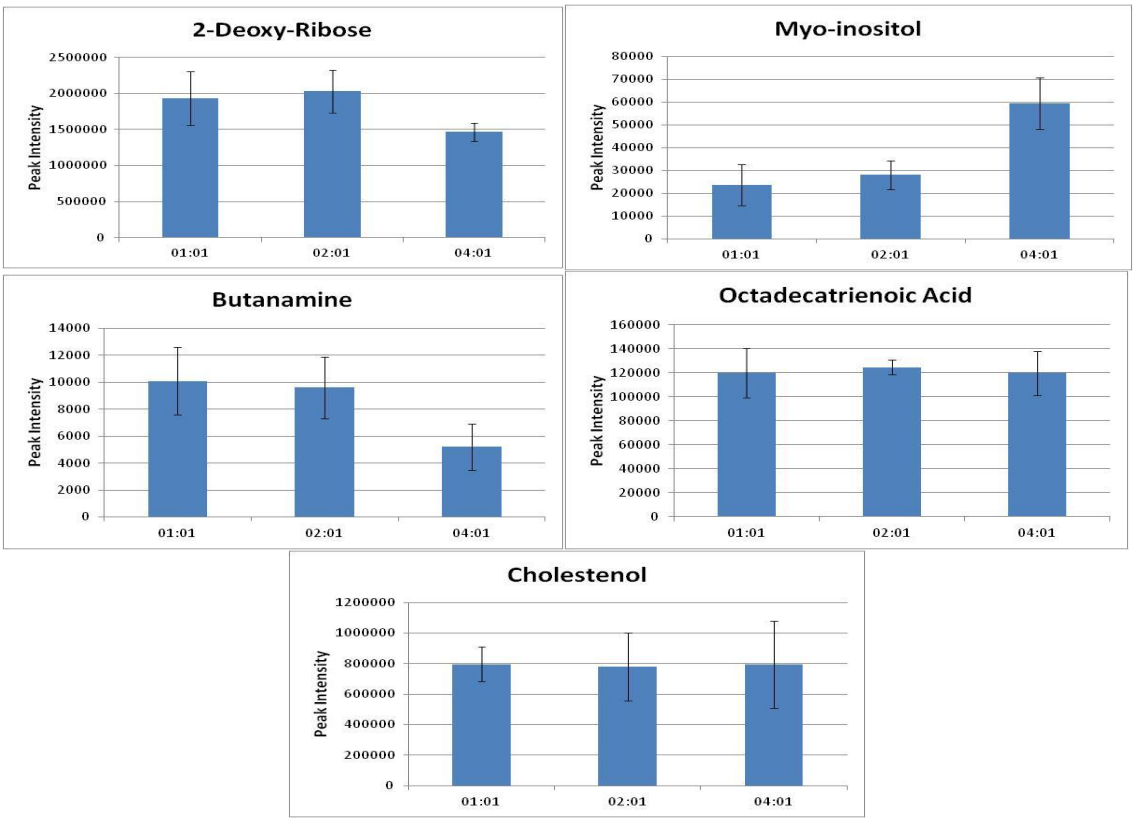

Figure 3.7 peak intensity of 5 annotated metabolites using different sample to derivatising agent proportion. Error bars signify standard deviation.

- **Injection Volume (Experiment Three):**

A significant increase in number of peaks in order of 0.5µL<1µL<2µL < 4µL of injection volume (Figure 3.9) were obtained. The same observations were seen in term of peak intensity (Figure 3.10).

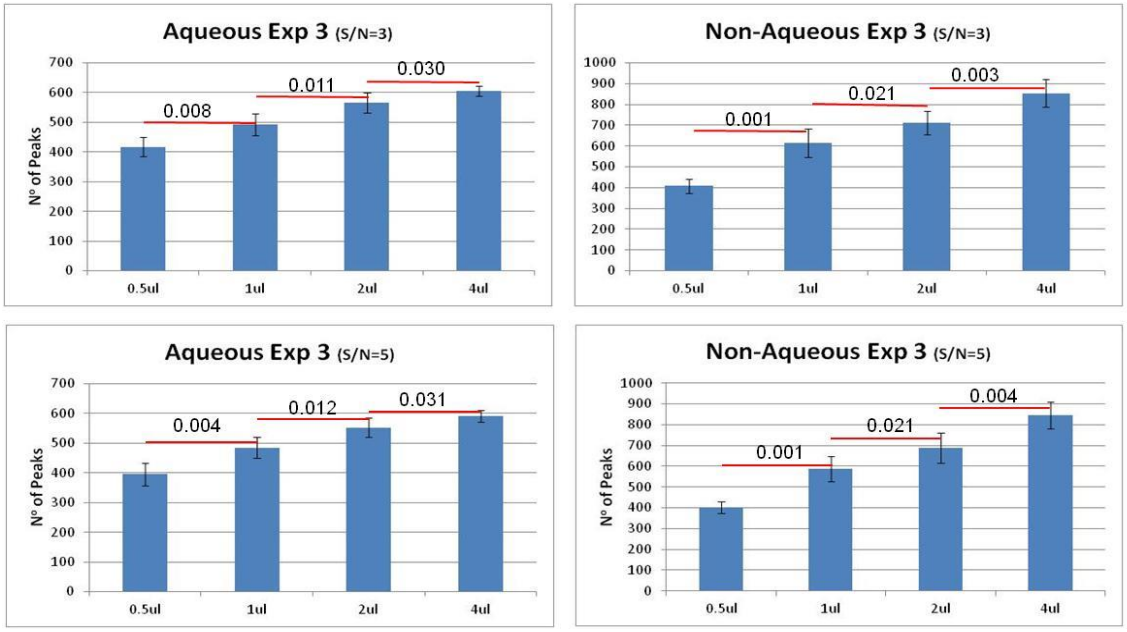

Figure 3.8 number of peaks obtained after using different injection volumes. Error bars signify standard deviation.

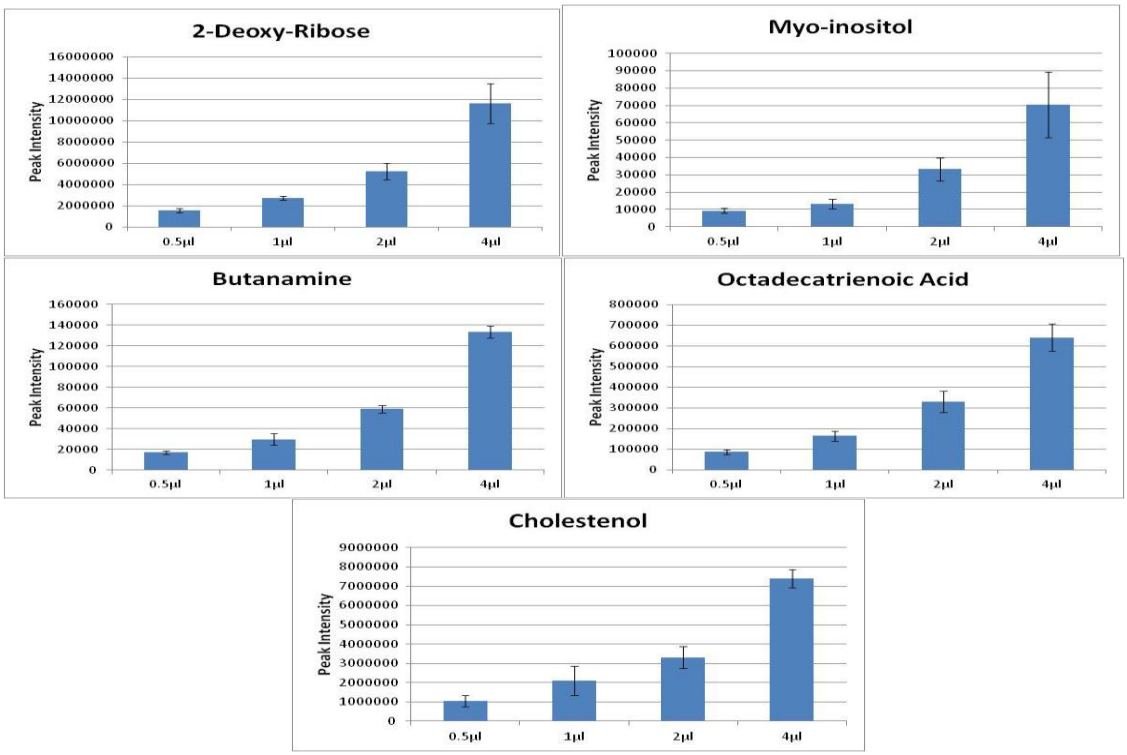

Figure 3.9 Peak intensity of metabolites at different injection volumes. Error bars signify standard deviation.

- **Gradient Length (Experiment Four):**

This study shows that increasing the gradient length increased the number of peaks detected. The short gradients (AQ=22mins and NAQ=34mins) measured the most peaks per minute, even compared to the 38 mins combined gradient (Figure 3.11). Moreover, we tried combining both phases, however, few peaks were obtained and therefore both phases were analysed separately. It can be clearly seen that less number of peaks were obtained using combined gradient compared to short, medium and long gradient lengths (Figure 3.12).

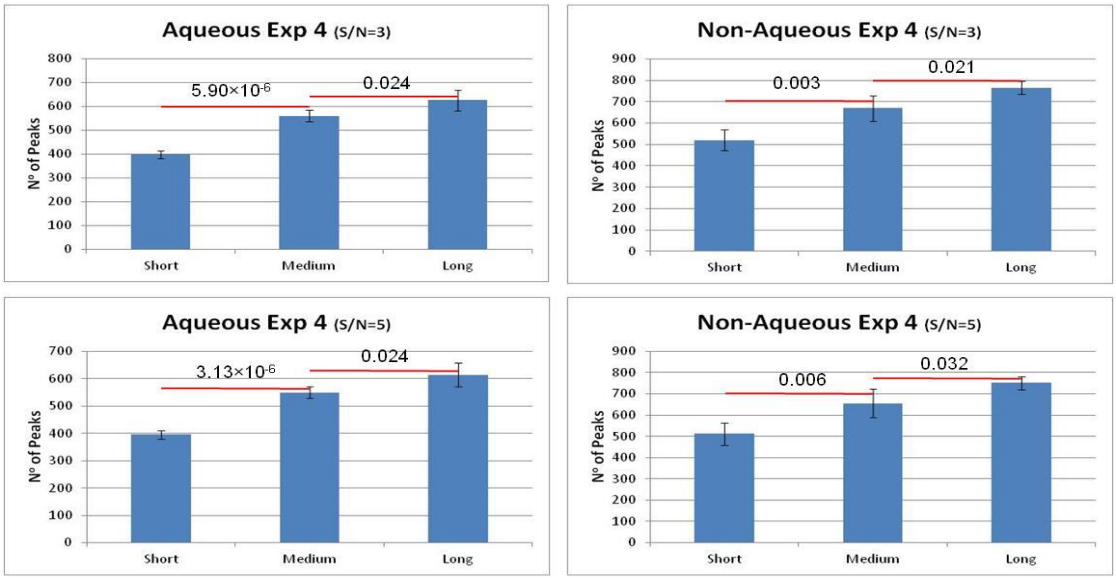

Figure 3.10 Number of peaks detected based on using different gradients length. Error bars signify standard deviation.

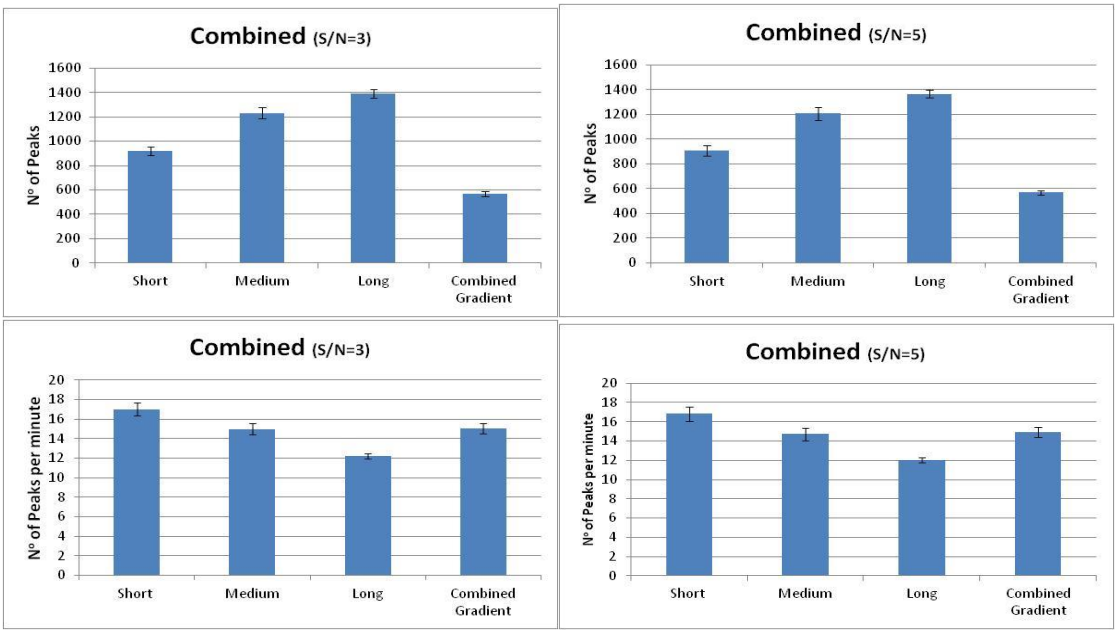

Figure 3.11 Number of peaks obtained when analysing both aqueous and non aqueous phase at different gradient lengths and combined gradient. Error bars signify standard deviation.

3.3.3 Reproducibility test of the proposed method (Experiment Five):

- Raw data reproducibility

This experiment aimed to study the reproducibility of the optimized GC-MS IVDE method. Based on the results obtained out of the optimization steps in section 3.3.2. The ideal conditions selected for the GC-MS analysis of the AQ and Non-AQ phase are as following:

Non-aqueous: 80ul of sample derivatised 2:1-1 uL Injection volume -49mins Medium gradient.
Aqueous: 40ul of sample derivatised 2:1-1uL Injection volume -33mins Medium gradient.

This experiment was performed by preparing 7 independent IVDE samples and derivatisations, up on both Aqueous and Non-Aqueous gradients. Following GC-MS analysis, the raw data were transformed to mzXML format, chromatograms were aligned and metabolic features were picked by XCMS. Then the data were normalized to TIC prior to applying signal threshold removal of 5.

Data reproducibility is reported as Relative Standard Deviation percentage (%RSD) with 30% acceptance tolerance was reported for metabolomics studies using GC-MS [281]. Method reproducibility was achieved by identifying a total of 2706 of features present in 100% of samples for both NAQ (1295) and AQ (1431) phase, then those features measured when a minimum of 70% sample cut off was applied. The %RSD results are shown in table 3.1.

Table 3.1 Measured metabolite features in the AQ and NAQ GC-MS method in experiment 5. Showing the number of metabolite peaks identified and their relative variability in 100%, 85%, 71% and 57% of 7 sample replicates. [a] percentage of samples a peak is detected in, [b] coefficient of variance of peak intensity between samples.

	RAW				RAW			
	GC AQ				GC NAQ			
%RSD	100%[a]	85%[a]	71%[a]	57%[a]	100%[a]	85%[a]	71%[a]	57%[a]
< 5[b]	66	74	86	91	103	117	99	102
5-10[b]	82	83	104	138	111	108	131	153
10-15[b]	101	106	114	239	167	199	347	309
15-30[b]	274	289	369	316	1009	1081	2061	2221
> 30[b]	894	981	1077	1142	1884	1931	1980	2168
Total	1417	1533	1750	1926	3247	3436	4618	4953

From the results, it can be concluded that reproducibility of LC-MS (reported in Chapter 2) is better than GC-MS. The variability in GC-MS analysis could be owed to the derivatization process. As mentioned before in GC-MS, the samples need to be derivatized before being injected into the column which will add more sample preparation stages including procedures of drying under nitrogen and transfers, therefore the removal of this pre-analytical steps will reduce the sample variability and processing time. GC-MS chromatography exhibits less matrix effects than LC/MS, this could be that during the derivatisation step, any residue following the extraction can be precipitated. From the result, it can also be deduced that GC-MS can provide reliable chromatographic fingerprinting approach for brain tissue with approximately 3K features detected in all the samples (100%).This result would also suggest brain extract contains a lot of compounds that are made volatile after derivatization.

- Data normalization

The most important part in the processing step is feature detection and selection. Here, a feature is an ion defined by a certain range of mass and RT. This step is usually called "peak detection and picking" in mass spectrometry literature where different signal detection methods are used to find a peak from a real signal in the presence of noise. To define a peak, it is required to meet certain criteria such as peak shape quality or reasonable signal-to-noise ratios. Different commercial and free tools exist for this purpose. In this study we mainly relied on XCMS[282] which is developed in R.

Normalization of the processed GC/LC-MS data is considered before application of any statistical analysis method to the data to minimize undesired bias [283] and avoid misleading results. The bias can be introduced from differences in the analytical procedures, in sample collection, biomolecule extraction, or from column separation nonlinearity and instrument variability [284] . Thus, normalization is used to address and ameliorate these issues. Raw data normalization using S/N TIC has improved %RSD as reported in Table 3.2.

In the raw brain data, the next step in determining the method's performance was to identify the number of metabolite features following GC separation and to assess the precision of these peaks. At this point features were counted as in "featuring" in all 7samples (100%), in 6 samples (85%), in 5 samples (71%), and 4 samples (57%) (Table

3.1), allowing for some noise or low abundant metabolites with high variation. The number of metabolite features measured in both AQ and NAQ phase were a total of 4664 peaks (signal/noise > 5). When the minimum cut off of peaks of 57% applied, 6879 metabolite features where identified.

In 100% of samples, metabolite features were reproducible with 13.5% and 41.5% of features have RSD of <15% and <30% in AQ and NAQ phase respectively. To improve reproducibility data was normalised to total ion count (TIC), with the normalization improving the reproducibly with 19.3% and 50.6% of features have RSD of <15% and <30% in AQ and NAQ phase respectively. The S/N>5 followed by TIC normalization applied has improved the reproducibility of the peaks measured.

Table 3.2 Measured metabolite features in the GC AQ and NAQ phase method in experiment 5. Showing the number of metabolite peaks identified and their relative variability in 100%, 85%, 71% and 57% of 7 sample replicates after transformation based on TIC normalization after S/N of 5. [a] percentage of samples a peak is detected in, [b] coefficient of variance of peak intensity between samples.

	TIC				TIC			
	GC AQ				GC NAQ			
%RSD	100%[a]	85%[a]	71%[a]	57%[a]	100%[a]	85%[a]	71%[a]	57%[a]
< 5[b]	97	110	123	101	148	169	176	193
5-10[b]	108	109	129	146	177	159	206	243
10-15[b]	163	142	209	293	205	252	479	406
15-30[b]	384	395	413	389	1080	1198	2121	2244
> 30[b]	665	777	876	997	1637	1658	1636	1867
Total	1417	1533	1750	1926	3247	3436	4618	4953

3.3.4 GC-MS Analysis Condition

In this study, electron impact ionization energy was set to 70 eV so that the MS spectra could be compared with a GCMS library acquired at the same voltage. To get a better separation, different temperature programmes were tested and the ideal GC condition was described in 1.2.5. An example of temperature adjustment to remove dead volume in GC-MS chromatogram of NAQ phase can be seen in Figure 3.13.

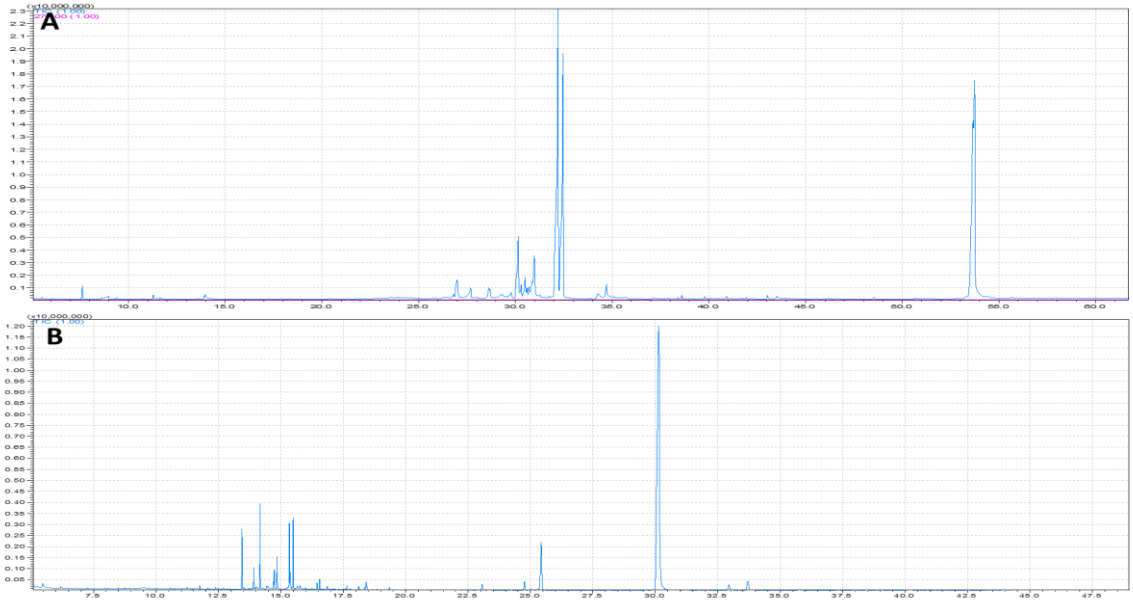

Figure 3.12 Showing (A)Atypical chromatogram of NAQ phase of 60 mins (B) NAQ chromatogram after dead volume removal (47 min). X axis represent the retention time in minutes and Y axis represent the intensity.

3.3.5 Metabolites Annotation

In GC-MS, a list of 60 compounds from both NAQ and AQ run were identified (Appendix B) using NIST and IEM libraries with a similarity index over 90%. These include: amino acids, amines, alcohols, sugars, organic acids, sterols, purines, and fatty acids. GC-MS applies electron ionization mode with 70 eV which can provide a standard spectrum for each compound, so it can compare samples with the database directly. This increases the efficiency in helping to identify unknowns. This is an advantage of GC-MS over LC-MS as in the latter fragmentation is less reproducible between instruments and identification is considered to be harder. GC-MS gives more information on the chemical composition. Therefore, using GC-MS to fingerprint of brain tissue to gain information about the chemical composition was successful. Many new metabolites were detected by GC-MS that could not be detected by LC-MS. These include fatty acids, amines, sugars, alcohols, sugar alcohols, amino-sugars, hydroxyl acids, organic acids, aromatics, sterols and purines.

3.4 Conclusion

In this study, a simple step derivatization procedure was applied for GC-MS analysis of the AQ and NAQ phase of rat brain samples. The GC-MS metabolomics protocol developed in this study achieved analytical reproducibility including data treatment and extracted features that were representative of the raw data. Modification of derivatisation procedures to simple steps provided a wide coverage of various volatile molecules and reported 60 metabolites of those identified in both AQ and NAQ phases(Appendix B-Table 3.1).

It can be concluded that this is a powerful metabolomics platform that can be used for our future brain studies. However, this still needs to be validated for application using complex samples. Therefore, the next chapter will test the applicability of the LC-MS (in Chapter 2) and GC-MS (in this chapter) brain IVDE method by analysing brain and plasma samples (as a proof of concept) of control and AD groups in volunteers. Another point to be addressed in the next chapter is managing and developing a standard data treatment protocol especially concerning the fusion of 6 analytical methods.

CHAPTER4: Multimodal metabolomics combining UPLC-qToF-MS and GC-MS data in human plasma and rat brain tissue

4.1. Introduction

AD is also known to have a long prodromal phase to the disease in which pathology accumulates without the presence of symptoms, making the discovery of a panel of biomarkers that can identify individuals in this phase of the disease highly relevant. A number of biomarker candidates have been frequently reported in the literature are the measurements of protein markers, amyloid beta, total tau and phosphorylated tau in cerebrospinal fluid (CSF) [118, 120, 285-287]. These are considered as lead marker candidates for AD. Moreover, brain imaging such as magnetic resonance imaging (MRI) [102, 288]and positron emission tomography (PET) [289, 290] with observations on specific brain region volume have also been suggested. However, the risk and difficulty in CSF samples collection along with high cost and difficulty in data interpretation of brain imaging suggests a growing need for more accessible biomarkers enable to recognize patients particularly at preclinical stage. Therefore, it is hoped by extending our coverage of the metabolome to include metabolites previously unstudied in AD will aid for this diagnosis approach.

Metabolomics is the unbiased analysis of the composition of small molecule metabolites in a given biological tissue or bio-fluid under a specific set of environmental conditions [291, 292]. In recent years the development of new methods has seen metabolomics progress from a novel analytical technique towards a mainstay of the biological toolbox. However, before this transformation can be completed a number of technical challenges remain to be overcome, foremost among these is maximizing coverage of the metabolome [263, 293]. A number of previous studies have done this by utilizing multiple complimentary techniques including liquid chromatography – mass spectrometry (LC-MS), nuclear magnetic resonance spectroscopy (NMR) and gas chromatography – mass spectrometry (GC-MS) [246, 248, 249, 294] enabling metabolic profiling to be performed in various biofluids such as blood [182, 193, 207, 295-297], urine [207, 298] and saliva [205, 206], demonstrating the easy accessibility of samples and the importance of this approach for the search of potential biomarkers. Another biofluid explored is CSF which is believed to reflect pathology of AD [179, 180, 182, 183]. Few studies presented alteration of metabolites in brain [210, 250, 251] to track metabolic pathway owing to the

scarcity of human brain tissue whereas, many studies alternatively used transgenic AD mice model [220, 221, 252, 253]. However, these strategies require individual sample preparation techniques which significantly increases the volume of sample and potentially variation and analysis time. Therefore, it is hoped by extending our coverage of the metabolome to include metabolites previously unstudied in AD will aid for this diagnosis approach.

The large and complex dataset generated using metabolomics studies is challenging and data processing and pre-processing procedure needed to simplify these data. In LC-MS based metabolomics the raw data are produced in 3-D format and data pre-processing step need to be applied to reduce data dimension to 2-D format. Our laboratory has previously developed a metabolomics workflow using Markerlynx [68], and Chapter 2 dataset processed was based on the established data pre-processing procedures. However, Markerlynx works only for Waters instruments and processes relatively small data sets, thus new data pre-processing techniques were necessary. XCMS was used to process data in this chapter as it has emerged as a powerful metabolomics data processing method. It is available from the R software (free-access programme), and it is highly adaptable to almost all types of LC-MS and GC-MS data sets with the help of format conversion tools [299, 300]

Following data pre-processing, large number of metabolic features will be generated that are difficult to manage and visualize. This raises the need for employing multivariate analysis and modelling (see introduction section 1.5.3 for more details). Models can either be non-supervised method, e.g. principal component analysis (PCA), where outliers and overall data distribution will be assessed, or supervised, such as partial least-squares (PLS), partial least-squares discriminate analysis (PLS-DA) and orthogonal partial least-squares discriminate analysis (OPLS-DA), where grouping of samples is possible to select their descriptive metabolic features or variables [301, 302].

To this end we developed a strategy that enables 6 analytical assays (4 LC-MS and 2 GC-MS) to be applied to a single in-vial dual extraction utilising as little as 3mg of brain tissue [303] or 20µl of plasma [256]. The method was designed to analyse samples in the future such as human brain, prioritising the information acquired over the length of the analysis.

The robustness and utility of this strategy was assessed by combining all the data and applying the method to 7 rat cerebellum samples and a pilot experiment of plasma samples of 20 Alzheimer's patients versus 20 healthy age matched controls split into stable and declining individuals to allow us to assess the ability of the platform to detect both large and subtle metabolic differences.

4.2. Materials and Methods

4.2.1. Chemicals and Reagents

All solvents including acetonitrile, ammonium formate, formic acid, methanol, methyl tertiary butyl ether (MTBE), toluene and water were all LC-MS grade, GC-MS reagents, internal standards and serum used to prepare quality control samples were purchased from Sigma-Aldrich except for acetonitrile which was purchased from VWR international. Three internal standards were added for LC-MS analysis, L-serine$^{13}C_3{}^{15}N$ (95%) and L-valine$^{13}C_5{}^{15}N$ (95%) for hydrophilic liquid interaction chromatography (HILIC), Tripentadecanoylglycerol for reversed phase (RP) and one internal standard for GCMS analysis, Succinic D4 acid for GC Aqueous. Sample derivatisation for GC-MS analysis was performed using N,O-Bis(trimethylsilyl)trifluoro-acetamide (BSTFA) with 1% trimethylchlorosilane (TMCS) purchased from Sigma-Aldrich.

4.2.2. Biological Material

Brain tissue samples were obtained from rat cerebellums which were harvested in the Biomedical services unit, King's College London as per Schedule 1 of the Animal (scientific procedures) Act of 1986. All animal procedures were approved by local animal welfare and the Ethics Review Body (King's College London). Plasma samples from 40 individuals, 20 Alzheimer's patients and 20 healthy controls were collected in Kupio (Finland) for the Addneuromed cohort were selected for analysis. [304]. Patient groups were balanced for age and gender, with mini-mental state examination score (MMSE) balanced between genders within each group (Table 4.1). MMSE was used as the primary cognitive measure, with Alzheimer's disease cooperative study scale – Ability of Daily

Living (ADCS-ADL) being used as a secondary cognitive measure specifically for AD patients.

Table 4.1. Characteristics of study cohort.

	Controls	**Alzheimer's**
Gender[a]	10/10	10/10
Age	74.8 +/- 5.0	75.3 +/- 6.1
MMSE	28.5 +/- 1.4	22.5 +/- 4.6
APOE4[b]	4	11
ADCS-ADL[c]	n/a	48.2 (+/- 16.4)

[a] male/female, [b] number of APOE4(genetic risk factor for AD) positive patients, [c] Alzheimer's disease Cooperative Study scale for Activities of Daily Living.

4.2.3. Plasma and brain samples derivatisation and Quality Control samples (QC) Preparation

The in vial dual extractions (IVDE) were performed as previously described for plasma [256] and brain tissue [303]. Following LC-MS analysis, the remaining aqueous and non-aqueous phases were split into separate vials and dried down under a stream of nitrogen at 37^{o}C. Samples were then re-suspended in a 1:1 solution of acetonitrile and the derivatising agents (BSTFA) with 1% TMCS, and were incubated at 37^{o}C for 1 hour. After incubation samples were again dried down under nitrogen and were subsequently re-suspended in 25µl of toluene for analysis. A graphical description of the analytical workflow used in this study is shown in Figure 4.1below. QC samples (Quality control) were prepared by using commercially available serum samples. Samples were analyzed in a randomized order with QC samples being analyzed after every 6 injections.

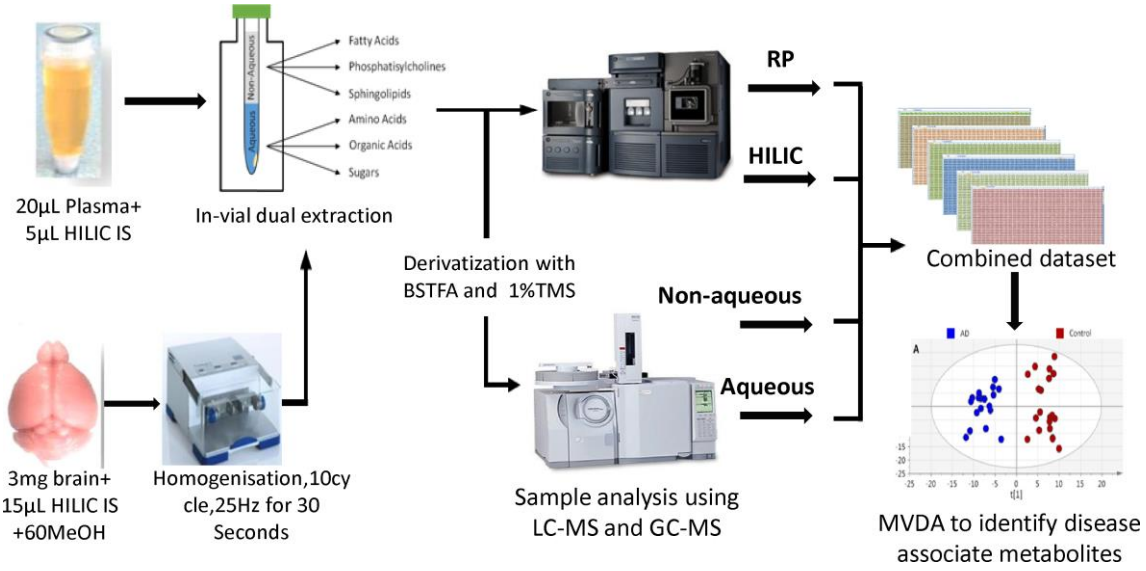

Figure 4.1 Analytical workflow from sample preparation to multiplatform analysis using LC-MS and GC-MS and onto multimodal and multivariate analysis.

4.2.4. Data Acquisition

The HILIC and reversed phase LC-MS analysis was performed on a Waters ultra-performance liquid chromatography (UPLC) system coupled to a quadrupole time-of-flight (Q-TOF) mass spectrometer (Waters, Milford, MA, USA) as described previously[256, 303]. GC-MS analysis was carried out on a Shimadzu QP-2010 with an AOC-20S auto sampler and AOC-20i auto injector (Shimadzu, Kyoto, Japan). The aqueous phase was analyzed in split less mode with 4µl of sample injected on a BP5MS column (length 30m, thickness 0.25mm, diameter 0.25mm). The carrier gas (helium) pressure was 79.5Kpa, with a total flow of 125ml/min, a column flow of 1.18ml/min, a linear velocity of 40cm/sec and a purge flow of 6ml/min. The gradient temperature started at 80^{o}C and was held for 5 minutes followed by a linear increase of 10^{o}C per minute to 200^{o}C, where the rate of increase was slowed to 2^{o}C per minute to a final temperature of 225^{o}C where it was held for 4 minutes. Analysis of 4µl non-aqueous phase was performed in the split less mode on the same column. The carrier gas (helium) pressure was set to 86.2Kpa with a total flow of 122.8ml/min a column flow of 1.16ml/min, a linear velocity of 40cm/sec and a purge flow of 6ml/min. The gradient temperature started at 100^{o}C and was held for 5 minutes followed by a linear increase of 15^{o}C per minute to 250^{o}C, where the rate of increase was slowed to 2^{o}C per minute to a final temperature of 310^{o}C where it

was held for 4 minutes. Mass spectral analysis of both phases was performed using electron impact ionisation between 50 and 600 *m/z* with an ion source temperature of 200^{o}C, an interface temperature of 280^{o}C with a scan speed of 833 and an event time of 0.7 seconds.

4.2.5. Data Processing

Initially all raw data files were converted into an mzXML format, LC-MS files were converted using msConvert (ProteoWizard), whilst GC-MS files were converted using GCMS Solutions® (Shimadzu). Converted data files were analyzed using XCMS [282] performed in the open source software package R, picking was performed using a ”massifquant” method for the GCMS data allows isotope trace feature detection and a ‘'centwave’’ method for LCMS data, allows the deconvolution of closely eluting or slightly overlapping peaks. Metabolite features were defined as any peak with an average intensity 5 times higher in the analytical samples than is measured for this peak in the extraction blanks. Measured metabolite features from all assays were combined into a single multimodal dataset that was analyzed using a range of multivariate tests including principle component analysis (PCA) and orthogonal projections to latent structures – discriminant analysis (OPLS-DA) and hierarchical clustering analysis (HCA) performed in SIMCA 14.0 (Umetrics, Umeå, Sweden). The data in all models was logarithmically transformed (base10) and pareto scaled. The performance of the generated models was assessed based on the cumulative correlation coefficients (R^2X[cum]) and predictive performance based on seven-fold cross validation (Q^2[cum]), with the significance of the model assessed based on the ANOVA of the cross-validated residuals (CV-ANOVA). Feature selection to create curated models was performed by iteratively removing variables using the variable influence to projections plot to achieve the fitted model with the optimal R^2 and Q^2 values [305].

The Curated PLS-DA models were produced using the variable importance to projection (VIP) scores, where the VIP is mean centred score of the contribution of a variable to the observed class separation. Metabolite features with a VIP less than 1 were iteratively removed to produce the optimal model based on R^2X, R^2Y, Q^2 and CV-ANOVA. The

predictive ability of the generated OPLS models were validated by using permutation test [306]. The results showed that none of the permuted Q^2 values is higher than the one in the original model which confirms the reliability of the produced models. Comparison of model performance of each individual method was performed, then followed by looking at how all of the methods performed together.

4.3. Results and Discussion

The total run time of this method was four hours which is unusually long in metabolomics, where methods need to be high-throughput. The present method was designed to acquire as much information as possible from one sample and the instrument time and cost of analysis were increased to achieve this end. The quality of the generated data was assessed by looking at the compositional similarity of QC samples based on all metabolite features using PCA (Figure 4.2). QCs clustered apart from QC1 which was the first injection into the run (highlighted in a box), the other QCs clustered once the columns were equilibrated, hence showing a clustering lower than biological variance suggesting across run reproducibility and stability. In a PCA analysis of just the QC samples it could be seen that the analytical drift across the run accounted for 17.2% of the overall variance observed in the QC. Reproducibility of the Aqueous phase internal standard was calculated in the raw data from plasma in both samples and QCs (Table 2). The %RSD was reported at less than 15 % across both samples and QCs, which is recommended in bio analytical method validation, which ultimately shows the values obtained have acceptable reproducibility. No shift in retention time over the runs was observed. There was limited overlap between the analytical methods used with no identified metabolites in common, this limited overlap demonstrates the importance of using complimentary separation techniques to obtain a new class of metabolites and increase the metabolic coverage.

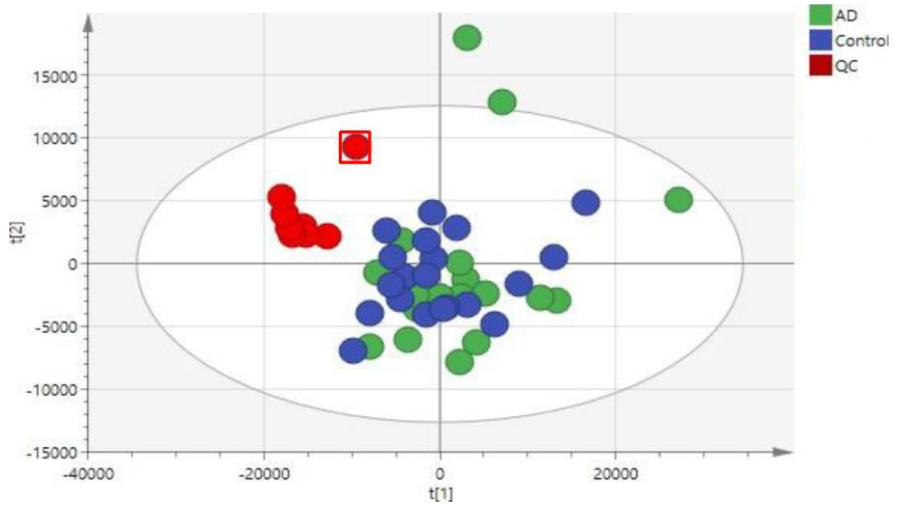

Figure 4.2 PCA score plot of plasma samples generated from the combined dataset from all 6 analytical methods combined. Plot showing controls, Alzheimer' and quality control samples, first QC is enclosed in a square.

Table 4.2: Reproducibility of internal standard in the GCMS aqueous phase.

	%RSD of IS in QCs	**%RSD of IS in Samples**
Plasma	3.22%	14.11%

QC =Quality Control samples, %RSD=% Relative Standard Deviation, IS: Internal Standard.

The selectivity and reproducibility of the method was assessed in both brain tissue (Table 4.3) and plasma (Table 4.4) by determining the number of peaks measured and their relative variance. In the raw brain data, the peaks detected in the 4 LC-MS methods were a total of 9459 peaks (signal/noise > 5), and reproducible with 61.8% of the metabolite features with coefficients of variance (CV) of less than 15% and 84.0% with CV's below 30% (Table 4.3). The data generated by GC-MS was also shown to be measuring 11248 (signal/noise > 5) metabolite features, however the reproducibility of the data is poor with only 1.5% of metabolite features showing CV's of less than 15% and 12.3% below 30% CV's. To improve the reproducibility, the data was normalized to total ion count (TIC), with this normalization significantly improving the reproducibility with 34.4% of total peaks now with CV's of less than 15% and 68.7 below 30%, however normalization appeared to have a limited effect on the LC-MS data. The initial selectivity and reproducibility of the method in plasma was assessed in the 8 serum QC samples run during

the pilot experiment. As with the data generated from brain tissue the LC-MS data was shown to be measuring a total of 9551 metabolite features as well as highly reproducible with 36.9% of peaks showing CV's of less than 15%, and 61.8% below 30% CV's, whilst 9.8% of the 7715 of the GC-MS metabolite features showing CV's lower than 15% and only 17.3% with CV's below 30%. The data when normalized to TIC, produced a modest increase in the reproducibility of the RP data from 33.3% and 74.0% to 50.7% and 75.2% and HILIC data from 41% and 60.5% to 50.5% and 71% with CV's below 15% and 30% respectively. Normalization of the GC-MS data also improved reproducibility from 16.5% to 30.9% to CV's below 15% and 30%. Inspection of the non-aqueous phase data which shows the least number of features with CV's <30% compared to LC-MS and GC-MS aqueous method. However, during method development the non-aqueous phase achieved CV's in line with the brain experiments shown in Table 3. The aqueous phase showed 34.9% of features with CV's below 15%, and 63.3% below 30% also in line with the brain experiment

Table 4.3. Reproducibility of RAW and TIC normalized data generated by each analytical method from brain tissue samples. Variability of metabolite features measured in 7 independent IVDE's from rat cerebellum.

	HILIC Pos		HILIC Neg		RP Pos		RP Neg		GC Aqueous		GC-non aqueous	
	RAW[a]	TIC[b]	RAW[a]	TIC[b]	RAW[a]	TIC[b]	RAW[a]	TIC[b]	RAW[a]	TIC[b]	RAW[a]	TIC[b]
<5%[c]	676	658	299	388	168	184	196	94	2	247	5	399
5-10%[c]	724	733	613	492	443	407	303	411	11	495	9	512
10-15%[c]	853	838	555	483	389	336	267	249	87	1147	64	1069
15-30%[c]	711	724	762	804	746	801	241	248	594	2119	611	1745
>30%[c]	309	320	524	586	653	671	27	32	5398	2084	4467	1431
Total	3273		2753		2399		1034		6092		5156	

[a] peak numbers for raw data [b] peak numbers for TIC normalized data [c] coefficient of variance of peak intensity between runs. GC; gas chromatography, HILIC; hydrophilic liquid interaction chromatography, Neg; negative, Pos; positive, RP; reversed phase.

Table 4.4: Reproducibility of RAW and TIC normalized data generated by each analytical method from plasma samples. Variability of metabolite features measured in 8 pooled QC samples.

	HILIC Pos		HILIC Neg		RP Pos		RP Neg		GC Aqueous		GC-non-aqueous	
	RAW[a]	TIC[b]	RAW[a]	TIC[b]	RAW[a]	TIC[b]	RAW[a]	TIC[b]	RAW[a]	TIC[b]	RAW[a]	TIC[b]
<5%[c]	592	668	102	336	78	175	56	241	18	87	3	17
5-10%[c]	684	794	458	473	203	398	236	272	95	254	6	29
10-15%[c]	349	447	256	284	261	369	230	253	609	809	27	58
15-30%[c]	668	748	488	472	1029	837	213	196	522	925	72	212
>30%[c]	1167	803	1180	919	996	788	305	78	2048	1217	4315	4107
Total	3460		2484		2567		1040		3292		4423	

[a] Peak numbers for raw data [b] peak numbers for TIC normalized data [c] coefficient of variance of peak intensity between runs. GC; gas chromatography, HILIC; hydrophilic liquid interaction chromatography, Neg; negative, Pos; positive, RP; reversed phase.

Having shown the method was reproducible the next stage in assessing its performance was to determine its ability to detect differences in a small pilot between biological classes using multimodal multivariate data analysis. Curated models were generated using both raw and TIC normalized data from all the 6 platforms combined into a single dataset to identify the metabolite features with the greatest predictive performance for discriminating diagnostic classes. The optimal model calculated between control and AD samples from the combination of all LC-MS and GC-MS raw data was based on 314 metabolite features, and showed a significant class separation ($R^2X = 0.489$, $R^2Y = 0.903$, $Q^2 = 0.794$, CV-ANOVA = 1.418×10^{-11}). However, in the same comparison a better separation was achieved by using the TIC normalized LC-MS and GC-MS data, with the final curated model based of 426 features (Figure 4.3A) ($R^2X = 0.585$, $R^2Y = 0.933$, $Q^2 = 0.869$, CV-ANOVA = 2.72×10^{-14}). Of the 426 metabolite features on which this model is based 95 were measured in HILIC positive, 84 were measured in HILIC negative, 63 came from RP positive, 72 from RP negative, with GC aqueous accounting for 69 and GC Non-aqueous for 43 of the features. In both the OPLS-DA (Figure 4.3A) and PCA (Figure 4.3B) analysis there is a visible separation between controls and AD, but also between the control samples themselves, the stable (control A) and declining control (B) samples. To investigate this further we performed hierarchical clustering analysis (HCA) (Figure 4.3C) to assess the compositional similarity of individual samples from the three sample groups. This analysis showed that the ‘declining’ control samples clustered in the same primary clade as the AD samples suggesting that they were more compositionally similar to the AD samples than they were to the ‘stable’ controls. Whilst these samples were diagnosed clinically as controls and showed no difference in cognitive ability at baseline, at a 12 month follow up these individuals had exhibited a significant decline in cognitive function (0.83 MMSE points, $p = 0.019$). When metabolite features were considered individually it could be seen that the ‘declining’ controls had a similar abundance to that which is observed in the AD samples or is intermediary between the ‘stable’ controls and AD samples (Figure 4.3C).

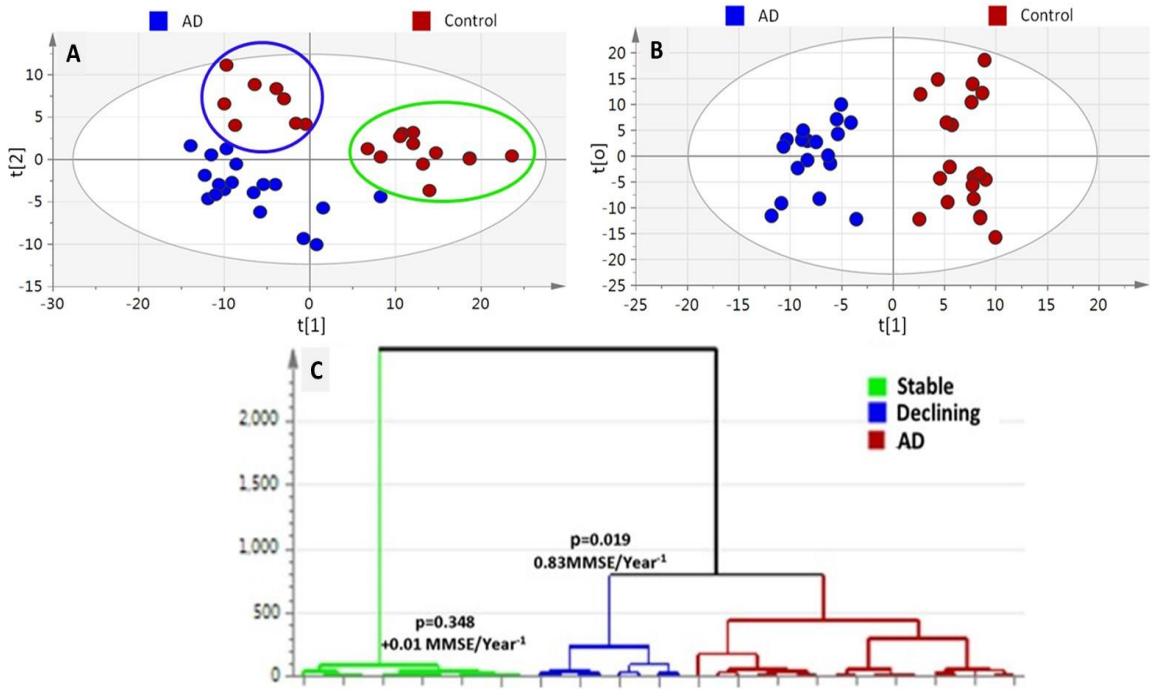

Figure 4.3 Multivariate analysis of all data using OPLS-DA and PCA scores plots and HCA dendrogram. A) PCA analysis (R^2X = 0.561, Q^2 = 0.498) based on the 426 metabolite features identified in curated OPLS-DA model, B) curated OPLS-DA model of healthy controls vs. AD patients (R^2X = 0.585, R2Y = 0.933, Q^2 = 0.869, CV-ANOVA = 2.72×10-14), C) HCA based on the PCA model to analyze compositional similarity of individual samples. In figure 4.3A and 4 .3B, blue circle refer to AD (Alzheimer's disease) samples and red circle refer to Control samples.

Having shown the ability of this method to discriminate controls from AD, the next step was to determine if the method could detect more subtle differences by looking for gender specific differences in metabolite composition. A curated 4 class OPLS-DA was generated model based on 808 metabolite features (R2X = 0.639, R2Y = 0.643, Q2 = 0.473, CV-ANOVA = 1.73×10-7), the primary separation in the first component was between controls and AD samples (Figure 4.4A) of both genders. Whilst no difference is seen in the control samples, there does appear to be a modest separation between the male and female AD patients. HCA was performed to assess this difference further (Figure 4.4C). This analysis confirmed that male and female AD patients are compositionally distinct both from each other and from controls, with female patients being more different to controls than males. This finding is potentially unsurprising owing to women's greater susceptibility to AD pathology relative to men [307, 308].

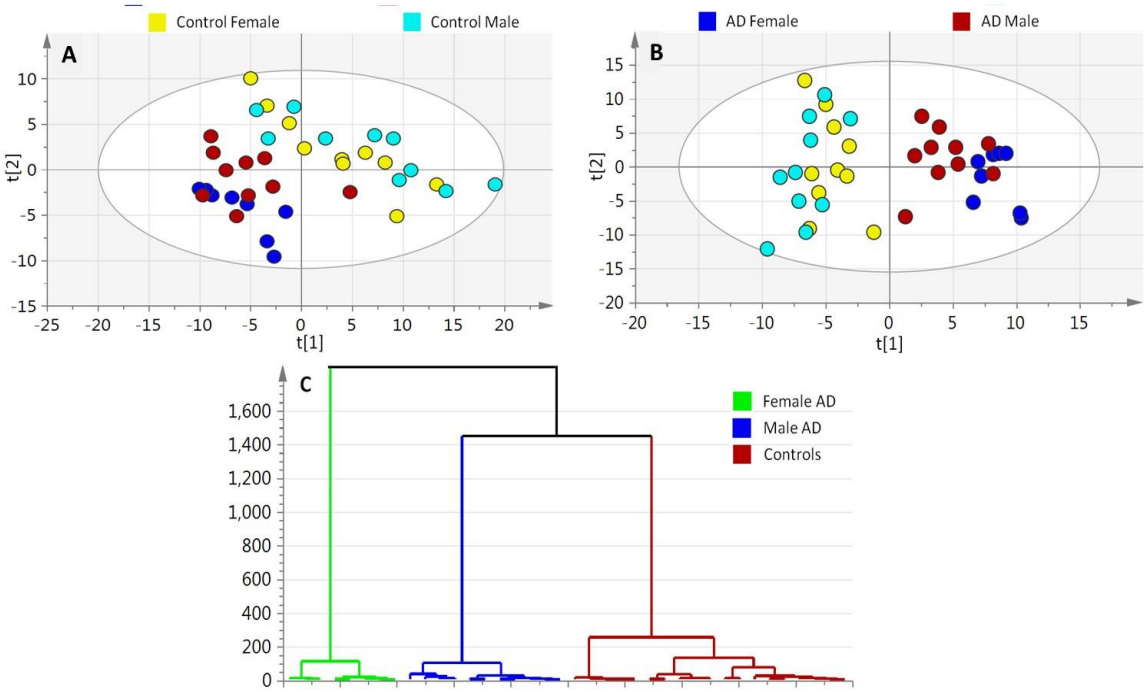

Figure 4.4 Gender specific analysis of all data that passed QC using a range of multivariate analysis approaches shown using A) PCA B) OPLS-DA and scores plots and C) HCA dendrogram.

Having observed that this method could discriminate between defined biological classes we wanted to determine whether metabolite composition could be directly correlated with a range of relevant clinical measures. Determining the association between metabolite composition and clinical outcomes was done using OPLS analysis with MMSE, age and ADCS-ADL set as Y variables. Using SIMCA's inner relations plot it can be seen that metabolite composition correlates with MMSE (Figure 4.5A) (R^2 = 0.893), age (Figure 4.5B) (R^2 = 0.636) and ADCS-ADL (Figure 4.5C) (R^2 =0.634). This direct correlation of metabolite composition to clinical outcomes further demonstrated biological relevance of the data generated using this multimodal method.

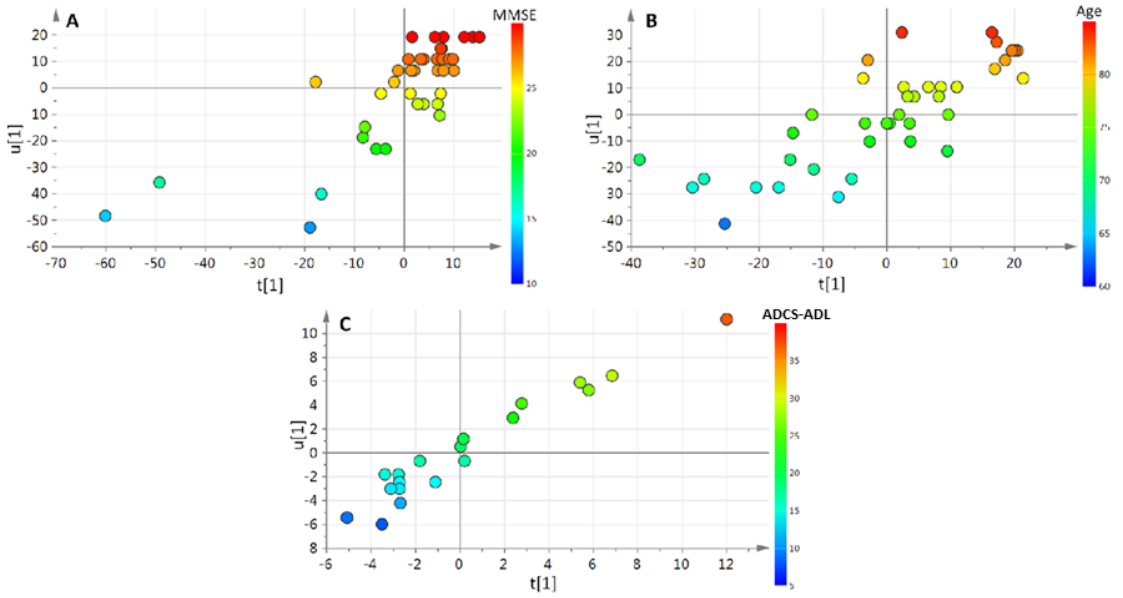

Figure 4.5 Inner relations plots of OPLS models demonstrating significant correlations between metabolite composition and a range of clinical outcomes. A) MMSE (R^2 = 0.893), B) age (R^2 = 0.636), and C) ADCS-ADL (R^2 = 0.634)

Metabolite annotation was performed by searching the *m/z* of measured metabolite features in a range of publicly accessible metabolite databases including the human metabolome database (HMDB), METLIN and LipidMap, by matching the fragmentation pattern of the peak being annotated to the fragmentation pattern shown for metabolites within the databases. In addition, some standards are available for these compounds allowing fragmentation spectra of these metabolites to be identified and easily confirmed.

Of the metabolite features that were important for driving the separation between the two groups of controls we annotated the excitatory neurotransmitter glutamate (Figure 4.6) which has previously been linked to the pathology and progression of Alzheimer's disease [309-313] .

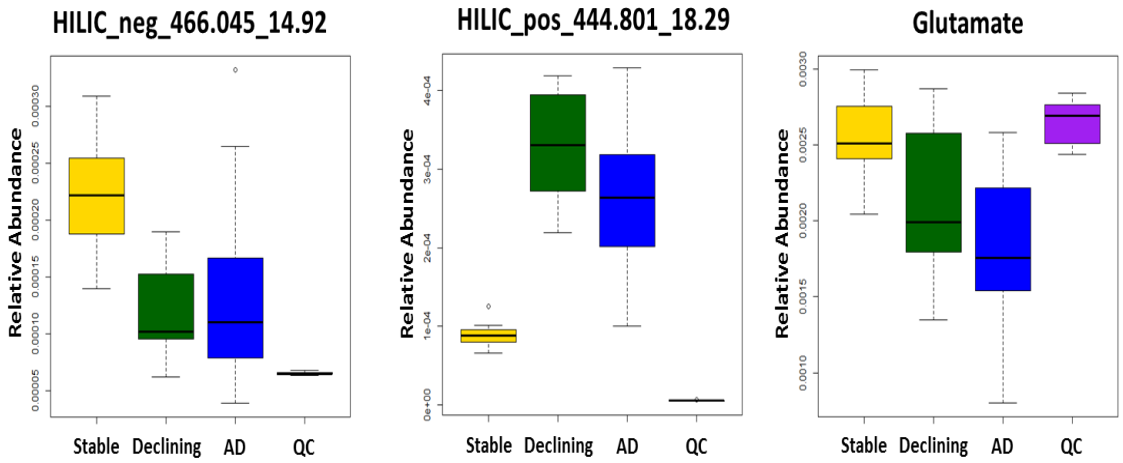

Figure 4.6 Boxplots showing examples of features discriminating between all three diagnostic groups. The feature name is the mode of chromatography followed by the ionization mode, then the feature mass and retention time in minutes. AD; Alzheimer's disease, HILIC; hydrophilic liquid interaction chromatography, QC; quality control.

In this small pilot, metabolic shifts potentially associated with subtle differences in biological phenotypes were observed. Hence, this multimodal method was able to discriminate 'stable', 'declining' controls and AD patients using a PCA, however promising this result, the number of samples does not warrant metabolite identification and validation using larger scale study is needed.

4.4 Conclusions

The study presented here in chapter 4 illustrates the utility of combining metabolomics data to measure large numbers of metabolite features from small sample volumes with multivariate statistics, to detect metabolic differences. Applying multimodal data to discriminate AD patients from healthy controls, also showed correlation of metabolite composition to clinical outcomes including mini-mental state examination (MMSE), age and Alzheimer's disease cooperative study scale – Ability of Daily Living (ADCS-ADL). In the next chapter, the metabolomics multimodal data protocol performed in this chapter combined with developed LC and GCMS methods (Chapter 2 and 3) will be applied to human brain samples.

CHAPTER 5: Brain metabolomics identifies dysregulation of Poly-unsaturated fatty acid metabolism

5.1 Introduction

Extracellular accumulation of amyloid-β (Aβ) plaques and intracellular accumulation of neurofibrillary tangles are the pathological hallmarks of AD. A growing body of evidence suggests that metabolic perturbations in various pathways may mediate the occurrence of Alzheimer pathology as well as the onset of cognitive impairment in patients [314]. The application of large- scale unbiased metabolomics techniques to study the role of metabolism in Alzheimer pathogenesis may facilitate a more complete understanding of Alzheimer pathology and mechanisms triggering symptom expression. Several metabolomic studies have previously examined the relationship between metabolism and AD pathology. While studies on serum, plasma, and cerebrospinal fluid have identified several metabolic pathways involving bile acids, sphingolipids, antioxidants, phospholipids, and amino acids that appear to be associated with disease [68, 181, 190, 193, 315, 316], it is likely that metabolomic studies on human brain tissue samples may provide direct insights into the molecular basis of Alzheimer pathogenesis. A handful of studies have performed metabolomics on brain tissue samples from both transgenic animal models and humans. Salek et al. found alterations in neurotransmitters, amino acids and antioxidants to be strongly associated with AD [2]. Graham *et al*. used metabolomics to analyze human brain neocortex samples (15 controls versus 15 AD) and were able to differentiate controls and AD samples [210]. Inoue et al. analyzed the parietal and frontal lobes of healthy controls and Alzheimer patients (10 versus10) and identified increased brain polyamine metabolism in AD brains [239].

In AD, there is a regional specificity in the vulnerability of various brain regions to pathology, with some regions exhibiting greater amyloid pathology whilst others are dominated by neurofibrillary tangles [317, 318]. However, previous studies have not examined changes in brain metabolite profiles in relation to the regional distribution of disease pathology. Equally important, few studies have addressed the relationships between brain metabolite signatures and the manifestation of clinical symptoms of AD in response to pathology. It is now well recognized that substantial levels of Alzheimer pathology can occur in the brains of cognitively normal individuals [319]. In the Baltimore Longitudinal Study of Aging (BLSA), we have categorized this group of

individuals as “asymptomatic” (ASM) [320], i.e., subject with significant AD neuropathology at death but without evidence for cognitive impairment during life, as assessed by longitudinal cognitive assessments.

In this study, we applied untargeted metabolomics to brain tissue collected through the autopsy sample of the BLSA in three groups of individuals (AD; N = 14, control; N = 14 and ASM; N = 15) and studied differences in brain metabolite levels within regions both vulnerable and resistant to AD pathology. We thus examined the middle frontal gyrus (MFG; vulnerable to Aβ deposition), inferior temporal gyrus (ITG; vulnerable to tau deposition), and the cerebellum (CB), which is relatively spared of classical AD pathology [321].

The relationships between metabolic shifts and specific features of Alzheimer pathology and disease outcome were assessed by applying untargeted metabolomics utilizing LC-MS and GC-MS method presented in chapter 2 and 3 to maximize the metabolite coverage obtained.

5.2 Materials and methods

5.2.1 Sample information

The ethics approval was obtained from the Institutional Review Board of the University of Maryland Baltimore County (03-AG-0325). The BLSA is a prospective, ongoing cohort study of community dwelling volunteer participants in Baltimore that originated in 1958. As such, it is among the largest and longest running longitudinal studies of aging in the United States [322, 323]. In general, at the time of entry into the study, participants had no physical or cognitive impairment. Detailed examinations, including neuropsychological assessments and neurological, laboratory, and radiological evaluations, were conducted every 2 years. Since 2003, participants older than 80 years have received yearly assessments. Written informed consent was obtained at each visit, and the study was approved by the local Institutional Review Board and the National Institute on Aging. After each visit, cognitive status was considered at consensus

diagnosis conferences relying on information from neuropsychological tests as well as clinical data as described previously[324]. Diagnoses of dementia and AD were based on the NINCDS-ADRDA criteria [6].

Table 5.1 Clinical Characteristics of study participants[a].

	CN	ASM	AD
Samples (Region)[b]	40 (11/15/14)	39 (9/15/15)	44 (15/15/14)
Gender[c]	7/33	12/27	23/21
Age	81 +/- 10.7	85.5 +/- 8.4	77.6 +/- 9.9***
MMSE[d]	27.8 +/- 2.4	29.0 +/- 0.9*	23.0 +/- 6.9**

[a] values are reported as the mean +/- standard deviation, and range, [b] total number of samples analysed per diagnostic class and the number of these samples split between three brain regions CB/MFG/ITG, [c] gender distribution (female/male),. [d]MMSE: Mini-mental state examination, , Significance relative to controls * <0.05,**p<0.01,***p<0.001. ASM, asymptomatic; CN, control; AD , Alzheimer.

5.2.2 Chemicals and reagents

All solvents and reagents, water, methanol, acetonitrile, ammonium formate, formic acid, and methyl tertiary butyl ether (MTBE), were LC-MS grade purchased from Sigma-Aldrich. Two internal standards for LC-MS analysis were added, L-serine $^{13}C3$ ^{15}N (95%) and L-valine $^{13}C5$ ^{15}N (95%), purchased from Sigma-Aldrich Sample derivatization for GC-MS analysis was performed using N,O-Bis (trimethylsilyl) trifluoro-acetamide (BSTFA) with 1% trimethylchlorosilane (TMCS) purchased from Sigma-Aldrich.

5.2.3 Sample preparation

The in-vial dual extractions were performed as previously described[303]. After LC-MS analysis, the remaining aqueous and non-aqueous phases were split into separate vials and dried down under a stream of nitrogen at 37˚C. Samples were then resuspended in a 1:1 solution of acetonitrile and the derivatizing agents N,O-Bis(Trimethylsilyl)trifluoroacetamide and 1% Trimethyl- chlorosilane, and were incubated at 37˚C for 1 h. After incubation, samples were again dried down under nitrogen at 37˚C and were subsequently resuspended in 25 µl of toluene for analysis.

5.2.4 Metabolite acquisition

Samples were analysed using HILIC-LC/MS, AQ and NAQ GC/MS. Analysis settings are described in detail in chapter 2, section 2.2.7 (HILIC-LC/MS) and chapter 3, section 3.2.5.

5.2.5 Data processing

Initially, all raw data files were converted into.mzXML format, LC-MS files were converted using msConvert (ProteoWizard) whilst GC-MS files were converted using GCMS Solutions (Shimadzu). Converted data files were analysed using XCMS and performed in the open source software package R, with peak picking performed on all MS assays using a "centwave" method, which allows the deconvolution of closely eluting or slightly overlapping peaks. After peak picking, metabolite features were defined as peaks with an average intensity 5 times higher in analytical samples than is measured in the extraction blanks. Metabolite features were analysed using a range of multivariate tests, with all the data logarithmically transformed (base10) and scaled to unit variance (UV), including principal component analysis (PCA) and partial least square discriminant analysis (PLS-DA) performed in SIMCA 13.0.4 (Umetrics, Umeå, Sweden). Model performance was assessed based on the cumulative correlation coefficients (R2X[cum]) and predictive performance based on 7-fold cross validation (Q2[cum]), with the significance of the model assessed based on the ANOVA of the cross-validated residuals (CV-ANOVA). Feature selection to create curated models was performed by iteratively removing metabolite features that had a score of less than 1 in the variable importance to projections plot to achieve the fitted model with the optimal R^2 and Q^2 values. All metabolite annotations were made by matching metabolite fragmentation patterns to those in both in-house and publicly available spectral libraries.

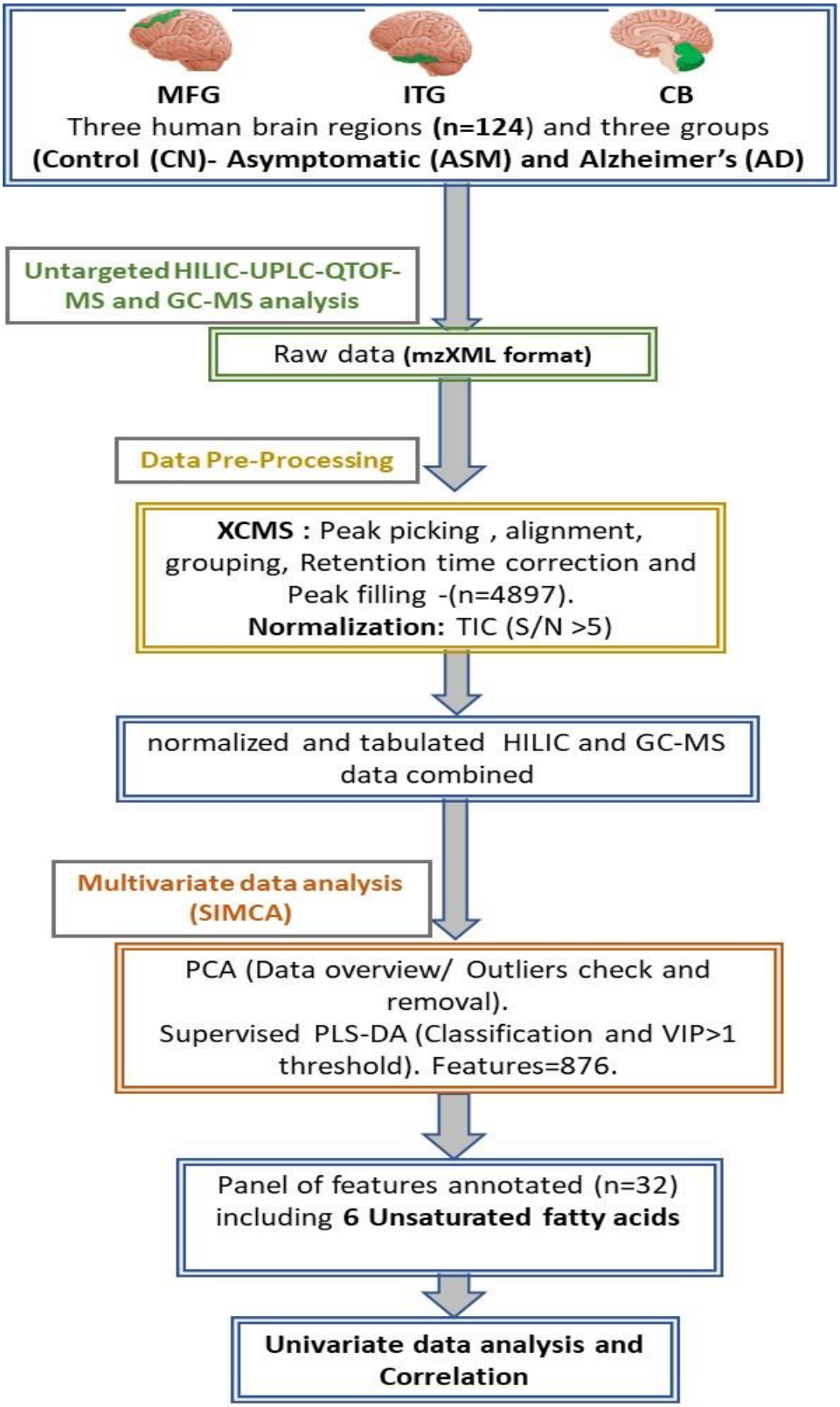

Figure 5.1 Data processing workflow. TIC: Total ion count, S/N: Signal to noise, PCA: Principal Componenet Analysis, PLS-DA: Partial least square discriminant analysis, VIP: Varible important to projection .

To compare the fatty acids among three groups (CN, ASM, and AD), we used nonparametric Kruskal–Wallis test for testing the null hypothesis that all three groups are equal and Mann–Whitney U test for pairwise comparisons. To control for type 1 errors in the p-values calculated using the Mann-Whitney U test, two false discovery rate strategies were employed. The first was to determine which p-values passed a Bonferroni corrected significance threshold and the second was to subject the p-values to a Benjamini-Hochberg procedure performed in "R.". Pearson's correlation coefficient applied to calculate the correlation of the abundance of unsaturated fatty acids and measures of amyloid-β and tau pathology. To evaluate the effect of fatty acids on longitudinal cognitive performance, we created domain-specific composite scores. We standardized each of the cognitive measures (using their baseline mean and standard deviation) and averaged the corresponding Z scores to form the composite score. Trail making tests A and B were first log transformed and then standardized. The following five cognitive domains were created: memory is the composite score of California Verbal Learning Test (CVLT), CVLT long delay free recall and learning and immediate free recall, attention is the composite score of Trail making test A and WAIS-R Digits Forward, executive function is the composite score of Trail making test B and WAIS-R Digits Backward, language is the composite score of letter fluency and semantic fluency, and visuospatial ability is the composite score of clock drawing and card rotation tests.

We then used separate linear mixed models with each cognitive domain as the outcome variable. The main predictor time (or time of follow up) was anchored at the last visit, and all the previous longitudinal follow-up visits were negative relative to the last visit. This kind of recentering of the time variable allows us to test the effect of the levels of each fatty acid on the cognitive performance at last visit and cognitive rates of change simultaneously in a single model. The predictors included fatty acid levels, sex, age at last visit, time, and interactions of time with fatty acid levels, sex, and age at last visit. All analyses were conducted in SAS 9.4 (Cary, NC).

5.3 Results

5.3.1 LC-MS and GC-MS analysis

The brain IVDE method described in Chapter 2(HILIC) and 3(GC-MS AQ and NAQ) were used to analyse the brain samples. The clinical characteristics of the three diagnostic groups analysed are summarised in Table 5.1. The three groups are not balanced for either age or gender, with the Alzheimer's group having significantly more female participants and lower mean age relative to both controls and asymptomatic patients. In this study, a total of 4,897 metabolite features were measured, 3,482 by LC-MS and 1,415 by GC-MS. Of these measured metabolite features, 126 were successfully annotated, representing 100 structurally distinct metabolites (Appendix C-Table 5.1).

5.3.2 Method assessment and Data quality test (PCA)

Following sample analysis, data from the 124 brain samples and the 22 QC underwent PCA analysis in SIMCA 14 to assess intra batch reproducibility. The %RSD of the three IS used were reported at less than 30 % across both samples and QCs, which is recommended in bioanalytical method validation, this ultimately shows the values obtained have acceptable reproducibility. In QC samples, %RSD was more reproducible with less than 15% variation (Table 5.2).

Table 5.2 Descriptive parameters from peak area of two internal standards used in this lipidomics analysis.

Internal Standard(IS)	Chromatography (Ionization Mode)	%RSD across all sample run(n=124)	% RSD in QC raw signal intensity	RT(min) / % RSD of RT
Histidine	HILIC (Positive)	17.38	7.38	12.17/0.2
Valine	HILIC (Positive)	14.58	4.58	14.80/0.2
Serine	HILIC (Positive)	23.96	9.96	17.18/0.3
Histidine	HILIC (Negative)	13.09	3.79	12.17/0.2
Valine	HILIC (Negative)	10.47	3.01	14.80/0.1
Serine	HILIC (Negative)	19.95	8.91	17.09/0.2

HILIC=Hydrophilic Interaction Liquid Chromatography, QC =Quality Control samples, RT=Retention time, %RSD=% Relative Standard Deviation.

5.3.3 Partial least square discriminant analysis of HILIC-LC-MS and GC-MS data.

Multivariate models were constructed based on all 4,897 metabolite features to assess the effects of both brain region and pathological diagnosis on metabolite composition. In curated PLS-DA models, it can be seen that both brain region (Figure 5.2A: $R^2X = 0.639$, $R^2Y = 0.622$, $Q^2 = 0.608$, cross validated ANOVA [CV-ANOVA] = 5.65 × 10−33) and pathological diagnosis (Figure 5.2B: $R^2X = 0.499$, $R^2Y = 0.439$, $Q^2 = 0.404$, CV-ANOVA = 4.72 × 10−21) are significantly associated with metabolite composition. The PLS-DA scores plots (Figure 5.2A) show that all three of the brain regions possess unique metabolite compositions, whilst the MFG and the ITG are compositionally distinct, shown by a modest separation in the second component (t[2]), and are more similar to each other than they are with the CB (Figure 5.2A), which is highly compositionally distinct, as shown by a clear separation in the first component (t[1]). As with the brain regions, PLS-DA analysis showed that the three diagnostic groups possessed unique chemical compositions, with less difference observed between control and ASM, shown by the modest separation in the second component, with the AD groups the most distinct with the greatest separation in the first component.

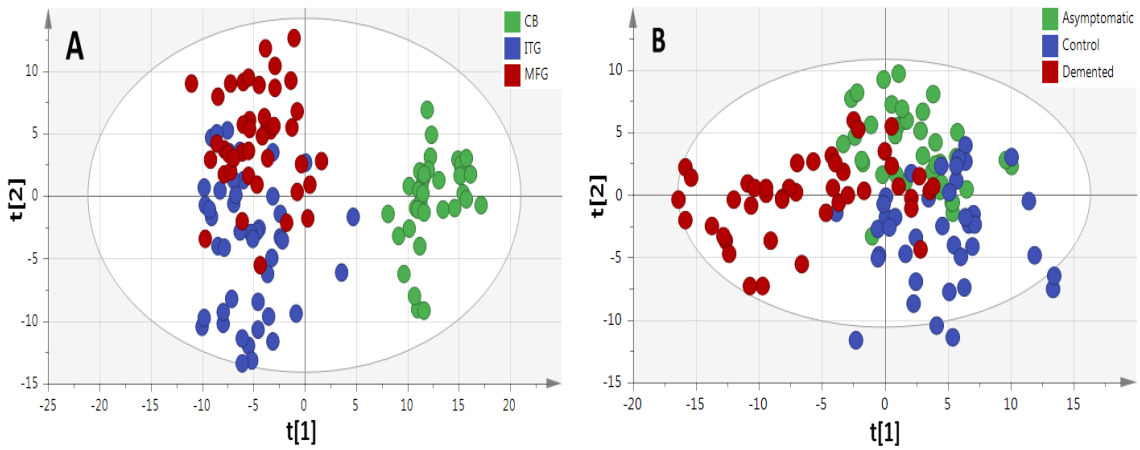

Figure 5.2 Scores plots from curated PLS-DA models comparing the metabolite composition of brain regions and diagnostic groups. A) Comparison of metabolite composition of cerebellum (CB), inferior temporal gyrus (ITG) and medial frontal gyrus (MFG) ($R^2X = 0.639$, $R^2Y = 0.622$, $Q^2 = 0.608$, CV-ANOVA = 5.65×10^{-33}) B) Comparison of metabolite composition of diagnostic groups, control, asymptomatic and demented ($R^2X = 0.499$, $R^2Y = 0.439$, $Q^2 = 0.404$, CV-ANOVA = 4.72×10^{-21}).

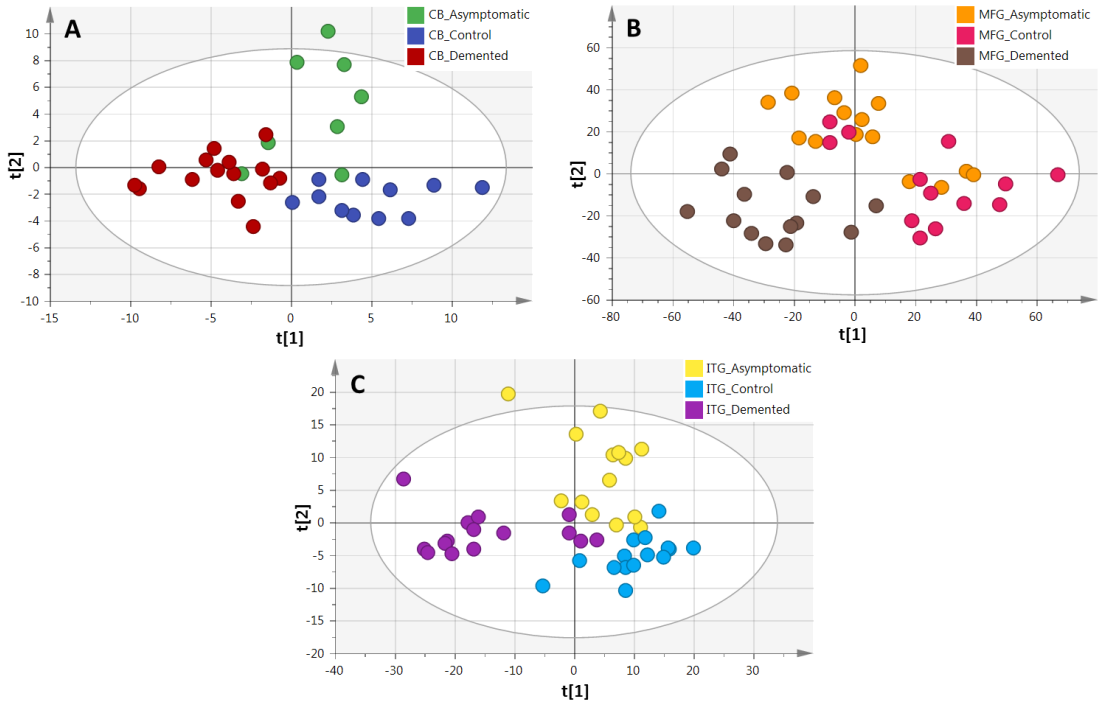

Figure 5.3 Scores plots from curated PLS-DA models comparing the metabolite composition of diagnostic groups in individual brain regions. A) Comparison of metabolite composition of diagnostic groups, control, asymptomatic and Alzheimer's in cerebellum samples ($R^2X = 0.527$, $R^2Y = 0.539$, $Q^2 = 0.424$, CV-ANOVA = 5.04×10^{-4}), B) Comparison of metabolite composition of diagnostic groups, control, asymptomatic and demented in medial frontal gyrus samples ($R^2X = 0.592$, $R^2Y = 0.563$, $Q^2 = 0.424$, CV-ANOVA = 3.28×10^{-7}), C) Comparison of metabolite composition of diagnostic groups, control, asymptomatic and demented in inferior temporal gyrus samples ($R^2X = 0.650$, $R^2Y = 0.563$, $Q^2 = 0.490$, CV-ANOVA = 1.62×10^{-5}).

Having shown that AD pathology is significantly associated with brain metabolite levels, we then examined specific metabolites and metabolic pathways driving the observed shifts. The metabolite features that were used to generate the optimal curated PLS-DA models in all three diagnostic groups were taken forward for further analyses of their relationships to AD pathology and disease status. The optimal curated PLS-DA model was comprised (Figure 5.2B) of 876 metabolite features putatively representing 160 metabolites as associated with diagnostic status, with 32 of these metabolites annotated (Table 5.3).

Having shown that metabolite composition differs significantly between diagnostic groups, further curated PLS-DA models were generated to see if the overall pattern was

replicated in each brain regions individually. It can be seen in Figure 5.3 that the pattern observed was replicated in each of the three brain regions.

Table 5.3 Annotated metabolites identified as being important compositional differences between the three diagnostic groups.

	CN VS ASM		CN VS AD	
	p-value	FC	p-value	FC
Cholesterol	7.5×10^{-3}	0.74	$6.8\times10^{-8*+}$	0.53
Linoleic Acid	7.3×10^{-3}	0.74	$8.8\times10^{-8*+}$	0.52
Cholestenol	1.0×10^{-1}	1.17	$1.0\times10^{-7*+}$	1.44
Docosahexanoic acid	1.7×10^{-1}	1.14	$1.7\times10^{-7*+}$	1.45
Carbamic acid	1.9×10^{-1}	1.15	$2.0\times10^{-7*+}$	1.53
Methylheptadecadiynoic acid	2.4×10^{-2}	0.79	$2.8\times10^{-7*+}$	0.59
Oleic acid	5.5×10^{-2}	0.73	$3.3\times10^{-7*+}$	0.34
Palmitic acid	1.9×10^{-2}	0.73	$4.8\times10^{-7*+}$	0.44
Hexanedioic acid	2.7×10^{-1}	1.11	$6.4\times10^{-7*+}$	1.42
Dimethylglycine	2.9×10^{-2}	0.89	$1.0\times10^{-6*+}$	0.74
Guanidobutanoate	1.9×10^{-1}	0.94	$3.7\times10^{-6*+}$	0.75
Ascorbate	1.5×10^{-1}	1.20	$1.9\times10^{-5*+}$	1.54
Aminobutanal	6.7×10^{-2}	0.94	$9.1\times10^{-5*+}$	0.86
Gluconic acid	1.4×10^{-2}	1.31	$1.0\times10^{-4*+}$	1.51
Cysteine	4.7×10^{-1}	1.06	$1.0\times10^{-4*+}$	1.33
Aspartate	6.2×10^{-2}	1.17	$1.5\times10^{-4*+}$	0.84
L-DOPA	9.2×10^{-2}	1.11	$1.8\times10^{-4*+}$	1.23
Fumaric acid	4.4×10^{-2}	0.91	$1.9\times10^{-4*+}$	0.85
Linolenic acid	7.5×10^{-2}	0.90	$2.5\times10^{-4*+}$	0.84
Indoleacetic acid	1.4×10^{-1}	0.93	$2.6\times10^{-4*+}$	0.82
Eicosapentaenoic acid	1.6×10^{-3}	0.25	$4.4\times10^{-4*}$	0.16
Allantoin	6.9×10^{-3}	1.19	$4.6\times10^{-4*}$	1.30
Hypoxanthine	4.7×10^{-1}	0.98	$5.4\times10^{-4*}$	0.88
Coumaric acid	5.9×10^{-2}	1.16	$7.6\times10^{-4*}$	1.28
Adenine	9.2×10^{-2}	1.10	$8.0\times10^{-4*}$	1.18
Oxoarginine	9.0×10^{-1}	0.99	$8.6\times10^{-4*}$	0.77
Deoxyflurouridine	5.2×10^{-1}	1.08	$1.0\times10^{-3*}$	1.45

Arginine	5.7×10^{-2}	1.24	$1.1\times10^{-3*}$	1.38
GABA	3.6×10^{-1}	1.07	4.4×10^{-3}	1.18
Myo-Inositol	5.7×10^{-1}	1.09	6.6×10^{-3}	0.70
Methylstearate	5.4×10^{-1}	0.85	2.6×10^{-2}	0.56
Octadecanal	1.6×10^{-1}	2.41	5.6×10^{-1}	0.68

DOPA: dihydroxy-phenylalanine, GABA: gamma-aminobutyrate. * passes FDR using Benjamini-Hochberg correction (0.05 threshold), + significant pass Bonferroni correction. ASM, asymptomatic; CN, control; AD , Alzheimer.

5.3.4 Feature selection and structural elucidation

These annotated metabolites were subsequently mapped onto known metabolic pathways using the Kyoto Encyclopedia of Genes and Genomes' pathway mapping tool [325]. This approach identified 113 metabolic pathways that contained at least one of the 31 metabolites. Of these 113 metabolic pathways, poly-unsaturated fatty acid (PUFA) metabolism was identified for more detailed analysis, as the metabolites in this pathway showed the strongest association with diagnostic status.

In GC-MS, Six PUFA were identified using NIST and IEM libraries with a similarity index over 90%. These are linoleic acid, linolenic acid, eicosapentanoic acid (EPA), oleic acid, arachidonic acid (AA) and Decosahexanoic acid(DHA). Calculated degree of similarity (similarity index). This is 100 when the spectra are perfectly identical. GC-MS applies electron ionization mode with 70 eV which can provide a standard spectrum for each compound, so it can compare samples with the database directly. This increases the efficiency and help to identify unknowns. This is an advantage of GC-MS over LC-MS as in the latter fragmentation is not as reproducible between instruments and identification is difficult.

We were able to run three PUFA standards, AA, EPA and DHA . Figure 5.4 ,5.5 & 5.6 represent the spectra obtained by similarity search results of the three Standards. This was matched with results of identified PUFA and validate the identification results for PUFA peaks in brain samples (also the the six identifies PUFA were the highest similarity index with over 90%).

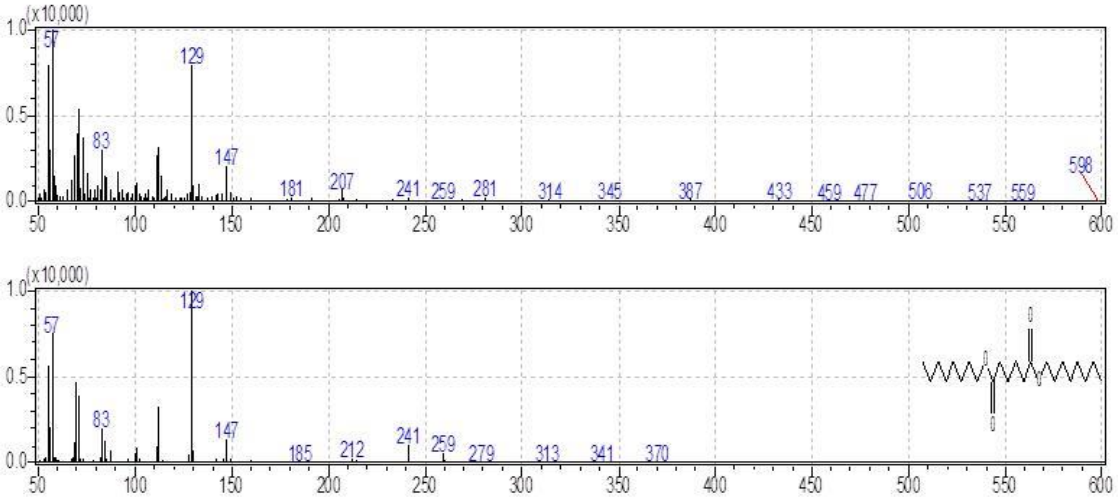

Figure 5.4 Spectrum of DHA analysed by GC-MS. The top spectrum shows the target spectrum of DHA that is the subject of the search. The bottom spectrum shows the spectrum registered in the library.

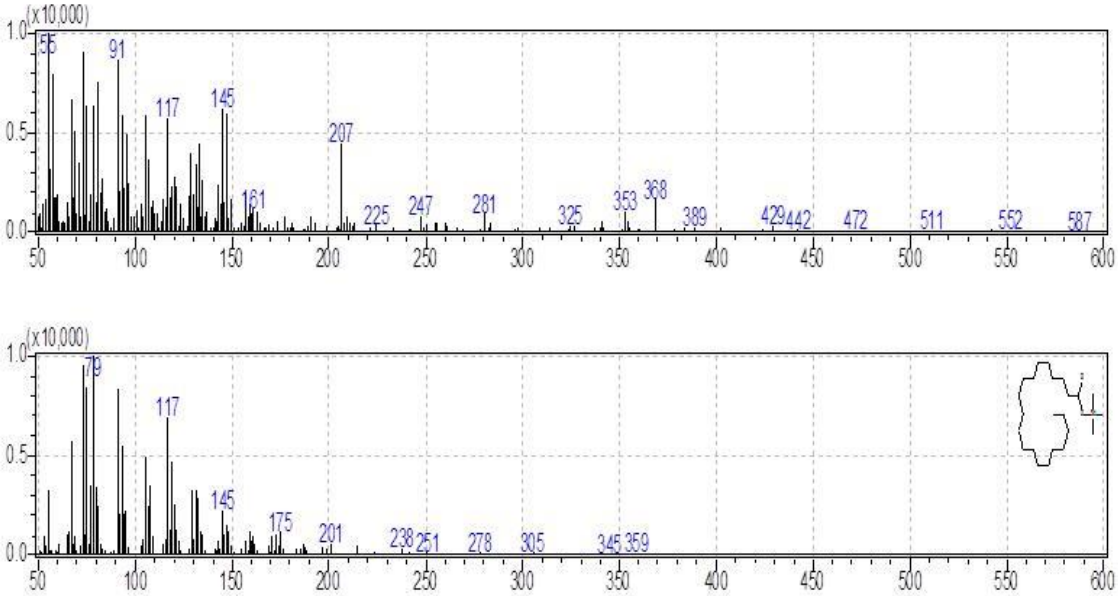

Figure 5.5 Spectrum of EPA analysed by GC-MS. The top spectrum shows the target spectrum of EPA that is the subject of the search. The bottom spectrum shows the spectrum registered in the library.

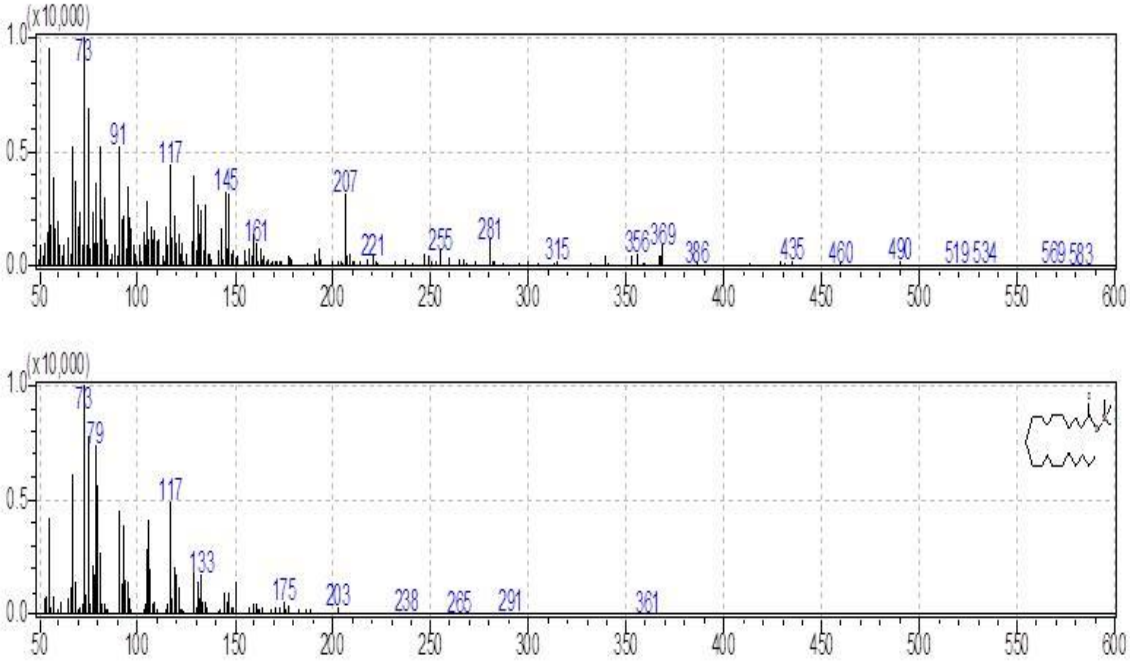

Figure 5.6 Spectrum of AA analysed by GC-MS. The top spectrum shows the target spectrum of AA that is the subject of the search. The bottom spectrum shows the spectrum registered in the library.

PUFA abundance in human brain regions

Table 5.4 and Figure 5.7 summarize results of analyses comparing brain tissue (PUFA) levels between the three groups. The overall pattern of results showed that brain tissue levels of the PUFAs, linoleic acid, linolenic acid, EPA, oleic acid, and (AA) were reduced in the ITG and MFG regions in AD relative to the control group. The AD group showed higher tissue levels of DHA in the ITG and MFG regions relative to controls. Within the CB, EPA levels also appeared to be lower in AD with oleic acid levels showing a similar trend relative to controls. Cerebellar DHA levels in AD were also higher relative to controls. Within the MFG, decrements in the levels of oleic acid, linoleic acid, linolenic acid, and arachidonic followed the pattern control> ASM >AD. Increments in DHA levels in the MFG followed the pattern AD>ASM >control. Six PUFA's, oleic acid, linoleic acid, linolenic acid, DHA, and EPA were shown to be highly associated with disease. Except for DHA all of the measured PUFA's were reduced in abundance with disease with only DHA increased in abundance (Table 5.4). These trends showed that whilst each of the brain regions is showing the same shifts in these species associated with disease,

however the shifts in the ITG appear to occur at an earlier stage of disease with the shifts in these metabolites equal to greater in asymptomatic patients relative to controls than is observed in Alzheimer's patients (Figure 5.7), whilst in the CB and MFG Alzheimer's patients exhibited a greater shift relative to controls than was observed in asymptomatic individuals.

Table 5.4 Relative changes in abundance of 6 poly-unsaturated fatty-acids between all three diagnostic groups in individual brain regions.

	CN Vs ASM						CN Vs AD						ASM Vs AD					
	CB		ITG		MFG		CB		ITG		MFG		CB		ITG		MFG	
	P[a]	FC[b]	P[a]	FC[b]	P[a]	FC[b]	P[a]	FC[b]	P[a]	FC[b]	P[a]	FC[b]	P[a]	FC[c]	P[a]	FC[c]	P[a]	FC[c]
Linoleic acid (ω-6)	7.6×10^{-1}	1.08	6.5×10^{-2}	0.66	7.7×10^{-2}	0.61	$3.5\times10^{-4*}$	0.42	9.0×10^{-3}	0.57	2.3×10^{-1}	1.34	2.4×10^{-1}	0.86	$1.0\times10^{-5*+}$	0.77	$2.7\times10^{-5*+}$	0.47
Oleic acid (ω-9)	1.1×10^{-1}	1.67	1.0×10^{-1}	0.50	4.7×10^{-3}	0.30	$7.2\times10^{-4*}$	0.26	1.0×10^{-2}	0.43	2.9×10^{-1}	1.64	1.6×10^{-1}	0.77	$5.1\times10^{-5*+}$	0.61	$3.7\times10^{-6*+}$	0.27
Docosahexanoic acid (ω-3)	8.9×10-7*+	0.34	4.5×10^{-2}	1.24	$3.1\times10^{-8*+}$	3.67	2.0×10^{-3}	1.43	2.1×10^{-2}	1.30	1.6×10^{-1}	0.91	2.9×10^{-3}	1.49	$3.3\times10^{-6*+}$	1.06	$1.4\times^{10-3}$	1.26
Arachidonic acid (ω-6)	6.1×10-1	0.90	1.1×10^{-1}	0.87	8.4×10^{-1}	0.96	1.6×10^{-3}	0.78	3.0×10^{-2}	0.83	4.1×10^{-1}	1.07	8.3×10^{-1}	1.02	2.8×10^{-2}	0.78	$9.0\times10^{-6*+}$	0.76
Linolenic acid(ω-3)	**3.3×10-1**	0.83	6.9×10^{-2}	0.88	7.9×10^{-1}	1.04	$5.9\times10^{-4*}$	0.81	1.9×10^{-2}	0.86	3.1×10^{-1}	1.06	8.3×10^{-1}	1.02	4.6×10^{-2}	0.81	$4.8\times10^{-6*+}$	0.80
Eicosapentaenoic acid (ω-3)	4.1×10-2	0.11	8.5×10^{-2}	0.26	1.6×10^{-1}	2.32	2.9×10^{-2}	0.09	5.5×10^{-2}	0.21	3.2×10^{-1}	2.24	1.3×10^{-1}	0.42	2.8×10^{-2}	0.80	2.1×10^{-3}	0.20

P: P-value calculated using mann-whitney U-test. [b] fold change relative to controls, [c] fold change relative to asymptomatic, [*] passes FDR using Benjamini-Hochberg correction (0.05 threshold), [+] significant pass Bonferroni correction. CB; Cerebellum, ITG; Inferior Temporal Gyrus, MFG; Medial Frontal Gyrus. ASM, asymptomatic; CN, control; AD , Alzheimer.

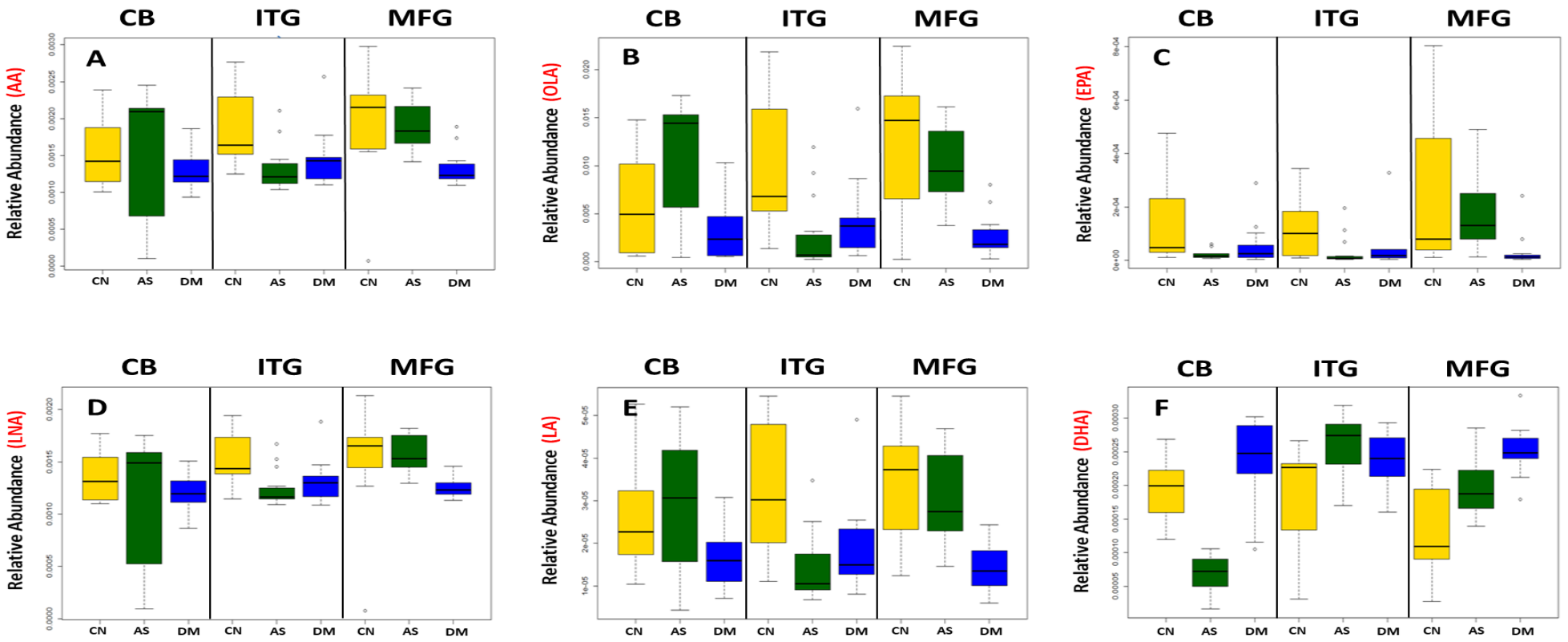

Figure 5.7 Boxplots showing the effect of disease status on the abundance of six PUFAs in the CB, ITG, and MFG. Dysregulation of six PUFAs shown by boxplots of three disease statuses separated by brain region. A) arachidonic acid (AA), B) oleic acid (OLA), C) eicosapentaenoic acid (EPA), D) linolenic acid (LNA), E) linoleic acid (LA), F) docosahexaenoic acid (DHA). ASM, asymptomatic; CN, control; AD , Alzheimer.

5.3.5 Correlation analysis of selected PUFA

As well as associating with disease status, levels of all six PUFA's in the MFG and ITG were shown to correlate significantly with both measures of neurofibrillary pathology estimated by Braak score and amyloid plaque burden assessed by the CERAD score (Table 5.6).

Table 5.5 Correlation analysis of the abundance of unsaturated fatty acids and measures of amyloid-β and tau pathology.

		Braak		CERAD	
		R^2	p-value	R^2	p-value
CB	**Eicosapentaenoic acid**	-0.310	0.0959	-0.3540	0.0550
	Linoleic	-0.129	0.4974	-0.1933	0.3060
	Arachidonic acid	-0.111	0.5590	-0.1848	0.0328
	Oleic acid	-0.280	0.1334	-0.2744	0.1423
	Docosahexanoic acid	0.411	0.0239	0.3376	0.0680
	Linolenic acid	-0.357	0.0528	0.2993	0.1081
ITG	**Eicosapentaenoic acid**	-0.332	0.0415	-0.3577	0.0275
	Linoleic	-0.382	0.0179	-0.3492	0.0317
	Arachidonic acid	-0.376	0.0199	-0.3641	0.0246
	Oleic acid	-0.335	0.0399	-0.3448	0.0340
	Docosahexanoic acid	0.310	0.0579	0.3227	0.0481
	Linolenic acid	-0.260	0.1154	-0.3183	0.0515
MFG	**Eicosapentaenoic acid**	-0.613	<0.0001	-0.5251	0.0006
	Linoleic	-0.572	0.0001	-0.5819	0.0001
	Arachidonic acid	-0.564	0.0002	-0.5527	0.0003
	Oleic acid	-0.640	<0.0001	-0.6363	<0.0001
	Docosahexanoic acid	0.602	<0.0001	-0.6919	<0.0001
	Linolenic acid	-0.634	<0.0001	-0.6673	<0.0001

Relationships between global measures of amyloid and tau pathologies and the regional abundances of 6 unsaturated fatty acids, values highlighted in bold are significant at $p<0.05$. CERAD; Consortium to Establish a Registry for Alzheimer's Disease.

Assessments of brain tissue levels of these PUFA's in relation to domain-specific measures of cognitive performance showed consistent patterns across domains and several significant cross sectional and longitudinal associations across the three brain regions were found (Appendix C-Tables 5.2-5.6). In general, the pattern of these associations showed that lower tissue levels of linoleic acid, linolenic acid, EPA, oleic acid, and AA were related to worse cognitive performance, whereas higher brain DHA levels were associated with poorer cognitive performance. The strongest associations with cognitive performance were between abundance of these fatty acids in the MFG and the final premortem memory, attention and executive function scores (Figure 5.10), as well as longitudinal trajectories in memory and language performance. The strongest association observed in the ITG between levels of these fatty acids was with longitudinal trajectory of visuospatial performance (Figure 5.9).

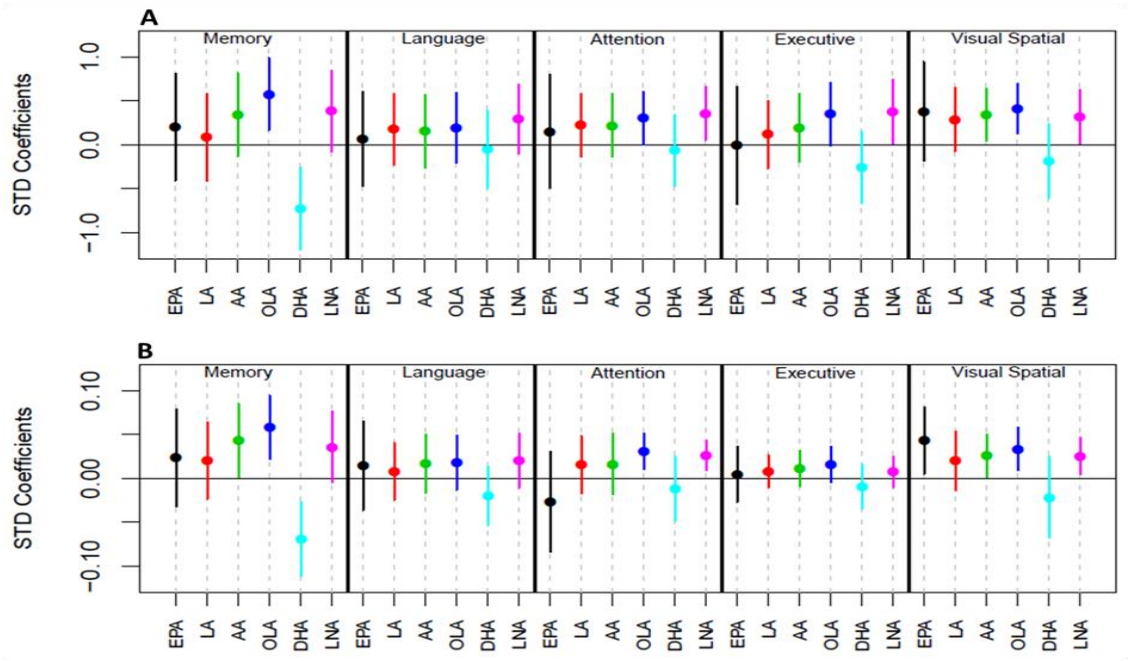

Figure 5.8 Forest plot showing the relationship of the abundance of six PUFA's in the CB and five measures of cognition. A) association between fatty acid abundance of PUFA levels and longitudinal cognitive performance B) associations between fatty acid abundance cognitive performance at the last visit prior to death. AA: arachidonic acid, DHA: docosahexaenoic acid, EPA: eicosapentaenoic acid, LA: linoleic acid, LNA: linolenic acid, OLA: oleic acid. This figure was produced by Dr.Yang Li and his permission was obtained to present.

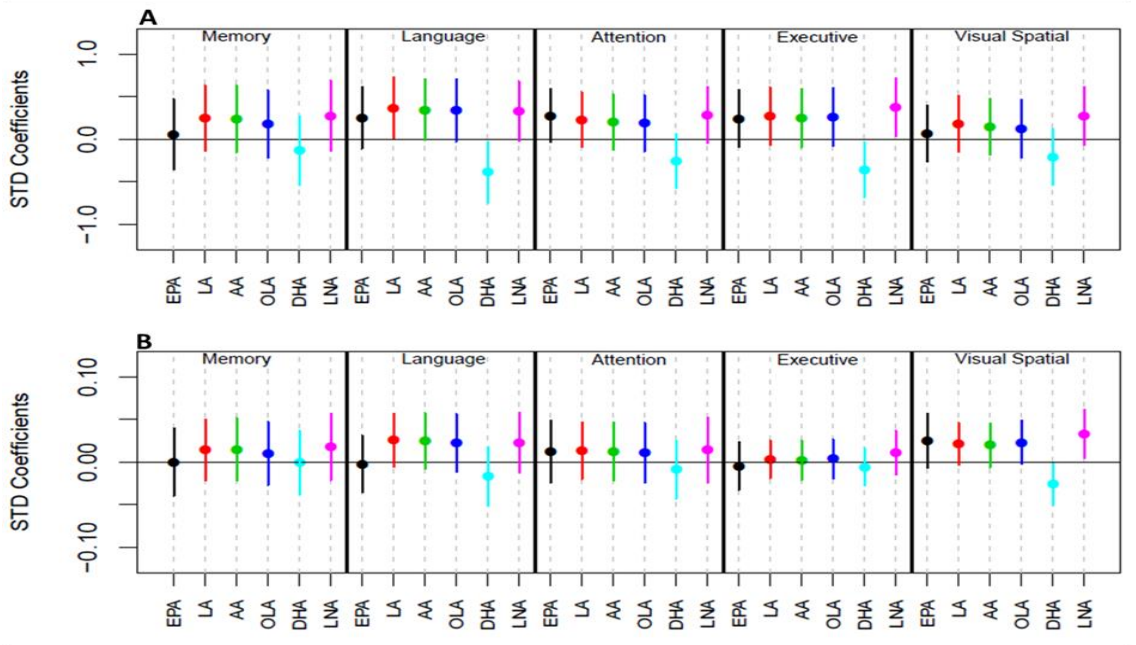

Figure 5.9 Forest plot showing the relationship of the abundance of six PUFA's in the ITG and five measures of cognition. A) association between fatty acid abundance of PUFA levels and longitudinal cognitive performance B) Associations between fatty acid abundance cognitive performance at the last visit prior to death. AA: arachidonic acid, DHA: docosahexaenoic acid, EPA: eicosapentaenoic acid, LA: linoleic acid, LNA: linolenic acid, OLA: oleic acid. This figure was produced by Dr.Yang Li and his permission was obtained to present.

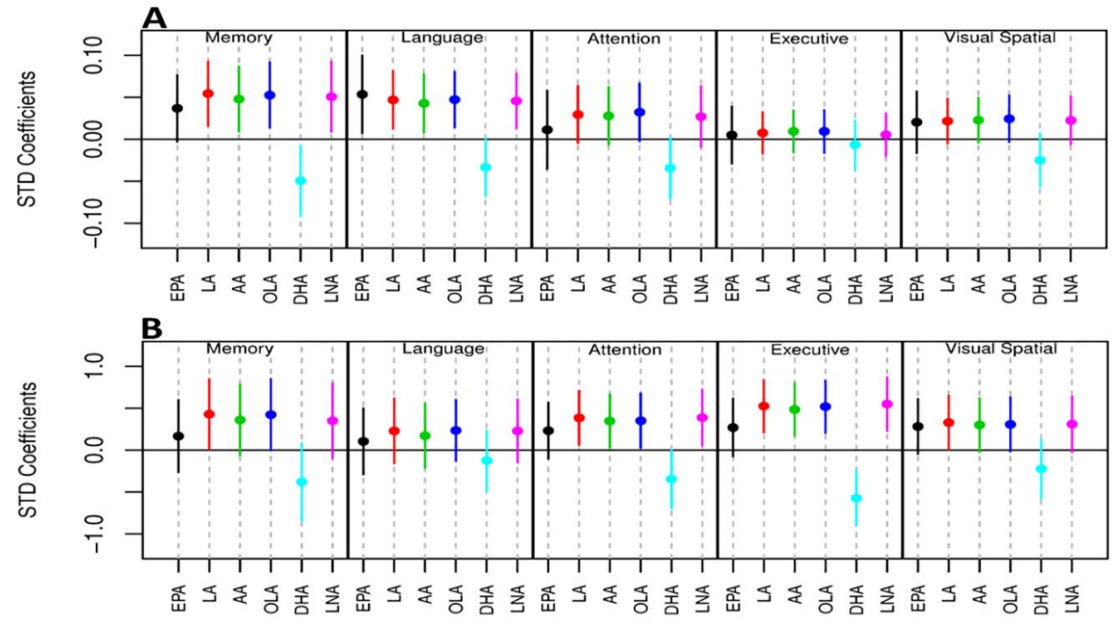

Figure 5.10 Fore`st plot showing the relationship of the abundance of six PUFA's in the MFG and five measures of cognition. A) association between fatty acid abundance of PUFA levels and longitudinal cognitive performance B) associations between fatty acid abundance cognitive performance at the last visit prior to death. AA: arachidonic acid, DHA: docosahexaenoic acid, EPA: eicosapentaenoic acid, LA: linoleic acid, LNA: linolenic acid, OLA: oleic acid. This figure was produced by Dr.Yang Li and his permission was obtained to present.

5.4 Discussion

The metabolic basis of vulnerability to AD pathology and the subsequent expression of symptoms of AD are poorly understood. In this study, we applied mass spectrometry-based metabolomics to human brain tissue samples from a well-characterized longitudinal cohort, i.e., the BLSA, to address this issue. Our results suggest that perturbations in brain UFA metabolism are closely related to AD pathogenesis. To the best of our knowledge, this report is the first to measure brain tissue levels of PUFAs to demonstrate a relationship with both severity of AD pathology and the expression of AD symptoms. Including brain tissue samples from "ASM" individuals who represent an intermediate group in the gradation of neuropathology from controls to AD patients in the absence of cognitive impairment during life allowed us to relate measures of brain UFAs to incremental levels of AD pathology and symptom expression.

Importantly, by measuring PUFA levels in brain regions both vulnerable to distinct pathological features of AD, i.e., MFG (amyloid deposition) and ITG (tau accumulation) as well as in a region relatively resistant to AD pathology, i.e., CB, we were able to ask whether the observed alterations in these metabolites were related to AD-defining pathological processes. We can categorize our results broadly as follows:

i. In the CB, the observed shifts in the abundance of the six UFAs measured do not follow a consistent trend (Figure 5.7) as observed in both the ITG and MFG, which are vulnerable to tau and amyloid pathology, respectively. Consistent shifts in the abundance of the UFAs are observed in the ITG, with the greatest difference between control and ASM participants. Consistent shifts are also observed in the MFG, with the ASM group being intermediate (Control>ASM >AD).

ii. There is an extensive body of literature exploring the potential mechanisms of Alzheimer pathology[326-328] with a number of metabolomic studies having examined associations with AD[190, 193, 256] , however few have studied these differences in human brain tissue [239, 255]. Our current report identified metabolite compositional

differences between three diagnostic groups, i.e., healthy controls, AD, and ASM, i.e., individuals with significant levels of Alzheimer pathology, but with no cognitive `1impairment during life (Figure 5.2). The overall pattern of metabolite shifts observed in the brain was mirrored in each of the individual brain regions (Figure 5.3), with the metabolism of PUFA's discriminating between the clinical groups in all brain regions.

iii. Whilst the CB was included in this study as a brain region showing low levels of Alzheimer pathology, we did observe significant alterations in the levels of the six PUFA's in this region relative to controls, suggesting that both Alzheimer pathology and other non-AD-related processes may contribute to or result from the metabolic differences observed in this brain region [235].

Previous studies have examined the abundance of PUFA's in the brain of AD patients. Nasaruddin *et al*. [329] reported that the abundance of 20 fatty acids was increased in Brodmann' 7 region of late stage AD patients. Four of these species, i.e., oleic, linoleic, linolenic, and AA were shown to be reduced in our present study, whereas levels of DHA were consistent. Cunnane *et al*. measured fatty acids in both plasma and brain tissue samples and reported lower levels of esterified DHA in the AD group specifically in phosphatidylserine in the middle frontal and superior temporal cortices [330]. It must be noted that DHA containing phospholipids are structurally and functionally distinct metabolites to the free fatty acids reported in this study.

The PUFAs can broadly be split into two classes, the omega-3 and omega-6 fatty acids. Alpha linolenic acid (omega-3) and linoleic acid (omega-6) are both "parental" essential fatty acids, both of which are converted into long chain PUFAs, AA from linoleic acid and DHA and EPA from linolenic acid. Amtul *et al*. [331] performed an in vitro study to deter- mine the effect of the omega-6 fatty acids linoleic acid and AA, and the omega-9 fatty acid oleic acid on the pathology of AD. Linoleic, oleic acid and AA were all shown to induce the polymerisation of both tau and Aβ , with AA also shown to induce $A\beta_{42}$ formation reducing the observed ratio of $A\beta_{40}/A\beta_{42}$. Whilst this information and additional literature [38] would point to oleic acid being pathogenic, there is also a

significant body of literature supporting the idea that oleic acid is protective against AD [332, 333]. Amtul *et al*. demonstrated that in in vitro models, oleic acid supplementation reduced secreted Aβ levels and validated these findings in a transgenic mouse model fed an oleic acid- rich diet [332]. The potential benefits of oleic acid supplementation in humans are highlighted by olive oil, which is rich in oleic acid and thought to be protective against age-related cognitive decline and onset of AD [332, 334, 335] , In a clinical trial, Martinez-Lapiscina *et al*. showed that patients randomised to an olive oil-rich diet had better cognitive function compared to those on a control diet [336].

Dietary supplementation with the omega-3 fatty acids DHA and EPA has also been shown to improve cognitive performance in several animal studies of AD [337-340]. Previous human studies have also reported promising effects on cognition in individuals receiving either DHA, EPA, or a combination of the two [341-343]. The mechanisms by which DHA supplementation may impact AD may be by modulating a beta deposition in the brain[344] . The potentially protective effects of EPA in the brain may be mediated through competitive inhibition of the action of lipoxygenases (LOX) (Figure 5.11), cyclooxygenases (COX), and cytochrome P450 (CYP450) against its omega-6 homologue arachidonic acid (AA) [345-348]. The breakdown of AA by COX and 5-LOX produces prostaglandin E2 and leukotriene B4 [347], which, respectively, are both highly proinflammatory [348, 54], whilst the breakdown of EPA by these enzymes to produce prostaglandin E3 and leukotriene B5 is less efficient [347] and whilst they are also proinflammatory, they are less potent than the products of AA [345, 346].

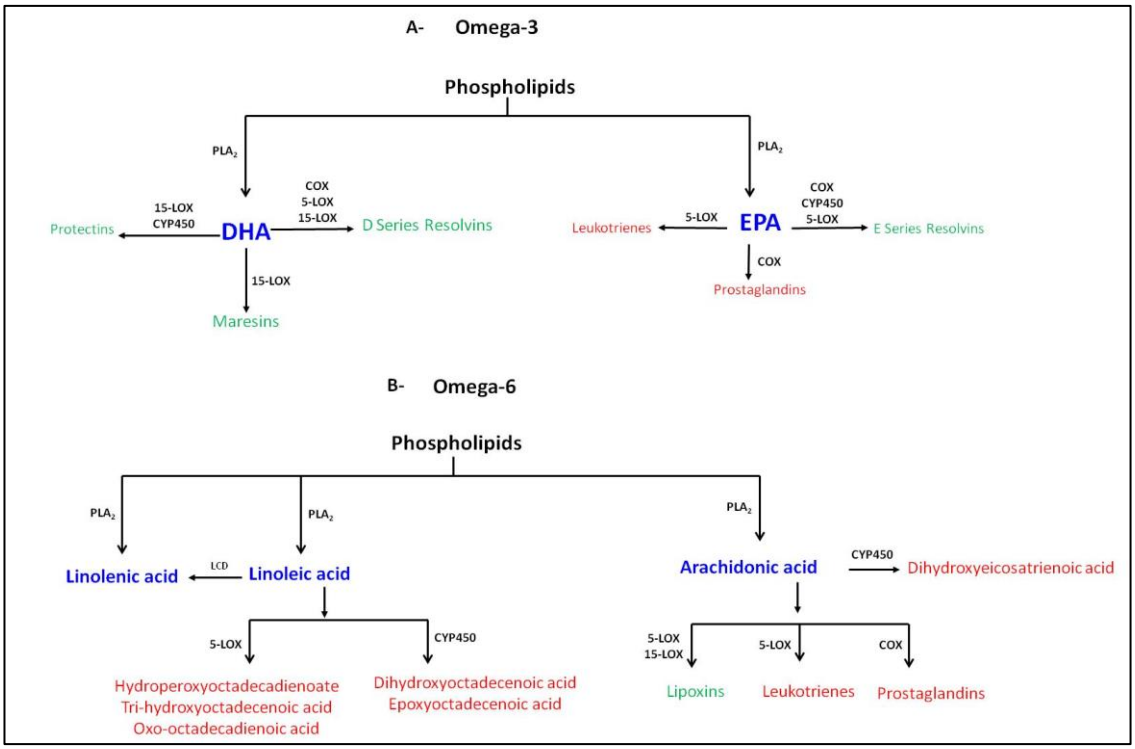

Figure 5.11 Overview of omega-3 and omega-6 PUFA metabolism showing the potential association between the measured PUFA's. Metabolites highlighted in red have been shown to pathogenic with metabolites highlighted in green shown to be protective of disease. COX: cyclooxygenase, CYP450: cytochrome P450, DHA: docosahexanoic acid, EPA: eicosapentaenoic acid, LCD: lineoyl-CoA desaturase, LOX: lipoxygenase, PLA_2: phospholipase A_2.

PUFAs are also precursors of the eicosanoids, which are a large class of highly potent regulatory lipid hormones (Figure 5.11), possessing a wide range of biological functions. Studies have shown that DHA and EPA containing phosphatidylcholines (PCs) are reduced in abundance in the blood of patients with AD [68, 349, 350]. It has been reported that COX, LOX, and CYP450, i.e., enzymes that break down EPA and the other five PUFAs measured, have all been shown to be up-regulated in patients with AD [351, 352], potentially explaining the decrease in the observed PUFA species. Breakdown of EPA and other PUFAs by COX leads to the production of prostaglandins with LOX breakdown leading to the production of leukotrienes, and breakdown by CYP450 producing epoxyeicosatrienoic acid, all of which have been associated with pathology in a range of diseases including AD [353-355]. The breakdown of DHA by these three enzymes produces resolvins, maresins, and protectins, which have been shown to be protective against numerous disease pathologies [356-358], including in AD [359, 360].

5.5 Conclusion

In this chapter, we identified significant differences in the abundance of six PUFAs in three brain regions with gradations in these metabolites being related to both severity of neuropathology at death as well as domain-specific cognitive performance during life. This suggests that dysregulation of PUFA's metabolism plays a role in AD pathology and that these results provide further evidence for the metabolic basis of AD pathogenesis. The next chapter will apply the brain IVDE method to explore lipids metabolites (Lipidomics).

Chapter 6: Comprehensive lipidomics analysis of brain reveals changes in sphingolipid metabolism in the inferior temporal gyrus (ITG) of patients with Asymptomatic Alzheimer's.

6.1 Introduction

As described in the introduction (Chapter 1), AD is accompanied with brain atrophy as a result of synaptic loss and neuronal death, and microscopically in the brain by the extracellular deposition of Aβ plaques, which arise as result of enzymatic cleavage of APP by β- and γ- secretase in sequential order; and the occurrence of NF tangles inside neurons, consisting of hyper-phosphorylated tau proteins formed in paired helical filaments [361-363]. Early pathological changes in the AD brain occur first in the hippocampus and cortex and then extend to the medial temporal lobe which is involved in the deficits in memory, hence as the disease progresses cognitive deficits begin to show. Other parts of the brain, like the cerebellum and midbrain, are also affected due to metabolic changes.

Metabolomics data regarding AD has shown abnormal concentrations of many lipids in various tissues, mainly CSF and plasma, suggesting evidence of irregular lipid metabolism [68, 182, 364, 365]. This could be related to AD's main genetic determinant APOE4, a lipoprotein that regulates lipid homeostasis by mediating lipid transport from one tissue or cell type to another and a major cholesterol carrier that supports lipid transport and injury repair in the brain [366, 367]. Many studies have identified irregularities in lipids concentration among AD as well as preclinical groups, suggesting their role in AD progression [82, 213] .

A rapidly growing body of literature is highlighting the importance of lipids in cell signalling and pathophysiological processes including phospholipids, sphingolipids (SPHL) and glycerides. Considering these findings, a comprehensive LC-MS lipidomics method of brain tissue was applied in this study based on an untargeted approach (described in Chapter 2). To our knowledge, no studies have analysed lipids directly in human brain and linked them to the progression of classic hallmarks of AD pathology. This is surprising considering that AD is a disease that primarily affects the brain, which is known to have the second highest concentration of lipids only behind rich adipose tissue. Therefore, understanding the lipid pathways in the prognosis of AD is of vital importance.

In this chapter, we present a comprehensive lipidomics analysis to identify metabolic changes associated with both Aβ and tau pathologies in the inferior temporal gyrus (vulnerable to tau deposition) and medial frontal gyrus (vulnerable to Aβ deposition) with the cerebellum as a low pathology control. Samples included three diagnostic groups, healthy controls, Alzheimer's patients and a third group of subjects that exhibit high levels of tau and amyloid pathology but were cognitively normal (called Asymptomatic patients) and that can be assumed to be in the early stages of AD.

All samples were analysed using the RP-LC-MS method described in chapter 2. We then carried out the analysis of correlation with pathology parameters (Braak staging (tau) and CERAD scoring (Aβ)) and cognition parameters. Our results show a significant increase in sphingolipid (SPHL) species in Asymptomatic group (ASM) brain in the Inferior temporal gyrus (ITG) region, these also revealed association with tau tangles.

6.2 Materials and Methods

6.2.1 Samples used for the analysis

All samples (n=124) were obtained from the Baltimore Longitudinal Study of Aging (BLSA), Baltimore, USA. At post-mortem 43 patients were stratified as healthy controls (CN), Alzheimer's patients(AD), and asymptomatic (ASM), patients with significant Alzheimer's pathology without exhibiting cognitive decline during life. Samples of three brain regions, cerebellum(CB) as pathology control region, inferior temporal gyrus (ITG) with high tau pathology and medial frontal gyrus (MFG) with high Aβ pathology were collected from all patients. The clinical characteristics (age, MMSE, PMI) of participants of the three diagnostic groups analysed are shown in Table 6.1 below.

Table 6.1 Demographic Characteristics of study participants. [a] value is reported as the mean +/- standard deviation, and range, [b] values are reported as the mean +/- standard deviation [c] values are reported as the mean +/- standard deviation, and range. MMSE: Mini-mental state examination, PMI: post mortem interval, *p<0.05, ** p<0.01***<0.001. ASM, asymptomatic; CN, control; AD , Alzheimer.

	CN	ASM	AD
Participants (f/m)	14 (4/10)	15 (5/10)	14 (7/7)
Age at death (Years)[a]	82.6 +/-11.0 (64.2-9.2)	89.2 +/- 7.9 (71.9-96.4)	87.9 +/- 8.9 (62.9-98.7)
MMSE[b]	27.8 +/- 2.4	29.0 +/- 0.9*	23.0 +/- 6.9**
Boston Naming	54.4 +/- 4.3	55.2 +/- 3.3	46.7 +/- 6.5***
Benton Retention	7.1 +/- 4.6	7.3 +/- 3.0	14.2 +/- 8.47***
PMI (Hours)[c]	16.9 +/- 6.4 (7.0-28.0)	14.8 +/- 8.1 (2.0-33.0)	14.7+/- 6.0 (3.0-23.0)

6.2.2 Chemicals and reagents

Solvents including water, MTBE and methanol were LC-MS grade purchased from Sigma-Aldrich (Poole, UK). Ammonium formate and the two internal standards, Cer (41:1) and SM (35:1) and commercially available serum samples were also purchased from Sigma-Aldrich.

6.2.3 Sample preparation

Human brain tissues were acquired from the BLSA. For all 124 biopsies, identical lipidomics procedures for sample preparation and LC-MS/MS analysis were executed. Sample preparation prior to analysis followed brain IVD extraction procedure as described in Chapter 2, Section 2.2.5. Samples were then analysed in a randomized order. Quality control (QC) samples were composed of a pool of commercially available serum samples (n=22) being extracted and analysed every 6 samples. Details of the analytical workflow are provided in Figure 6.1 below.

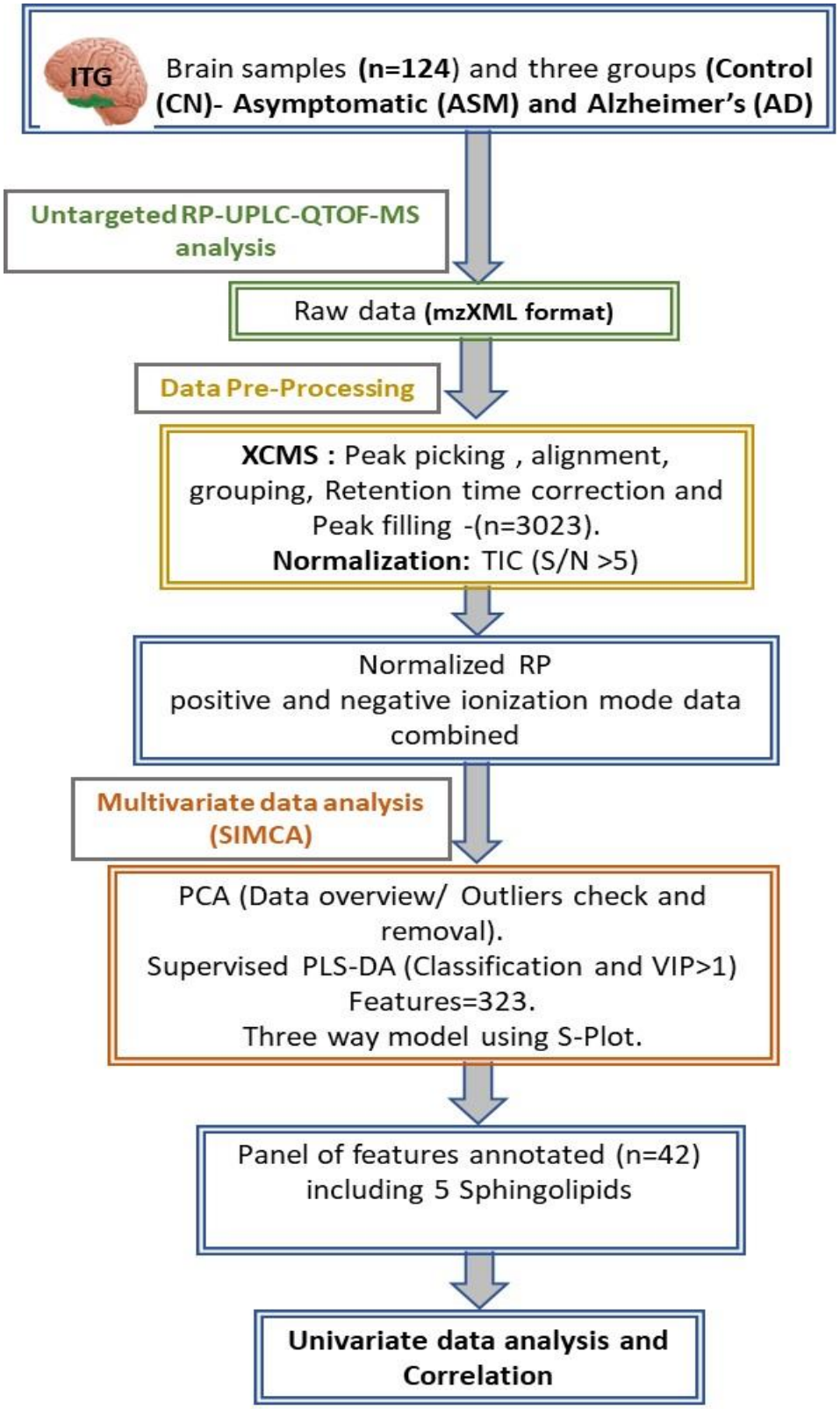

Figure 6.1 Lipidomics Data processing workflow. RP: Reversed phase, TIC: Total ion count, S/N: Signal to noise, PCA: Principal Componenet Analysis, PLS-DA: Partial least square discriminant analysis, VIP: Varible important to projection .

6.2.4 Chromatography

Samples were analysed using RP-LC/MS. Analysis was performed using Waters Aquity coupled to Waters Xevo QTOF (Waters,Milford, USA). Analysis was completed in both positive and negative ionization mode with LC and MS settings designed for each phase are described in detail in chapter 2, section 2.2.6.

6.2.5 Data collection and Pre-processing

All data was collected by Waters Xevo QTOF which used MS^e technique, two collision energies applied that grant data collection at two levels. The first level obtained data using 5 V of collision energy, the second level obtained data at higher collision energy of 50 V. This can assist in structural elucidation and to simultaneously collect accurate mass of parent ion and fragmentation data.

Following LC-MS analysis of samples, the MS raw data were transformed into mzXML format using msConvert (ProteoWizard). XCMS software package in R was then used to analyse the converted mzXML data files, underwent preprocessing steps of peak picking and alignment processed, using a 'centwave' method which enables the deconvolution of closely eluting or slightly overlapping peaks. Following peak picking, metabolite features were defined as peaks with an average intensity five times higher in analytical samples than in the extraction blanks.

6.2.6 Data Processing

Metabolite features were analysed using a multivariate data analysis, including principle component analysis (PCA), Partial least square – discriminant analysis (PLS-DA) and Orthogonal partial least square – discriminant analysis (OPLS-DA). All were performed in SIMCA 13.0.4 (Umetrics, Umeå, Sweden). The performance of the model was evaluated using the cumulative correlation coefficients (R^2X[cum]) and predictive performance based on seven-fold cross validation (Q^2[cum]. Feature selection to create curated models was performed by removing metabolite features that had VIP plot score

of <1 to achieve the fitted model with the optimal R^2 and Q^2 values. The optimal Curated PLS-DA model has total of 323 features. Statistical analysis on features of interest was performed using one-way ANOVA with multiple comparison testing performed using Benjamini and Hochberg applied to TIC normalised data in SPSS software. Spearman's correlation analysis was applied to investigate the correlation with clinical of pathology parameters: Braak staging and Cerad score. All correlation analysis was also conducted in SPSS 22 (IBM: Armonk, United States). The potential disease pathology indicators selection was based on those features exhibiting high magnitude of variation in the s-plot with value (p[1]) >0.15 and statistical significance.

6.3 Results

6.3.1 Brain lipidomics analysis

The lipidomics brain IVDE method described in Chapter 2 was used to analyse the brain samples. A final list of 3023 metabolite features (m/z at retention time) were obtained after data pre-processing and alignment using XCMS divided in to 2014 features from RP positive ionization mode and 1009 features from negative ionization mode.

6.3.2 Method assessment and data quality

Following sample analysis, XCMS data underwent PCA analysis in SIMCA 14 to overview data and check for outliers. The %RSD of both IS used were reported at less than 30 % across samples and QCs, shows the values obtained have acceptable reproducibility. In Table 6.2, %RSD in QC samples was lower with <15% variation. IS high reproducibility would indicate analytical stability since it is important to ensure the reproducibility of the whole run and allow for instrument calibration, this is to asses any instrumental variability and ensure mass accuracy over the analytical run time.

Table 6.2 Descriptive parameters from peak area of two internal standards used in this lipidomics analysis.

Internal Standard	Chromatography (Ionization mode)	%RSD across all sample run (n=124)	% RSD in QC raw signal intensity	RT(min) / % RSD of RT
Cer (17:1/24:1)	RP (Positive)	18.73	7.8	17.17/0.2
Cer (17:1/24:1)	RP (Negative)	18.51	8.2	22.01/0.2
SM (18:1/17:0)	RP (Positive)	24.66	12.7	11.45/0.4

RP=Reversed Phase, Cer=Ceramide, SM= Sphingomyelines, %RSD=% Relative Standard Deviation, RT=Retention time, QC =Quality Control samples.

6.3.3 Partial Least Square Discriminant Analysis (PLS-DA) of lipidomics data

PLS-DA models were constructed based on 3023 metabolite features to assess the effect of both brain regions and pathological diagnosis on metabolite composition. In curated PLS-DA models both pathological diagnosis (Figure 6.2B - $R^2X = 0.469$, $R^2Y = 0.443$, $Q^2 = 0.422$, CV-ANOVA = $4.63x10\text{-}^{19}$) and brain region (Figure 6.2A - $R^2X = 0.594$, $R^2Y = 0.582$, $Q^2 = 0.529$, CV-ANOVA = $3.54x10^{-23}$) have a significant effect on metabolite composition. From the scores plot (Figure 6.2A) it can be observed that ITG and MFG regions are more similar to each other although they are metabolically compositionally distinct, with CB showing to be highly distinct. The same is observed when comparing the three diagnostic groups, asymptomatic and control groups appear to be more like each other than the group representing Alzheimer's patients. It can be seen (Figure 6.3) that the pattern observed was replicated in each of the three brain regions with the effect size appearing comparable in the ITG and MFG and slightly weaker model in the CB (Figure 6.3).

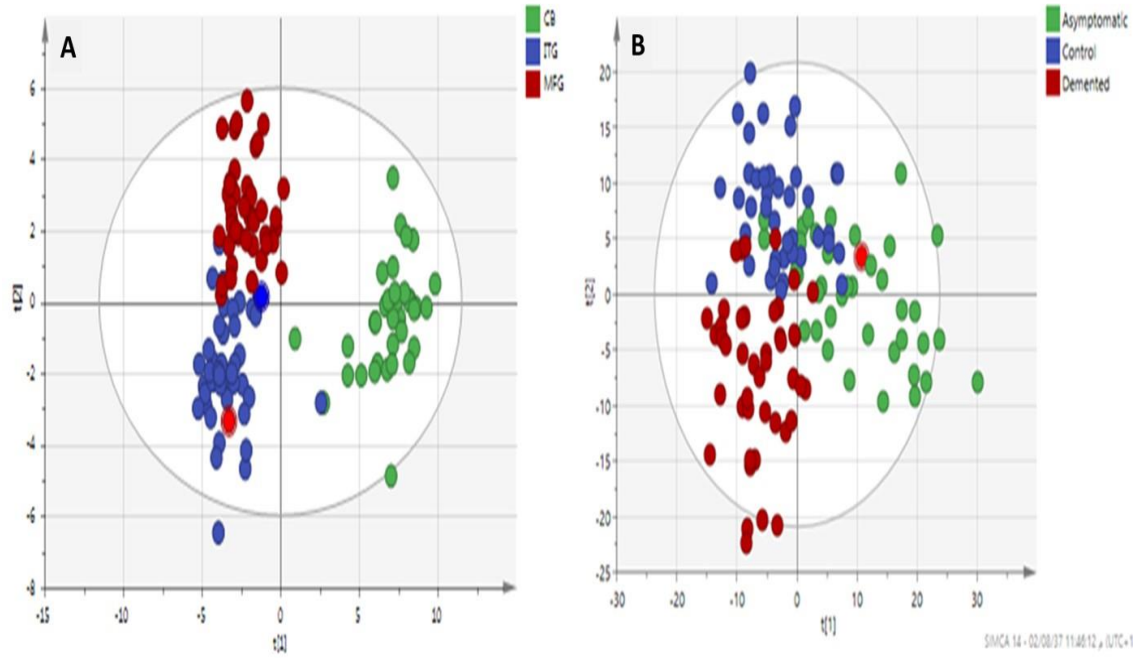

Figure 6.2 Curated PLS-DA scores plots models comparing the metabolite composition of brain regions and diagnostic groups. (A) Comparisons of metabolite composition of cerebellum (CB), inferior temporal gyrus (ITG) and medial frontal gyrus (MFG) $R^2X = 0.594$, $R^2Y = 0.582$, $Q^2 = 0.529$, CV-ANOVA = $3.54x10^{-23}$). (B) Comparison of metabolite composition of diagnostic groups, control(CN), asymptomatic (ASM) and Alzheimer's (AD) ($R^2X = 0.469$, $R^2Y = 0.443$, $Q^2 = 0.422$, CV-ANOVA = $4.63x10^{-19}$).

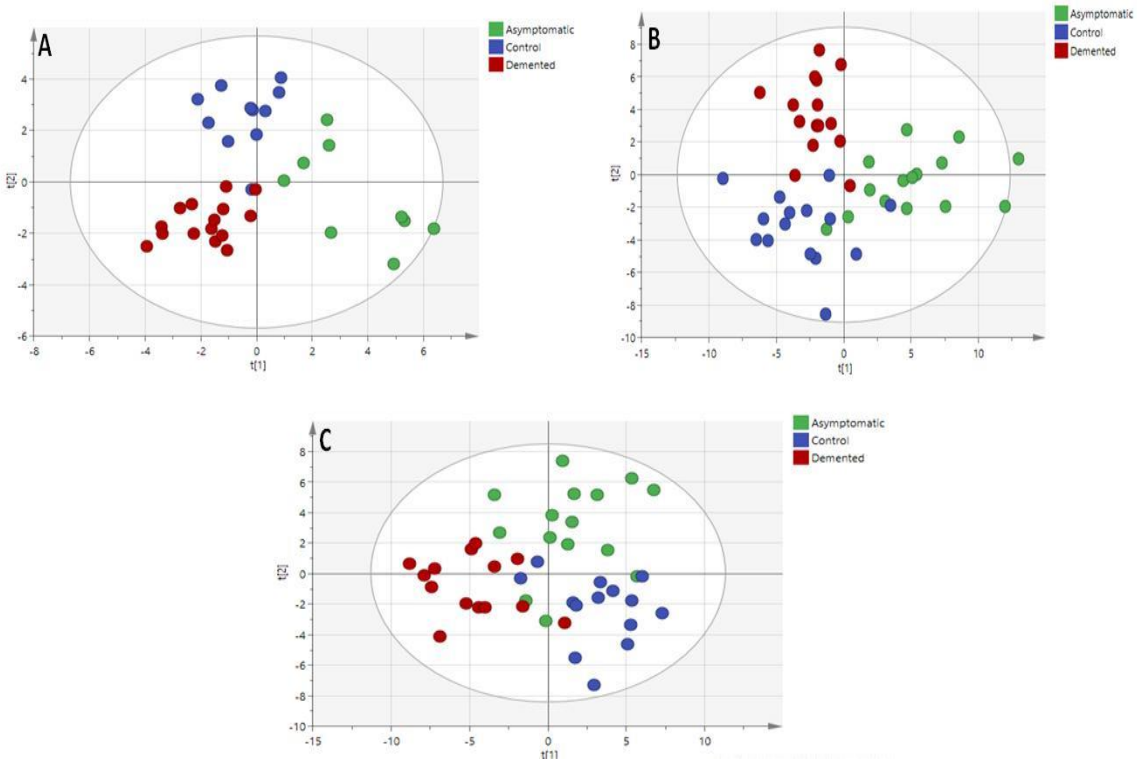

Figure 6.3 Curated PLS-DA scores plots comparing the metabolite composition of diagnostic groups in individual brain regions. (A) Comparisons of metabolite composition of diagnostic groups, control, asymptomatic and Alzheimer's in cerebellum samples (R^2X = 0.516, R^2Y = 0.527, Q^2 = 0.412, CV-ANOVA = 7.03×10^{-6}). (B) Comparisons of metabolite composition of diagnostic groups, control, asymptomatic and Alzheimer's in inferior temporal gyrus samples (R^2X = 0.589, R^2Y = 0.561, Q^2 = 0.471, CV-ANOVA = 2.17×10^{-5}). (C) Comparisons of metabolite composition of diagnostic groups, control, asymptomatic and Alzheimer's in medial frontal gyrus samples (R^2X = 0.553, R^2Y = 0.561, Q^2 = 0.410, CV-ANOVA = 4.23×10^{-5}).

The metabolic features used to create the optimal curated PLS-DA models of all three diagnostic classes (Figure 6.2B) were taken forward as being the most interesting to pathology. The optimal PLS-DA model obtained comprised of 323 features that discriminated different groups to be highly associated with disease progression.

6.3.4 Orthogonal partial least square discriminant analysis of lipidomics data

OPLS-DA models were created using 323 features obtained from the optimal PLS-DA model, as a further data mining approach. The samples were grouped by class (CN or ASM or AD) with first model composed of all three diagnostic groups within the same model (Figure 6.4A). It can be seen that the AD group is different from the controls groups (CN and ASM). Based on this OPLS-DA model of the two controls groups and AD group was performed (Figure 6.4B- refers to as three-way model). The three-way model OPLS-DA returned an R2 and Q2 value of 0.873 and 0.425 respectively (Figure 6.4B). The model was considered an acceptable predictive model. From the OPLS-DA model an S-plot was produced (Figure 6.4C), in order to obtain the features that varied the most between diagnosis groups. The features with p[1] of >0.10 and p(corr)[1] of > 0.20 were selected (Table 6.4C). The model produced 42 features that underwent further investigation and annotation.

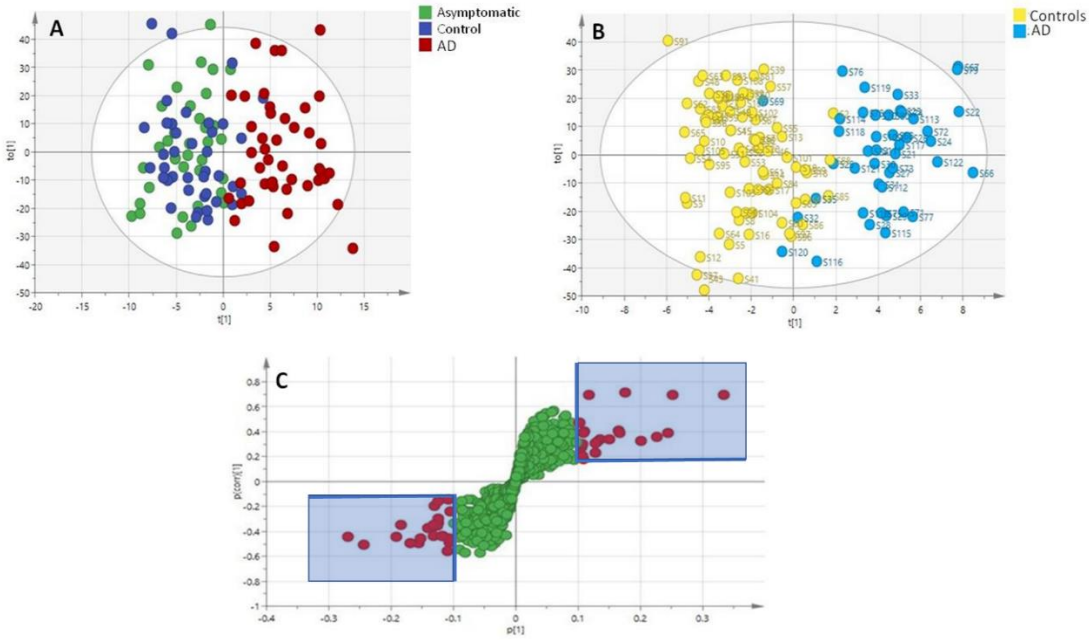

Figure 6.4 The figure depicts pareto scaled OPLS-DA model of Lipidimics data (n=323). (A) Three groups showing clear separation between AD and Controls (ASM and CN). (B) OPLS-DA for three-way model by combining ASM and CN as one group and AD as second group with model validation value R^2= 0.873 Q^2= 0.425. (C) S-Plot with features exhibiting great magnitude of variation (p [1] of >0.10 and p(corr) [1] of > 0.20) are in red colour. These features can be found in Table 6.3.

Table 6.3 Features obtained from the data S-plot analysis.

	m/z	RT (min)		m/z	RT (min)
POSITIVE IONIZATION MODE	811.8	15.36	NEGATIVE IONIZATION MODE	747.54	15.75
	889.7	28.6		748.51	19.15
	858.6	17.31		916.63	21.44
	860.8	18.3		764.50	18.19
	866.7	17.5		778.56	21.81
	617.7	16.08		804.54	18.62
	632.8	19.37		788.52	18.68
	645.8	18.83		646.59	23.05
	604.8	17.58		742.53	19.32
	684.6	16.38		849.61	21.84
	686.8	16.67		742.52	19.32
	661.7	17.76		838.52	18.28
	671.8	17.95		851.65	21.96
	644.7	19.64		862.63	22.67
	548.8	13.65		819.52	20.05
	585.8	13.41		464.30	5.77
	520.8	11.60		788.52	18.68
	597.7	10.82		832.49	16.04
	711.7	18.22			
	730.6	16.42			
	787.8	16.55			
	704.8	10.52			
	630.8	12.17			
	646.8	16.86			

6.3.4 Lipid feature selection

Out of the 42 features detected in the s-plot (Table 6.3), we were able to confirm the structural elucidation of 15 features (see Table 6.4 below), with sphingolipids (SPHLs) making up for over half of the annotated metabolites, and a massive body of literature also linked SPHLs to AD pathology. To this end, SPHLs were identified for more detailed analysis as these metabolites showed the strongest correlation with the disease group.

Table 6.4 List of annotated lipids displaying p-value and fold change and listed by lipid family.

	CN Vs ASM		CN Vs AD		ASM Vs AD	
	p-value	FC[b]	p-value	FC[b]	p-value	FC[c]
Cer(18:1/16:0)	8.4×10^{-2}	1.34	3.0×10^{-2}	0.61	1.8×10^{-2}	0.82
Cer(18:1/18:0)	6.8×10^{-3}*	0.74	2.3×10^{-1}	0.52	4.0×10^{-2}	0.16
Cer(18:1/22:0)	6.3×10^{-2}	1.11	8.0×10^{-1}	1.44	2.4×10^{-2}	1.30
Cer(18:1/24:0)	7.8×10^{-3}*	1.14	8.5×10^{-1}	1.31	5.4×10^{-3}	0.78
Cer(18:1/24:1)	6.3×10^{-3}*	1.15	7.5×10^{-1}	1.53	8.7×10^{-3}	1.26
Cer(18:1/26:1)	6.4×10^{-3}*	1.06	7.5×10^{-1}	0.59	9.7×10^{-2}	1.11
SM (18:1/16:0)	4.6×10^{-1}	0.73	3.4×10^{-1}	0.34	8.8×10^{-1}	1.21
SM (18:1/22:0)	2.8×10^{-2}	0.63	8.2×10^{-1}	0.44	3.2×10^{-2}	0.91
DG (13:0/21:0)	7.5×10^{-1}	1.11	6.7×10^{-3}	1.42	2.1×10^{-2}	0.80
DG (17:0/20:3)	1.0×10^{-2}*	0.89	7.3×10^{-2}	1.31	1.1×10^{-2}	0.93
PC (22:4/20:4)	8.1×10^{-1}	0.94	1.1×10^{-2}	1.38	1.6×10^{-2}	1.05
PC (18:1/22:0)	6.4×10^{-1}	1.20	3.3×10^{-2}	0.46	1.5×10^{-1}	1.31
PE (20:5/19:0)	6.4×10^{-1}	1.04	1.2×10^{-1}	0.88	4.4×10^{-2}	0.85
PA (33:0)	2.8×10^{-1}	1.19	8.9×10^{-3}	1.90	1.6×10^{-2}	1.58
TG (55:8)	2.1×10^{-1}	0.59	4.1×10^{-1}	0.94	1.5×10^{-1}	1.22

Cer=ceramides, SM=Sphingomyelin, PC=Phosphatidylcholine, DG=Diacylglycerol, TAG=Triacylglycerol, PE=Phosphatidylethanolamine, PA=Phosphatidicacid, *pass Benjamin and Hochberge correction (q=<0.05). ASM, asymptomatic; CN, control; AD , Alzheimer.

6.3.5 Structural elucidation and identification: Sphingolipids.

In total 184 metabolites were annotated out of the features detected in this lipidomics study (Appendix D-Table 6.1). Following the selection of highly correlated features using multivariate modeling, these features underwent putative identification using database and MS[e] technology on the Waters Xevo instrument by checking for fragments for structural identification. A set of rules were also applied to filter the search results as described in Chapter 2 (Section 2.3.4). Table 6.5 displays the fragments of each molecule as observed on MS[e] data. Moreover, in this lipidomics study, two internal standards were used, Cer (17:1/24:1) and SM (18:1/17:0), which also help during the identification

process to elucidate side chain cleavages and retention time order of related structures. Figure 6.1 & 6.2 (Appendix D) represent the MS spectra (both channel 1 and channel 2) of the two Standards.

Cers were identified as $[M+H_2O-H]^+$ as sphinganine molecules. Initial observations showed a fragment ion in each m/z at 264 Da which represents the sphinganine head group of (18:1), this m/z is unique and does not match with other molecules. The unsaturated fatty acid 24:1 has *m/z* 630.88 with 2 less Da due to the double bond and loss of Hydrogen. SM was identified as $[M+H]^+$. The fragment ion of m/z 184.07 Da is known to refer to the Choline head group that is distinctive to 2 lipids classes which are phosphatidylcholines (PC) and SM. However, when matching the results from open access data base and the retention time of our in-house database, no PC molecule were associated with the detected m/z, providing support that the 2 features with 184.07 (choline head group) are SM.

Table 6.5 Identification based on the observed ions, collision induced dissociation fragmentation of lipids, and retention time (product ion *m/z* 264.2 and 184.07 for ceramides and Sphingomyelins species corresponds to sphingosine base chain and choline head group respectively.)

Identified as	Observed ion	Fragments	RT (min)
Cer (d18:1/16:0)/Cer16:0	$[M+H_2O-H]^+$	520.83 & 264.24	11.60
Cer (d18:1/18:0)/Cer18:0	$[M+ H_2O -H]^+$	548.85 & 264.24	13.65
Cer (d18:1/18:1)/Cer18:1	$[M+ H_2O -H]^+$	546.85 & 264.24	12.33
Cer (d18:1/20:0)/Cer20:0	$[M+H_2O-H]^+$	576.81 & 264.24	14.84
Cer (d18:1/22:0)/Cer22:0	$[M+H_2O-H]^+$	604.87 & 264.24	17.58
Cer (d18:1/24:0)/Cer24:0	$[M+H_2O-H]^+$	632.89 & 264.24	19.37
Cer (d18:1/24:1)/Cer24:1	$[M+H_2O-H]^+$	630.88 & 264.24	17.96
Cer (d18:1/26:1)/Cer26:1	$[M+H_2O-H]^+$	644.78 & 264.24	19.64
SM (d18:1/16:0)/SM16:0	$[M+H]^+$	704.83& 184.24	10.52
SM(d18:1/22:0)/SM 22:0	$[M+H]^+$	787.87& 184.24	16.55

6.3.6 Sphingolipids abundance in the three human brain regions.

In this study we analysed sphingolipids in human brain of CN, ASM and AD groups from three brain regions which are ITG, MFG and CB. Lipids sphingomyelines (SM (18:1/16:0) and SM (18:1/22:0) will be referred to as (SM 16:0, SM22:0) and ceramides will be referred to as (Cer16:0, Cer18:0, Cer22:0, Cer24:0, Cer24:1 and Cer26:1) throughout the rest of the chapter.

Mann Whitney test value was used to show mean significant difference of identified SPHL species between groups in individual brain regions. SPHLs showed a similar trend increasing in ASM and AD compared to CN in ITG region. The same trends were observed in the MFG region, however, in MFG region no significant change were observed in SPHLs abundance between groups, except SM 24:0 which show significant increase in AD compared to CN. Based on these observations, SPHL abundance in ITG brain region (Table 6.6 and Figure 6.7) was processed using one-way ANOVA with Benjamini and Hochberg correction to control the false discovery rate (FDR). All p-values were represented as q values after correction. Lipids with $q<0.05$ were selected for correlation analysis.

Table 6.6 Sphingolipids passed multiple comparison correction (n=5) in ITG brain region.

ITG Region	Overall q-Value	CN vs ASM	CN vs AD	ASM vs AD
Cer22:0	0.011*	**0.013**	0.883	0.065
Cer24:0	0.002*	**0.002**	0.725	**0.019**
Cer26:1	0.006*	**0.017**	0.999	**0.016**
SM 16:0	0.032*	**0.019**	**0.027**	0.902
SM 22:0	0.043*	**0.017**	**0.049**	0.787

* Pass ANOVA Kruskal Wallis test with Benjamini and Hochberg multiple corrections, values highlighted in bold are significant at $q<0.05$. ASM, asymptomatic; CN, control; AD , Alzheimer.

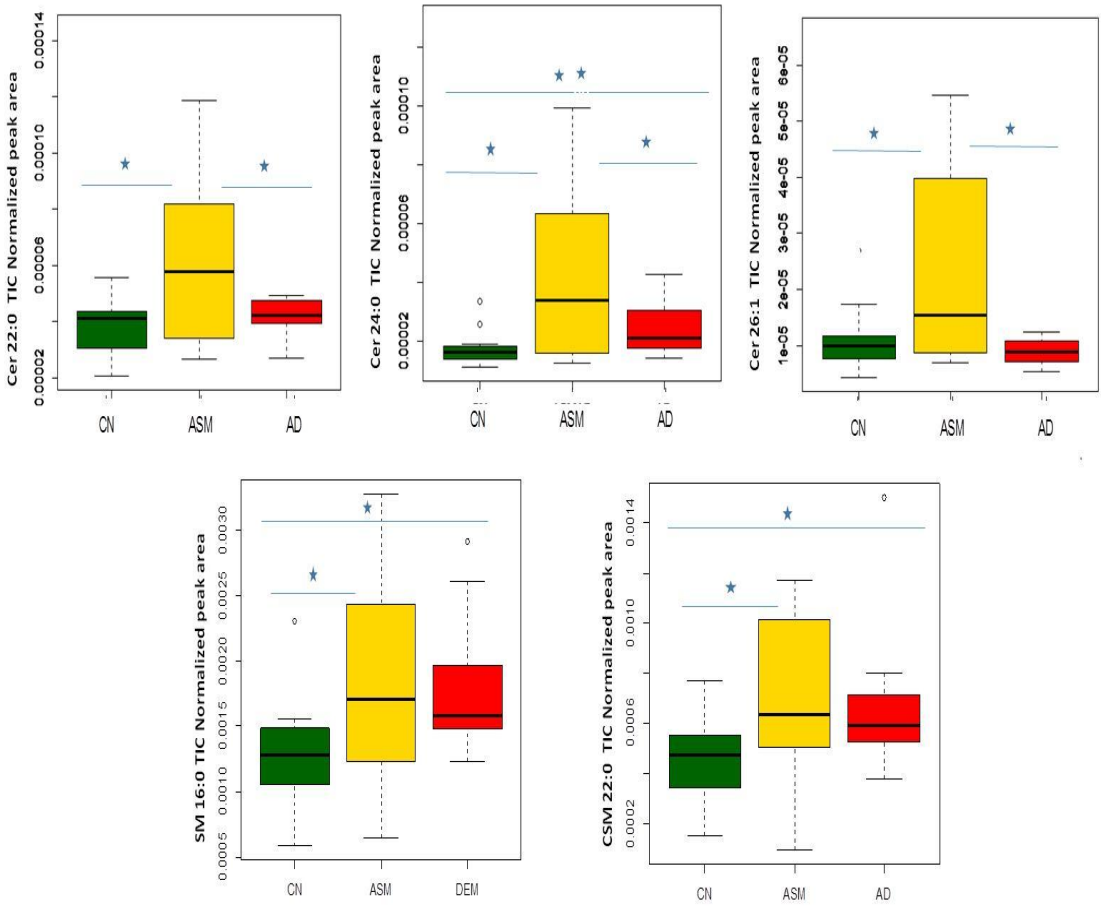

Figure 6.5 Boxplots showing the effect of disease status on the abundance of five sphingolipid in the Inferior Temporal Gyrus(ITG). *pass ANOVA Kruskal-Wallis with Benjamin and Hochberg multiple correction (*<0.05 threshold).

6.3.7 Correlation analysis of selected sphingolipids in brain's ITG region

From the gathered data, significant changes were observed in the brain's ITG region, with our findings showing elevated ceramides and sphingomyelins levels in this region. The results of ANOVA Kruskal wallis test with Benjamini and Hochberge multiple correction revealed that the abundance of very long chain Cer24:0 and Cer26:1 level show significant increase in ASM vs CN (q= 0.002 and 0.017) and in ASM vs AD (q= 0.019 and 0.016) (Table 6.6). On the other hand, SM16:0 and SM22:0 levels were significantly higher in ASM (q= 0.019 and 0.017) and in AD (q= 0.027 and 0.049) compared to CN respectively.

Spearman's correlation analysis of the 3 Cers and 2 SMs that passed multiple corrections were performed using the three diagnostic groups (Table 6.7). It is important to note that ASM is a group with no cognitive decline but with AD pathology (Aβ and tau). Cer levels in the ITG region were shown to be correlated with tau tangles (Table 6.7). and no correlation was observed with any of the cognitive tests. CB is considered as spared region of the brain, believed not to show changes in pathology and also correlation analysis in this region revealed no correlation with neither pathology nor cognition parameters.

Table 6.7 Correlation analysis of sphingolipid abundance and measures of Aβ and tau pathology in ITG region.

	Braak		CERAD	
	R^2	p-value	R^2	p-value
Cer 22:0	0.209	0.183	0.053	0.741
Cer 24:0	**0.405**	**0.008**	0.244	0.120
Cer 26:1	-0.168	0.288	-0.110	0.488
SM 16:0	**0.518**	**0.0001**	0.297	0.056
SM 22:0	**0.419**	**0.006**	0.295	0.058

Relationships between global measures of amyloid and tau pathologies and the abundances of five Sphingolipids, values highlighted in bold are significant at $p<0.05$. CERAD; Consortium to Establish a Registry for Alzheimer's Disease.

6.4 Discussion

Introduction and study overview

Many studies have suggested sphingolipids role in AD pathology. However, role of SPHL metabolism in disease aetiology and mechanism of AD pathology is yet to be understood. In this study, we applied mass spectrometry-based metabolomics to human brain tissue from the longitudinal cohort i.e. BLSA to explore this mechanism in three brain regions. As mentioned previously, ASM group represents the early stage of AD pathology, with this group having Alzheimer's neuropathology without exhibiting cognitive decline during life. Up on observing changes between groups in different brain regions, it can be noticed that changes in SPHL levels occur mainly in the ITG brain region (Appendix D Figure 6.1). Therefore, it was decided to focus on the trends Cers and SM in ITG region.

Interestingly, ITG has high tau pathology and it is described to contribute to early disease pathology where functions as memory, understanding and language are controlled. Five lipids passed multiple corrections, comprised of two SM (SM16:0 and 22:0) both with the omega-9 fatty acid oleic (18:1) chain and 3 Cers (Cer22:0, 24:0 and 26:1). Correlation analysis revealed association of SPHL metabolism with tau tangles. Our data observed an increase in Cers and SM species level in ASM and AD compared to CN groups in the ITG region of brain. The alteration in both early and late AD stage suggested that these species might have a role in disease pathology and shift in cognition. SPHL are class of lipids composed of a backbone of sphingoid base, including but not limited to ceramides (Cers) sphingomyelins (SMs) and sulfatides. They regulate diverse cellular processes such as a apoptosis, cell senescence, cell cycle and cellular differentiation [368].

Many studies have revealed elevated levels of SPHL in human AD brain [213, 369]. Han *et al.* 2002 performed MS lipidomics analysis of Cers in white and grey matter in post-mortem brain tissue of AD subjects at early clinical stage (very mild dementia) This showed a remarkable increase in Cers level in very mild samples compared to age matched controls in white matter. They also found no change in Cers at all stages of AD in the MFG region [210]. Bandaru, Troncoso *et al* 2009 [370] have also reported no change in Cers in MFG grey matter except for Cer24:0, this molecule showed significant increase in AD *versus* CN, these findings are in agreement with what we observed in this study, with only Cer24:0 in the MFG region showing to be significant and increased in AD (q=0.024) and ASM (q=0.047) groups brain compared to CN. The same group reported that Cers production can be due to sulfatide degradation (another class of sphingolipids) as sulfatide depletion was reported in AD brain [213]. Also, investigated Cer and SM levels in AD plasma providing new insight into the AD sphingolipidome and the potential use of metabolite signatures as potential biomarkers [190].

In the case of SM levels previous studies in AD brain have reported both increases and decreases. One 2012 study stated significantly elevated CSF SM levels in patients with prodromal AD and no change between those with mild and moderate AD compared to controls [371]. The authors of this study hypothesized that the observed increase in SM abundance is believed to be an outcome of cellular response to a high cer abundance. SM

can be obtained from Cer via catabolic pathway leading to elevated SM abundance. Another assumption is this increase in SM can be owed to neuronal death and brain atrophy, this explanation is commonly used with lipid levels since SM exist in membranes and form the myelin sheet in the nerve cells maintaining it is structure.

Following the metabolic pathway of SPHL synthesis, it was also reported that the dramatic increases seen in Cers content could be related to abnormal de novo ceramide synthesis from sphinganine and fatty acyl CoA by the action of ceramide synthase or the hydrolysis of SM by activation of sphingomyelinase (SMase), enzyme that facilitates the SM conversion to ceramide. SMase found to present in several forms (Neutral and Acidic). Acidic SMase was reported to be high in AD brains [372] suggesting lower SM levels in the AD brain.

Contrary to this hypothesis our results observed an elevation of two SM species (SM 16:0 and SM 22:0) in ASM and AD brains. This is in line with other publications which reported elevated SM levels in AD brains compared to age matched controls [370, 373]. Yet again, two studies described a significant decrease in SM levels in AD brain, so it might be the case that particular fatty acid chains are changing and not all the lipid family as a whole [372, 374].

It has been proven that membrane associated oxidative stress occurs in association with lipid alterations and Aβ accumulation in AD brain. Aβ has been reported to be involved in the pathogenesis of AD, owing to its association with levels of oxidative stress in the brain [375]. Furthermore, both AD brain tissue and neurons treated with Aβ show excessive oxidative stress, and constant increase in Cer and membrane cholesterol abundance, suggesting irregularities in SPHL and cholesterol metabolism in AD brain [369], including elevated Cer and cholesterol levels in patients with mild symptoms. In our work although we did find specific Cers to be elevated, cholesterol in its free form was found to be very much decreased with pathology and early in AD as (in Chapter 5-Table 5.3).

Considering these observations, it could be suggested that changes Cers would occur early during AD pathogenesis. In 2004 a study by Lee et al showed that treating cultural cells with Aβ lead to Cers accumulation. Also, it was reported that Cers production can affect Aβ production [376] and APP process [377] causing neuronal dysfunction and cell death in AD. Another study suggested that increased Cers concentration result in activation of the enzymes acetyltransferases 1 and 2, BACE1 protein acetylation and therefore protecting protein degradation. This would mean a leading role for Cers in Aβ production [378]. It was also reported that immunization with Aβ caused reduction in Aβ plaque but did not improve cognition due to CNS inflammatory response observed at phase II trial [379]. With these findings in mind, Aβ effect on increasing Cers level would trigger inflammatory effects and this would induce ROS and lead to cognitive dysfunction as a result of cell and neuronal death.

However, this would not be the case in the very early stage, since Cers levels in the ASM group were the highest and these volunteers had not experienced cognitive decline symptoms, unless sustained Cers inflammation could lead to cognitive decline. Yet again, Cers in our study were higher in the ITG, at early and late AD stage, in an area which is susceptible to tau and correlated to tau measures.

To corroborate this assumption, we performed correlation analysis for the five SPHL that passed multiple correction with AD pathology represented as Braak staging (tau tangle) and Cerad score (Aβ accumulation). According to our results (Table 6.7), the correlation analysis of SPHL species with pathology parameters, showed strong correlation of 3 SPHL with tau tangles in the ITG. It was reported that progression of tau pathology through the brain correlated with decline in cognitive function [380]. None of the SPHL correlated with either Braak or CERAD scores in the MFG region, confirming that the observed increases were associated to tau accumulation in the ITG region.

Tau pathology in AD is credited to dead neurons releasing of tau aggregates. This axonal protein's role is to regulate microtubules stability and it mainly accumulates in areas of the brain that are essential for learning and memory such as the ITG [381]. A number of recent studies used various AD models have manifested the active release and inter-neuronal transport of tau [382, 383]. Bright *et al* in 2015 found that human secreted tau

increased Aβ production, since secreted extracellular tau (eTau) leads to neurons hyperactivity and this is a possible process by which eTau regulates Aβ production suggesting that stopping tau spread and progression could prevent Aβ deposition, cognitive decline and thus apoptosis [384].

This theory is proposing that controlling the release of tau would assist the transneuronal expansion of misfolding. Therefore, elucidating the mechanism of tau transfer and spread early in disease is crucial. Braak and Braak *et al* 1991, hypothesized that tau pathology proceed Aβ plaque formation and that tau load correlated better with severity and progression of the disease compared to Aβ plaque [385]. This is a theory that is gaining a lot of support recently, especially in the ADNI imaging studies, where results have shown that tau was a better predictor of AD progression [386].

Our results show Three SPHL to correlate with tau at early stage of AD in the region vulnerable to tau (ITG) (Figure 6.7), suggesting that these SPHL levels increase with disease progression with no correlation seen to cognitive tests. It has been suggested that this could be due to the absence of severe inflammation at this stage and oxidative stress which plays a role in changes in the tau structure to promote its aggregation and lipids peroxidation [387]. We would hypothesize that tau induces Cers production but not to the degree of causing neuronal death and affecting mental functions.

Considering tau as hallmark in AD and Cers as inflammatory species that contribute to cell apoptosis, studying the mechanism by which tau would promote the elevation in Cers is crucially important, especially since this mechanism is believed to take place at the very early stages of disease.

Several studies indicated that Cer and sphingosine mediate apoptosis, growth arrest, and senescence, while their phosphorylated derivatives promote proliferative and antiapoptotic activities. It has been suggested that Cers involved in hyper phosphorylation of tau via activation of protein kinases [388] , such as GSK-3β, MAPK and Cdk5, activated on cellular membranes and thus dysregulation of lipid metabolism may affect the activity of these kinases that are involved in stress signalling cascade hence deterioration in lipids metabolism impact these enzymes function [389, 390]. Cdk5 may

regulate the clearance of tau aggregates by stimulating the autophagy pathway [391, 392]. Thus, the importance of exploring the mechanisms by which tau aggregates, is secreted leading to propagating the tau pathology are still unknown. Maccioni *et al.* 2010 suggested that tau hyper phosphorylation may be a convergent point of toxicity in the AD brain stressing the importance of tau in targeting therapeutic in AD [393].

It was also reported that neuronal survival could be antagonized with very small shifts in ceramide metabolism [363] . Moreover, shift in SPHL metabolism toward accumulation of Cer with the reduction of anti-apoptotic signalling, has been suggested as a function of the disease progression [394].Interestingly, there have been a great emphasize that defect in autophagy (defined as "a vesicle and lysosome-mediated degradative pathway that is essential for protein homeostasis and cell health" are likely to contribute to AD neurodegenerative mechanism [395].

Studies have also related long chain Cer, to tau phosphorylation vis the regulation of phosphoprotein phosphatase 2A (PP2A) signalling and activity [396, 397]. PP2A is a key tau phosphatase, found to be low in AD brain. Activation of PP2A is believed to reduce tau phosphorylation level. Cers are the only endogenous small lipid molecules along with metal cation and polyamines that were shown to regulate PPA2 activity[398] either by blocking I2 inhibitor binding [399] or inhibiting demethylation of PP2A mediated by lithium effects on ceramide [400] . According to this mechanism Cers will increase PP2A activity leading to reduction in tau phosphorylation and therefore inflammation and neuronal dysfunction. This could explain the lack of cognitive decline with high Cers level in ASM group and it is correlation to tau, however this would represent a protective role to ceramides and the evidence is somehow more robust in the inflammatory role. Together with this ceramide do remain increased once AD is diagnosed in our study.

Recent research has postulated that its "glial cells and not neurons that cause regional shift in human brain aging, with glial-specific genes predicting age with greater precision than neuron-specific genes". This emphasizes the importance of understanding neuron-glial interaction in aging [401]. Satoi et al reported abnormal expression of cers in the astroglia by immunohistochemical analysis of AD brain [402]. Using animal models, a

link between tau pathology and the activation of microglial activation has been reported in brain regions of mice over-expressing human tau deposits [403, 404] . A study by Patil *et al.* 2007 reported the involvement of free fatty acid palmitic acid (PA) in increasing cer release by astroglial cells. This increase in cer levels upon PA treatment of astroglia did not cause cellular stress in astroglia or affect the astroglial cell viability compared with controls [405] . With the aim of investigating fatty acid metabolism in different brain region, the same group [406] examined PA effect in the cortex (AD affected region) and cerebellum (as control region), high fatty acid metabolism was observed in cortical astroglia compared to cerebellar astroglia which would indicate region vulnerability in AD.

Considering fatty acids metabolism in AD. We have reported dysregulation in unsaturated fatty acids metabolism in chapter 5 [407] with region specificity effect on AD pathology and cognition using the same samples employed to conduct this lipidomics study. PA was reported as one of the 32 annotated metabolites that highly associated with disease pathology (see Table 5.3 in Chapter 5). It can be noticed that PA trends in MFG region is similar to CB. However, a distinct significant decrease in PA was seen in the ASM and AD compared to CN in ITG region (q=0.0001 and q=0.01). This suggests abnormal metabolism of PA particularly in ASM groups in ITG region where SPHL metabolism deregulations were also observed (See Appendix D Figure 6.2). The other fatty acids related to our SPHLs were oleic, arachidonic, linoleic, linolenic, eicosapentanoic and all were decreased (Control>ASM>AD) in ITG region.

Changes in SPHL abundance as earliest incidents of AD development were investigated by number of studies in biofluids. A study in our research group [365] has reported increased Cer levels in plasma AD at younger age suggesting a role of Cers in the very early stage of disease. Moreover, another study correlated higher plasma SM levels with slower cognitive decline among AD patients, illustrating SM as potential sensitive blood based biomarker for disease progression[408] . Recent study by Varma *et al. 2018*, identified SPHL as relevant biomarker for early detection of AD, showing connection with disease progression and pathology over the preclinical and prodromal stages of AD in both brain and blood, and suggested that amending the disturbance in this class of lipids would aid finding therapeutic strategy in AD [409].

Imaging techniques such as MRI and PET scan are used in AD to observe brain regions volume and to trace labelled molecules allowing imaging of Aβ and tau. A recent study conducted by researchers in Washington University using PET brain scans of individuals with mild AD symptoms and those cognitively normal, suggested that tau protein build up in the brain as "better marker of AD symptoms" than the long-studied Aβ build up. This was seen mainly in the temporal lobe where tau deposition occurs, with this data supporting AD hypothesis that tau pathology follows functional changes in brain that leads to the onset of early symptoms and somehow shifting the theory that Aβ is the main target for AD therapies [386].

6.5 Conclusions

The work presented in this chapter suggested SPHL species, as indicators associated with disease pathology and progression. The changes in these species were observed in ITG brain region with correlation to tau. These observations would suggest that tau pathology could be linked to SPHLs metabolism at very early stages in Alzheimer's disease.

CHAPTER 7: General conclusions and future work

Study strengths and limitations

The main strengths of the study applied in chapter 5 and 6 are the well-characterized longitudinal BLSA cohort with serial cognitive assessments and detailed neuropathological examination at death. Inclusion of the "ASM" group of individuals allows us to relate the observed shifts in metabolism with both severity of pathology and the expression of AD symptoms. Inclusion of distinct brain regions representing areas both vulnerable and resistant to AD pathology is another key strength of this study.

We applied four distinct metabolomic assays utilizing a range of complementary instruments and chromatographic techniques that together provided a wide coverage of the brain metabolome. The main limitation of this study is the relatively small sample size. There are few cohorts with extensive longitudinal cognitive assessments during life and detailed neuropathological assessments at death as the BLSA. Our findings therefore merit confirmation in larger studies. Another limitation of this study is one shared by all untargeted metabolomics approaches, which is the difficulty in assigning metabolite identities to metabolite features within the data set. With the advent of large publicly available metabolite databases, it is hoped that larger numbers of metabolites will be identified in future studies using these methods.

Chapters conclusions

AD is a major global burden in terms of the economic cost of care and the psychological effect on patients and their families. Finding a diagnosis that does not rely on AD symptoms is a major challenge in AD. Recent approaches depend on expert's opinion by testing patient's cognition and assessing their physical ability. This adds variability when diagnosing different types of dementia. Other challenge is the difficulty in following AD progression, with patient's category usually divided into moderate to severe dementia, just considering a battery of cognitive tests and their performance.

Taking all this together, investigating molecular markers that can provide meaningful trends to follow disease progression, cognitive decline and provide accurate measures to diagnose AD is an urgent need and the focus of many in the field.

This thesis applied MS based metabolomics to look at molecular markers in the AD brain and possibly to provide a map of brain metabolism with pathology. With the current literature indicating that AD pathology appears 20 years earlier prior to AD symptoms, the stage where symptoms have not developed is very important for early intervention In our investigations we were lucky to have participants with AD pathology (tau and AB) and in absence of cognitive decline (referred to as ASYM-Asymptomatic).

Furthermore, the need to design clinical trials with objective outcomes to halt disease progression also emphasizes the urgent need to find molecular markers of interest to help predict disease prior to symptoms of cognitive decline. The brain is the first organ affected by AD and changes in this organ will give insight into molecular shifts at different disease stages.

Many markers have been reported on the literature including genes and proteins, these show inconsistencies particularly when it comes to finding marker to diagnose AD from different disease state forms and at early stage. In this work, our aim was to look at molecular changes in brain and to expand the knowledge of brain metabolism by investigating small molecular markers and their role in relation to AD pathology and progression.

A number of investigations were undertaken and the results were presented and discussed in the following thesis chapters.

In chapter 2, an untargeted metabolomics method was developed aimed at investigating brain small molecules using LC-Q-Tof-MS. The method development consisted of several validation procedures designed to examine reproducibility and metabolites coverage with different sample volumes. In chapter 3, GC-MS was used to develop untargeted metabolomics method aimed at obtaining a wider and more diverse coverage of brain metabolites.

In chapter 4, using multimodal data obtained in the previous chapters, it was possible to discriminate Alzheimer's disease (AD) patients from healthy controls, it also showed the method has potential to resolve subtle biological differences and to correlate metabolite composition directly to clinical outcomes.

In Chapter 5, the untargeted screening method developed in chapter 2 (LC-MS) and chapter 3 (GC-MS), along with proposed data processing approach in chapter 4. This was applied to a total of 124 tissues from human brain. The results showed six PUFA to be strongly associated with Alzheimer's disease. Of these, 5 were decreased with disease, with only docosahexanoic acid increasing in abundance, with the greatest shifts observed in the ITG of ASM patients. The ITG has been implicated in driving early stages AD, so with the largest shifts in PUFA metabolism occurring in this brain region of ASM patients, suggested that these shifts maybe triggering symptom onset of Alzheimer's disease.

In chapter 6, we continued with processing the Lipidomics (RP-LC-MS) data. The results showed disturbance in sphingolipids species including 2SM (SM(16:0) and (22:0)) and 3Cer (Cer(22:0), (24:0) and (26:1)) with some of these species reported in the literature already. All were significantly higher in the ASM and AD group compared to controls in ITG only. Cers more significantly changed between groups whereas SMs significantly correlated with Braak. The results of this chapter suggest that tau pathology could be linked to SPHLs metabolism at very early stages in Alzheimer's disease.

Future Work

Future work would be to incorporate brain region from a greater number of participants. Another interesting aspect could be to analyze UFA concentration in brain regions along with corresponding plasma or serum. This would allow the observation of metabolites variation across the blood brain barrier, further increasing the understanding of UFA in AD brain as considering using of biofluids is important for markers to be applied successfully in clinical scenario. Extending the finding of FA in Chapter 5, quantitation of eicosanoids in relation to FA would be interesting approach.

Another possible future investigation would be to compare FA and SPHLs concentration from AD cases with a range of alternative types of dementia, brain tumor, epilepsy and stroke. This result will be useful to investigate how these metabolites change when compared with a range of conditions. An approach like this could identify novel pathway

targets in AD and help to improve understanding of disease leading to novel therapeutic treatment.

Another aspect would be to investigate if trends in UFA and SPHLs observed in AD are primary or secondary response to the disease. It should also be necessary to see if there are any correlations between these metabolites and major lipoproteins linked to AD in the literature.

To briefly summarize, the project performed in this thesis identified many metabolites of interest in AD brain, including UFA and SPHLs. Further validation to these results can provide leads to future research and improve the understanding of underlying mechanisms in AD. Therefore, replication in larger samples will provide more clear outcomes and reduce variability of small sample sizes.

Further important future work would be to develop AD-Metabolomics data repository or database which primarily involve sharing metabolomics data in brain. This will help for example to produce a validated map of human brain lipids that would help to study the brain lipidome effect of AD, involve mapping different brain regions and establish disease pathways.

References

1. 2017. http://www.nlm.nih.gov/medlineplus/neurologicdiseases.html. [cited accessed on November 2017.
2. Salek, R.M., et al., *A metabolomic study of the CRND8 transgenic mouse model of Alzheimer's disease.* Neurochem Int, 2010. **56**(8): p. 937-47.
3. Rice, M.L., et al., *Language symptoms of developmental language disorders: An overview of autism, Down syndrome, fragile X, specific language impairment, and Williams syndrome.* Applied Psycholinguistics, 2005. **26**(1): p. 7-27.
4. Geschwind, D.H. and P. Levitt, *Autism spectrum disorders: developmental disconnection syndromes.* Curr Opin Neurobiol, 2007. **17**(1): p. 103-11.
5. Niedermeyer, E., W. Froescher, and R.S. Fisher, *Epileptic seizure disorders. Developments in diagnosis and therapy.* Journal of neurology, 1985. **232**(1): p. 1-12.
6. McKhann, G., et al., *Clinical diagnosis of Alzheimer's disease: report of the NINCDS-ADRDA Work Group under the auspices of Department of Health and Human Services Task Force on Alzheimer's Disease.* Neurology, 1984. **34**(7): p. 939-44.
7. Jankovic, J., *Parkinson's disease: clinical features and diagnosis.* Journal of Neurology, Neurosurgery & Psychiatry, 2008. **79**(4): p. 368.
8. Alzheimer, A., et al., *An English translation of Alzheimer's 1907 paper, "Uber eine eigenartige Erkankung der Hirnrinde".* Clin Anat, 1995. **8**(6): p. 429-31.
9. Alzheimer's Association Report 2011. *Alzheimer's disease facts and figures. Alzheimers & Dementia, 2011.* **7***(2): p. 208-44.*
10. Alzheimer's Association Report *201.7 Alzheimer's disease facts and figures.* Alzheimer's & Dementia, 201**7**. **13**(4): p. 325-373.
11. Langa, K.M., *Is the risk of Alzheimer's disease and dementia declining?* Alzheimers Res Ther, 2015. **7**(1): p. 34.
12. Ferri, C.P., et al., *Global prevalence of dementia: a Delphi consensus study.* Lancet, 2005. **366**(9503): p. 2112-7.
13. Hort, J., et al., *EFNS guidelines for the diagnosis and management of Alzheimer's disease.* European Journal of Neurology, 2010. **17**(10): p. 1236-1248.
14. www.alzheimersresearchuk.org. 2017.
15. Ryman, D.C., et al., *Symptom onset in autosomal dominant Alzheimer disease: a systematic review and meta-analysis.* Neurology, 2014. **83**(3): p. 253-60.
16. Tanzi, R.E. and L. Bertram, *Twenty years of the Alzheimer's disease amyloid hypothesis: a genetic perspective.* Cell, 2005. **120**(4): p. 545-55.
17. Haass, C., et al., *The Swedish mutation causes early-onset Alzheimer's disease by β-secretase cleavage within the secretory pathway.* Nature Medicine, 1995. **1**: p. 1291.
18. Sando, S.B., et al., *APOE ε4 lowers age at onset and is a high risk factor for Alzheimer's disease; A case control study from central Norway.* BMC Neurology, 2008. **8**(1): p. 9.
19. Bekris, L.M., et al., *Genetics of Alzheimer Disease.* Journal of geriatric psychiatry and neurology, 2010. **23**(4): p. 213-227.
20. Braak, H. and E. Braak, *Evolution of the neuropathology of Alzheimer's disease.* Acta Neurol Scand Suppl, 1996. **165**: p. 3-12.
21. Zhang, H., et al., *Proteolytic processing of Alzheimer's beta-amyloid precursor protein.* J Neurochem, 2012. **120 Suppl 1**: p. 9-21.
22. Selkoe, D.J., *Alzheimer's disease: genes, proteins, and therapy.* Physiol Rev, 2001. **81**(2): p. 741-66.
23. Haass, C. and D.J. Selkoe, *Soluble protein oligomers in neurodegeneration: lessons from the Alzheimer's amyloid beta-peptide.* Nat Rev Mol Cell Biol, 2007. **8**(2): p. 101-12.

24. Oddo, S., et al., *Triple-transgenic model of Alzheimer's disease with plaques and tangles: intracellular Abeta and synaptic dysfunction.* Neuron, 2003. **39**(3): p. 409-21.
25. Jarrett, J.T., E.P. Berger, and P.T. Lansbury, *The C-Terminus of the β Protein is Critical in Amyloidogenesisa.* Annals of the New York Academy of Sciences, 1993. **695**(1): p. 144-148.
26. Soscia, S.J., et al., *The Alzheimer's disease-associated amyloid beta-protein is an antimicrobial peptide.* PLoS One, 2010. **5**(3): p. e9505.
27. Kumar, D.K., et al., *Amyloid-beta peptide protects against microbial infection in mouse and worm models of Alzheimer's disease.* Sci Transl Med, 2016. **8**(340): p. 340ra72.
28. Chen, W.T., et al., *Distinct effects of Zn2+, Cu2+, Fe3+, and Al3+ on amyloid-beta stability, oligomerization, and aggregation: amyloid-beta destabilization promotes annular protofibril formation.* J Biol Chem, 2011. **286**(11): p. 9646-56.
29. Curtain, C.C., et al., *Alzheimer's disease amyloid-beta binds copper and zinc to generate an allosterically ordered membrane-penetrating structure containing superoxide dismutase-like subunits.* J Biol Chem, 2001. **276**(23): p. 20466-73.
30. Motter, R., et al., *Reduction of beta-amyloid peptide42 in the cerebrospinal fluid of patients with Alzheimer's disease.* Ann Neurol, 1995. **38**(4): p. 643-8.
31. Herukka, S.K., et al., *CSF Abeta42 and tau or phosphorylated tau and prediction of progressive mild cognitive impairment.* Neurology, 2005. **64**(7): p. 1294-7.
32. Hansson, O., et al., *Association between CSF biomarkers and incipient Alzheimer's disease in patients with mild cognitive impairment: a follow-up study.* Lancet Neurol, 2006. **5**(3): p. 228-34.
33. Grundke-Iqbal, I., et al., *Abnormal phosphorylation of the microtubule-associated protein tau (tau) in Alzheimer cytoskeletal pathology.* Proc Natl Acad Sci U S A, 1986. **83**(13): p. 4913-7.
34. Liang, Z., et al., *Dysregulation of Tau Phosphorylation in Mouse Brain during Excitotoxic Damage.* Journal of Alzheimer's disease : JAD, 2009. **17**(3): p. 531-539.
35. Iqbal, K., et al., *Mechanisms of tau-induced neurodegeneration.* Acta Neuropathol, 2009. **118**(1): p. 53-69.
36. Su, J.H., B.J. Cummings, and C.W. Cotman, *Plaque biogenesis in brain aging and Alzheimer's disease. I. Progressive changes in phosphorylation states of paired helical filaments and neurofilaments.* Brain Res, 1996. **739**(1-2): p. 79-87.
37. Goedert, M., D.S. Eisenberg, and R.A. Crowther, *Propagation of Tau Aggregates and Neurodegeneration.* Annual Review of Neuroscience, 2017. **40**(1): p. 189-210.
38. Behl, C., et al., *Hydrogen peroxide mediates amyloid beta protein toxicity.* Cell, 1994. **77**(6): p. 817-27.
39. Kamat, P.K., et al., *Mechanism of Oxidative Stress and Synapse Dysfunction in the Pathogenesis of Alzheimer's Disease: Understanding the Therapeutics Strategies.* Mol Neurobiol, 2016. **53**(1): p. 648-661.
40. Zuo, L., et al., *The Role of Oxidative Stress-Induced Epigenetic Alterations in Amyloid-β Production in Alzheime's Disease.* Oxid Med and Cell Longevity, 2015. p. 13.
41. Costa, R.O., et al., *Inhibition of mitochondrial cytochrome c oxidase potentiates Aβ-induced ER stress and cell death in cortical neurons.* Molecular and Cellular Neuroscience, 2013. **52**: p. 1-8.
42. Caspersen, C., et al., *Mitochondrial Abeta: a potential focal point for neuronal metabolic dysfunction in Alzheimer's disease*, 2005. **19**(14): p. 2040-1.
43. Du, H. and S. ShiDu Yan, *Unlocking the Door to Neuronal Woes in Alzheimer's Disease: Aβ and Mitochondrial Permeability Transition Pore.* Pharmaceuticals, 2010. **3**(6): p. 1936.
44. Rodrigues, C.M., et al., *Amyloid beta-peptide disrupts mitochondrial membrane lipid and protein structure: protective role of tauroursodeoxycholate.* Biochem Biophys Res Commun, 2001. **281**(2): p. 468-74.

45. Keller, J.N., et al., *Impairment of Glucose and Glutamate Transport and Induction of Mitochondrial Oxidative Stress and Dysfunction in Synaptosomes by Amyloid β-Peptide: Role of the Lipid Peroxidation Product 4-Hydroxynonenal.* Journal of Neurochemistry, 1997. **69**(1): p. 273-284.
46. Meier-Ruge, W., C. Bertoni-Freddari, and P. Iwangoff, *Changes in brain glucose metabolism as a key to the pathogenesis of Alzheimer's disease.* Gerontology, 1994. **40**(5): p. 246-52.
47. An, Y., et al., *Evidence for brain glucose dysregulation in Alzheimer's disease.* Alzheimers Dement, 2018. **14**(3): 318-329.
48. Mosconi, L., *Brain glucose metabolism in the early and specific diagnosis of Alzheimer's disease. FDG-PET studies in MCI and AD.* Eur J Nucl Med Mol Imaging, 2005. **32**(4): p. 486-510.
49. Ishii, K., et al., *Reduction of Cerebellar Glucose Metabolism in Advanced Alzheimer's Disease.* Journal of Nuclear Medicine, 1997. **38**(6): p. 925-928.
50. Feng, Y., et al., *Cleavage of GSK-3beta by calpain counteracts the inhibitory effect of Ser9 phosphorylation on GSK-3beta activity induced by H_2O_2.* J Neurochem, 2013. **126**(2): p. 234-42.
51. Cho, M.H., et al., *Increased phosphorylation of dynamin-related protein 1 and mitochondrial fission in okadaic acid-treated neurons.* Brain Res, 2012. **1454**: p. 100-10.
52. Ghribi, O., M.M. Herman, and J. Savory, *Lithium inhibits Aβ-induced stress in endoplasmic reticulum of rabbit hippocampus but does not prevent oxidative damage and tau phosphorylation.* Journal of Neuroscience Research, 2003. **71**(6): p. 853-862.
53. Graham, S.F., et al., *Age-associated changes of brain copper, iron, and zinc in Alzheimer's disease and dementia with Lewy bodies.* J Alzheimers Dis, 2014. **42**(4): p. 1407-13.
54. Maynard, C.J., et al., *Overexpression of Alzheimer's disease amyloid-beta opposes the age-dependent elevations of brain copper and iron.* J Biol Chem, 2002. **277**(47): p. 44670-6.
55. Deibel, M.A., W.D. Ehmann, and W.R. Markesbery, *Copper, iron, and zinc imbalances in severely degenerated brain regions in Alzheimer's disease: possible relation to oxidative stress.* J Neurol Sci, 1996. **143**(1-2): p. 137-42.
56. Parthasarathy, S., et al., *Molecular-level examination of Cu^{2+} binding structure for amyloid fibrils of 40-residue Alzheimer's beta by solid-state NMR spectroscopy.* J Am Chem Soc, 2011. **133**(10): p. 3390-400.
57. Sayre, L.M., et al., *In situ oxidative catalysis by neurofibrillary tangles and senile plaques in Alzheimer's disease: a central role for bound transition metals.* J Neurochem, 2000. **74**(1): p. 270-9.
58. Huang, X., et al., *The A beta peptide of Alzheimer's disease directly produces hydrogen peroxide through metal ion reduction.* Biochemistry, 1999. **38**(24): p. 7609-16.
59. Vetrivel, K.S., et al., *Association of gamma-secretase with lipid rafts in post-Golgi and endosome membranes.* J Biol Chem, 2004. **279**(43): p. 44945-54.
60. van Meer, G., D.R. Voelker, and G.W. Feigenson, *Membrane lipids: where they are and how they behave.* Nature reviews. Molecular cell biology, 2008. **9**(2): p. 112-124.
61. Prasad, M.R., et al., *Regional Membrane Phospholipid Alterations in Alzheimer's Disease.* Neurochemical Research, 1998. **23**(1): p. 81-88.
62. Nitsch, R.M., et al., *Evidence for a membrane defect in Alzheimer disease brain.* Proc Natl Acad Sci USA, 1992. **89**(5): p. 1671-5.
63. Guan, Z., et al., *Decrease and structural modifications of phosphatidylethanolamine plasmalogen in the brain with Alzheimer disease.* J Neuropathol Exp Neurol, 1999. **58**(7): p. 740-7.
64. Prasad, M.R., et al., *Regional membrane phospholipid alterations in Alzheimer's disease.* Neurochem Res, 1998. **23**(1): p. 81-8.

65. Stokes, C.E. and J.N. Hawthorne, *Reduced phosphoinositide concentrations in anterior temporal cortex of Alzheimer-diseased brains.* J Neurochem, 1987. **48**(4): p. 1018-21.
66. Pettegrew, J.W., et al., *Brain membrane phospholipid alterations in Alzheimer's disease.* Neurochem Res, 2001. **26**(7): p. 771-82.
67. Ginsberg, L., et al., *Disease and anatomic specificity of ethanolamine plasmalogen deficiency in Alzheimer's disease brain.* Brain Res, 1995. **698**(1-2): p. 223-6.
68. Whiley, L., et al., *Evidence of altered phosphatidylcholine metabolism in Alzheimer's disease.* Neurobiol Aging, 2014. **35**(2): p. 271-8.
69. Han, X., *Lipid alterations in the earliest clinically recognizable stage of Alzheimer's disease: implication of the role of lipids in the pathogenesis of Alzheimer's disease.* Curr Alzheimer Res, 2005. **2**(1): p. 65-77.
70. Astarita, G. and D. Piomelli, *Towards a whole-body systems [multi-organ] lipidomics in Alzheimer's disease.* Prostaglandins, leukotrienes, and essential fatty acids, 2011. **85**(5): p. 197-203.
71. Walter, A., et al., *Glycerophosphocholine is elevated in cerebrospinal fluid of Alzheimer patients.* Neurobiol Aging, 2004. **25**(10): p. 1299-303.
72. Mulder, C., et al., *Decreased lysophosphatidylcholine/phosphatidylcholine ratio in cerebrospinal fluid in Alzheimer's disease.* Journal of Neural Transmission, 2003. **110**(8): p. 949-955.
73. Kolesnick, R.N., *Sphingomyelin and derivatives as cellular signals.* Prog Lipid Res, 1991. **30**(1): p. 1-38.
74. He, X., et al., *Deregulation of sphingolipid metabolism in Alzheimer's disease.* Neurobiol Aging, 2010. **31**(3): p. 398-408.
75. Cutler, R.G., et al., *Involvement of oxidative stress-induced abnormalities in ceramide and cholesterol metabolism in brain aging and Alzheimer's disease.* Proc Natl Acad Sci U S A, 2004. **101**(7): p. 2070-5.
76. Han, X., D.M. Holtzman, and D.W. McKeel, Jr., *Plasmalogen deficiency in early Alzheimer's disease subjects and in animal models: molecular characterization using electrospray ionization mass spectrometry.* J Neurochem, 2001. **77**(4): p. 1168-80.
77. Dinkins, M.B., et al., *Exosome reduction in vivo is associated with lower amyloid plaque load in the 5XFAD mouse model of Alzheimer's disease.* Neurobiol Aging, 2014. **35**(8): p. 1792-800.
78. Bandaru, V.V., et al., *ApoE4 disrupts sterol and sphingolipid metabolism in Alzheimer's but not normal brain.* Neurobiol Aging, 2009. **30**(4): p. 591-9.
79. Kosicek, M., et al., *Nano-HPLC-MS analysis of phospholipids in cerebrospinal fluid of Alzheimer's disease patients-a pilot study.* Anal Bioanal Chem, 2010. **398**(7-8): p. 2929-37.
80. Kosicek, M., et al., *Elevated cerebrospinal fluid sphingomyelin levels in prodromal Alzheimer's disease.* Neurosci Lett, 2012. **516**(2): p. 302-5.
81. Koudinov, A.R. and N.V. Koudinova, *Essential role for cholesterol in synaptic plasticity and neuronal degeneration.* Faseb j, 2001. **15**(10): p. 1858-60.
82. Di Paolo, G. and T.-W. Kim, *Linking Lipids to Alzheimer's Disease: Cholesterol and Beyond.* Nature Reviews. Neuroscience, 2011. **12**(5): p. 284-296.
83. Puglielli, L., et al., *Acyl-coenzyme A: cholesterol acyltransferase modulates the generation of the amyloid beta-peptide.* Nat Cell Biol, 2001. **3**(10): p. 905-12.
84. Simons, M., et al., *Cholesterol depletion inhibits the generation of beta-amyloid in hippocampal neurons.* Proc Natl Acad Sci U S A, 1998. **95**(11): p. 6460-4.
85. Wahrle, S., et al., *Cholesterol-dependent gamma-secretase activity in buoyant cholesterol-rich membrane microdomains.* Neurobiol Dis, 2002. **9**(1): p. 11-23.
86. Bhattacharyya, R. and D.M. Kovacs, *ACAT inhibition and amyloid beta reduction.* Biochim biophys acta, 2010. **1801**(8): p. 960-965.

87. McKhann, G., et al., *Clinical diagnosis of Alzheimer's disease.* Report of the NINCDS-ADRDA Work Group* under the auspices of Department of Health and Human Services Task Force on Alzheimer's Disease, 1984. **34**(7): p. 939-939.
88. Albert, M.S., et al., *The diagnosis of mild cognitive impairment due to Alzheimer's disease: recommendations from the National Institute on Aging-Alzheimer's Association workgroups on diagnostic guidelines for Alzheimer's disease.* Alzheimers Dement, 2011. **7**(3): p. 270-9.
89. Jack, C.R., Jr., et al., *Introduction to the recommendations from the National Institute on Aging-Alzheimer's Association workgroups on diagnostic guidelines for Alzheimer's disease.* Alzheimers Dement, 2011. **7**(3): p. 257-62.
90. Jack, C.R., Jr., et al., *Introduction to the recommendations from the National Institute on Aging-Alzheimer's Association workgroups on diagnostic guidelines for Alzheimer's disease.* Alzheimer's & Dementia,, 2011. **7**(3): p. 257-262.
91. Folstein, M.F., S.E. Folstein, and P.R. McHugh, *"Mini-mental state". A practical method for grading the cognitive state of patients for the clinician.* J Psychiatr Res, 1975. **12**(3): p. 189-98.
92. Rosen, W.G., R.C. Mohs, and K.L. Davis, *A new rating scale for Alzheimer's disease.* Am J Psychiatry, 1984. **141**(11): p. 1356-64.
93. Reisberg, B., et al., *The Global Deterioration Scale for assessment of primary degenerative dementia.* Am J Psychiatry, 1982. **139**(9): p. 1136-9.
94. Berg, L., *Clinical Dementia Rating (CDR).* Psychopharmacol Bull, 1988. **24**(4): p. 637-9.
95. Morris, J.C., *The Clinical Dementia Rating (CDR): current version and scoring rules.* Neurology, 1993. **43**(11): p. 2412-4.
96. Braak, H., et al., *Staging of Alzheimer disease-associated neurofibrillary pathology using paraffin sections and immunocytochemistry.* Acta Neuropathologica, 2006. **112**(4): p. 389-404.
97. Mirra, S.S., et al., *The Consortium to Establish a Registry for Alzheimer's Disease (CERAD). Part II. Standardization of the neuropathologic assessment of Alzheimer's disease.* Neurology, 1991. **41**(4): p. 479-86.
98. Apostolova, L.G., et al., *Conversion of mild cognitive impairment to Alzheimer disease predicted by hippocampal atrophy maps.* Arch Neurol, 2006. **63**(5): p. 693-9.
99. Mungas, D., et al., *Longitudinal volumetric MRI change and rate of cognitive decline.* Neurology, 2005. **65**(4): p. 565-71.
100. Shi, F., et al., *Hippocampal volume and asymmetry in mild cognitive impairment and Alzheimer's disease: Meta-analyses of MRI studies.* Hippocampus, 2009. **19**(11): p. 1055-64.
101. Bobinski, M., et al., *MRI of entorhinal cortex in mild Alzheimer's disease.* The Lancet. **353**(9146): p. 38-40.
102. Hampel, H., et al., *Age transformation of combined hippocampus and amygdala volume improves diagnostic accuracy in Alzheimer's disease.* J Neurol Sci, 2002. **194**(1): p. 15-9.
103. Selnes, P., et al., *Diffusion tensor imaging surpasses cerebrospinal fluid as predictor of cognitive decline and medial temporal lobe atrophy in subjective cognitive impairment and mild cognitive impairment.* J Alzheimers Dis, 2013. **33**(3): p. 723-36.
104. Zhang, Y., et al., *Diffusion tensor imaging of cingulum fibers in mild cognitive impairment and Alzheimer disease.* Neurology, 2007. **68**(1): p. 13-19.
105. Stebbins, G.T. and C.M. Murphy, *Diffusion tensor imaging in Alzheimer's disease and mild cognitive impairment.* Behav Neurol, 2009. **21**(1): p. 39-49.
106. Schuff, N., et al., *Changes of hippocampal N-acetyl aspartate and volume in Alzheimer's disease. A proton MR spectroscopic imaging and MRI study.* Neurology, 1997. **49**(6): p. 1513-21.

107. Gujar, S.K., et al., *Magnetic resonance spectroscopy.* J Neuroophthalmol, 2005. **25**(3): p. 217-26.
108. Cohen, A.D. and W.E. Klunk, *Early detection of Alzheimer's disease using PiB and FDG PET.* Neurobiol Dis, 2014. **72 Pt A**: p. 117-22.
109. Herholz, K., et al., *Direct comparison of spatially normalized PET and SPECT scans in Alzheimer's disease.* J Nucl Med, 2002. **43**(1): p. 21-6.
110. Schroeter, M.L., et al., *Neural Correlates of Alzheimer's Disease and Mild Cognitive Impairment: A Systematic and Quantitative Meta-Analysis involving 1,351 Patients.* NeuroImage, 2009. **47**(4): p. 1196-1206.
111. Corder, E.H., et al., *Gene dose of apolipoprotein E type 4 allele and the risk of Alzheimer's disease in late onset families.* Science, 1993. **261**(5123): p. 921-3.
112. Mayeux, R., et al., *Utility of the apolipoprotein E genotype in the diagnosis of Alzheimer's disease. Alzheimer's Disease Centers Consortium on Apolipoprotein E and Alzheimer's Disease.* N Engl J Med, 1998. **338**(8): p. 506-11.
113. Reiman, E.M., et al., *Fibrillar amyloid-beta burden in cognitively normal people at 3 levels of genetic risk for Alzheimer's disease.* Proc Natl Acad Sci USA, 2009. **106**(16): p. 6820-5.
114. Holtzman, D.M., et al., *Apolipoprotein E isoform-dependent amyloid deposition and neuritic degeneration in a mouse model of Alzheimer's disease.* Proc Natl Acad Sci U S A, 2000. **97**(6): p. 2892-7.
115. Jiang, Q., et al., *ApoE promotes the proteolytic degradation of Aβ.* Neuron, 2008. **58**(5): p. 681-693.
116. Takata, M., et al., *Detection of amyloid beta protein in the urine of Alzheimer's disease patients and healthy individuals.* Neurosci Lett, 2008. **435**(2): p. 126-30.
117. Mayeux, R., et al., *Plasma amyloid beta-peptide 1-42 and incipient Alzheimer's disease.* Ann Neurol, 1999. **46**(3): p. 412-6.
118. Galasko, D., et al., *High cerebrospinal fluid tau and low amyloid beta42 levels in the clinical diagnosis of Alzheimer disease and relation to apolipoprotein E genotype.* Arch Neurol, 1998. **55**(7): p. 937-45.
119. Sunderland, T., et al., *Biomarkers in the diagnosis of Alzheimer's disease: are we ready?* J Geriatr Psychiatry Neurol, 2006. **19**(3): p. 172-9.
120. Nagga, K., et al., *Cerebrospinal fluid phospho-tau, total tau and beta-amyloid(1-42) in the differentiation between Alzheimer's disease and vascular dementia.* Dement Geriatr Cogn Disord, 2002. **14**(4): p. 183-90.
121. Sjogren, M., et al., *Both total and phosphorylated tau are increased in Alzheimer's disease.* J Neurol Neurosurg Psychiatry, 2001. **70**(5): p. 624-30.
122. Forlenza, O.V., et al., *Cerebrospinal fluid biomarkers in Alzheimer's disease: Diagnostic accuracy and prediction of dementia.* Alzheimers Dement (Amst), 2015. **1**(4): p. 455-63.
123. Maddalena, A., et al., *Biochemical diagnosis of Alzheimer disease by measuring the cerebrospinal fluid ratio of phosphorylated tau protein to beta-amyloid peptide42.* Arch Neurol, 2003. **60**(9): p. 1202-6.
124. Shaw, L.M., et al., *Cerebrospinal fluid biomarker signature in Alzheimer's disease neuroimaging initiative subjects.* Ann Neurol, 2009. **65**(4): p. 403-13.
125. Whiley, L. and C. Legido-Quigley, *Current strategies in the discovery of small-molecule biomarkers for Alzheimer's disease.* Bioanalysis, 2011. **3**(10): p. 1121-42.
126. Fiehn, O., *Metabolomics – the link between genotypes and phenotypes.* Plant Molecular Biology, 2002. **48**(1): p. 155-171.
127. Nicholson, J.K., J.C. Lindon, and E. Holmes, *'Metabonomics': understanding the metabolic responses of living systems to pathophysiological stimuli via multivariate statistical analysis of biological NMR spectroscopic data.* Xenobiotica, 1999. **29**(11): p. 1181-9.
128. Goodacre, R., et al., *Metabolomics by numbers: acquiring and understanding global metabolite data.* Trends Biotechnol, 2004. **22**(5): p. 245-52.

129. Holmes, E., I.D. Wilson, and J.K. Nicholson, *Metabolic Phenotyping in Health and Disease.* Cell, 2008. **134**(5): p. 714-717.
130. Nicholson, J.K. and J.C. Lindon, *Systems biology: Metabonomics.* Nature, 2008. **455**(7216): p. 1054-6.
131. Soga, T., et al., *Differential metabolomics reveals ophthalmic acid as an oxidative stress biomarker indicating hepatic glutathione consumption.* J Biol Chem, 2006. **281**(24): p. 16768-76.
132. Patti, G.J., O. Yanes, and G. Siuzdak, *Innovation: Metabolomics: the apogee of the omics trilogy.* Nat Rev Mol Cell Biol, 2012. **13**(4): p. 263-9.
133. Mathe, E.A., et al., *Noninvasive urinary metabolomic profiling identifies diagnostic and prognostic markers in lung cancer.* Cancer Res, 2014. **74**(12): p. 3259-70.
134. Jung, J., et al., *Noninvasive diagnosis and evaluation of curative surgery for gastric cancer by using NMR-based metabolomic profiling.* Ann Surg Oncol, 2014. **21 Suppl 4**: p. S736-42.
135. Wang, Y., et al., *LC-MS-Based Metabolomics Discovers Purine Endogenous Associations with Low-Dose Salbutamol in Urine Collected for Antidoping Tests.* Analytical Chemistry, 2016. **88**(4): p. 2243-2249.
136. Raterink, R.-J., et al., *Recent developments in sample-pretreatment techniques for mass spectrometry-based metabolomics.* TrAC Trends in Analytical Chemistry, 2014. **61**: p. 157-167.
137. Want, E.J., et al., *Global metabolic profiling procedures for urine using UPLC–MS.* Nature protocols, 2010. **5**(6): p. 1005-1018.
138. Nicholson, J.K., E. Holmes, and J.C. Lindon, *Chapter 1 - Metabonomics and Metabolomics Techniques and Their Applications in Mammalian Systems*, in *The Handbook of Metabonomics and Metabolomics*, Elsevier Science, 2007. p. 1-33.
139. Dunn, W.B., et al., *The importance of experimental design and QC samples in large-scale and MS-driven untargeted metabolomic studies of humans.* Bioanalysis, 2012. **4**(18): p. 2249-64.
140. Gika, H.G., I.D. Wilson, and G.A. Theodoridis, *LC–MS-based holistic metabolic profiling. Problems, limitations, advantages, and future perspectives.* Journal of Chromatography B, 2014. **966**: p. 1-6.
141. Vasilopoulou, C.G., M. Margarity, and M.I. Klapa, *Metabolomic Analysis in Brain Research: Opportunities and Challenges.* Frontiers in Physiology, 2016. **7**: p. 183.
142. Dunn, W.B., et al., *Mass appeal: metabolite identification in mass spectrometry-focused untargeted metabolomics.* Metabolomics, 2013. **9**(1): p. 44-66.
143. Metz, T.O., et al., *The future of liquid chromatography-mass spectrometry (LC-MS) in metabolic profiling and metabolomic studies for biomarker discovery.* Biomark Med, 2007. **1**(1): p. 159-185.
144. Markley, J.L., et al., *The future of NMR-based metabolomics.* Current Opinion in Biotechnology, 2017. **43**: p. 34-40.
145. Emwas, A.H., *The strengths and weaknesses of NMR spectroscopy and mass spectrometry with particular focus on metabolomics research.* Methods Mol Biol, 2015. **1277**: p. 161-93.
146. Chatham, J.C. and S.J. Blackband, *Nuclear magnetic resonance spectroscopy and imaging in animal research*, 2001. **42**(3): p. 189-208.
147. Berendt, R.T., et al., *Solid-state NMR spectroscopy in pharmaceutical research and analysis.* TrAC Trends in Analytical Chemistry, 2006. **25**(10): p. 977-984.
148. Corcoran, O., *NMR Spectroscopy As a Versatile Analytical Platform for Toxicology Research.* Handbook of Toxicogenomics, J. Borlak (Ed.). *doi:10.1002/3527603719.ch8*. 2005.
149. Inoue, K., et al., *Metabolic profiling of Alzheimer's disease brains.* Sci Rep, 2013. **3**: p. 2364.

150. Whiley,L. and C. Legido-Quigley, *Current strategies in the discovery of small-molecule biomarkers for Alzheimer's disease.* Bioanalysis, 2011. **3**(10): p. 1121-1142.
151. Schwudke, D., et al., *Shotgun lipidomics by tandem mass spectrometry under data-dependent acquisition control.* Methods Enzymol, 2007. **433**: p. 175-91.
152. Kind, T., et al., *FiehnLib: Mass Spectral and Retention Index Libraries for Metabolomics Based on Quadrupole and Time-of-Flight Gas Chromatography/Mass Spectrometry.* Analytical Chemistry, 2009. **81**(24): p. 10038-10048.
153. Simón-Manso, Y., et al., *Metabolite Profiling of a NIST Standard Reference Material for Human Plasma (SRM 1950): GC-MS, LC-MS, NMR, and Clinical Laboratory Analyses, Libraries, and Web-Based Resources.* Analytical Chemistry, 2013. **85**(24): p. 11725-11731.
154. Giddings, J.C., *Comparison of Theoretical Limit of Separating Speed in Gas and Liquid Chromatography.* Analytical Chemistry, 1965. **37**(1): p. 60-63.
155. McNair, H.M. and K.M. Trivedi, *Gas Chromatography and Pharmaceutical Analyses*, in *Chromatography of Pharmaceuticals*. 1992, American Chemical Society. p. 67-84.
156. Santos, F.J. and M.T. Galceran, *The application of gas chromatography to environmental analysis.* TrAC Trends in Analytical Chemistry, 2002. **21**(9): p. 672-685.
157. Svec, F., *Introduction to Modern Liquid Chromatography, 3rd Edition Lloyd R. Snyder, Joseph J. Kirkl and, John W. Dolan Wiley, Hoboken, NJ, USA, December 2009 ISBN 978-0-470-16754-0 912 pages, Hardcover US$125.* Journal of Separation Science, 2010. **33**(12): p. 1877-1877.
158. Neue, U.D., *HPLC Columns, Theory, Technology, and Practice.* Instrumentation Science & Technology, 1998. **26**(4): p. 439-440.
159. Alpert, A.J., *Hydrophilic-interaction chromatography for the separation of peptides, nucleic acids and other polar compounds.* J Chromatogr, 1990. **499**: p. 177-96.
160. Zhou, B., et al., *LC-MS-based metabolomics.* Mol Biosyst, 2012. **8**(2): p. 470-81.
161. Fenn, J.B., et al., *Electrospray ionization–principles and practice.* Mass Spectrometry Reviews, 1990. **9**(1): p. 37-70.
162. Ramautar, R., *CE-MS in metabolomics: status quo and the way forward.* Bioanalysis, 2016. **8**(5): p. 371-374.
163. Ramautar, R., G.W. Somsen, and G.J. de Jong, *CE-MS for metabolomics: developments and applications in the period 2012-2014.* Electrophoresis, 2015. **36**(1): p. 212-24.
164. Marney, L.C., et al., *Methods of discovery-based and targeted metabolite analysis by comprehensive two-dimensional gas chromatography with time-of-flight mass spectrometry detection.* Methods Mol Biol, 2014. **1198**: p. 83-97.
165. Vincent, G., et al., *Citrate release by perfused rat hearts: a window on mitochondrial cataplerosis.* Am J Physiol Endocrinol Metab, 2000. **278**(5): p. E846-56.
166. Sato, Y., et al., *Quantitative and wide-ranging profiling of phospholipids in human plasma by two-dimensional liquid chromatography/mass spectrometry.* Anal Chem, 2010. **82**(23): p. 9858-64.
167. Bamba, T., et al., *Metabolic profiling of lipids by supercritical fluid chromatography/mass spectrometry.* J Chromatogr A, 2012. **1250**: p. 212-9.
168. Southam, A.D., et al., *Distinguishing between the metabolome and xenobiotic exposome in environmental field samples analysed by direct-infusion mass spectrometry based metabolomics and lipidomics.* Metabolomics, 2014. **10**(6): p. 1050-1058.
169. Uarrota, V.G., et al., *Metabolomics combined with chemometric tools (PCA, HCA, PLS-DA and SVM) for screening cassava (Manihot esculenta Crantz) roots during postharvest physiological deterioration.* Food Chem, 2014. **161**: p. 67-78.
170. Pérez-Enciso, M. and M. Tenenhaus, *Prediction of clinical outcome with microarray data: A partial least squares discriminant analysis (PLS-DA) approach*. Vol. 112. 2003. 581-92.
171. Madsen, R., T. Lundstedt, and J. Trygg, *Chemometrics in metabolomics--a review in human disease diagnosis.* Anal Chim Acta, 2010. **659**(1-2): p. 23-33.

172. Broadhurst, D.I. and D.B. Kell, *Statistical strategies for avoiding false discoveries in metabolomics and related experiments.* Metabolomics, 2006. **2**(4): p. 171-196.
173. Jackson, J.E., *Getting Started*, in *A User's Guide to Principal Components*. 2004, John Wiley & Sons, Inc. p. 4-25.
174. Trygg, J. and S. Wold, *Orthogonal projections to latent structures (O-PLS).* Journal of Chemometrics, 2002. **16**(3): p. 119-128.
175. Bylesjö, M., et al., *OPLS discriminant analysis: combining the strengths of PLS-DA and SIMCA classification.* Journal of Chemometrics, 2006. **20**(8-10): p. 341-351.
176. Sitter, B., et al., *High-resolution magic angle spinning (HR MAS) MR spectroscopy in metabolic characterization of human cancer.* Progress in Nuclear Magnetic Resonance Spectroscopy, 2009. **54**(3): p. 239-254.
177. Kaddurah-Daouk, R., et al., *Cerebrospinal fluid metabolome in mood disorders-remission state has a unique metabolic profile.* Sci Rep, 2012. **2**: p. 667.
178. Quinones, M.P. and R. Kaddurah-Daouk, *Metabolomics tools for identifying biomarkers for neuropsychiatric diseases.* Neurobiol Dis, 2009. **35**(2): p. 165-76.
179. Kaddurah-Daouk, R., et al., *Alterations in metabolic pathways and networks in Alzheimer's disease.* Transl Psychiatry, 2013. **3**: p. e244.
180. Motsinger-Reif, A.A., et al., *Comparing metabolomic and pathologic biomarkers alone and in combination for discriminating Alzheimer's disease from normal cognitive aging.* Acta Neuropathologica Communications, 2013. **1**: p. 28-28.
181. Kaddurah-Daouk, R., et al., *Metabolomic changes in autopsy-confirmed Alzheimer's disease.* Alzheimers Dement, 2011. **7**(3): p. 309-17.
182. Trushina, E., et al., *Identification of Altered Metabolic Pathways in Plasma and CSF in Mild Cognitive Impairment and Alzheimer's Disease Using Metabolomics.* PLOS ONE, 2013. **8**(5): p. e63644.
183. Ibanez, C., et al., *A new metabolomic workflow for early detection of Alzheimer's disease.* J Chromatogr A, 2013. **1302**: p. 65-71.
184. Ibáñez, C., et al., *Toward a Predictive Model of Alzheimer's Disease Progression Using Capillary Electrophoresis–Mass Spectrometry Metabolomics.* Analytical Chemistry, 2012. **84**(20): p. 8532-8540.
185. Czech, C., et al., *Metabolite Profiling of Alzheimer's Disease Cerebrospinal Fluid.* PLOS ONE, 2012. **7**(2): p. e31501.
186. Kork, F., et al., *A possible new diagnostic biomarker in early diagnosis of Alzheimer's disease.* Curr Alzheimer Res, 2009. **6**(6): p. 519-24.
187. Jukarainen, N.M., et al., *Quantification of ^{1}H NMR spectra of human cerebrospinal fluid: a protocol based on constrained total-line-shape analysis.* Metabolomics, 2008. **4**(2): p. 150-160.
188. Fonteh, A.N., et al., *Free amino acid and dipeptide changes in the body fluids from Alzheimer's disease subjects.* Amino Acids, 2007. **32**(2): p. 213-24.
189. Li, N.J., et al., *Plasma metabolic profiling of Alzheimer's disease by liquid chromatography/mass spectrometry.* Clin Biochem, 2010. **43**(12): p. 992-7.
190. Oresic, M., et al., *Metabolome in progression to Alzheimer's disease.* Transl Psychiatry, 2011. **1**: p. e57.
191. Foley, P., *Lipids in Alzheimer's disease: A century-old story.* Biochim Biophys Acta, 2010. **1801**(8): p. 750-3.
192. Tukiainen, T., et al., *A multi-metabolite analysis of serum by 1H NMR spectroscopy: early systemic signs of Alzheimer's disease.* Biochem Biophys Res Commun, 2008. **375**(3): p. 356-61.
193. Han, X., et al., *Metabolomics in early Alzheimer's disease: identification of altered plasma sphingolipidome using shotgun lipidomics.* PLoS One, 2011. **6**(7): p. e21643.
194. Sing, C.F. and J. Davignon, *Role of the apolipoprotein E polymorphism in determining normal plasma lipid and lipoprotein variation.* American Journal of Human Genetics, 1985. **37**(2): p. 268-285.

195. Sato, Y., et al., *Identification of a new plasma biomarker of Alzheimer's disease using metabolomics technology.* J Lipid Res, 2012. **53**(3): p. 567-76.
196. Proitsi, P., et al., *Plasma lipidomics analysis finds long chain cholesteryl esters to be associated with Alzheimer's disease.* Translational Psychiatry, 2015. **5**: p. e494.
197. Goodenowe, D.B., et al., *Peripheral ethanolamine plasmalogen deficiency: a logical causative factor in Alzheimer's disease and dementia.* J Lipid Res, 2007. **48**(11): p. 2485-98.
198. Li, D., et al., *Plasma phospholipids and prevalence of mild cognitive impairment and/or dementia in the ARIC Neurocognitive Study (ARIC-NCS).* Alzheimer's & Dementia : Diagnosis, Assessment & Disease Monitoring, 2016. **3**: p. 73-82.
199. Gonzalez-Dominguez, R., T. Garcia-Barrera, and J.L. Gomez-Ariza, *Metabolomic study of lipids in serum for biomarker discovery in Alzheimer's disease using direct infusion mass spectrometry.* J Pharm Biomed Anal, 2014. **98**: p. 321-6.
200. Gonzalez-Dominguez, R., T. Garcia-Barrera, and J.L. Gomez-Ariza, *Using direct infusion mass spectrometry for serum metabolomics in Alzheimer's disease.* Anal Bioanal Chem, 2014. **406**(28): p. 7137-48.
201. Klavins, K., et al., *The ratio of phosphatidylcholines to lysophosphatidylcholines in plasma differentiates healthy controls from patients with Alzheimer's disease and mild cognitive impairment.* Alzheimer's & Dementia: Diagnosis, Assessment & Disease Monitoring, 2015. **1**(3): p. 295-302.
202. Wood, P.L., et al., *Targeted lipidomics distinguishes patient subgroups in mild cognitive impairment (MCI) and late onset Alzheimer's disease (LOAD).* BBA Clin, 2016. **5**: p. 25-8.
203. Gonzalez-Dominguez, R., et al., *Metabolomic-Driven Elucidation of Serum Disturbances Associated with Alzheimer's Disease and Mild Cognitive Impairment.* Curr Alzheimer Res, 2016. **13**(6): p. 641-53.
204. Fukuhara, K., et al., *NMR-based metabolomics of urine in a mouse model of Alzheimer's disease: identification of oxidative stress biomarkers.* J Clin Biochem Nutr, 2013. **52**(2): p. 133-8.
205. Liang, Q., et al., *High-throughput metabolomics analysis discovers salivary biomarkers for predicting mild cognitive impairment and Alzheimer's disease.* RSC Advances, 2016. **6**(79): p. 75499-75504.
206. Liang, Q., et al., *Metabolomics-based screening of salivary biomarkers for early diagnosis of Alzheimer's disease.* RSC Advances, 2015. **5**(116): p. 96074-96079.
207. Cui, Y., et al., *Lysophosphatidylcholine and amide as metabolites for detecting alzheimer disease using ultrahigh-performance liquid chromatography-quadrupole time-of-flight mass spectrometry-based metabonomics.* J Neuropathol Exp Neurol, 2014. **73**(10): p. 954-63.
208. Peng, J., et al., *Development of isotope labeling liquid chromatography mass spectrometry for mouse urine metabolomics: quantitative metabolomic study of transgenic mice related to Alzheimer's disease.* J Proteome Res, 2014. **13**(10): p. 4457-69.
209. Graham, S.F., C. Holscher, and B.D. Green, *Metabolic signatures of human Alzheimer's disease (AD): ^{1}H NMR analysis of the polar metabolome of post-mortem brain tissue.* Metabolomics, 2014. **10**(4): p. 744-753.
210. Graham, S.F., et al., *Investigation of the Human Brain Metabolome to Identify Potential Markers for Early Diagnosis and Therapeutic Targets of Alzheimer's Disease.* Analytical Chemistry, 2013. **85**(3): p. 1803-1811.
211. Farooqui, A.A. and L.A. Horrocks, *Plasmalogens: workhorse lipids of membranes in normal and injured neurons and glia.* Neuroscientist, 2001. **7**(3): p. 232-45.
212. Wood, P.L., et al., *Non-targeted lipidomics of CSF and frontal cortex grey and white matter in control, mild cognitive impairment, and Alzheimer's disease subjects.* Acta Neuropsychiatr, 2015. **27**(5): p. 270-8.

213. Han, X., et al., *Substantial sulfatide deficiency and ceramide elevation in very early Alzheimer's disease: potential role in disease pathogenesis.* J Neurochem, 2002. **82**(4): p. 809-18.
214. Cheng, H., et al., *Apolipoprotein E mediates sulfatide depletion in animal models of Alzheimer's disease.* Neurobiol Aging, 2010. **31**(7): p. 1188-96.
215. Chishti, M.A., et al., *Early-onset amyloid deposition and cognitive deficits in transgenic mice expressing a double mutant form of amyloid precursor protein 695.* J Biol Chem, 2001. **276**(24): p. 21562-70.
216. Hsiao, K., et al., *Correlative memory deficits, Abeta elevation, and amyloid plaques in transgenic mice.* Science, 1996. **274**(5284): p. 99-102.
217. Mucke, L., et al., *High-level neuronal expression of abeta 1-42 in wild-type human amyloid protein precursor transgenic mice: synaptotoxicity without plaque formation.* J Neurosci, 2000. **20**(11): p. 4050-8.
218. Pan, X., et al., *Alzheimer's disease–like pathology has transient effects on the brain and blood metabolome.* Neurobiology of Aging, 2016. **38**: p. 151-163.
219. González-Domínguez, R., et al., *Region-specific metabolic alterations in the brain of the APP/PS1 transgenic mice of Alzheimer's disease.* Biochimica et Biophysica Acta (BBA) - Molecular Basis of Disease, 2014. **1842**(12, Part A): p. 2395-2402.
220. Lalande, J., et al., *^{1}H NMR metabolomic signatures in five brain regions of the AbetaPPswe Tg2576 mouse model of Alzheimer's disease at four ages.* J Alzheimers Dis, 2014. **39**(1): p. 121-43.
221. Trushina, E., et al., *Defects in Mitochondrial Dynamics and Metabolomic Signatures of Evolving Energetic Stress in Mouse Models of Familial Alzheimer's Disease.* PLOS ONE, 2012. **7**(2): p. e32737.
222. Dedeoglu, A., et al., *Magnetic resonance spectroscopic analysis of Alzheimer's disease mouse brain that express mutant human APP shows altered neurochemical profile.* Brain Res, 2004. **1012**(1-2): p. 60-5.
223. Woo, D.C., et al., *Regional metabolic alteration of Alzheimer's disease in mouse brain expressing mutant human APP-PS1 by ^{1}H HR-MAS.* Behav Brain Res, 2010. **211**(1): p. 125-31.
224. Salek, R.M., et al., *A metabolomic study of the CRND8 transgenic mouse model of Alzheimer's disease.* Neurochemistry International, 2010. **56**(8): p. 937-947.
225. Lin, S., et al., *Ultrahigh resolution mass spectrometry-based metabolic characterization reveals cerebellum as a disturbed region in two animal models.* Talanta, 2014. **118**: p. 45-53.
226. Forster, D.M., M.F. James, and S.R. Williams, *Effects of Alzheimer's disease transgenes on neurochemical expression in the mouse brain determined by ^{1}H MRS in vitro.* NMR Biomed, 2012. **25**(1): p. 52-8.
227. Wang, H., et al., *Age-related alterations in the metabolic profile in the hippocampus of the senescence-accelerated mouse prone 8: a spontaneous Alzheimer's disease mouse model.* J Alzheimers Dis, 2014. **39**(4): p. 841-8.
228. Hu, Z.-P., et al., *Metabonomic Profiling of TASTPM Transgenic Alzheimer's Disease Mouse Model.* Journal of Proteome Research, 2012. **11**(12): p. 5903-5913.
229. Graham, S.F., et al., *^{1}H NMR metabolomics investigation of an Alzheimer's disease (AD) mouse model pinpoints important biochemical disturbances in brain and plasma.* Metabolomics, 2013. **9**(5): p. 974-983.
230. Lin, S., et al., *Hippocampal metabolomics using ultrahigh-resolution mass spectrometry reveals neuroinflammation from Alzheimer's disease in CRND8 mice.* Anal Bioanal Chem, 2013. **405**(15): p. 5105-17.
231. González-Domínguez, R., et al., *Metabolomic screening of regional brain alterations in the APP/PS1 transgenic model of Alzheimer's disease by direct infusion mass spectrometry.* Journal of Pharmaceutical and Biomedical Analysis, 2015. **102**: p. 425-435.

232. Pan, X., et al., *Alzheimer's disease like pathology has transient effects on the brain and blood metabolome, 2013.* Neurobiology of Aging. **38**: p. 151-163.
233. Li, N., et al., *A UPLC/MS-based metabolomics investigation of the protective effect of ginsenosides Rg1 and Rg2 in mice with Alzheimer's disease.* Journal of Ginseng Research. **40**(1): p. 9-17.
234. Paglia, G., et al., *Unbiased Metabolomic Investigation of Alzheimer's Disease Brain Points to Dysregulation of Mitochondrial Aspartate Metabolism.* Journal of Proteome Research, 2016. **15**(2): p. 608-618.
235. Xu, J., et al., *Graded perturbations of metabolism in multiple regions of human brain in Alzheimer's disease: Snapshot of a pervasive metabolic disorder.* Biochim Biophys Acta, 2016. **1862**(6): p. 1084-92.
236. Ansoleaga, B., et al., *Deregulation of purine metabolism in Alzheimer's disease.* Neurobiology of Aging, 2015. **36**(1): p. 68-80.
237. Krzysztof Blusztajn, J., et al., *Levels of phospholipid catabolic intermediates, glycerophosphocholine and glycerophosphoethanolamine, are elevated in brains of Alzheimer's disease but not of Down's syndrome patients*. Vol. 536. 1991. 240-4.
238. Takayama, T., et al., *A novel approach for LC-MS/MS-based chiral metabolomics fingerprinting and chiral metabolomics extraction using a pair of enantiomers of chiral derivatization reagents.* Analytica Chimica Acta, 2015. **898**: p. 73-84.
239. Inoue, K., et al., *Metabolic profiling of Alzheimer's disease brains.* Scientific Reports, 2013. **3**: p. 2364.
240. Liu, P., et al., *Altered arginine metabolism in Alzheimer's disease brains.* Neurobiology of Aging. **35**(9): p. 1992-2003.
241. Cheng, H., et al., *Specific changes of sulfatide levels in individuals with preclinical Alzheimer's disease: an early event in disease pathogenesis.* Journal of neurochemistry, 2013. **127**(6): p. 10.1111/jnc.12368.
242. Botosoa, E., et al., *NMR metabolomic of frontal cortex extracts: First study comparing two neurodegenerative diseases, Alzheimer disease and amyotrophic lateral sclerosis*. Vol. 33. 2012. 281–286.
243. Miatto, O., et al., *In vitro ^{31}P NMR spectroscopy detects altered phospholipid metabolism in Alzheimer's disease.* Can J Neurol Sci, 1986. **13**(4): p. 535-9.
244. Kell, D.B., *Metabolomics and systems biology: making sense of the soup.* Curr Opin Microbiol, 2004. **7**(3): p. 296-307.
245. Pan, Z.a.D.R., *Comparing and combining NMR spectroscopy and mass spectrometry in metabolomics.* Analytical and Bioanalytical Chemistry, 2007. **387**(2): p. 525-527.
246. Psychogios, N., et al., *The Human Serum Metabolome.* PLOS ONE, 2011. **6**(2): p. e16957.
247. Zhang, T., et al., *Evaluation of Coupling Reversed Phase, Aqueous Normal Phase, and Hydrophilic Interaction Liquid Chromatography with Orbitrap Mass Spectrometry for Metabolomic Studies of Human Urine.* Analytical Chemistry, 2012. **84**(4): p. 1994-2001.
248. Crockford, D.J., et al., *Statistical heterospectroscopy, an approach to the integrated analysis of NMR and UPLC-MS data sets: application in metabonomic toxicology studies.* Anal Chem, 2006. **78**(2): p. 363-71.
249. Kleijn, R.J., et al., *Metabolic flux analysis of a glycerol-overproducing Saccharomyces cerevisiae strain based on GC-MS, LC-MS and NMR-derived C-labelling data.* FEMS Yeast Res, 2007. **7**(2): p. 216-31.
250. Ansoleaga, B., et al., *Deregulation of purine metabolism in Alzheimer's disease.* Neurobiol Aging, 2015. **36**(1): p. 68-80.
251. Jove, M., et al., *Metabolomics of human brain aging and age-related neurodegenerative diseases.* J Neuropathol Exp Neurol, 2014. **73**(7): p. 640-57.
252. Gonzalez-Dominguez, R., et al., *Metabolomic screening of regional brain alterations in the APP/PS1 transgenic model of Alzheimer's disease by direct infusion mass spectrometry*. J Pharm Biomed Anal, 2015. **102**: p. 425-35.

253. Gonzalez-Dominguez, R., et al., *Metabolomic investigation of systemic manifestations associated with Alzheimer's disease in the APP/PS1 transgenic mouse model.* Mol Biosyst, 2015. **11**(9): p. 2429-40.
254. Guest, P.C., F.L. Guest, and D. Martins-de Souza, *Making Sense of Blood-Based Proteomics and Metabolomics in Psychiatric Research.* International Journal of Neuropsychopharmacology, 2016. **19**(6): p. pyv138.
255. Graham, S.F., et al., *Investigation of the Human Brain Metabolome to Identify Potential Markers for Early Diagnosis and Therapeutic Targets of Alzheimer's Disease.* Analytical Chemistry, 2013. **85**(3): p. 1803-1811.
256. Whiley, L., et al., *In-vial dual extraction for direct LC-MS analysis of plasma for comprehensive and highly reproducible metabolic fingerprinting.* Anal Chem, 2012. **84**(14): p. 5992-9.
257. Spijker, S., *Dissection of Rodent Brain Regions*, in *Neuroproteomics*, K.W. Li, Editor. 2011, Humana Press: Totowa, NJ. p. 13-26.
258. US Department of Health and Human Services, F.a.D.A., Centre for Drug Evaluation and Research (CDER), Centre for Veterinary Medicine (CVM). , *Bioanalytical Method Validation.* 2001.
259. Folch, J., et al., *Preparation of lipid extracts from brain tissue.* J Biol Chem, 1951. **191**(2): p. 833-41.
260. Abbott, S.K., et al., *An improved high-throughput lipid extraction method for the analysis of human brain lipids.* Lipids, 2013. **48**(3): p. 307-18.
261. Matyash, V., et al., *Lipid extraction by methyl-tert-butyl ether for high-throughput lipidomics.* Journal of Lipid Research, 2008. **49**(5): p. 1137-1146.
262. Bligh, E.G. and W.J. Dyer, *A rapid method of total lipid extraction and purification.* Canadian Journal of Biochemistry and Physiology, 1959. **37**(8): p. 911-917.
263. Yanes, O., et al., *Expanding coverage of the metabolome for global metabolite profiling.* Anal Chem, 2011. **83**(6): p. 2152-61.
264. Masson, P., et al., *Optimization and Evaluation of Metabolite Extraction Protocols for Untargeted Metabolic Profiling of Liver Samples by UPLC-MS.* Analytical Chemistry, 2010. **82**(18): p. 7779-7786.
265. Chen, S., et al., *Simultaneous extraction of metabolome and lipidome with methyl tert-butyl ether from a single small tissue sample for ultra-high performance liquid chromatography/mass spectrometry.* J Chromatogr A, 2013. **1298**: p. 9-16.
266. Fernie, A.R., et al., *Metabolite profiling: from diagnostics to systems biology.* Nat Rev Mol Cell Biol, 2004. **5**(9): p. 763-9.
267. Forcisi, S., et al., *Liquid chromatography-mass spectrometry in metabolomics research: mass analyzers in ultra high pressure liquid chromatography coupling.* J Chromatogr A, 2013. **1292**: p. 51-65.
268. Larive, C.K., G.A. Barding, and M.M. Dinges, *NMR Spectroscopy for Metabolomics and Metabolic Profiling.* Analytical Chemistry, 2015. **87**(1): p. 133-146.
269. Crockford, D.J., et al., *Statistical Heterospectroscopy, an Approach to the Integrated Analysis of NMR and UPLC-MS Data Sets: Application in Metabonomic Toxicology Studies.* Analytical Chemistry, 2006. **78**(2): p. 363-371.
270. Constantinou, C., et al., *GC−MS Metabolomic Analysis Reveals Significant Alterations in Cerebellar Metabolic Physiology in a Mouse Model of Adult Onset Hypothyroidism.* Journal of Proteome Research, 2011. **10**(2): p. 869-879.
271. Horning, E.C. and M.G. Horning, *Human Metabolic Profiles Obtained by GC and GC/MS.* Journal of Chromatographic Science, 1971. **9**(3): p. 129-140.
272. Koek, M.M., et al., *Quantitative metabolomics based on gas chromatography mass spectrometry: status and perspectives.* Metabolomics, 2011. **7**(3): p. 307-328.
273. Guarino, A.M. and H.M. Fales, *Gas Chromatography-Mass Spectrometry*, in *Concepts in Biochemical Pharmacology: Part 2*, B.B. Brodie, J.R. Gillette, and H.S. Ackerman, Editors. 1971, Springer Berlin Heidelberg: Berlin, Heidelberg. p. 178-208.

274. Rosenthal, D., *Theoretical limitations of gas chromatographic/mass spectrometric identification of multicomponent mixtures.* Analytical Chemistry, 1982. **54**(1): p. 63-66.
275. Lenz, E.M. and I.D. Wilson, *Analytical strategies in metabonomics.* J Proteome Res, 2007. **6**(2): p. 443-58.
276. Alañón, M.E., M.S. Pérez-Coello, and M.L. Marina, *Wine science in the metabolomics era.* TrAC Trends in Analytical Chemistry, 2015. **74**: p. 1-20.
277. Cajka, T. and O. Fiehn, *Toward Merging Untargeted and Targeted Methods in Mass Spectrometry-Based Metabolomics and Lipidomics.* Anal Chem, 2016. **88**(1): p. 524-45.
278. Raterink, R.-J., et al., *Recent developments in sample-pretreatment techniques for mass spectrometry-based metabolomics.* TrAC Trends in Analytical Chemistry, 2014. **61**(Supplement C): p. 157-167.
279. Farré, M., M. Petrovic, and D. Barceló, *Recently developed GC/MS and LC/MS methods for determining NSAIDs in water samples.* Analytical and Bioanalytical Chemistry, 2007. **387**(4): p. 1203-1214.
280. Ghassempour, A., et al., *Monitoring of the fermentation media of citric acid by the trimethylsilyl derivatives of the organic acids formed.* J Agric Food Chem, 2004. **52**(21): p. 6384-8.
281. Dunn, W.B., et al., *Procedures for large-scale metabolic profiling of serum and plasma using gas chromatography and liquid chromatography coupled to mass spectrometry.* Nat Protoc, 2011. **6**(7): p. 1060-83.
282. Smith, C.A., et al., *XCMS: processing mass spectrometry data for metabolite profiling using nonlinear peak alignment, matching, and identification.* Anal Chem, 2006. **78**(3): p. 779-87.
283. Listgarten, J. and A. Emili, *Statistical and computational methods for comparative proteomic profiling using liquid chromatography-tandem mass spectrometry.* Mol Cell Proteomics, 2005. **4**(4): p. 419-34.
284. Chen, M., et al., *A modified data normalization method for GC-MS-based metabolomics to minimize batch variation.* Springerplus, 2014. **3**: p. 439.
285. Lewczuk, P., et al., *Tau protein phosphorylated at threonine 181 in CSF as a neurochemical biomarker in Alzheimer's disease: original data and review of the literature.* J Mol Neurosci, 2004. **23**(1-2): p. 115-22.
286. Buerger, K., et al., *Differential diagnosis of Alzheimer disease with cerebrospinal fluid levels of tau protein phosphorylated at threonine 231.* Arch Neurol, 2002. **59**(8): p. 1267-72.
287. Blennow, K., E. Vanmechelen, and H. Hampel, *CSF total tau, Abeta42 and phosphorylated tau protein as biomarkers for Alzheimer's disease.* Mol Neurobiol, 2001. **24**(1-3): p. 87-97.
288. Schuff, N., et al., *MRI of hippocampal volume loss in early Alzheimer's disease in relation to ApoE genotype and biomarkers.* Brain, 2009. **132**(Pt 4): p. 1067-77.
289. Klunk, W.E., et al., *Imaging brain amyloid in Alzheimer's disease with Pittsburgh Compound-B.* Ann Neurol, 2004. **55**(3): p. 306-19.
290. Mosconi, L., et al., *FDG-PET changes in brain glucose metabolism from normal cognition to pathologically verified Alzheimer's disease.* European journal of nuclear medicine and molecular imaging, 2009. **36**(5): p. 811-822.
291. Fiehn, O., *Metabolomics--the link between genotypes and phenotypes.* Plant Mol Biol, 2002. **48**(1-2): p. 155-71.
292. Snowden, S., S.E. Dahlen, and C.E. Wheelock, *Application of metabolomics approaches to the study of respiratory diseases.* Bioanalysis, 2012. **4**(18): p. 2265-90.
293. Sana, T.R., K. Waddell, and S.M. Fischer, *A sample extraction and chromatographic strategy for increasing LC/MS detection coverage of the erythrocyte metabolome.* J Chromatogr B Analyt Technol Biomed Life Sci, 2008. **871**(2): p. 314-21.
294. Ibanez, C., A. Cifuentes, and C. Simo, *Recent advances and applications of metabolomics to investigate neurodegenerative diseases.* Int Rev Neurobiol, 2015. **122**: p. 95-132.

295. Wang, G., et al., *Plasma metabolite profiles of Alzheimer's disease and mild cognitive impairment.* J Proteome Res, 2014. **13**(5): p. 2649-58.
296. Toledo, J.B., et al., *Metabolic network failures in Alzheimer's disease: A biochemical road map.* Alzheimers Dement, 2017. **13**(9): p. 965-984.
297. Gonzalez-Dominguez, R., T. Garcia-Barrera, and J.L. Gomez-Ariza, *Metabolite profiling for the identification of altered metabolic pathways in Alzheimer's disease.* J Pharm Biomed Anal, 2015. **107**: p. 75-81.
298. Tang, Z., et al., *Urinary Metabolomics Reveals Alterations of Aromatic Amino Acid Metabolism of Alzheimer's Disease in the Transgenic CRND8 Mice.* Curr Alzheimer Res, 2016. **13**(7): p. 764-76.
299. Tautenhahn, R., C. Bottcher, and S. Neumann, *Highly sensitive feature detection for high resolution LC/MS.* BMC Bioinformatics, 2008. **9**: p. 504.
300. Smith, C.A., et al., *XCMS: Processing Mass Spectrometry Data for Metabolite Profiling Using Nonlinear Peak Alignment, Matching, and Identification.* Analytical Chemistry, 2006. **78**(3): p. 779-787.
301. Wiklund, S., et al., *Visualization of GC/TOF-MS-Based Metabolomics Data for Identification of Biochemically Interesting Compounds Using OPLS Class Models.* Analytical Chemistry, 2008. **80**(1): p. 115-122.
302. Saccenti, E., et al., *Reflections on univariate and multivariate analysis of metabolomics data.* Metabolomics, 2014. **10**(3): p. 361-374.
303. Ebshiana, A.A., et al., *Metabolomic Method: UPLC-q-ToF Polar and Non-Polar Metabolites in the Healthy Rat Cerebellum Using an In-Vial Dual Extraction.* PLOS ONE, 2015. **10**(4): p. e0122883.
304. Lovestone, S., et al., *AddNeuroMed--the European collaboration for the discovery of novel biomarkers for Alzheimer's disease.* Ann N Y Acad Sci, 2009. **1180**: p. 36-46.
305. Eriksson, L., et al., *Multi- and Megavariate Data Analysis: Principles and Applications*. 2001: Umetrics Academy.
306. Triba, M.N., et al., *PLS/OPLS models in metabolomics: the impact of permutation of dataset rows on the K-fold cross-validation quality parameters.* Mol Biosyst, 2015. **11**(1): p. 13-9.
307. Andersen, K., et al., *Gender differences in the incidence of AD and vascular dementia: The EURODEM Studies.* Neurology, 1999. **53**(9): p. 1992.
308. Barnes, L.L., et al., *Sex differences in the clinical manifestations of Alzheimer disease pathology.* Arch Gen Psychiatry, 2005. **62**(6): p. 685-91.
309. Danysz, W. and C.G. Parsons, *The NMDA receptor antagonist memantine as a symptomatological and neuroprotective treatment for Alzheimer's disease: preclinical evidence.* Int J Geriatr Psychiatry, 2003. **18**(Suppl 1): p. S23-32.
310. Danysz, W. and C.G. Parsons, *Alzheimer's disease, beta-amyloid, glutamate, NMDA receptors and memantine--searching for the connections.* Br J Pharmacol, 2012. **167**(2): p. 324-52.
311. Greenamyre, J.T., et al., *Glutamate transmission and toxicity in Alzheimer's disease.* Prog Neuropsychopharmacol Biol Psychiatry, 1988. **12**(4): p. 421-30.
312. Hynd, M.R., H.L. Scott, and P.R. Dodd, *Glutamate-mediated excitotoxicity and neurodegeneration in Alzheimer's disease.* Neurochem Int, 2004. **45**(5): p. 583-95.
313. Kirvell, S.L., M. Esiri, and P.T. Francis, *Down-regulation of vesicular glutamate transporters precedes cell loss and pathology in Alzheimer's disease.* J Neurochem, 2006. **98**(3): p. 939-50.
314. de la Monte, S.M. and M. Tong, *Brain metabolic dysfunction at the core of Alzheimer's disease.* Biochem Pharmacol, 2014. **88**(4): p. 548-59.
315. Greenberg, N., et al., *A proposed metabolic strategy for monitoring disease progression in Alzheimer's disease.* Electrophoresis, 2009. **30**(7): p. 1235-9.
316. Mapstone, M., A.K. Cheema, and M.S. Fiandaca, *Plasma phospholipids identify antecedent memory impairment in older adults.* 2014. **20**(4): p. 415-8.

317. Braak, H. and E. Braak, *Diagnostic criteria for neuropathologic assessment of Alzheimer's disease.* Neurobiol Aging, 1997. **18**(4 Suppl): p. S85-8.
318. Jellinger, K.A. and C. Bancher, *Neuropathology of Alzheimer's disease: a critical update.* J Neural Transm Suppl, 1998. **54**: p. 77-95.
319. Bennett, D.A., et al., *Neuropathology of older persons without cognitive impairment from two community-based studies.* Neurology, 2006. **66**(12): p. 1837-44.
320. Iacono, D., et al., *Mild cognitive impairment and asymptomatic Alzheimer disease subjects: equivalent beta-amyloid and tau loads with divergent cognitive outcomes.* J Neuropathol Exp Neurol, 2014. **73**(4): p. 295-304.
321. Larner, A.J., *The cerebellum in Alzheimer's disease.* Dement Geriatr Cogn Disord, 1997. **8**(4): p. 203-9.
322. Ferrucci, L., *The Baltimore Longitudinal Study of Aging (BLSA): A 50-Year-Long Journey and Plans for the Future.* The journals of gerontology. Series A, Biological sciences and medical sciences, 2008. **63**(12): p. 1416-1419.
323. Shock, N.W.a.G., Richard C. and Costa, Paul T, Jr. and Andres, Reubin and Lakatta, Edward G. and Arenberg, David and Tobin, Jordan D., *Normal Human Aging: The Baltimore Longitudinal Study on Aging.* NIH Publication, Washington, D.C, US Government Printing Office., 1984.
324. Kawas, C., et al., *Age-specific incidence rates of Alzheimer's disease: the Baltimore Longitudinal Study of Aging.* Neurology, 2000. **54**(11): p. 2072-7.
325. Kanehisa, M. and S. Goto, *KEGG: Kyoto Encyclopedia of Genes and Genomes.* Nucleic Acids Research, 2000. **28**(1): p. 27-30.
326. de Calignon, A., et al., *Propagation of tau pathology in a model of early Alzheimer's disease.* Neuron, 2012. **73**(4): p. 685-697.
327. Hardy, J.A. and G.A. Higgins, *Alzheimer's disease: the amyloid cascade hypothesis.* Science, 1992. **256**(5054): p. 184-5.
328. Iqbal, K., et al., *Tau pathology in Alzheimer disease and other tauopathies.* Biochim Biophys Acta, 2005. **1739**(2-3): p. 198-210.
329. Nasaruddin, M.L., et al., *Wide-ranging alterations in the brain fatty acid complement of subjects with late Alzheimer's disease as detected by GC-MS.* Am J Transl Res, 2016. **8**(1): p. 154-65.
330. Cunnane, S.C., et al., *Plasma and brain fatty acid profiles in mild cognitive impairment and Alzheimer's disease.* J Alzheimers Dis, 2012. **29**(3): p. 691-7.
331. Amtul, Z., et al., *Detrimental effects of arachidonic acid and its metabolites in cellular and mouse models of Alzheimer's disease: structural insight.* Neurobiol Aging, 2012. **33**(4): p. 831.e21-31.
332. Amtul, Z., et al., *Oleic acid ameliorates amyloidosis in cellular and mouse models of Alzheimer's disease.* Brain Pathol, 2011. **21**(3): p. 321-9.
333. Park, Y.S., et al., *Prolyl endopeptidase inhibitory activity of unsaturated fatty acids.* J Agric Food Chem, 2006. **54**(4): p. 1238-42.
334. Lopez-Miranda, J., et al., *Olive oil and health: summary of the II international conference on olive oil and health consensus report, Jaen and Cordoba (Spain) 2008.* Nutr Metab Cardiovasc Dis, 2010. **20**(4): p. 284-94.
335. Pelletier, A., et al., *Mediterranean diet and preserved brain structural connectivity in older subjects.* Alzheimers Dement, 2015. **11**(9): p. 1023-31.
336. Martinez-Lapiscina, E.H., et al., *Virgin olive oil supplementation and long-term cognition: the PREDIMED-NAVARRA randomized, trial.* J Nutr Health Aging, 2013. **17**(6): p. 544-52.
337. Cole, G.M. and S.A. Frautschy, *Docosahexaenoic acid protects from amyloid and dendritic pathology in an Alzheimer's disease mouse model.* Nutr Health, 2006. **18**(3): p. 249-59.
338. Cole, G.M. and S.A. Frautschy, *DHA may prevent age-related dementia.* J Nutr, 2010. **140**(4): p. 869-74.

339. Hashimoto, M., et al., *Docosahexaenoic acid provides protection from impairment of learning ability in Alzheimer's disease model rats.* J Neurochem, 2002. **81**(5): p. 1084-91.
340. Swanson, D., R. Block, and S.A. Mousa, *Omega-3 Fatty Acids EPA and DHA: Health Benefits Throughout Life.* Advances in Nutrition: An International Review Journal, 2012. **3**(1): p. 1-7.
341. Freund-Levi, Y., et al., *Omega-3 fatty acid treatment in 174 patients with mild to moderate Alzheimer disease: OmegAD study: a randomized double-blind trial.* Arch Neurol, 2006. **63**(10): p. 1402-8.
342. Morris, M.C., et al., *Consumption of fish and n-3 fatty acids and risk of incident Alzheimer disease.* Arch Neurol, 2003. **60**(7): p. 940-6.
343. Quinn, J.F., et al., *Docosahexaenoic acid supplementation and cognitive decline in Alzheimer disease: a randomized trial.* Jama, 2010. **304**(17): p. 1903-11.
344. Grimm, M.O., et al., *Docosahexaenoic acid reduces amyloid beta production via multiple pleiotropic mechanisms.* J Biol Chem, 2011. **286**(16): p. 14028-39.
345. Goldman, D.W., W.C. Pickett, and E.J. Goetzl, *Human neutrophil chemotactic and degranulating activities of leukotriene B5 (LTB5) derived from eicosapentaenoic acid.* Biochem Biophys Res Commun, 1983. **117**(1): p. 282-8.
346. Hawkes, J.S., M.J. James, and L.G. Cleland, *Biological activity of prostaglandin E3 with regard to oedema formation in mice.* Agents Actions, 1992. **35**(1-2): p. 85-7.
347. James, M.J., R.A. Gibson, and L.G. Cleland, *Dietary polyunsaturated fatty acids and inflammatory mediator production.* Am J Clin Nutr, 2000. **71**(1 Suppl): p. 343s-8s.
348. Rola-Pleszczynski, M., et al., *Differential regulation of cytokine and cytokine receptor genes by PAF, LTB4 and PGE2.* J Lipid Mediat, 1993. **6**(1-3): p. 175-81.
349. Schaefer, E.J., et al., *Plasma phosphatidylcholine docosahexaenoic acid content and risk of dementia and Alzheimer disease: the Framingham Heart Study.* Arch Neurol, 2006. **63**(11): p. 1545-50.
350. Simpson, B.N., et al., *Blood metabolite markers of cognitive performance and brain function in aging.* J Cereb Blood Flow Metab, 2016. **36**(7): p. 1212-23.
351. Ikonomovic, M.D., et al., *Increased 5-lipoxygenase immunoreactivity in the hippocampus of patients with Alzheimer's disease.* J Histochem Cytochem, 2008. **56**(12): p. 1065-73.
352. Manev, H., *5-Lipoxygenase gene polymorphism and onset of Alzheimer's disease.* Med Hypotheses, 2000. **54**(1): p. 75-6.
353. Bazan, N.G., V. Colangelo, and W.J. Lukiw, *Prostaglandins and other lipid mediators in Alzheimer's disease.* Prostaglandins Other Lipid Mediat, 2002. **68-69**: p. 197-210.
354. Funk, C.D., *Prostaglandins and leukotrienes: advances in eicosanoid biology.* Science, 2001. **294**(5548): p. 1871-5.
355. Sanchez-Mejia, R.O., et al., *Phospholipase A2 reduction ameliorates cognitive deficits in a mouse model of Alzheimer's disease.* Nat Neurosci, 2008. **11**(11): p. 1311-8.
356. Ariel, A. and C.N. Serhan, *Resolvins and protectins in the termination program of acute inflammation.* Trends Immunol, 2007. **28**(4): p. 176-83.
357. Serhan, C.N., et al., *Resolvins: a family of bioactive products of omega-3 fatty acid transformation circuits initiated by aspirin treatment that counter proinflammation signals.* J Exp Med, 2002. **196**(8): p. 1025-37.
358. Serhan, C.N., et al., *Maresins: novel macrophage mediators with potent antiinflammatory and proresolving actions.* J Exp Med, 2009. **206**(1): p. 15-23.
359. Farooqui, A.A., *Lipid mediators and their metabolism in the nucleous: implications for Alzheimer's disease.* J Alzheimers Dis, 2012. **30 Suppl 2**: p. S163-78.
360. Mizwicki, M.T., et al., *1alpha,25-dihydroxyvitamin D3 and resolvin D1 retune the balance between amyloid-beta phagocytosis and inflammation in Alzheimer's disease patients.* J Alzheimers Dis, 2013. **34**(1): p. 155-70.

361. Gouras, G.K., et al., *Intraneuronal β-amyloid accumulation and synapse pathology in Alzheimer's disease.* Acta neuropathologica, 2010. **119**(5): p. 523-541.
362. Grundke-Iqbal, I., et al., *Abnormal phosphorylation of the microtubule-associated protein tau (tau) in Alzheimer cytoskeletal pathology.* Proceedings of the National Academy of Sciences of the United States of America, 1986. **83**(13): p. 4913-4917.
363. Barth, B.M., S.J. Gustafson, and T.B. Kuhn, *Neutral Sphingomyelinase Activation Precedes NADPH Oxidase-Dependent Damage in Neurons Exposed to the Proinflammatory Cytokine TNFα.* Journal of neuroscience research, 2012. **90**(1): p. 229-242.
364. Blusztajn, J.K., et al., *Levels of phospholipid catabolic intermediates, glycerophosphocholine and glycerophosphoethanolamine, are elevated in brains of Alzheimer's disease but not of Down's syndrome patients.* Brain Research, 1990. **536**(1): p. 240-244.
365. Kim, M., et al., *Association between Plasma Ceramides and Phosphatidylcholines and Hippocampal Brain Volume in Late Onset Alzheimer's Disease.* J Alzheimers Dis, 2016.
366. Elliott, D.A., C.S. Weickert, and B. Garner, *Apolipoproteins in the brain: implications for neurological and psychiatric disorders.* Clinical lipidology, 2010. **51**(4): p. 555-573.
367. Mahley, R.W. and J. Stanley C. Rall, *Apolipoprotein E: Far More Than a Lipid Transport Protein.* Annual Review of Genomics and Human Genetics, 2000. **1**(1): p. 507-537.
368. Ben-David, O. and A.H. Futerman, *The Role of the Ceramide Acyl Chain Length in Neurodegeneration: Involvement of Ceramide Synthases.* NeuroMolecular Medicine, 2010. **12**(4): p. 341-350.
369. Cutler, R.G., et al., *Involvement of oxidative stress-induced abnormalities in ceramide and cholesterol metabolism in brain aging and Alzheimer's disease.* Proceedings of the National Academy of Sciences of the United States of America, 2004. **101**(7): p. 2070-2075.
370. Bandaru, V.V.R., et al., *ApoE4 disrupts sterol and sphingolipid metabolism in Alzheimer's but not normal brain.* Neurobiology of aging, 2009. **30**(4): p. 591-599.
371. Kosicek, M., et al., *Elevated cerebrospinal fluid sphingomyelin levels in prodromal Alzheimer's disease.* Neuroscience Letters, 2012. **516**(2): p. 302-305.
372. He, X., et al., *Deregulation of sphingolipid metabolism in Alzheimer's disease.* Neurobiology of Aging, 2010. **31**(3): p. 398-408.
373. Pettegrew, J.W., et al., *Brain Membrane Phospholipid Alterations in Alzheimer's Disease.* Neurochemical Research, 2001. **26**(7): p. 771-782.
374. Cutler, R.G. and M.P. Mattson, *Sphingomyelin and ceramide as regulators of development and lifespan.* Mechanisms of Ageing and Development, 2001. **122**(9): p. 895-908.
375. Smale, G., et al., *Evidence for Apoptotic Cell Death in Alzheimer's Disease.* Experimental Neurology, 1995. **133**(2): p. 225-230.
376. Puglielli, L., et al., *Ceramide Stabilizes β-Site Amyloid Precursor Protein-cleaving Enzyme 1 and Promotes Amyloid β-Peptide Biogenesis.* Journal of Biological Chemistry, 2003. **278**(22): p. 19777-19783.
377. Sawamura, N., et al., *Modulation of Amyloid Precursor Protein Cleavage by Cellular Sphingolipids.* Journal of Biological Chemistry, 2004. **279**(12): p. 11984-11991.
378. Ko, M.H. and L. Puglielli, *Two endoplasmic reticulum (ER)/ER Golgi intermediate compartment-based lysine acetyltransferases post-translationally regulate BACE1 levels.* J Biol Chem, 2009. **284**(4): p. 2482-92.
379. Head, E., et al., *A Two-Year Study with Fibrillar β-Amyloid (Aβ) Immunization in Aged Canines: Effects on Cognitive Function and Brain Aβ.* The Journal of Neuroscience, 2008. **28**(14): p. 3555-3566.
380. Nelson, P.T., et al., *Correlation of Alzheimer Disease Neuropathologic Changes With Cognitive Status: A Review of the Literature.* Journal of neuropathology and experimental neurology, 2012. **71**(5): p. 362-381.

381. Hyman, B., et al., *Alzheimer's disease: cell-specific pathology isolates the hippocampal formation.* Science, 1984. **225**(4667): p. 1168-1170.
382. de Calignon, A., et al., *Propagation of tau pathology in a model of early Alzheimer's disease.* Neuron, 2012. **73**(4): p. 685-97.
383. Liu, L., et al., *Trans-Synaptic Spread of Tau Pathology In Vivo.* PLoS ONE, 2012. **7**(2): p. e31302.
384. Bright, J., et al., *Human secreted tau increases amyloid-beta production.* Neurobiology of Aging, 2015. **36**(2): p. 693-709.
385. Braak, H. and E. Braak, *Neuropathological stageing of Alzheimer-related changes.* Acta Neuropathol, 1991. **82**(4): p. 239-59.
386. Brier, M.R., et al., *Tau and Aβ imaging, CSF measures, and cognition in Alzheimer's disease.* Science translational medicine, 2016. **8**(338): p. 338ra66-338ra66.
387. Madeo J, E.C., *The Role of Oxidative Stress in Alzheimer's Disease.* J Alzheimers Dis Parkinsonism, 2013. **3:116. doi:10.4172/2161-0460.1000116**.
388. Avila, J., *Tau phosphorylation and aggregation in Alzheimer's disease pathology.* FEBS Letters, 2006. **580**(12): p. 2922-2927.
389. Hernandez, P., et al., *Tau phosphorylation by cdk5 and Fyn in response to amyloid peptide Abeta (25-35): involvement of lipid rafts.* J Alzheimers Dis, 2009. **16**(1): p. 149-56.
390. Schenck, A., et al., *The Endosomal Protein Appl1 Mediates Akt Substrate Specificity and Cell Survival in Vertebrate Development.* Cell, 2008. **133**(3): p. 486-497.
391. García-Arencibia, M., et al., *Autophagy, a guardian against neurodegeneration.* Seminars in Cell & Developmental Biology, 2010. **21**(7): p. 691-698.
392. Frost, B. and M.I. Diamond, *Prion-like mechanisms in neurodegenerative diseases.* Nat Rev Neurosci, 2010. **11**(3): p. 155-9.
393. Maccioni, R.B., et al., *The Revitalized Tau Hypothesis on Alzheimer's Disease.* Archives of Medical Research, 2010. **41**(3): p. 226-231.
394. Katsel, P., C. Li, and V. Haroutunian, *Gene Expression Alterations in the Sphingolipid Metabolism Pathways during Progression of Dementia and Alzheimer's Disease: A Shift Toward Ceramide Accumulation at the Earliest Recognizable Stages of Alzheimer's Disease?* Neurochemical Research, 2007. **32**(4): p. 845-856.
395. Zare-shahabadi, A., et al., *Autophagy in Alzheimer's Disease.* Reviews in the neurosciences, 2015. **26**(4): p. 385-395.
396. Chalfant, C.E., et al., *Long Chain Ceramides Activate Protein Phosphatase-1 and Protein Phosphatase-2A: activation is stereospecific and regulated by phosphatidic acid.* Journal of Biological Chemistry, 1999. **274**(29): p. 20313-20317.
397. Mukhopadhyay, A., et al., *Direct interaction between the inhibitor 2 and ceramide via sphingolipid-protein binding is involved in the regulation of protein phosphatase 2A activity and signaling.* The FASEB Journal, 2009. **23**(3): p. 751-763.
398. Voronkov, M., S.P. Braithwaite, and J.B. Stock, *Phosphoprotein phosphatase 2A: a novel druggable target for Alzheimer's disease.* Future Medicinal Chemistry, 2011. **3**(7): p. 821-833.
399. Mukhopadhyay, A., et al., *Direct interaction between the inhibitor 2 and ceramide via sphingolipid-protein binding is involved in the regulation of protein phosphatase 2A activity and signaling*, 2009. **23**(3): p. 751-63.
400. Chen, C.-L., et al., *Lithium Inhibits Ceramide- and Etoposide-Induced Protein Phosphatase 2A Methylation, Bcl-2 Dephosphorylation, Caspase-2 Activation, and Apoptosis.* Molecular Pharmacology, 2006. **70**(2): p. 510-517.
401. Soreq, L., et al., *Major Shifts in Glial Regional Identity Are a Transcriptional Hallmark of Human Brain Aging.* Cell Reports, 2017. **18**(2): p. 557-570.
402. Satoi, H., et al., *Astroglial expression of ceramide in Alzheimer's disease brains: A role during neuronal apoptosis.* Neuroscience, 2005. **130**(3): p. 657-666.

403. Sasaki, A., et al., *Microglial activation in brain lesions with tau deposits: Comparison of human tauopathies and tau transgenic mice TgTauP301L.* Brain Research, 2008. **1214**(Supplement C): p. 159-168.
404. Wang, G., et al., *Astrocytes secrete exosomes enriched with proapoptotic ceramide and prostate apoptosis response 4 (PAR-4): potential mechanism of apoptosis induction in Alzheimer disease (AD).* J Biol Chem, 2012. **287**(25): p. 21384-95.
405. Patil, S., J. Melrose, and C. Chan, *Involvement of astroglial ceramide in palmitic acid-induced Alzheimer-like changes in primary neurons.* The European journal of neuroscience, 2007. **26**(8): p. 2131-2141.
406. Patil, S., et al., *Brain region-specificity of palmitic acid-induced abnormalities associated with Alzheimer's disease.* BMC Research Notes, 2008. **1**: p. 20-20.
407. Snowden, S.G., et al., *Association between fatty acid metabolism in the brain and Alzheimer disease neuropathology and cognitive performance: A nontargeted metabolomic study.* PLoS Medicine, 2017. **14**(3): p. e1002266.
408. Mielke, M.M., et al., *Plasma sphingomyelins are associated with cognitive progression in Alzheimer's Disease.* Journal of Alzheimer's disease, 2011. **27**(2): p. 259-269.
409. Varma, V.R., et al., *Brain and blood metabolite signatures of pathology and progression in Alzheimer disease: A targeted metabolomics study.* PLOS Medicine, 2018. **15**(1): p. e1002482.

Appendix A

Table 2.1 Metabolites annotated from the HILIC method. Annotations were made by matching fragmentation of analyte peaks to fragmentations in publicly accessible databases. Displaying the molecular formula, molecular weight in Da, retention time (RT) in minutes and intensity in positive and negative ionisation modes in arbitrary units for all metabolites. – represents metabolites not detected in this ionisation mode.

Name	**Formula**	**Molecular Weight (Da)**	**RT (mins)**	**Intensity**	
				Positive	Negative
Acetylalanine	C5H9NO3	131.0582	15.56	6.2	-
Acetylaspartate	C6H9NO5	175.0480	7.66	6.4	56.2
Acetylaspartylglutamate	C11H16N2O8	304.0906	8.38	7.2	28.6
Acetylcarnitine	C9H17NO4	203.1157	14.08	27.0	0.4
Acetylneuraminate	C11H19NO9	309.1059	23.88	0.4	-
Acetylserine	C5H9NO4	147.0531	8.31	-	22.3
Adenosine	C10H13N5O4	267.0967	12.92	33.3	-
Adenosine monophosphate	C10H14N5O7P	347.0630	15.60	6.2	-
Adrenaline	C9H13NO3	183.0895	6.74	2.9	-
Alanine	C3H7NO2	89.0476	16.61	184.5	39.2
Aminobutyrate	C4H9NO2	103.0633	16.25	-	84.5
Arachidonoyl glycidol	C23H36O3	360.2664	5.01	7.8	-
Arginine	C6H14N4O2	174.1116	26.47	40.9	7.4
Ascorbate	C6H8O6	176.0320	10.72	4.2	69.1
Asparagine	C4H8N2O3	132.0534	17.01	-	1.4
Aspartate	C4H7NO4	133.0375	7.81	109.2	33.6
Butyrlcarnitine	C11H21NO4	231.1470	12.11	1.7	-
Carnitine	C7H15NO3	161.1051	17.06	135.5	-
Carnosine	C9H14N4O3	226.1065	28.8	2.1	-
Citrate	C6H8O7	192.0270	10.7	-	1.2
Citrulline	C6H13N3O3	175.0956	17.17	2.7	2.2
Coumarate	C9H8O3	164.0473	14.40	26.7	-
Creatine	C4H9N3O2	131.0694	16.62	576.9	20.5
Creatinine	C4H7N3O	113.0589	16.61	15.6	1.0
Cystathionine	C7H14N2O4S	222.0674	21.74	7.4	1.2

Cysteine	C3H7NO2S	121.0197	15.30	2.8	-
Cytidine	C9H13N3O5	243.0855	17.33	2.1	1.2
Deoxyfluorouridine	C9H11FN2O5	246.0651	12.20	-	6.2
Dimethylarginine	C8H18N4O2	202.1429	24.45	1.4	-
Dimethylglycine	C4H9NO2	103.0633	17.21	24.9	-
Fumarate	C4H4O4	116.0109	7.78	-	0.8
Gluconate	C6H12O7	196.0583	15.64	-	43.1
Glutamate	C5H9NO4	147.0531	16.17	79.1	61.6
Glutamine	C5H10N2O3	146.0691	16.78	27.9	95.2
Glutamyl-glutamate	C10H14N2O7	274.0801	15.61	8.2	-
Glutamyl-leucine	C11H19N2O5	259.1293	15.48	2.8	-
Glutathione	C10H17N3O6S	307.0838	15.06	22.8	-
Glycine	C2H5NO2	75.0320	17.13	2.2	1.3
Glycolate	C2H4O3	76.0160	6.51	-	4.5
Guanidinobutanoate	C5H11N3O2	145.0851	15.73	8.4	-
Guanine	C5H5N5O	151.0494	11.90	13.5	7.9
Guanosine	C10H13N5O5	283.0916	11.87	2.3	18.4
Hexose-deoxy sugar	C6H12O5	164.0679	14.39	-	5.2
Hexose-Phosphate	C6H13O9P	260.0297	14.94	-	17.4
Histidine	C6H9N3O2	155.0694	25.13	14.6	6.1
Hydroxyphenylglycine	C8H9NO3	167.0582	16.61	-	0.7
Hydroxyproline	C5H9NO3	131.0582	16.17	-	1.6
Hypoxanthine	C5H4N4O	136.0385	9.45	489.9	108.7
Indoleacetate	C10H9NO2	175.0633	9.17	5.0	-
Inosine	C10H12N4O5	268.0807	10.03	45.7	388.8
Kynurenine	C10H12N2O3	208.0847	12.19	0.9	-
Lactate	C3H6O3	90.0316	7.57	-	6.1
leucine/Isoleucine	C6H13NO2	131.0946	12.69	20.3	1.6
Lysine	C6H14N2O2	146.1055	26.62	4.7	16.3
Lysophosphatidylserine	C24H48NO9P	326.3033	6.89	4.9	-
Malate	C4H6O5	134.0215	8.66	-	9.5
Malonate	C3H4O4	104.0109	7.27	0.4	-
Methionine	C5H11NO2S	149.0510	13.43	7.3	1.2
Methyladenosine	C11H15N5O4	281.1124	17.16	0.9	0.7

Methylaspartate	C5H9NO4	147.0531	8.39	48.4	20.3
Methylbutyroylcarnitine	C12H23NO4	245.1627	11.8	0.3	-
Methylfuranone	C6H8O2	98.0368	15.66	-	223.4
Methylhistidine	C7H11N3O2	169.0851	25.54	2.2	-
Methylsulfolene	C5H8O2S	132.0245	13.44	16.9	-
Methylthioadenosine	C11H15N5O3S	297.0895	10.61	1.3	-
Methylthiophene	C5H6S	98.0190	7.80	1.2	-
myo-inositol	C6H12O6	180.0633	15.83	5.3	5.0
Nicotinamide	C6H6N2O	122.0480	9.57	104.8	-
Nicotinate	C6H5NO2	123.0320	9.14	-	0.6
Ornithine	C5H12N2O2	132.0898	26.39	0.5	14.4
Oxoproline	C5H7NO3	129.0425	16.77	217.42	30.2
Pantothenate	C9H17NO5	219.1106	6.74	10.1	2.2
Pentose sugar	C5H10O5	150.0528	13.55	-	10.7
Phenylalanine	C9H11NO2	165.0789	12.03	9.2	0.4
Phosphatidylcholine	C40H80NO8P	733.5621	9.08	63.6	-
Phosphenolpyruvate	C3H5O6P	167.9823	12.09	-	0.4
Phosphocreatine	C4H10N3O5P	211.0358	15.05	4.1	-
Pipecolate	C6H11NO2	129.0789	14.76	1.7	-
Proline	C5H9NO2	115.0633	14.99	30.2	0.3
Propionylcarnitine	C10H19NO4	217.1314	12.92	1.3	-
Putrescine	C4H12N2	88.1000	34.8	-	0.8
Riboflavin	C17H20N4O6	376.1382	7.9	5.5	-
Serine	C3H7NO3	105.0425	17.06	4.2	1.9
Spermidine	C7H19N3	145.1578	30.46	1.1	-
Taurine	C2H7NO3S	125.0146	15.00	119.9	286.3
Thiouracil	C4H4N2OS	128.0044	8.4	-	0.9
Threonine/Homoserine	C4H9NO3	119.0582	16.37	6.9	-
Thymidine	C10H14N2O5	242.0902	8.2	-	1.6
Thymine	C5H6N2O2	126.0429	9.30	0.6	25.6
Tocopherol	C29H50O2	430.3810	20.89	5.1	-
Tryptophan	C11H12N2O2	204.0898	12.74	4.2	1
Tyrosine	C9H11NO3	181.0738	14.39	8.8	14.9
Uracil	C4H4N2O2	112.0272	9.14	27.3	6.3

Urate	C5H4N4O3	168.0283	11.19	2.3	3.8
Uridine	C9H12N2O6	244.0695	9.18	1.7	12.1
Valine	C5H11NO2	117.0789	14.66	4.6	0.9
Xanthine	C5H4N4O2	152.0334	8.88	78.1	51.7
Xanthosine	C10H12N4O6	284.0756	11.85	-	2.8
Xanthurenate	C10H7NO4	205.0375	11.20	1.4	-

Table 2.2 Metabolites annotated from the reversed phase method. Annotations were made by matching fragmentation of analyte peaks to fragmentations in publicly accessible databases. Displaying the molecular formula, molecular weight in Da, retention time (RT) in minutes and intensity in positive and negative ionisation modes in arbitrary units for all metabolites. – represents metabolites not detected in this ionisation mode.

Name	Formula	Molecular Weight (Da)	RT (mins)	Intensity	
				Positive	Negative
Eicosatetraenoic acid	C20H32O2	304.2395	18.20	7.4	-
Docosahexaenoic acid	C22H32O2	328.2400	5.02	-	16.8
Oxo-nonadecanoic acid	C19H36O3	312.2661	20.81	14.1	-
Glucopyranosyl-octacosaneteraol	C34H68O9	620.4783	18.45	0.4	-
Glucopyranosyl-triacontanetanetriol	C36H70O9	646.4954	20.90	2.0	-
Octadecatrienal	C18H30O	262.2281	19.43	0.8	
Hexadecynyl acetate	C18H32O2	280.2388	4.61	-	1.7
Hydroxycholestanol	C27H48O2	404.363	15.06	-	3.7
DG(40:5)	C43H74O5	670.5535	20.79	1.8	-
DG(34:2)	C37H68O5	592.5103	27.07	0.7	-
DG(42:3)	C45H82O5	702.6099	17.58	3.9	-
DG(37:2)	C40H74O5	634.5490	27.14	1.2	-
SM(d36:0)	C41H85N2O6P	732.6091	13.20	0.7	-
SM(d41:1)	C46H93N2O6P	800.6832	18.55	1.9	-
SM(d42:1)	C47H95N2O6P	814.6965	24.13	3.9	-
SM(d42:2)	C47H93N2O6P	812.6822	20.20	18.9	-
C16:1 OH	C39H77N2O7P	716.5468	16.53		10.2

TG(52:7)	C55H92O6	848. 6842	28.10	6.2	-
TG(49:3)	C52H94O6	814.6965	19.44	3.5	-
TG(48:3)	C51H92O6	800.6823	17.70	1.4	-
TG(50:3)	C53H96O6	828.7112	19.97	1.1	-
TG(54:7)	C57H96O6	876.7199	30.36	3.1	-
TG(54:6)	C57H98O6	878.7420	30.43	1.1	-
TG(56:8)	C59H98O6	902.7421	30.71	1.2	-
Tetradecanyl-8-ladderance-octanyl)-glycerophospho-glycerol	C40H75O8P	714.5224	23.40	6.2	-
PI(36:3)	C45H81O13P	860.5627	21.29	-	6.93
PI(32:0)	C41H79O13P	811.5319	20.97	-	19.00
PI(38:2)	C47H87O13P	891.5596	19.08	-	34.13
PA(33:0)	C36H71O8P	662.4854	15.97	1.4	-
PA(36:1)	C39H75O8P	524.4359	26.03	32.8	-
PA(O-38:2)	C41H79O7P	714.5610	23.33	7.2	-
PA(35:1)	C38H75O7P	674.5328	20.86	1.7	-
PA(0-39:0)	C42H85O7P	732.6091	14.89	0.9	-
Didocasanoyl-glycerosulfocholine	C51H101O8PS	904.6917	15.92	3.2	-
GlcCer(36:1)	C42H81NO8	727.5962	24.19	5.5	-
GlcCer(d40:1)	C48H93NO8	811.6851	23.04	16.7	-
GlcCer(d40:2)	C46H87NO8	781.6351	23.60	-	4.3
Cerebroside D	C43H81NO9	755.6033	17.50	1.5	-
TermetomycesphinA	C41H77NO10	743.5492	18.71	-	2.9
Cholestanediol	C27H48O2	404.3636	14.84	-	1.4
PC(31:2)	C39H74NO8P	715.5134	18.85	2.4	-
PC(36:2)	C44H84NO7P	770.7432	18.36	1.5	-
PC(33:2)	C41H78NO8P	743.5492	20.21	1.7	12.1
PC(32:3)	C42H74NO8P	751.5152	18.77	-	57.7
PC(33:1)	C41H80NO8P	745.5574	21.30	-	0.3
PC(37:6)	C45H78NO8P	791.5417	19.61	-	1.9
PC(32:2)	C40H76NO8P	729.5322	15.98	13.7	-
PC(38:9)	C46H74NO8P	799.5298	20.62	-	1.4

PC(38:9)	C46H74NO8P	799.5298	19.11	-	45.4
PC(35:6)	C43H74NO8P	763.5146	18.70	2.3	22.4
PC(35:3)	C43H80NO8P	769.5688	20.70	41.5	-
PC(35:6)	C43H74NO8P	763.5146	17.63	2.1	-
PC(35:3)	C43H80NO8P	769.5???	25.57	1.5	-
PC(36:3)	C44H82NO8P	783.5663	15.49	15.7	-
PC(44:1)	C52H103NO8P	900.7242	24.05	19.9	-
PC(P-38:6)	C46H80NO7P	789.5609	18.20	1.0	-
PC(44:0)	C52H105NO8P	902.7421	28.94	18.6	-
PC(45:0)	C53H107NO8P	916.6589	27.84	11.5	-
PG(38:3)	C44H81O10P	801.0817	17.50	14.8	-
PG(36:2)	C42H79O10P	775.0444	17.53	1.4	-
PG(0-42:0)	C48H97O9P	848.6842	19.75	2.7	-
PE(40:6)	C45H78NO8P	791.5417	19.61	-	31.3
PE(33:1)	C38H74NO8P	703.5118	16.54	24.6	-
PE(35:2)	C40H80NO8P	729.5307	25.83	4.9	-
PE(38:3)	C43H80NO8P	769.5688	25.96	24.2	-
PE(33:2)	C38H72NO8P	701.4996	18.18		36.9
PE(34:2)	C39H74NO8P	715.5134	18.85	-	12.4
PE(36:4)	C41H76NO8P	739.5154	12.76	0.1	-
PE(36:2)	C41H78NO8P	743.5492	14.70	2.4	-
PE(36:5)	C41H72NO8P	737.9865	21.03	2.5	-
PE(36:1)	C41H76NO8P	745.5574	20.23	-	0.3
PE(38:6)	C43H74NO8P	763.5116	18.70	12.2	-
PE(38:4)	C43H78NO8P	768.0551	23.40	7.4	-
PE(46:1)	C51H100NO8P	885.7367	22.07	7.6	-
PE(O-36:0)	C41H86NO6P	719.6105	12.32	0.1	-
PE(O-40:0)	C45H92NO7P	789.6791	16.03	1.0	-
PE(44:8)	C49H82NO8P	844.5151	19.64	3.2	-
LPC(20:4)	C28H50NO7P	543.3353	1.80	3.1	-
LPC(24:1)	C32H64NO7P	605.4384	6.13	2.1	-
LPE(22:0)	C27H56NO7P	537.7098	15.76	-	10.1
LPE(24:1)	C29H58NO7P	563.7471	16.41	-	7.2
PS(39:3)	C45H82NO10P	827.5655	21.55	-	1.9

PS(37:3)	C43H78NO10P	799.5298	10.64	-	1.5
PS(36:1)	C42H80NO10P	789.5609	13.75	0.8	-
PS(36:0)	C42H82NO10P	791.5800	14.77	0.4	-
PS(36:5)	C42H72NO10P	781.9955	12.70	1.1	-
PS(0-34:0)	C40H80NO9P	749.5511	14.55	0.3	-
Cer(36:1)	C36H67NO3	565.5435	17.49	-	8.6
Cer(38:1)	C38H67NO3	593.5725	19.16	-	3.7
Cer(40:1)	C40H67NO3	621.6163	20.60	-	1.9
Cer(42:1)	C42H67NO3	649.6446	20.83	-	1.2
Cer(d44:2)	C44H85NO3	675.6477	24.30	5.6	-
Cer(d40:1)	C40H80NO6P	701.5575	15.13	3.8	-
PC aa C38:0	C46H92NO8P	817.6561	26.70	3.2	-
PC aa C40:1	C48H94NO8P	843.6717	20.24	6.6	6.4
PC aa C40:6	C48H84NO8P	833.5935	18.78	1.5	68.1
PC aa C38:6	C44H76NO8P	805.5622	15.60	16.8	-
PC aa C40:2	C48H92NO8P	841.6561	21.07	-	3.6

Appendix B

Table 2.1 List of metabolites identified by GC-MS aqueous, and non-aqueous, based on Similarity Index search of 90 and over(AQ and NAQ)

Extraction Phase	Retention Time	Name of compounds
Non-Aqueous	7.777	Octadecanal
	7.882	Octadecenoic acid
	8.384	Oleic acid
	8.679	Gamma-Linolenic acid
	9.193	Hexadecanoic acid (Palmitic acid)
	10.288	Hexanedioic acid
	10.810	Linoleic acid
	11.277	Methylheptadecadiynoic acid
	11.474	Methylstearate
	12.592	Arachidonic acid
	14.581	Benzesulfonamide
	16.225	Carbamic acid
	16.358	Cholestenol
	16.743	Cholesterol
	16.933	Docosahexanoic acid
	17.531	Eicosapentaenoic acid
	17.717	Cyclobarbital
	18.521	Tricosanoic acid
	18.712	Allopregnane
	19.150	Cyclohexanooxazin-2(1H)-one, 3,9-dihydro-6,8-isopropylideno-9-methyl-
	21.906	Propanedioic acid-, diethyl ester
	23.466	Ergosta-5,22-dien-3-ol, 24-methyl
	25.086	9,12-Octadecadienoic acid-, trimethylsilyl ester
	28.866	4-Pyrimidinecarboxylicacid,2,6-bis[(tert-butyldimethylsilyl)oxy]-,tert-utyldimethylsilyl ester
	29.353	Eicosanoic acid, trimethylsilyl ester
	29.710	16-Epiestriol, tris(pentafluoropropionate)

	30.723	3,4-Dihydrocoumarin
	31.332	2-Amino-2-(hydroxymethyl)propane-1,3-diol, N-(trifluoroacetyl)-,tris(tert butyldimethylsilyl) ether
	31.520	6,26-Pentatriacontadien-2-one
	31.928	Methionine, N-neopentyloxycarbonyl-, tetradecyl ester
	32.211	1,4-Cyclohexadiene-1-propanoic acid, 3-(dichloromethyl)-3-methyl-6-oxo-, ethyl ester
	32.519	Cyclobarbital
	32.667	Cholesterol trimethylsilyl ether
	34.173	3.alpha-(Trimethylsiloxy)cholest-5-ene
	34.371	3-Hydroxy-11-ketocholanic acid
	37.130	Card-20(22)-enolide
	37.326	3-Cyclopentylpropionic acid, phenyl ester
	43.292	Undecanoic acid,11-chloro-trimethylsilyl ester
	43.53	Succinic acid, dodec-9-yn-1-yl undecyl ester
	44.12	Cyclobarbital
	45.31	Cyclopropanetetradecanoicacid,2-octyl-methyl ester
Aqueous	10.957	Propanoic acid, 2-oxo-3-(trimethylsilyl)-, trimethylsilyl ester
	11.015	Glycerol, tris(trimethylsilyl) ether
	12.858	Propanedioic acid, methyl-bis(tert-butyldimethylsilyl) ester
	13.967	Ribitol, 1,2,3,4,5-pentakis-O-(trimethylsilyl)
	15.098	Acetamide, N-n-heptyl-
	15.273	Butanamide, 3-(1-oxo-2-phenylethylhydrazono)-N-(2-methylpropyl)-
	16.253	Isopropylmalic acid, O-(tert-butyldimethylsilyl)-, bis(tert-butyldimethylsilyl) ester
	16.685	Myristic acid, 2,3-bis(trimethylsiloxy)propyl ester
	17.227	Mannose, 6-deoxy-2,3,4,5-tetrakis-O-(trimethylsilyl)-, L-
	18.317	Levoglucosan, tris(trimethylsilyl)-
	18.866	D-Xylose, tetrakis(trimethylsilyl)-
	20.36	Galactofuranose
	21.970	Imidazolidine-1,3-dicarboxaldehyde, 4,5-diphenylamino-

	22.08	2-Deoxy-Ribose
	22.34	Myo-Inositol
	22.53	Malonic acid, 2-trifluoroacetamido-2-trimethylsiloxy-, di(trimethylsilyl)-
	25.587	Piperazine, 1-n-propyl-4-[3-phenpropyl]-
	29.413	Cholesta-3,5-diene
	32.35	Heptanoic acid, 6-oxo-trimethylsilyl ester
	32.52	Tetracosanoic acid

Appendix C

Table 5.1 Summary of the association of all annotated metabolites with disease pathology.

	CN Vs ASM		CN Vs AD		ASM Vs AD	
	p-value[a]	FC[b]	p-value[a]	FC[b]	p-value[a]	FC[c]
Acetylaspartate	4.7×10^{-2}	0.93	9.1×10^{-3}	0.91	6.5×10^{-1}	0.98
Acetylaspartylglutamate	8.4×10^{-1}	0.99	9.1×10^{-2}	0.90	1.5×10^{-1}	0.91
Acetylcarnitine	5.0×10^{-2}	1.21	1.1×10^{-2}	1.28	5.5×10^{-1}	1.06
Adenine	9.2×10^{-2}	1.10	8.0×10^{-4}	1.18	1.4×10^{-1}	1.08
Adenosine	1.2×10^{-1}	1.23	9.5×10^{-1}	0.99	1.0×10^{-1}	0.81
Adenosylmethionine	9.1×10^{-1}	0.98	4.4×10^{-3}	0.68	2.1×10^{-3}	0.69
Alanine	7.4×10^{-1}	1.02	1.6×10^{-2}	0.87	2.5×10^{-2}	0.85
Allantoin	7.0×10^{-3}	1.19	4.7×10^{-4}	1.30	2.0×10^{-1}	1.09
Aminobutanal	6.8×10^{-2}	0.94	9.2×10^{-5}	0.86	6.9×10^{-2}	0.92
AMP	6.0×10^{-1}	0.90	3.3×10^{-2}	1.50	9.4×10^{-3}	1.66
Arachidonic acid	9.5×10^{-2}	0.88	2.9×10^{-5}	0.75	1.4×10^{-2}	0.84
Arginine	5.7×10^{-2}	1.24	1.1×10^{-3}	1.38	2.9×10^{-1}	1.12
Ascorbate	1.6×10^{-1}	1.20	1.9×10^{-5}	1.54	6.2×10^{-3}	1.29
Asparagine	2.4×10^{-1}	1.17	3.0×10^{-2}	1.29	4.3×10^{-1}	1.10
Aspartate	6.3×10^{-2}	0.91	1.5×10^{-4}	0.84	1.0×10^{-1}	0.92
Benzesulfonamide	6.7×10^{-2}	0.76	4.6×10^{-7}	0.40	6.7×10^{-4}	0.52
Butyrylcarnitine	1.9×10^{-1}	1.17	1.2×10^{-2}	1.40	1.4×10^{-1}	1.19
Carbamic acid	1.9×10^{-1}	1.15	2.0×10^{-7}	1.53	4.0×10^{-4}	1.32
Carnitine	7.5×10^{-1}	0.98	7.2×10^{-1}	1.02	5.6×10^{-1}	1.04
Carnosine	2.9×10^{-1}	0.91	2.0×10^{-1}	1.21	6.6×10^{-2}	1.33
Cholestenol	1.1×10^{-1}	1.17	1.0×10^{-7}	1.44	3.0×10^{-3}	1.24
Cholesterol	7.6×10^{-3}	0.74	6.9×10^{-8}	0.53	1.1×10^{-2}	0.72
Citrulline	1.7×10^{-1}	1.25	7.4×10^{-1}	0.96	1.2×10^{-1}	0.77
Coumaric acid	9.8×10^{-2}	1.16	1.1×10^{-3}	1.28	2.3×10^{-1}	1.10
Creatine	1.6×10^{-1}	0.95	3.2×10^{-2}	0.92	4.5×10^{-1}	0.97
Creatinine	5.1×10^{-1}	0.98	3.5×10^{-1}	0.98	8.7×10^{-1}	1.00
Csytathionine	6.3×10^{-1}	1.09	7.3×10^{-1}	1.06	9.0×10^{-1}	0.98
Cysteine	4.7×10^{-1}	1.06	1.1×10^{-4}	1.33	2.1×10^{-3}	1.26

Cytidine	2.8×10^{-1}	1.14	8.5×10^{-3}	1.28	2.2×10^{-1}	1.13
Cytosine	8.4×10^{-1}	0.98	7.4×10^{-1}	1.03	6.4×10^{-1}	1.06
Dehydroascorbic acid	8.6×10^{-1}	0.94	1.9×10^{-2}	2.14	1.4×10^{-2}	2.28
Deoxyflurouridine	5.3×10^{-1}	1.08	1.0×10^{-3}	1.45	2.1×10^{-2}	1.34
Deoxy-Ribose	6.1×10^{-1}	0.94	3.6×10^{-1}	0.90	6.7×10^{-1}	0.95
Dimethylglycine	2.9×10^{-2}	0.89	1.1×10^{-6}	0.74	2.3×10^{-4}	0.84
Docosahexanoic acid	1.8×10^{-1}	1.14	1.7×10^{-7}	1.45	1.6×10^{-3}	1.27
Dopamine	1.4×10^{-1}	0.91	4.7×10^{-3}	0.82	2.3×10^{-1}	0.90
Eicosapentaenoic acid	1.6×10^{-3}	0.25	4.4×10^{-4}	0.16	1.8×10^{-1}	0.63
Fumaric acid	4.5×10^{-2}	0.91	1.9×10^{-4}	0.85	1.6×10^{-1}	0.93
GABA	3.6×10^{-1}	1.07	4.4×10^{-3}	1.18	8.7×10^{-2}	1.11
Galactofuranose	5.7×10^{-1}	1.06	6.8×10^{-2}	1.17	2.3×10^{-1}	1.11
Gluconic acid	1.5×10^{-2}	1.31	1.0×10^{-4}	1.51	1.6×10^{-1}	1.15
Glucose	5.1×10^{-1}	0.95	3.3×10^{-1}	1.07	1.4×10^{-1}	1.13
Glutamate	9.5×10^{-1}	1.00	1.0×10^{-1}	0.96	1.9×10^{-1}	0.96
Glutamine	7.1×10^{-1}	1.02	8.3×10^{-1}	0.99	5.4×10^{-1}	0.97
Glutathione	8.3×10^{-1}	1.02	1.3×10^{-1}	1.13	3.4×10^{-1}	1.10
Glycine	3.8×10^{-1}	1.07	2.6×10^{-1}	0.93	8.8×10^{-2}	0.87
Guanidobutanoate	2.0×10^{-1}	0.94	3.7×10^{-6}	0.75	5.9×10^{-5}	0.80
Guanine	4.5×10^{-2}	0.83	1.0×10^{-3}	0.75	3.2×10^{-1}	0.91
Guanosine	7.5×10^{-2}	0.83	5.0×10^{-3}	0.76	4.4×10^{-1}	0.92
Hexanedioic acid	2.8×10^{-1}	1.11	6.4×10^{-7}	1.42	5.3×10^{-4}	1.28
Histidine	9.1×10^{-1}	0.99	7.6×10^{-3}	0.71	7.8×10^{-3}	0.72
Homocysteine	8.0×10^{-1}	0.97	2.0×10^{-1}	1.14	1.6×10^{-1}	1.17
Hydroxyanthranillate	5.4×10^{-1}	0.95	3.6×10^{-1}	0.92	7.4×10^{-1}	0.97
Hydroxyguanine	8.3×10^{-2}	3.06	2.1×10^{-1}	1.05	9.0×10^{-2}	0.34
Hypoxanthine	4.7×10^{-1}	0.98	5.5×10^{-4}	0.88	4.1×10^{-3}	0.91
Indoleacetic acid	1.4×10^{-1}	0.93	2.6×10^{-4}	0.82	4.8×10^{-2}	0.89
Inosine	2.8×10^{-1}	0.93	8.9×10^{-1}	0.99	3.1×10^{-1}	1.07
Kynurenic acid	7.3×10^{-1}	0.96	3.2×10^{-1}	0.87	5.2×10^{-1}	0.91
Lactic acid	9.1×10^{-1}	1.00	7.1×10^{-1}	0.99	8.2×10^{-1}	0.99
L-DOPA	9.3×10^{-2}	1.11	1.9×10^{-4}	1.23	6.1×10^{-2}	1.10
Leucine/Isoleucine	4.5×10^{-1}	1.05	3.4×10^{-2}	1.14	1.7×10^{-1}	1.09
Linoleic acid	7.0×10^{-3}	0.74	8.9×10^{-8}	0.52	6.7×10^{-3}	0.71

Linolenic acid	7.5×10^{-2}	0.90	2.6×10^{-4}	0.84	1.6×10^{-1}	0.93
Lysine	1.9×10^{-1}	1.20	3.1×10^{-2}	1.41	2.9×10^{-1}	1.18
Malate	9.8×10^{-1}	1.00	1.8×10^{-1}	0.91	2.7×10^{-1}	0.91
Methionine	4.2×10^{-1}	1.09	2.1×10^{-1}	1.14	6.1×10^{-1}	1.05
Methyl-aspartic acid	8.2×10^{-1}	0.99	4.6×10^{-2}	0.88	7.5×10^{-2}	0.89
Methylheptadecadiynoate	2.5×10^{-2}	0.79	2.8×10^{-7}	0.59	1.2×10^{-2}	0.75
Methylstearate	5.4×10^{-1}	0.85	2.6×10^{-2}	0.56	2.0×10^{-1}	0.66
Myo-Inositol	5.8×10^{-1}	1.09	6.6×10^{-3}	0.70	9.7×10^{-3}	0.65
Nicotinamide	6.9×10^{-1}	0.98	6.8×10^{-1}	0.98	9.6×10^{-1}	1.00
Nicotinic acid	2.5×10^{-1}	1.13	1.7×10^{-2}	0.80	1.7×10^{-3}	0.71
Nitrotyrosine	9.6×10^{-3}	1.25	1.6×10^{-3}	1.33	4.9×10^{-1}	1.06
Noradrenaline	2.9×10^{-1}	1.16	9.8×10^{-3}	1.35	1.9×10^{-1}	1.16
Octadecanal	1.6×10^{-1}	2.41	5.6×10^{-1}	0.68	5.5×10^{-2}	0.28
Oleic acid	5.5×10^{-2}	0.73	3.3×10^{-7}	0.34	3.9×10^{-4}	0.46
Ornithine	8.5×10^{-2}	1.18	2.1×10^{-3}	1.29	3.1×10^{-1}	1.09
Oxoarginine	9.0×10^{-1}	0.99	8.6×10^{-4}	0.77	2.3×10^{-2}	0.78
Oxoglutarate	9.3×10^{-1}	0.99	5.5×10^{-2}	1.10	1.1×10^{-1}	1.11
Palmitic acid	2.0×10^{-2}	0.73	4.9×10^{-7}	0.44	1.9×10^{-3}	0.61
Pantothenate	3.3×10^{-1}	0.88	3.3×10^{-2}	0.75	1.1×10^{-1}	0.85
Phenylalanine	2.1×10^{-1}	1.09	5.5×10^{-2}	1.14	4.3×10^{-1}	1.05
Phosphocholine	3.5×10^{-1}	1.06	9.5×10^{-3}	1.14	2.6×10^{-1}	1.07
Phosphocreatine	3.7×10^{-1}	0.87	1.1×10^{-1}	0.77	4.4×10^{-1}	0.88
Proline	2.6×10^{-1}	1.06	8.5×10^{-1}	1.01	3.4×10^{-1}	0.95
Propionylcarnitine	1.3×10^{-1}	1.29	2.7×10^{-2}	1.37	6.5×10^{-1}	1.07
Serine	6.9×10^{-1}	1.04	6.7×10^{-1}	0.96	4.3×10^{-1}	0.92
Spermidine	8.4×10^{-1}	0.95	1.8×10^{-1}	0.72	2.1×10^{-1}	0.76
Succinate	6.6×10^{-1}	0.96	7.0×10^{-2}	1.13	3.4×10^{-2}	1.18
Taurine	5.0×10^{-1}	0.96	9.3×10^{-1}	1.01	4.7×10^{-1}	1.04
Threonine	3.4×10^{-1}	1.07	8.9×10^{-2}	1.11	5.6×10^{-1}	1.04
Tryptophan	1.5×10^{-1}	1.16	1.2×10^{-1}	1.19	7.8×10^{-1}	1.03
Tyrosine	2.6×10^{-2}	1.22	2.7×10^{-3}	1.30	4.4×10^{-1}	1.07
Uracil	8.5×10^{-1}	1.01	1.8×10^{-3}	1.22	1.8×10^{-3}	1.21
Uric acid	5.9×10^{-1}	1.06	4.5×10^{-2}	0.80	2.0×10^{-2}	0.76
Uridine	9.6×10^{-1}	1.00	1.3×10^{-1}	0.88	1.5×10^{-1}	0.89

Valine	4.1×10^{-2}	1.21	5.6×10^{-3}	1.25	7.6×10^{-1}	1.03
Xanthine	3.2×10^{-1}	1.04	1.2×10^{-1}	0.95	2.0×10^{-2}	0.92
Xanthosine	9.7×10^{-1}	1.00	7.5×10^{-1}	1.02	7.3×10^{-1}	1.03

[a] p-value calculated using mann-whitney U-test. [b] fold change relative to controls, [c] fold change relative to asymptomatic. AMP; adenosine-monophosphate, Asymp; asymptomatic, Cont; control, Dem; demented, GABA; gamma-aminobutanoate, L-DOPA; L-dihydroxy-phenylalanine.

Table 5.2 Correlation of the abundance of 6 unsaturated fatty acids with measures of both cross sectional and longitudinal memory performance.

		Last Score*		Longitudinal decline+	
		Estimate	p-value	Estimate	p-value
CB	Eicosapentaenoic acid	0.185	0.551	0.020	0.490
	Linoleic acid	0.042	0.867	0.019	0.394
	Arachidonic acid	0.275	0.264	0.039	0.093
	Oleic acid	0.489	0.032	0.047	0.029
	Docosahexanoic acid	-0.607	0.022	-0.052	0.035
	Linolenic acid	0.305	0.209	0.023	0.290
ITG	Eicosapentaenoic acid	0.073	0.731	0.000	0.988
	Linoleic acid	0.238	0.231	0.010	0.599
	Arachidonic acid	0.236	0.244	0.011	0.585
	Oleic acid	0.182	0.373	0.006	0.751
	Docosahexanoic acid	-0.131	0.528	0.003	0.866
	Linolenic acid	0.282	0.188	0.014	0.515
MFG	Eicosapentaenoic acid	0.109	0.620	0.027	0.206
	Linoleic acid	0.344	0.121	0.039	0.075
	Arachidonic acid	0.283	0.200	0.034	0.116
	Oleic acid	0.350	0.121	0.039	0.080
	Docosahexanoic acid	-0.347	0.148	-0.038	0.105
	Linolenic acid	0.268	0.249	0.034	0.139

Table 5.3 Correlation of the abundance of 6 unsaturated fatty acids with measures of both cross sectional and longitudinal language performance.

		Last Score*		Longitudinal decline+	
		Estimate	p-value	Estimate	p-value
CB	Eicosapentaenoic acid	0.068	0.804	0.015	0.583
	Linoleic acid	0.176	0.404	0.008	0.644
	Arachidonic acid	0.154	0.472	0.017	0.347
	Oleic acid	0.194	0.346	0.018	0.273
	Docosahexanoic acid	-0.053	0.817	-0.020	0.272
	Linolenic acid	0.294	0.154	0.020	0.225
ITG	Eicosapentaenoic acid	0.253	0.178	-0.002	0.907
	Linoleic acid	0.371	0.050	0.026	0.127
	Arachidonic acid	0.348	0.067	0.025	0.156
	Oleic acid	0.341	0.077	0.023	0.207
	Docosahexanoic acid	-0.384	0.044	-0.017	0.354
	Linolenic acid	0.329	0.074	0.023	0.217
MFG	Eicosapentaenoic acid	0.105	0.605	0.054	0.032
	Linoleic acid	0.230	0.253	0.047	0.015
	Arachidonic acid	0.173	0.383	0.043	0.026
	Oleic acid	0.236	0.215	0.047	0.012
	Docosahexanoic acid	-0.125	0.499	-0.033	0.074
	Linolenic acid	0.229	0.242	0.046	0.015

Table 5.4 Correlation of the abundance of 6 unsaturated fatty acids with measures of both cross sectional and longitudinal attention span.

		Last Score*		Longitudinal decline+	
		Estimate	p-value	Estimate	p-value
CB	Eicosapentaenoic acid	0.152	0.650	-0.027	0.382
	Linoleic acid	0.222	0.234	0.016	0.384
	Arachidonic acid	0.220	0.244	0.016	0.392
	Oleic acid	0.306	0.058	0.031	0.003
	Docosahexanoic acid	-0.065	0.755	-0.011	0.555
	Linolenic acid	0.356	0.031	0.026	0.003
ITG	Eicosapentaenoic acid	0.277	0.093	0.013	0.502
	Linoleic acid	0.230	0.173	0.013	0.455
	Arachidonic acid	0.202	0.236	0.013	0.494
	Oleic acid	0.189	0.269	0.011	0.549
	Docosahexanoic acid	-0.256	0.123	-0.009	0.631
	Linolenic acid	0.284	0.102	0.014	0.475
MFG	Eicosapentaenoic acid	0.233	0.184	0.011	0.640
	Linoleic acid	0.385	0.027	0.030	0.117
	Arachidonic acid	0.347	0.042	0.028	0.138
	Oleic acid	0.352	0.042	0.032	0.096
	Docosahexanoic acid	-0.345	0.064	-0.034	0.087
	Linolenic acid	0.387	0.031	0.027	0.173

Table 3.5 Correlation of the abundance of 6 unsaturated fatty acids with measures of both cross sectional and longitudinal executive function.

		Last Score*		Longitudinal decline+	
		Estimate	p-value	Estimate	p-value
CB	Eicosapentaenoic acid	-0.007	0.984	0.005	0.765
	Linoleic acid	0.119	0.552	0.008	0.396
	Arachidonic acid	0.193	0.336	0.011	0.288
	Oleic acid	0.349	0.068	0.016	0.126
	Docosahexanoic acid	-0.258	0.227	-0.009	0.476
	Linolenic acid	0.376	0.053	0.008	0.383
ITG	Eicosapentaenoic acid	0.244	0.160	-0.004	0.764
	Linoleic acid	0.273	0.123	0.003	0.768
	Arachidonic acid	0.248	0.165	0.002	0.855
	Oleic acid	0.262	0.145	0.004	0.742
	Docosahexanoic acid	-0.357	0.038	-0.006	0.620
	Linolenic acid	0.379	0.037	0.011	0.400
MFG	Eicosapentaenoic acid	0.270	0.134	0.005	0.775
	Linoleic acid	0.525	0.002	0.008	0.545
	Arachidonic acid	0.484	0.005	0.009	0.468
	Oleic acid	0.518	0.003	0.009	0.477
	Docosahexanoic acid	-0.575	0.002	-0.007	0.654
	Linolenic acid	0.550	0.002	0.006	0.670

Table 5.6 Correlation of the abundance of 6 unsaturated fatty acids with measures of both cross sectional and longitudinal visual spatial awareness.

		Last Score*		Longitudinal decline+	
		Estimate	p-value	Estimate	p-value
CB	Eicosapentaenoic acid	0.383	0.166	0.055	0.013
	Linoleic acid	0.296	0.091	0.025	0.218
	Arachidonic acid	0.349	0.020	0.033	0.015
	Oleic acid	0.422	0.004	0.042	0.002
	Docosahexanoic acid	-0.182	0.366	-0.025	0.248
	Linolenic acid	0.329	0.033	0.035	0.004
ITG	Eicosapentaenoic acid	0.038	0.815	0.030	0.079
	Linoleic acid	0.160	0.317	0.029	0.034
	Arachidonic acid	0.131	0.417	0.028	0.056
	Oleic acid	0.128	0.434	0.032	0.027
	Docosahexanoic acid	-0.218	0.173	-0.033	0.014
	Linolenic acid	0.266	0.113	0.042	0.008
MFG	Eicosapentaenoic acid	0.258	0.118	0.025	0.186
	Linoleic acid	0.330	0.043	0.025	0.094
	Arachidonic acid	0.305	0.059	0.026	0.084
	Oleic acid	0.303	0.065	0.028	0.065
	Docosahexanoic acid	-0.235	0.176	-0.031	0.074
	Linolenic acid	0.298	0.076	0.023	0.144

Appendix D

Table 6.1 show annotated metababolites of lipidomics study between groups.

	Control Vs ASM		Control Vs AD		ASM Vs AD	
	p-value	FC[b]	p-value	FC[b]	p-value	FC[c]
LPE(18:0)	4.56E-01	1.08	5.92E-02	1.24	2.76E-01	1.15
LPC(16:1)	7.47E-01	0.97	3.85E-01	1.13	3.23E-01	1.16
LPC(16:0)	9.68E-01	1.00	9.66E-02	1.14	1.26E-01	1.14
LPE(20:0)	9.76E-01	1.00	4.27E-01	1.11	4.52E-01	1.10
LPC(18:3)	5.91E-01	1.07	5.27E-02	1.30	1.56E-01	1.21
Cer(d34:1)	6.51E-02	1.57	2.25E-01	1.16	1.71E-01	0.74
LPC(18:1)	8.21E-01	0.98	2.17E-01	1.11	2.31E-01	1.13
LPC(18:0)	9.66E-01	1.00	1.52E-01	1.14	1.42E-01	1.14
Cer(36:2)	1.38E-01	1.48	7.96E-01	1.03	1.66E-01	0.70
Cer(36:1)	5.77E-02	1.52	1.93E-02	1.24	3.04E-01	0.82
Cer(38:1)	5.02E-02	1.23	2.26E-01	1.12	4.40E-01	0.92
DG(34:0)	7.56E-01	1.02	5.44E-01	0.97	3.87E-01	0.95
Cer(40:1)	3.02E-02	1.31	9.95E-01	1.00	1.51E-02	0.76
DG(35:3)	2.55E-01	1.07	4.41E-01	0.96	3.33E-02	0.90
DG(36:4)	7.44E-01	0.96	1.41E-02	1.33	6.92E-03	1.38
Cer(42:1)	4.48E-03	2.16	6.38E-01	1.09	7.78E-03	0.51
Cer(42:1)	4.54E-03	1.70	7.38E-01	1.05	3.98E-03	0.62
DG(37:0)	5.43E-01	1.04	2.23E-01	0.92	5.50E-02	0.88
Cer(43:2)	5.35E-03	1.87	6.63E-01	1.06	9.61E-03	0.57
PA(O-33:1)	3.44E-02	1.64	5.86E-01	1.10	7.05E-02	0.67
DG(38:0)	8.92E-01	1.02	7.47E-01	1.05	8.89E-01	1.02
Cer(44:2)	1.53E-03	1.89	7.35E-01	1.05	2.70E-03	0.55
DG(40:8)	5.95E-01	0.93	5.40E-03	1.49	1.11E-03	1.61
PA(33:0)	2.22E-01	1.23	6.14E-04	1.97	1.64E-02	1.59
DG(40:6)	3.01E-01	1.22	9.63E-04	1.87	1.53E-02	1.53
SM(32:1)	5.12E-01	1.13	7.39E-01	1.04	6.13E-01	0.92

SM(32:2)	5.45E-01	1.10	4.59E-03	1.69	1.62E-02	1.54
PE(P-34:1)	1.00E-01	1.34	3.66E-01	1.11	2.54E-01	0.83
SM(34:1)	2.83E-01	1.14	2.32E-01	1.10	7.46E-01	0.97
DG(44:12)	7.99E-01	1.04	1.34E-03	1.76	2.00E-03	1.69
PE(36:2)	4.75E-01	1.12	6.43E-01	1.07	7.40E-01	0.95
SM(36:2)	5.70E-01	0.96	8.82E-01	1.01	5.04E-01	1.05
PC(P33:1)	1.01E-01	1.34	5.99E-01	1.07	1.81E-01	0.80
SM(36:1)	8.64E-02	0.87	3.76E-01	1.07	4.80E-03	1.22
PA(O-39:0)	4.93E-01	1.12	8.00E-01	1.04	6.16E-01	0.93
PE(P-38:6)	3.36E-01	1.12	8.11E-01	1.02	4.35E-01	0.91
PS(0-34:0)	5.00E-02	0.68	6.53E-01	1.09	2.19E-02	1.59
PC(33:1)	4.69E-01	1.10	9.91E-01	1.00	4.76E-01	0.91
PE(P-38:4)	8.41E-01	0.98	6.61E-01	0.97	8.61E-01	0.99
PC(34:2)	7.16E-01	0.98	1.27E-01	0.93	4.26E-01	0.95
SM(38:1)	6.35E-01	0.94	1.22E-01	0.84	3.02E-01	0.89
PC(35:0)	1.86E-01	0.97	9.89E-01	1.00	1.54E-01	1.03
PCae(36:5)	4.96E-01	0.95	6.36E-01	1.03	2.64E-01	1.08
PC aa(36:4)	1.15E-01	1.19	7.18E-01	0.96	5.12E-02	0.80
PC(35:3)	3.40E-01	1.10	8.85E-01	1.01	4.01E-01	0.92
PC(26:1)	1.39E-01	0.89	7.87E-02	0.89	9.67E-01	1.00
PE(P-40:7)	1.94E-01	1.27	6.96E-01	1.06	2.91E-01	0.83
PC(34:4)	3.46E-02	0.88	3.69E-01	0.96	1.72E-01	1.09
PE(P-40:5)	9.48E-01	0.99	4.35E-01	1.15	3.89E-01	1.17
PC aa(36:5)	5.44E-01	1.04	1.36E-01	0.90	2.77E-02	0.86
SM(38:1)	5.55E-01	1.04	1.62E-01	0.90	3.80E-02	0.87
PC(36:4)	3.17E-01	0.91	7.86E-01	0.97	4.98E-01	1.08
PC(36:3)	1.15E-01	0.81	9.60E-01	0.99	8.76E-02	1.23
PC(36:2)	9.07E-01	0.99	1.97E-01	0.90	2.44E-01	0.91
Glucer(d40:0)	7.72E-01	1.02	3.04E-01	0.96	2.19E-01	0.94
SM(40:1)	2.32E-01	1.41	7.36E-01	1.04	2.77E-01	0.74
PC(37:1)	1.15E-01	1.06	9.91E-01	1.00	1.06E-01	0.95
Glucer(d39:1)	7.06E-01	1.10	3.38E-01	1.10	1.00E+00	1.00
PC ae(38:6)	7.72E-01	0.98	3.07E-01	0.94	5.53E-01	0.96
PC(38:4)	4.01E-01	0.92	7.19E-01	1.04	2.43E-01	1.13

PG(38:3)	1.15E-01	1.46	3.75E-01	1.14	2.75E-01	0.78
GlcCer(d40:1)	5.70E-02	0.89	2.79E-01	1.05	4.93E-03	1.19
Pcaa(38:6)	1.34E-01	1.43	3.38E-01	1.20	4.23E-01	0.84
SM(40:2)	4.12E-01	1.18	4.77E-01	0.90	1.71E-01	0.76
SM(40:1)	6.97E-02	0.90	3.37E-01	0.96	2.45E-01	1.06
PC(37:0)	1.49E-01	0.92	1.00E-01	0.92	9.70E-01	1.00
PC(38:4)	5.06E-01	1.17	6.79E-01	1.09	7.50E-01	0.93
PC(38:3)	4.50E-02	2.14	3.46E-01	1.32	1.54E-01	0.62
SM(42:2)	6.37E-02	1.40	3.90E-01	1.13	1.97E-01	0.81
PC(37:6)	8.50E-02	1.36	4.17E-01	1.12	2.39E-01	0.82
SM(42:1)	8.36E-02	1.55	4.69E-01	1.12	1.69E-01	0.72
SM(43:2)	1.02E-01	1.45	3.59E-01	1.15	2.74E-01	0.79
Pcae(40:1)	8.28E-01	1.04	4.60E-01	1.12	6.05E-01	1.08
PC aa(40:6)	1.95E-02	0.86	6.14E-01	1.03	7.65E-03	1.20
SM(42:1)	3.48E-01	0.86	2.95E-02	1.48	7.80E-03	1.73
PC(30:4)	5.72E-01	0.96	2.16E-01	0.92	5.15E-01	0.96
SM(42:0)	5.55E-01	0.96	1.95E-01	0.91	4.99E-01	0.95
SM(44:2)	1.71E-01	1.38	2.48E-01	1.23	6.08E-01	0.89
PC aa(40:1)	1.51E-01	0.88	7.51E-02	1.14	2.82E-03	1.29
PS(36:2)	2.07E-01	1.29	4.48E-01	1.13	4.78E-01	0.87
TG(50:0)	9.66E-02	1.37	9.63E-02	1.22	4.83E-01	0.89
PC ae(42:3)	2.50E-01	0.91	2.12E-01	1.12	3.19E-02	1.24
PC(42:9)	1.00E-01	0.81	9.53E-01	0.99	8.84E-02	1.22
TG(52:5)	5.10E-01	1.13	2.80E-01	0.87	1.73E-01	0.77
PC(42:7)	2.12E-01	1.21	1.55E-02	1.37	3.23E-01	1.14
Glc cer(40:1)	2.65E-02	0.77	7.31E-01	1.04	1.20E-02	1.34
PC(42:4)	8.77E-02	0.84	5.16E-01	1.07	2.82E-02	1.28
TG(51:0)	3.00E-01	2.26	6.69E-02	0.66	1.86E-01	0.29
PC(44:5)	9.62E-01	1.01	9.03E-01	1.01	9.48E-01	1.01
TG(52:0)	4.78E-01	1.09	4.72E-02	1.16	5.56E-01	1.07
TG(52:0)	6.38E-01	1.05	4.94E-02	1.16	3.58E-01	1.10
PC(44:1)	2.38E-01	1.33	5.42E-01	1.11	4.18E-01	0.84
TG(54:6)	2.42E-01	2.21	2.27E-01	0.73	1.47E-01	0.33

Hexadecynyl acetate	4.26E-01	1.09	7.18E-02	0.89	8.40E-02	0.82
Tetradecanedioic acid	5.71E-01	0.95	7.08E-01	1.03	4.20E-01	1.08
Octadecadenoic acid	7.52E-01	0.96	5.19E-01	1.08	4.29E-01	1.13
hydroxycalciol	3.27E-01	1.17	2.65E-01	1.17	9.91E-01	1.00
LPE alkenyl 18:1	7.63E-01	1.04	1.19E-01	1.19	2.46E-01	1.15
LPE(18:1)	7.12E-01	1.03	7.79E-02	1.15	2.52E-01	1.11
LPC(15:0)	8.53E-01	0.99	3.73E-01	1.06	3.05E-01	1.08
Lyso PE(20:4)	9.29E-01	0.99	4.04E-01	1.07	4.44E-01	1.08
LPE(20:1)	9.77E-01	1.00	7.78E-01	0.98	8.35E-01	0.98
LPE(20:0)	7.74E-01	0.98	4.11E-01	1.07	2.63E-01	1.10
Cer(36:1)	1.18E-01	1.36	3.67E-02	1.21	5.09E-01	0.89
Cer(38:1)	2.82E-01	1.18	9.64E-01	1.00	2.44E-01	0.84
Cer(42:2)	1.09E-02	1.48	9.52E-01	1.01	1.54E-02	0.68
PA(34:1)	7.65E-02	1.44	1.02E-01	1.26	4.85E-01	0.88
Cer(41:0)	3.21E-02	1.34	4.68E-01	0.94	1.22E-02	0.70
Cer(42:1)	1.47E-02	1.52	4.97E-01	0.92	6.86E-03	0.60
PA(36:1)	2.46E-01	1.17	9.73E-02	1.13	8.05E-01	0.97
PE(34:2)	9.06E-01	1.01	5.78E-01	1.04	6.64E-01	1.03
PE(34:1)	5.87E-01	0.97	4.66E-01	0.96	8.82E-01	0.99
PE(34:0)	7.44E-01	0.97	6.54E-01	1.03	4.51E-01	1.06
PE(35:3)	7.05E-01	1.05	5.16E-01	1.07	8.34E-01	1.02
PC(32:1)	7.00E-01	1.03	2.24E-01	0.93	1.45E-01	0.91
PC(33:2)	2.66E-01	1.07	3.01E-01	1.06	8.14E-01	0.99
PE(36:2)	6.41E-01	1.03	2.26E-02	0.91	2.79E-02	0.88
PE(36:1)	7.76E-01	1.01	7.85E-01	0.99	5.79E-01	0.97
PE ae(38:6)	7.37E-01	0.98	9.59E-01	1.00	6.94E-01	1.03
PS(32:6)	1.29E-01	1.39	3.16E-01	1.22	4.63E-01	0.88
PE(38:4)	5.78E-01	0.96	2.12E-01	0.92	5.97E-01	0.96
PC(34:1)	3.14E-01	1.05	2.27E-01	0.95	6.92E-02	0.91
PC(35:3)	4.53E-01	1.10	8.60E-01	1.02	5.59E-01	0.93
PE ae(40:6)	6.57E-01	0.96	4.07E-01	0.94	7.70E-01	0.98

PE(39:6)	8.49E-01	1.01	7.40E-01	1.01	9.02E-01	1.00
PS(36:7)	2.83E-01	0.92	3.26E-01	1.07	3.74E-02	1.16
PE(39:5)	6.16E-01	0.96	8.21E-01	1.02	4.57E-01	1.06
PE(39:5)	8.61E-01	0.99	7.23E-02	0.86	7.98E-02	0.87
PC(36:4)	6.68E-01	0.97	4.66E-01	0.96	8.20E-01	0.99
PE(40:6)	7.70E-01	1.02	3.33E-01	0.94	2.66E-01	0.92
PG(36:6)	8.54E-01	0.98	8.75E-01	1.02	7.29E-01	1.05
PE(42:9)	8.85E-01	0.99	1.03E-01	0.86	1.46E-01	0.87
PE(40:3)	4.39E-01	0.94	1.43E-01	0.88	3.96E-01	0.94
PS(38:3)	3.54E-01	0.90	5.84E-01	0.95	6.25E-01	1.05
PS(37:1)	7.29E-01	1.03	3.29E-02	0.88	4.53E-02	0.85
PS(37:0)	9.36E-01	1.00	5.66E-01	0.97	6.35E-01	0.98
PA(44:5)	9.16E-01	0.99	5.78E-01	0.97	6.66E-01	0.98
PS(38:6)	9.30E-01	1.01	8.61E-01	1.02	9.36E-01	1.01
Glccer(d42:0)	8.28E-02	0.85	6.87E-01	0.97	1.17E-01	1.14
PC(40:10)	6.55E-01	0.95	5.15E-01	0.94	9.20E-01	0.99
PS(39:3)	3.90E-01	0.92	9.12E-01	0.99	4.07E-01	1.08
PI(35:1)	3.10E-01	0.91	4.93E-01	1.06	7.27E-02	1.17
GlcCer(44:1)	1.43E-01	0.81	5.83E-01	0.93	1.99E-01	1.15
PS(40:2)	9.07E-01	1.01	2.24E-01	1.08	2.84E-01	1.07
PI(36:4)	6.46E-01	1.05	7.34E-01	1.04	9.15E-01	0.99
PI(34:2)	5.84E-01	1.05	6.38E-01	1.05	9.56E-01	0.99
PE(46:6)	1.56E-02	0.83	3.07E-01	0.93	8.91E-02	1.13
PE(46:5)	5.68E-02	0.72	2.37E-01	0.83	5.16E-02	1.16
PI(38:5)	8.92E-01	0.99	1.18E-01	0.90	1.43E-01	0.91
PI(40:6)	8.59E-01	0.98	4.58E-01	1.07	3.40E-01	1.09

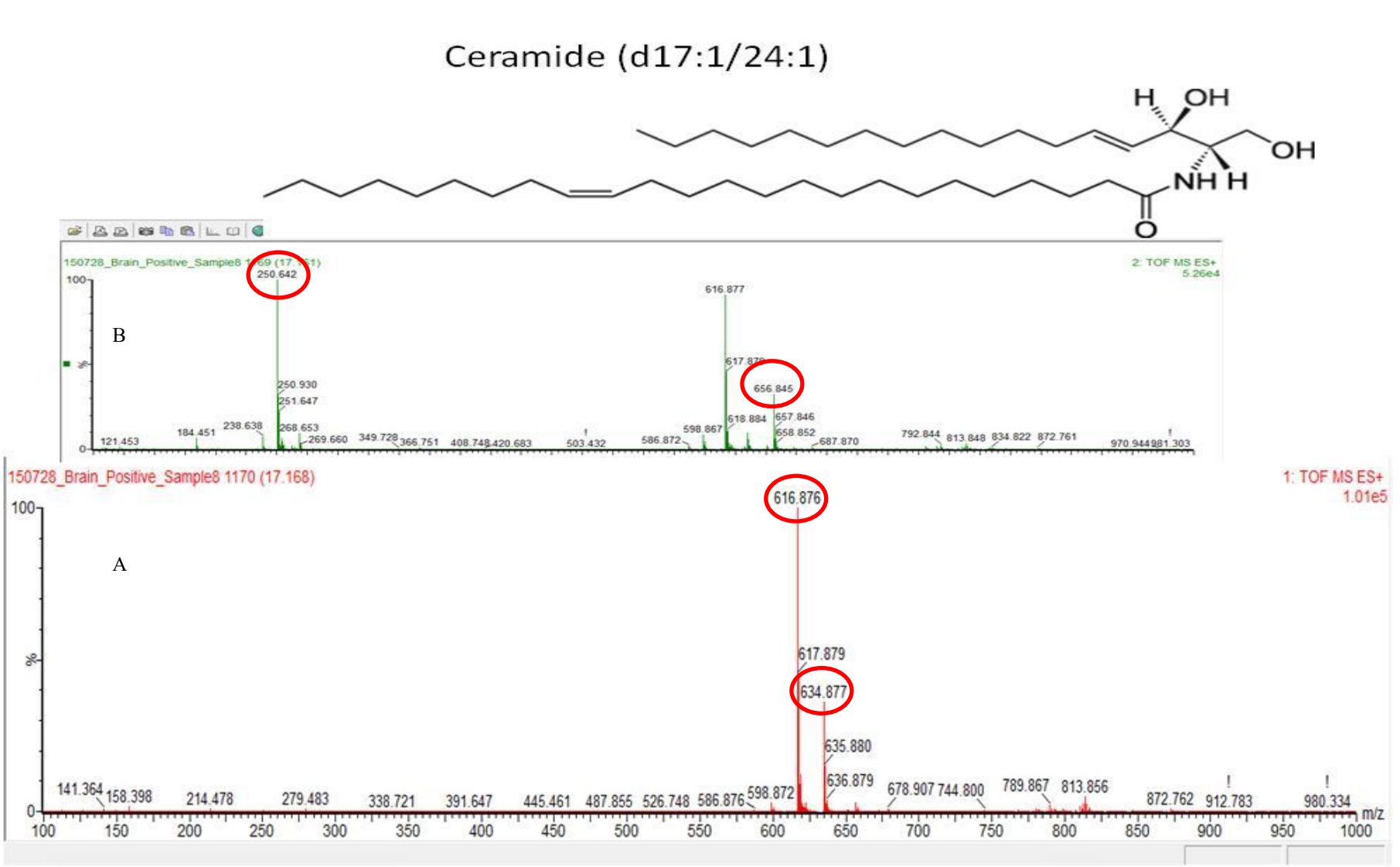

Figure 6.1 Mass spectrum of lipid internal standard-ceramide (d17:1/24:1). A) Channel 1 showing two main parent ions. B) Channel 2 showing daughter ions. Cer (d17:1/24:1), parent ion $[M+H)^+$ = 634.87, RT=17.1 min, parent ion $[M - H_2O + H]^+$ = 616.87.

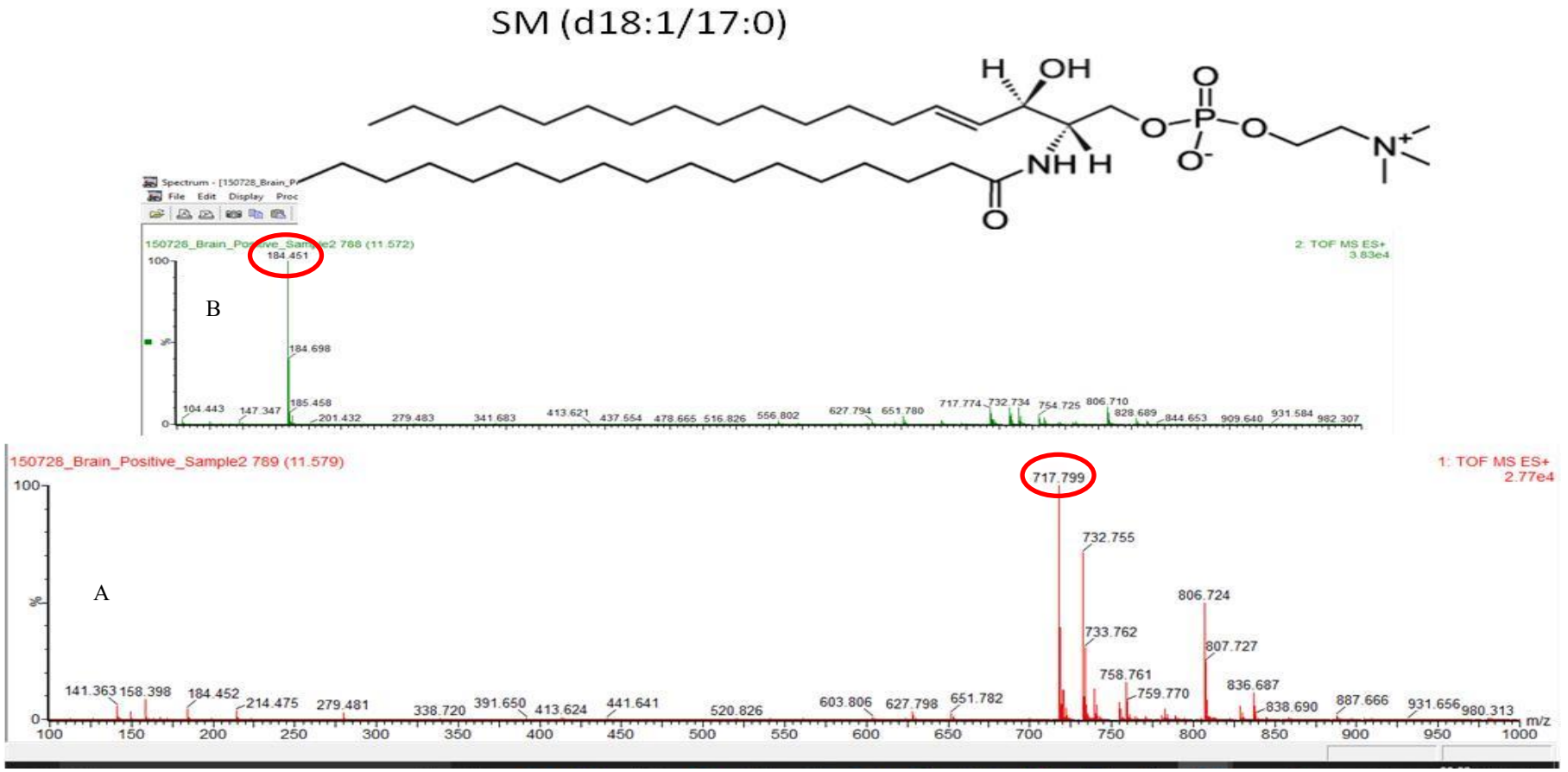

Figure 6.2 Mass spectrum of lipid internal standard- sphingomyeline (/d18:117:0). A) Channel 1showing parent ion. B) Channel 2 showing daughter ions. SM (d18:1/17:0), $[M+H]^+$ =717.79, RT=11.5min, Daughter ion -Phosphocholine = 184.4.

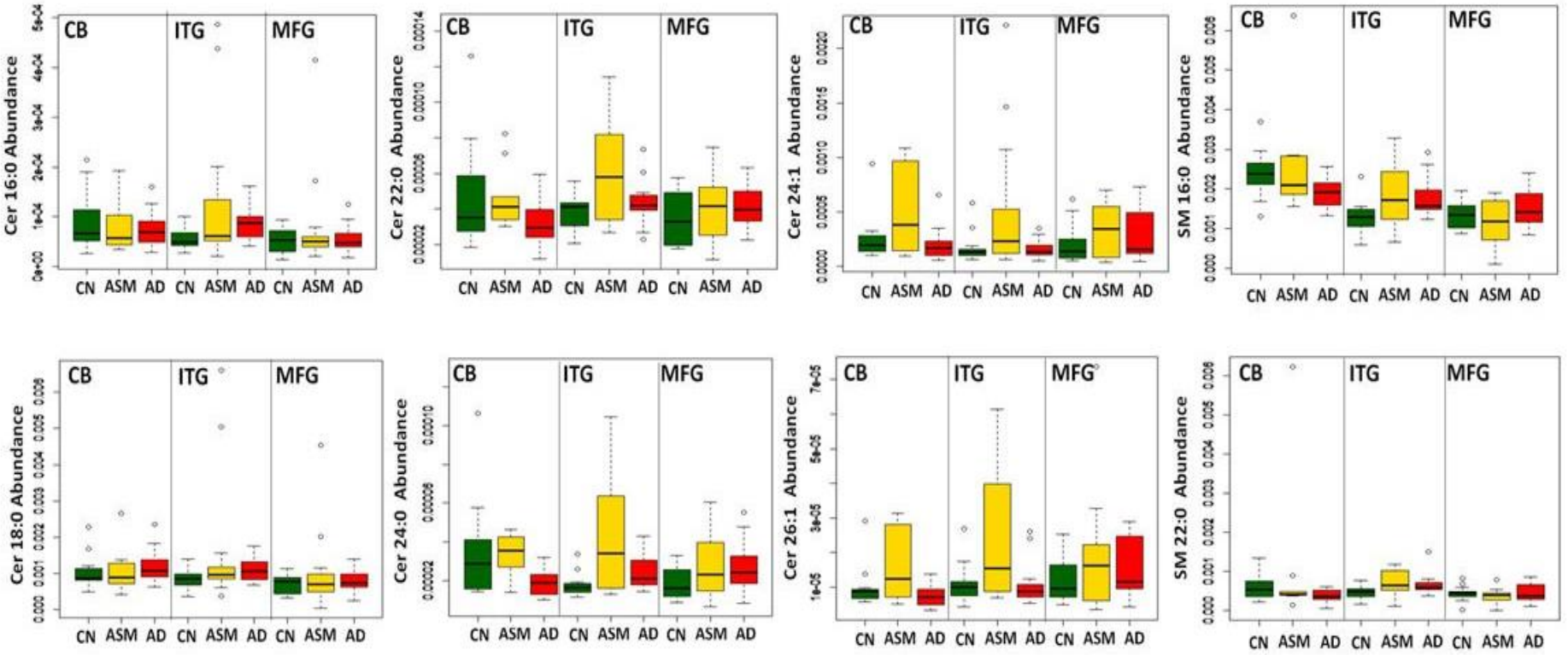

Figure 6.3 Boxplots showing the effect of disease status on the abundance of all SPHLs annotated (n=8) in the Cerebellum(CB), Inferior Temporal Gyrus(ITG) and Middle Frontal Gyrus(MFG).

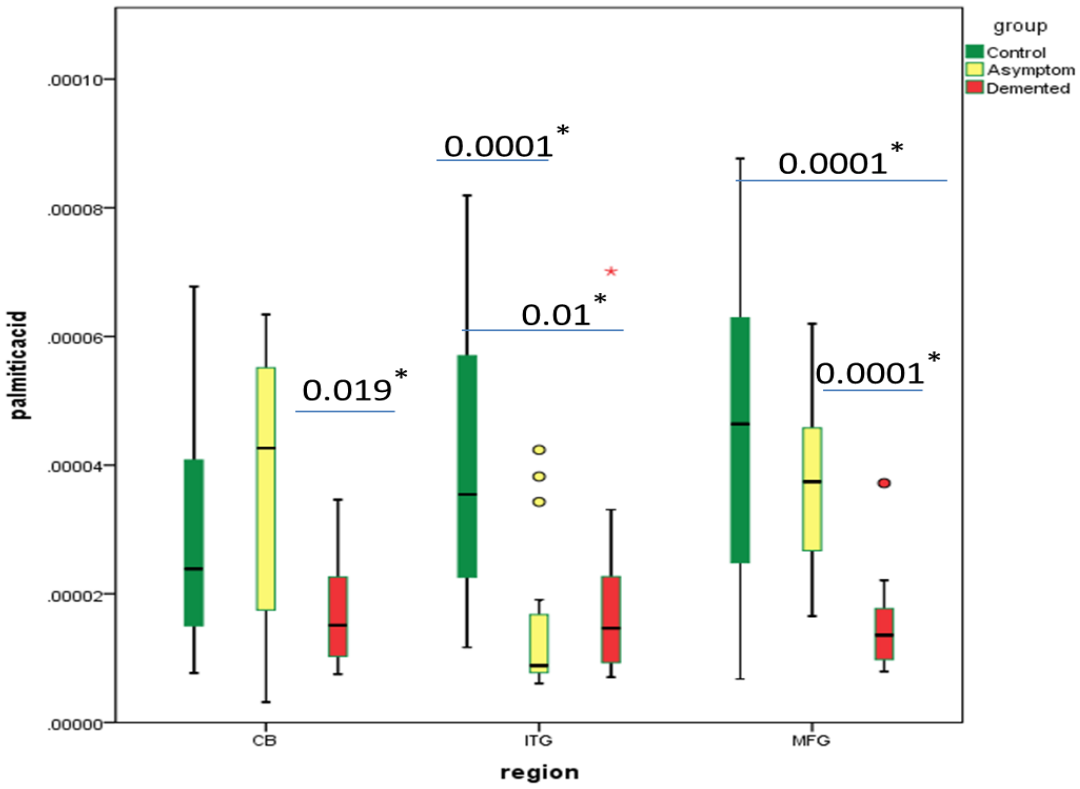

Figure 6.4 Boxplot of palmitic acid abundance in brain ITG region. * ANOVA kruskal wallis with Benjamini-Hochberg multiple correction, *outlier.